

# **DESIGN OF NONLINEAR CONTROLLERS FOR VARIABLE SPEED VARIABLE PITCH WIND TURBINE**

Thesis

Submitted in partial fulfillment of the requirement for the award of degree of

**DOCTOR OF PHILOSOPHY**

By

**SARAVANAKUMAR R.**



**DEPARTMENT OF ELECTRICAL AND ELECTRONICS ENGINEERING  
NATIONAL INSTITUTE OF TECHNOLOGY KARNATAKA  
SURATHKAL, MANGALORE-575025**

**March, 2016**



# **D E C L A R A T I O N**

*by the Ph.D. Research Scholar*

I hereby declare that the Research Thesis entitled “**DESIGN OF NONLINEAR CONTROLLERS FOR VARIABLE SPEED VARIABLE PITCH WIND TURBINE**” which is being submitted to the National Institute of Technology Karnataka, Surathkal in partial fulfillment of the requirements for the award of the Degree of **Doctor of Philosophy in Electrical and Electronics Engineering** is a bonafide report of the research work carried out by me. The material contained in this Research Thesis has not been submitted to any University or Institution for the award of any degree.

**SARAVANAKUMAR R.**

(Reg. No: 110654EE11F02)

Department of Electrical and Electronics Engineering

Place: NITK Surathkal

Date:



# CERTIFICATE

This is to certify that the Research Thesis entitled “**DESIGN OF NONLINEAR CONTROLLERS FOR VARIABLE SPEED VARIABLE PITCH WIND TURBINE**” submitted by **SARAVANAKUMAR R.** (Register Number: **110654EE11F02**) as the record of the research work carried out by him, is *accepted as the Research Thesis submission* in partial fulfillment of the requirements for the award of degree of **Doctor of Philosophy**.

Dr. Debashisha Jena

(Research Guide)

(Name and Signature with Date and Seal)

Chairman-DRPC

(Signature with Date and Seal)



## **ACKNOWLEDGEMENTS**

I would like to express my sincere gratitude to my advisor Dr. Debashisha Jena. Without the help obtained from him, the work behind this thesis could hardly have been done. He has been the most instrumental person for my academic and research achievements. He provided guidance, advice, expertise, never ending encouragement, patience and support which are invaluable input into my life that lies ahead.

I wish to thank my research progress assessment committee (RPAC) members Dr. H.S Nagaraja and Dr. Ashvini Chaturvedi, for their constructive feedback and guidance from research problem definition stage to thesis submission stage. Without their help the thesis would not have taken this shape.

I would like to thank Mr. Jora M. Gonda, former HOD for providing the necessary resources in the department to carry out my research. Also, I would like to thank Dr U. Vinatha, HOD, for encouragement and providing valuable suggestions.

My sincere thanks to Prof K. Chandrasekaran and Dr. I. Jayaraman for their valuable guidance and support. Special thanks to Mr. Andrew Scholbrock from National Renewable Energy Limited for solving challenges in my projects.

I take this opportunity to thank all teaching and non-teaching staff of EEE Department, NITK Surathkal.

I express my heartfelt thanks to all research scholars in the EEE department for their valuable support.

Finally, I would like to thank my family members for their patience, care and love which drew me with inspiration to carry out my research.

**Saravanakumar R**





# ABSTRACT

In recent years, wind energy emerges as one of the prominent renewable energy source because of environmental, social and economical benefits. The wind turbines (WT) are classified as fixed speed wind turbine (FSWT) and variable speed wind turbine (VSWT). Compared to FSWT, VSWT offers many advantages such as improved energy capture, reduction in transient load and better power conditioning. In VSWT, the operating regions are classified into two major categories, i.e., below and above rated wind speed. At below rated wind speed, the main objective of the controller (i.e. torque control) is to optimize the wind energy capture by avoiding the transients in the turbine components; especially in the drive train. Whereas, at above rated wind speed, the major objective of the controller (i.e. pitch control) is to maintain the rated power of the WT. At below rated wind, speed the control problem is that the WT rotor should track the optimal rotor speed for extracting the maximum power. This can be achieved by adjusting the generated torque, which is derived from estimated wind speed. So, exact estimation of the wind speed plays one of the major roles in deriving the maximum power from the VSWT. In general, wind speed is measured by the anemometer for deriving the optimal rotor speed to adjust the control input, i.e., generator torque, but the anemometer only measures the single wind speed, i.e., at the point of installation, which is not the accurate effective wind speed. At the same time, anemometer increases the overall cost, maintenance and reduces the reliability of the entire systems.

In this work, estimation of effective wind speed is achieved by using different nonlinear estimation algorithms such as Modified Newton Rapshon (MNR), Neural Network trained with different algorithms, and nonlinear time series estimation. This work presents the combination of linear and nonlinear controllers for variable speed variable pitch wind turbines (VSVPWT) operating at below and above rated wind speeds. The mathematical model of the turbine is derived from two mass model, which deal with flexible modes induced by low speed shaft stiffness. The performances of the controllers are tested with nonlinear FAST (Fatigue, Aerodynamics, Structures, and

Turbulence) WT dynamic simulation. The WT simulations are performed in three different cases of wind speed profiles such as below rated wind speed (region-2), above rated wind speed (region-3) and a smooth transition between these two wind speeds (region-2.5). Initially, the conventional control technique such as Aerodynamic torque feed forward (ATF) and Indirect Speed Control (ISC) are adapted to the WT. However, the performance measures of those techniques do not take into account the dynamical aspect of the wind and aero turbine, leading to significant power loss. In addition, it was found that they were not robust with respect to disturbances. In order to overcome the above drawbacks, nonlinear controllers i.e. sliding mode control (SMC), integral sliding mode control (ISMC) and terminal sliding mode (TSMC) have been applied. At region 3 the main aim is to prevent excess power and to mitigate the load using pitch control. There is no standard method to operate WT in transition region i.e. region 2.5 which is between region 2 and 3. This work discusses about the use of a nonlinear control i.e. ISMC and TSMC in region 2 and fuzzy based proportional integral (PI) control in region 3. The benefit of using this combination is analysed for the point of how much electrical energy can be gained in transition region with reduced variation in pitch angle and generator speed. The controllers for WT are tested with different types of wind speed profiles and in the presence of sensor and actuator faults. The thesis concludes that higher tracking dynamic will ensure maximum power capture at the cost of high turbulence in the control action. Conversely a slower tracking dynamic ensures smooth torque, i.e., less transient load on the drive train at the cost of low power capture.

**Keywords:** Wind turbine, nonlinear controllers, sliding mode control, integral sliding mode control, fuzzy PI controller, terminal sliding mode controller, FAST.

## Contents

List of Figures .....	iii
List of Tables.....	ix
List of Abbreviations.....	xi
List of Nomenclatures .....	xv
1 INTRODUCTION .....	1
1.1 Introduction .....	1
1.2 Wind Turbine .....	1
1.3 Literature Survey on Estimation of Effective Wind Speed.....	7
1.4 Literature survey on Estimation of Effective Wind Speed Based Control .....	21
1.5 Classical Control Techniques for Wind Turbine.....	25
1.6 Literature Survey on Control for Maximum Power Extraction of VSWT.....	30
1.7 Wind Turbine Simulators .....	33
1.8 Motivation of the Work.....	35
1.9 Contribution of the Thesis.....	36
1.10 Conclusion.....	38
2 DESIGN AND IMPLEMENTATION OF NONLINEAR ESTIMATOR AND CONTROLLER FOR SINGLE MASS MODEL WIND TURBINE.....	39
2.1 Introduction .....	39
2.2 Problem Formulation.....	40
2.3 Estimation of Wind Speed and Control.....	41
2.4 Iterative Methods for Estimation of Effective Wind Speed Estimation.....	42
2.5 Neural Network Based Effective Wind Speed Estimation.....	45
2.6 Nonlinear Identification Based Effective Wind Speed Estimation .....	60
2.7 Results and Discussion for Wind Speed Estimation .....	62
2.8 Results and Discussion for NSSFE and NDSFE Controller .....	64
2.9 Evaluation of Performance of the Controllers.....	68
2.10 Proposed Controllers .....	73
2.11 Simulation Results and Discussion for Single Mass Model .....	88
2.12 Comparison Between Single-Mass and Two-Mass Model .....	96
2.13 Conclusion.....	97

3 DESIGN AND IMPLEMENTATION OF NONLINEAR CONTROLLERS FOR TWO MASS MODEL OF WIND TURBINE WITH FAST NREL .....	99
3.1 Introduction .....	99
3.2 Modified Nonlinear Static State Feedback Linearization with Estimator (MNSSFEL) for Two Mass Model.....	100
3.3 SMC Design for Two Mass Model .....	101
3.4 Integral Sliding Mode Controller Design for Two Mass Model.....	104
3.5 Simulation Results and Discussion for Two Mass Model .....	105
3.6 Conclusion.....	118
4 CONTROLLER DESIGN FOR ABOVE RATED WIND SPEED AND TRANSITION REGION .....	119
4.1 Introduction .....	119
4.2 Conventional Baseline Controller of the Industrial State of Art.....	120
4.3 Conventional Pitch Controller for Above Rated Wind Speed .....	121
4.4 Simulation Results for SMC and ISMC with Conventional PI Pitch Control .	126
4.5 Proposed Fuzzy PI Pitch Controller .....	131
4.6 Simulation Results For Baseline + PI and ISMC + Fuzzy PI .....	132
4.7 Conclusion.....	140
5 FAULT ANALYSIS OF WIND TURBINE WITH NREL FAST.....	141
5.1 Introduction .....	141
5.2 Actuator and Sensor Faults .....	141
5.3 Terminal Sliding Mode Controller for Single Mass Model .....	143
5.4 Result and Discussion of TSMC for Single Mass Model .....	146
5.5 TSMC for optimal power capture for FAST two mass model.....	150
5.6 Comparison of results of ISMC, TSMC and baseline controller for Two Mass Model with FAST.....	154
5.7 Fault Description .....	157
5.8 Simulation Result for Both the Faults .....	158
5.9 Conclusion.....	159
6 CONCLUSIONS AND FUTURE WORK .....	161
Appendix I .....	165
Appendix II.....	167
References.....	177
Publications.....	187

## LIST OF FIGURES

Figure 1.1: Power coefficient versus tip-speed ratio characteristics.....	3
Figure 1.2: Electrical power characteristics of 600 kW wind turbine. ....	3
Figure 1.3: Two mass model of the wind turbine. ....	6
Figure 1.4: NN based training scheme for wind velocity estimator. ....	10
Figure 1.5: NN based Wind velocity estimation with five tan-sigmoid neurons and one linear neuron. ....	10
Figure 1.6: NN based control of wind turbine rotor speed. ....	11
Figure 1.7: NN-based control module of rotor speed with compensation function....	11
Figure 1.8: Block diagram of small wind turbine driven PMSG and PI controller. ....	12
Figure 1.9: GRBFN-based wind speed estimation. ....	14
Figure 1.10: Block diagram of the GRBFN-based sensor less maximum wind power tracking. ....	14
Figure 1.11: The principle of wind speed estimation. ....	16
Figure 1.12: Wind speed estimation using an ESN. ....	16
Figure 1.13: Block diagram of the wind prediction sensor less WECS-controlled system. ....	18
Figure 1.14: Schematic diagram of the effective wind speed filter. ....	19
Figure 1.15: Entire sensor less control scheme for variable-pitch PMSG WTPGS. ...	20
Figure 1.16: WT control. ....	21
Figure 1.17: Nonlinear Static and Dynamic state feedback control with estimator control scheme. ....	23
Figure 1.18: Nonlinear state space feedback linearization with PI controller and wind speed estimator.....	23
Figure 1.19: Feed forward pitch control with estimator and 3D lookup table.....	24
Figure 1.20: LQR control of wind turbine. ....	24
Figure 1.21: Control scheme based on aerodynamic torque and effective wind speed estimation.....	25
Figure 1.22: ISC Control.....	27
Figure 1.23: Simulink model for simulating the FAST nonlinear turbine with controller and pitch actuator. ....	34
Figure 1.24: Proposed control scheme for WT.....	36
Figure 2.1: Power operating region of wind turbines. ....	40
Figure 2.2: WT control scheme. ....	40
Figure 2.3: $C_q$ vs Lamda curve. ....	43
Figure 2.4: Fundamental block diagram for wind speed nonlinear estimator with controller.....	45
Figure 2.5: Schematic of a single neuron.....	46
Figure 2.6: Schematic of a single layer network.....	47
Figure 2.7: Schematic of a multilayer network.....	48
Figure 2.8: Flow chart for BPNN. ....	52

Figure 2.9: Block diagram for DENN algorithm. ....	56
Figure 2.10: Flowchart for PSO NN. ....	59
Figure 2.11: HWM structure.....	60
Figure 2.12: Measured hub height wind Profile. ....	62
Figure 2.13: Wind speed comparisons for NSSFE. ....	63
Figure 2.14: Zoomed version of Wind speed comparisons for NSSFE.....	63
Figure 2.15: Wind speed comparisons for NDSFE. ....	63
Figure 2.16: Zoomed version of Wind speed comparisons for NDSFE.....	64
Figure 2.17: Rotor speed comparisons for NSSFE.....	65
Figure 2.18: Zoomed version rotor speed comparisons for NSSFE.....	65
Figure 2.19: Rotor speed comparisons for NDSFE. ....	66
Figure 2.20: Zoomed version of rotor speed comparisons for NDSFE. ....	66
Figure 2.21: Generator torque comparisons for NSSFE.....	66
Figure 2.22: Generator torque comparisons for NDSFE. ....	67
Figure 2.23: Generator torque power spectrum magnitude for NSSFE.....	67
Figure 2.24: Generator torque power spectrum magnitude for NDSFE.....	67
Figure 2.25: Comparison of various Standard deviations for various techniques. ....	70
Figure 2.26: Comparison of various maximum generator torques for various techniques. .....	70
Figure 2.27: Comparison of various error variances for estimation techniques. ....	71
Figure 2.28: Comparison of various error co variances for estimation techniques. ....	71
Figure 2.29: Test wind profile of mean 7 m/s.....	76
Figure 2.30 : Rotor speed comparisons of ATF, ISC, SMC and FSMC.....	77
Figure 2.31: Rotor speed comparisons for NSSFE and NDSFE. ....	77
Figure 2.32: Generator torque comparisons of different control strategy. ....	78
Figure 2.33: Generator torque comparisons NSSFE and NDSFE. ....	78
Figure 2.34: Rotor speed comparisons of different control strategy. ....	80
Figure 2.35: Rotor speed comparisons for NSSFE and NDSFE. ....	81
Figure 2.36: Generator torque comparisons NSSFE and NDSFE. ....	81
Figure 2.37: Generator torque comparisons of different control strategy. ....	81
Figure 2.38: Generator torque PSD for SMC and FSMC.....	84
Figure 2.39: Comparison of rotor speed with different level of constant disturbance for SMC (Transient wind speed) .....	88
Figure 2.40: Comparison of rotor speed with different level of constant disturbance for ISMC (Transient wind speed).....	88
Figure 2.41: Rotor speed comparisons for AFISMC with different level of constant disturbance (Transient wind speed). ....	89
Figure 2.42: Comparison of rotor speed with different types of disturbance for AFISMC (Transient wind speed).....	89
Figure 2.43: Comparison of rotor speed with different disturbance for SMC (smooth wind speed). ....	93
Figure 2.44: Comparison of rotor speed with different disturbance for ISMC (smooth wind speed). ....	93

Figure 2.45: Comparison of rotor speed with different disturbance for AFISMC (smooth wind speed).....	93
Figure 2.46: Rotor speed comparison for NSSFE, NSDFE and AFISMC with constant 4kNm disturbance. ....	95
Figure 2.47: Comparison for single and two mass model based control law for FAST model.....	97
Figure 3.1: Test Wind Speed Profile.....	106
Figure 3.2: Rotor speed comparison using mathematical model. ....	106
Figure 3.3: Rotor speed comparison for SMC and ISMC for two mass model.....	107
Figure 3.4: Electromagnetic torque comparison for SMC and ISMC. ....	107
Figure 3.5: Low speed shaft torque comparison for SMC and ISMC. ....	108
Figure 3.6: Rotor speed comparison for ATF, ISC, MNSSFE and SMC for FAST simulator .....	109
Figure 3.7: Boxplot for Low Speed Shaft Torque using FAST Simulator. ....	110
Figure 3.8: Boxplot for generator torque using FAST Simulator.....	110
Figure 3.9: Boxplot for rotor speed using FAST Simulator. ....	111
Figure 3.10: PSD for Low Speed Shaft Torque using FAST Simulator.....	111
Figure 3.11: Comparison for baseline control with other controllers for LSS, Control torque and RMS of rotor speed. ....	112
Figure 3.12: Comparison for baseline control with other controllers for generated average power. ....	112
Figure 3.13: Rotor speed comparison for SMC and ISMC for FAST simulator.....	114
Figure 3.14: Boxplot for Low Speed Shaft Torque using FAST Simulator. ....	115
Figure 3.15: Boxplot for generator torque using FAST Simulator.....	115
Figure 3.16: Boxplot for rotor speed using FAST Simulator. ....	116
Figure 3.17: PSD for Low Speed Shaft Torque using FAST Simulator.....	116
Figure 3.18: Comparison for baseline control with other controllers for LSS, and Control torque. ....	116
Figure 3.19: Comparison for baseline control with other controllers for generated average power. ....	117
Figure 4.1: Simulation model for the CART3 baseline Controller.....	120
Figure 4.2: Best fit line of the pitch sensitivity in region 3. ....	124
Figure 4.3: Baseline pitch control system gain scheduling law.....	125
Figure 4.4: Gain scheduling control law.....	126
Figure 4.5: Simulation results of 600kW CART 3 WT using SMC and ISMC in full range of operation (Step change wind profile). a) Wind speed profile b) Generator Speed c) Electrical Power d) Generator Torque e) Pitch angle .....	127
Figure 4.6: Simulation results of 600kW CART 3 WT using SMC and ISMC in full range of operation (Vertical wind profile). a) Wind speed profile b) Generator Speed c) Electrical Power d) Generator Torque e) Pitch angle .....	128

Figure 4.7: Simulation results of 600kW CART 3 WT using SMC and ISMC in full range of operation (Vertical wind profile). a) Wind speed profile b) Generator Speed c) Electrical Power d) Generator Torque e) Pitch angle .....	129
Figure 4.8: Different types of wind speed in region 2.5. ....	129
Figure 4.9: Power comparison for SMC and ISMC in region 2.5 for different wind speed profile. ....	130
Figure 4.10: Simulation results of 600kW CART 3 WT using SMC and ISMC in full range of operation (above rated wind profile). a) Wind speed profile b) Generator Speed c) Electrical Power d) Pitch angle.....	130
Figure 4.11: Comparison for baseline and ISMC controller a) wind profile with mean 7m/s b) Electrical power comparison for 7m/s c) wind profile with mean 8m/s d) Electrical power comparison for 8m/s. ....	132
Figure 4.12: Comparison of baseline PI and ISMC + Fuzzy PI a) wind profile mxws1 b) Electrical power comparison c) Pitch angle comparison and d) Generator speed comparison.....	133
Figure 4.13: Comparison of baseline PI and ISMC + Fuzzy PI a) mxws2 wind profile b) Electrical power comparison c) Pitch angle comparison and d) Generator speed comparison.....	134
Figure 4.14: Comparison of baseline PI and ISMC + Fuzzy PI a) Darrow wind profile b) Electrical power comparison c) Pitch angle comparison.....	135
Figure 4.15: Comparison of baseline PI and ISMC + Fuzzy PI a) Hansen wind profile b) Electrical power comparison c) Pitch angle comparison.....	135
Figure 4.16: Comparison of baseline PI and ISMC + Fuzzy PI a) Mixed wind profile b) Electrical power comparison c) Pitch angle comparison and d) PSD compassion of pitch signal.....	136
Figure 4.17: Comparison of baseline PI and ISMC + Fuzzy PI a) Above rated wind profile b) Electrical power comparison c) Pitch angle comparison and d) PSD compassion of pitch signal.....	137
Figure 4.18: Comparison of baseline PI and ISMC + Fuzzy PI a) Mixed wind profile form 5 to 25 m/s b) Electrical power comparison c) Generator speed comparison and d) Pitch angle comparison.....	139
Figure 5.1: Different types of faults.....	142
Figure 5.2: Actuator and sensor faults. ....	143
Figure 5.3: Wind speed profile. ....	146
Figure 5.4: Rotor speed comparison for SMC and TSMC controller for mathematical model without disturbance.....	146
Figure 5.5: Rotor speed comparison for SMC and TSMC controller for mathematical model with random disturbance between 1000 to 4000Nm. ....	147
Figure 5.6: Rotor speed comparison for SMC and TSMC controller for mathematical model with presence of actuator offset. ....	147
Figure 5.7: Rotor speed comparison for SMC and TSMC controller for mathematical model with presence random disturbance more than 4500kNm.....	149
Figure 5.8: Mean power comparison for SMC and TSMC. ....	149



Figure 5.9: Different wind speed profiles .....	154
Figure 5.10: Power comparison for mxtest1 and mxtest2 wind speed profiles. ....	155
Figure 5.11: Power comparison for mxtest3 and mxtest4 wind speed profiles. ....	155
Figure 5.12: Anova1 plot for different control strategy.....	156
Figure 5.13: Power comparison one actuator fault. ....	157
Figure 5.14: Power comparison two actuator fault. ....	157
Figure 5.15: Mixed wind profile. ....	158
Figure 5.16: Electrical power comparison for conventional, ISMC and TSMC with generator and sensor fault. ....	158
Figure 5.17: Generator torque comparison for conventional, ISMC and TSMC with generator and sensor fault. ....	158



## LIST OF TABLES

Table 2.1: Commonly used activation function .....	48
Table 2.2: Comparisons of different estimation and control strategies for classical, MNR, BPNN and PSONN.....	69
Table 2.3: Comparisons of different estimation and control strategies for DENN HWM and NARX. ....	70
Table 2.4: MNR, BPNN and PSONN based nonlinear estimation models for wind speed. ....	72
Table 2.5: DENN, HWM and NARX based nonlinear estimation models for wind speed. ....	72
Table 2.6: Fuzzy rules $S_{smc}, \dot{S}_{smc}$ and $\phi_{Fuzzy}$ .....	75
Table 2.7 : Different control strategy with high transient wind speed.....	79
Table 2.8: Different control strategy with +30% parameter uncertainty.....	80
Table 2.9: Different control strategy with filtered wind speed.....	82
Table 2.10: Different control strategy with +30% parameter uncertainty.....	83
Table 2.11: Different control strategy with mean wind speed of 8 m/sec .....	83
Table 2.12: Different control strategy with mean wind speed of 8.5 m/sec .....	83
Table 2.13: Mean error in rotor speed for different control strategy with different wind profile.....	83
Table 2.14: Fuzzy rules $S_{ismc}, \dot{S}_{ismc}$ and $k_{fuzzy}$ .....	87
Table 2.15: Performance analysis of SMC with and without constant disturbances (wind speed 7 m/sec).....	90
Table 2.16: Performance analysis of ISMC with and without constant disturbances (wind speed 7 m/sec) .....	90
Table 2.17: Performance analysis of AFISMC with different types of disturbances ..	91
Table 2.18: Performance analysis of AFISMC with different types of disturbances ..	91
Table 2.19: Performance analysis of AFISMC with different types of disturbances. (8.5m/sec wind profile).....	92
Table 2.20: Analysis of electrical efficiency with respect to different level of disturbance for a wind speed of 7 m/sec.....	92
Table 2.21: Performance analysis of SMC with and without constant disturbances for smooth wind speed of 7 m/sec .....	94
Table 2.22: Performance analysis of ISMC with and without constant disturbances for smooth wind speed of 7 m/sec .....	94
Table 2.23: Performance analysis of AFISMC with different types disturbances for smooth wind speed of 7 m/sec .....	95
Table 2.24: Performance comparison for NSSFE, NDSFE and AFISMC .....	95
Table 3.1: Comparison of different control strategy based on two mass model using mathematical model.....	106
Table 3.2: Comparisons for various control strategy (Two mass model).....	108

Table 3.3: Comparison of different control strategy based on two mass model using FAST simulator.....	109
Table 3.4: SMC performance for different wind speed profiles.....	113
Table 3.5: MNSSFPE performance for different wind speed profiles.....	113
Table 3.6: Comparison of different control strategy based on two mass model using FAST simulator.....	114
Table 3.7: SMC performance for different wind speed profiles.....	117
Table 3.8: ISMC performance for different wind speed profiles.....	117
Table 4.1: Sensitivity of the aerodynamic power to blade pitch angle in region 3 (above rated wind speed) .....	123
Table 4.2: Performance of SMC and ISMC in region 2.5 .....	130
Table 4.3: Power Comparison ISMC and Baseline PI in below rated wind speed....	133
Table 4.4: Turbulence realization by using mean power comparison for different mean wind speed (7 and 11 m/s) .....	137
Table 4.5: Turbulence realization by using mean power comparison for different mean wind speed (13 and 15 m/s) .....	138
Table 4.6: Turbulence realization by using mean power comparison for different mean wind speed (17 and 19 m/s) .....	138
Table 4.7: Results of paired t-test .....	139
Table 5.1: Comparisons of control strategies without disturbance.....	148
Table 5.2: Comparisons of control strategies with random disturbance.....	148
Table 5.3: Comparisons of control strategies with actuator offset .....	148
Table 5.4: Mean wind power comparison.....	150
Table 5.5: Standard deviation of the different controllers with different wind speed profiles .....	155
Table 5.6: one actuator offset.....	156
Table 5.7: Two actuator offset.....	157
Table 5.8: Fault Scenarios.....	157
Table 5.9: Performance analysis of different controller in the presence of generator sensor and actuator fault. ....	159

## LIST OF ABBREVIATIONS

AFISMC	Adaptive Fuzzy Integral Sliding Mode Control
ANFIS	Adaptive Neuro Fuzzy Inference Systems
ANN	Artificial Neural Network
ARX	Auto Regressive Exogenous
ATF	Aerodynamic Torque Feedforward
BPANN	Backpropagation Artificial Neural Network
BPNN	Backpropagation Neural Network
CART	Controls Advanced Research Turbine
DAC	Disturbance Accommodation Control
DE	Differential Evolution
DENN	Differential Evolution Neural Network
DFIG	Doubly Fed Induction Generator
DOF	Degree of Freedom
EEWS	Estimation of Effective Wind Speed
EKF	Extended Kalman Filter
ELM	Extreme Learning Machine
ESN	Echo state network
FAST	Fatigue, Aerodynamics, Structures, and Turbulence
FL	Fuzzy Logic
FOINC	Fractional Order Incremental Conductance Algorithm
FIS	Fuzzy Inference System
FLC	Fuzzy Logic Controller
FLS	Fuzzy Logic System
FSMC	Fuzzy Sliding Mode Control
FSWT	Fixed Speed Wind Turbine
GA	Genetic Algorithm
GSA	Gravitational Search Algorithm
GRBFN	Gaussian Radial Basis Function Network
GSC	Grid Side Control
HSMC	Higher Order Sliding Mode Control

HCS	Hill-Climb Searching
HWM	Hammerstein Wiener Model
I&I	Immersion and Invariance
INC	Incremental Conductance
IREDA	Indian Renewable Energy Development Agency
ISC	Indirect Speed Control
ISMC	Integral Sliding Mode Control
ISE	Integral Square Error
KF	Kalman Filter
LQR	Linear Quadratic Regulator
LS	Least Square
MLFFNN	Multilayer Feed Forward Neural Network
MLPNN	Multilayer Perceptron Neural Network
MNES	Ministry of Non-conventional Energy Sources
MNR	Modified Newton-Raphson
MNSNFE	Modified Nonlinear Static State Feedback with Estimator
MPPT	Maximum Power Point Tracking
MPSO	Modified Particle Swarm Optimization
NARX	Nonlinear Autoregressive Exogenous Model
NDSFE	Nonlinear Dynamic State Feedback with Estimator
NN	Neural Network
NR	Newton-Raphson
NREL	National Renewable Energy Limited
NSSFE	Nonlinear Static State Feedback with Estimator
OT	Optimal Torque
OT	Optimal Torque Control
P	Proportional
PI	Proportional Integral
PMG	Permanent Magnet Generator
P&O	Perturbation and Observation
PMSG	Permanent Magnet Synchronous Generator

PSD	Power Spectral Density
PSO	Particle Swarm Optimization
PSF	Power Signal Feedback
PSOINN	Particle Swarm Optimization Neural Network
PWM	Pulse Width Modulation
RSC	Rotor Side Control
SMC	Sliding Mode Control
STD	Standard Deviation
SVM	Support Vector Machine
SVR	Support Vector Regression
TSK	Takagi-Sugeno Kang
TSR	Tip-Speed Ratio
TSMC	Terminal Sliding Mode Control
VSVPWT	Variable Speed Variable Pitch Wind Turbine
VSWT	Variable Speed Wind Turbine
WECS	Wind Energy Conversion System
WT	Wind Turbine
WRBFN	Wilcoxon Radial Basis Function Network
WTPGS	Wind Turbine Power Generation System





## LIST OF NOMENCLATURES

$P_{air}$	Power in air flow
$P_{windturbine}$	Turbine power
$C_p$	Power coefficient
$\lambda$	Tip speed ratio
$R$	Radius of the rotor
$\omega_r$	Rotor speed
$U$	Wind speed
$\rho$	Air density
$P_a$	Aerodynamic power
$T_a$	Aerodynamic torque
$C_q$	Torque coefficient
$\beta$	Pitch angle
$J_r$	Rotor inertia
$T_{ls}$	Low speed shaft torque
$\omega_g$	Generator speed
$T_{hs}$	High speed shaft torque
$J_g$	Generator inertia
$K_r$	Rotor external damping
$K_g$	Generator external damping
$J_t$	Total turbine inertia
$K_t$	Turbine total external damping
$T_{em}$	Electromagnetic torque
$T_g$	Generator torque
$n_g$	Gear ratio
$\theta_g$	Generator-side angular deviation
$\theta_{ls}$	Gearbox-side angular deviation
$\lambda_{opt}$	Optimal tip speed ratio
$\beta_{opt}$	Optimal pitch angle
$B_{ls}$	Low speed shaft stiffness
$K_{ls}$	Low speed shaft damping

$\hat{\omega}_{s,low}$	Estimated below rated wind speed
$\hat{\omega}_{s,high}$	Estimated above rated wind speed
$\alpha_{\omega_s}$	Bandwidth of the estimator
$k_{tr}$	Transition parameter
$C_{p\max}$	Maximum power coefficient
$P_{wt}^{\max}$	Optimal turbine output power
$\eta_{\max}^{DFM}$	Maximum DFM efficiency
$P_t^{\max}$	Estimated maximum output power of the electrical generator
$P_e$	Electrical power
$\omega$	Electrical frequency
$W$	Neural network weights
$b$	Bias
$x_i$ and $y_i$	Input and output space
$\hat{\omega}_{ref}$	Estimated rotor reference speed
$\omega_{ref}$ or $\omega_{ropt}$ or $\omega_r^*$	Reference or Optimal rotor reference speed
$\hat{\omega}_r$	Estimated rotor speed
$K_c$	Proportional gain
$a_0, b_0, b_1$	Positive constants
$e$	Rotor speed error
$T_s$	Sampling time
$\phi_{\min}$	Absolute relative error
$n_{\max}$	Maximum Iteration
$\eta$	Learning rate
$d_j$	Target output
$y_j$	Actual output
$\varphi(s)$	Activation function
$C$	Crossover rate
$F$	Mutation factor
$g$	Maximum number of generation
$E$	Mean square error
$\eta_{aero}$	Aerodynamic efficiency
$\eta_{elec}$	Electrical efficiency
$P_{aopt}$	Optimal aerodynamic power

$S_{smc}$	Sliding surface of SMC
$k$	Sliding gain
$\phi$	Thickness of boundary layer
$\phi_{Fuzzy}$	Fuzzy based thickness of boundary layer
$S_{ismc}$	Sliding surface of ISMC
$k_i$	Integral gain
$k_{fuzzy}$	Fuzzy sliding gain
$\lambda_1$ and $\beta_1$	Positive constants
$\theta$	Full span rotor collective blade pitch angle
$\Delta\theta$	Small perturbation of the blade pitch angle
$\omega_{\varphi n}$	Natural frequency
$\zeta_{\varphi}$	Damping ratio
$K_P$	Proportional Gain
$K_I$	Integral gain
$K_D$	Derivative gain



# **CHAPTER 1**

## **1 INTRODUCTION**

### **1.1 INTRODUCTION**

In this chapter, the general introduction about the wind turbine (WT) systems are given. The single mass and two mass mathematical model of the WT are explained. The brief literature of different techniques for effective wind speed estimation and mechanism of control of WT are described in this chapter. The FAST NREL 600kW WT model, and the wind speed generation by using the TurbSim are also explained. The contribution and organization of the thesis is presented in the last section.

### **1.2 WIND TURBINE**

Burning of fossil fuels has the significant influence of global climate change (Anaya-Lara, O. et al. 2009). Wind energy is one of the fastest growing and environment friendly renewable energy source. In past two decades the capacity of the wind turbines have been developed from 20KW to 2MW, even large wind turbines are also designed and tested (Amirat, Y. et al. 2007). Wind energy is playing an important role in future national energy scene (Fung, K.T. et al. 1981) and (Sesto, E. and Casale, C. 1998). Wind turbines convert the kinetic energy of the wind to electrical energy by rotating the blades. Greenpeace states that about 10% electricity can be supplied by the wind by the year 2020. At good windy sites, it is already competitive with that of traditional fossil fuel generation technologies (Herbert, G.M.J. et al. 2007). Ministry of Non-conventional Energy Sources (MNES), Indian Renewable Energy Development Agency (IREDA) and the wind industry are working together to accomplish these improvements through various research and development programs.

The global wind power industry produced 3,69,579 MW in the year 2014. Some of the countries with the higher total installed wind power capacity are Germany 39,165 MW, Spain 22,987MW, The United States 65,879 MW and India 22,465 MW (Global Wind

Energy Council). WT subsequently converts the kinetic energy of the wind into electrical energy. Wind interaction with blades generates lift and extracts the turning force, which in turn rotate a shaft that into a gear box. The gearbox is used to increase the speed which in appropriate proportion to the generator. It uses the magnetic field to convert the rotational energy into electrical energy (Herbert, G.M.J. et al. 2007).

The WT extracts the kinetic energy from the blade swept area. The power estimation in air flow ( $P_{air}$ ) is given by

$$P_{air} = \frac{1}{2} \rho A v^3 \quad (1.1)$$

The amount of estimated power as given in equation (1.1) is transferred into the WT rotor that reduces the power coefficient ' $C_p$ ' and is given by

$$C_p = \frac{P_{wind\ turbine}}{P_{air}} \quad (1.2)$$

According to the Betz limit, the maximum value of ' $C_p$ ' is never more than the 59.3% of the power from an air stream. In real time the typical ' $C_p$ ' variation range is 25-45%. The tip speed ratio ' $\lambda$ ' is defined as the ratio between linear tip speed and wind speed and is given in equation (1.3)

$$\lambda = \frac{\omega_r R}{v} \quad (1.3)$$

Figure 1.1 shows the characteristics dependency on tip speed ratio ( $\lambda$ ) and the power coefficient ( $C_p$ ). The power coefficient becomes maximum at a particular tip speed ratio for fixed rotational speed ( $\omega_r$ ) and wind speed ( $v$ ). So for a variable rotational speed it is possible to operate at maximum ' $C_p$ ' over a range of wind speed. In this context; we define following terms:

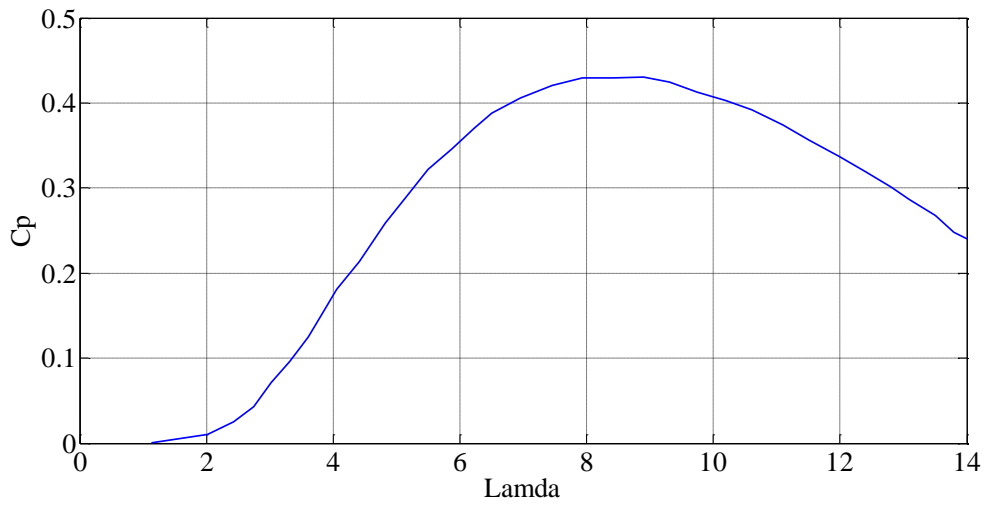


Figure 1.1: Power coefficient versus tip-speed ratio characteristics.

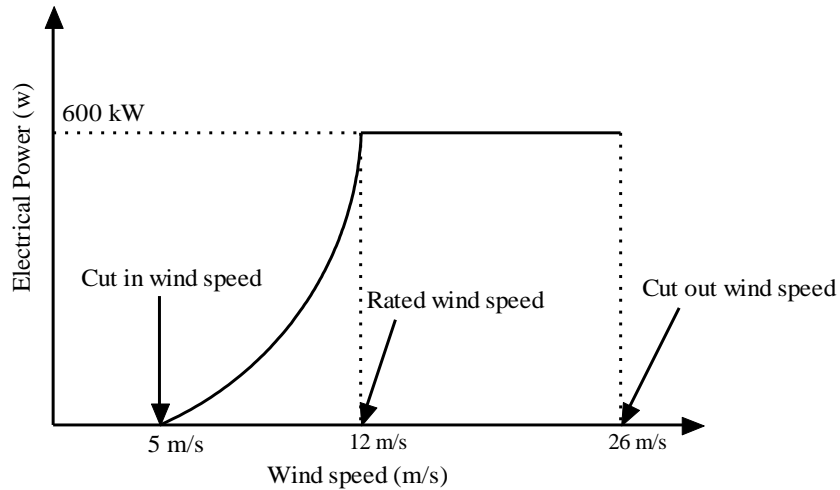


Figure 1.2: Electrical power characteristics of 600 kW wind turbine.

Cut in wind speed: It is minimum speed which requires to run the machine.

Rated wind speed: The wind speed at which the rated power is obtained.

Cut out wind speed: It is maximum wind speed which the turbine allows to deliver the power.

Figure 1.2 shows the power curve for 600kW wind turbine. For the wind speed below 5 m/s the wind turbine remains shut down because the wind is too low for useful energy production. However, once it start operation the power output increases and follows a broadly cubic relationship with wind speed (although modified by the variation in  $C_p$ ) until rated wind speed is reached. Above rated wind speed the aerodynamic rotor is

arranged to limit the mechanical power extracted from the wind and so reduce the mechanical loads on the drive train. At very high wind speeds the turbine is shut down.

### **1.2.1 Types of wind turbine**

In (Bansal, R. et al. 2005) the authors have reviewed issues related to power generation from wind energy systems. This study discussed about factors affecting wind power, classification of wind turbine, wind turbine design, problems associated with grid connection, reactive power control of wind turbine and recent trends of power generation from off shore wind turbine sites. Fixed speed wind turbine consists of a squirrel cage induction machine connected to the grid. Generally, wind turbine is of two types, i.e. fixed speed and variable speed wind turbine (Anaya-Lara, O. et al. 2009). The generator operating slip changes slightly as the operating power level changes, so the rotational speed is not entirely constant. However, as the operating slip variation is usually less than 1%, this type of wind turbine is normally referred to as fixed speed. For the large size wind turbines the technology has switched from fixed speed to variable speed. The drivers behind these developments are mainly the ability to comply with grid connection requirements and the reduction in mechanical loads achieved with variable-speed operation. Currently the most common variable-speed wind turbine configurations are as follows:

- Doubly fed induction generator (DFIG) wind turbine
- Fully rated converter (FRC) wind turbine based on a synchronous or induction generator.

### **1.2.2 SINGLE MASS AND TWO MASS MODEL OF THE WIND TURBINE**

Wind turbine is a device which converts the kinetic energy of the wind into electric energy. Simulation complexity of the WT purely depends on the type of control objectives. In case of WT modelling complex simulators are required to verify the dynamic response of multiple components and aerodynamic loading. Generally dynamic loads and interaction of large components are verified by the aero elastic simulator. For designing a WT controller, instead of going with complex simulator, the design objective can be achieved by using simplified mathematical model (Boukhezzar,



B. 2011). In this work, wind turbine model is described by the set of nonlinear ordinary differential equations with limited degree of freedom.

Equation (1.4) gives the nonlinear expression for aerodynamic power capture by the rotor

$$P_a = \frac{1}{2} \rho \pi R^2 C_p(\lambda, \beta) v^3 \quad (1.4)$$

From equation (1.4) it is clear that the aerodynamic power ' $P_a$ ' is directly proportional to the cube of the wind speed. The power coefficient ' $C_p$ ' is a function of blade pitch angle ' $\beta$ ' and tip speed ratio ' $\lambda$ '. Generally wind speed variations are stochastic in nature with respect to time. Because of this, tip speed ratio gets affected, which leads to variation in power coefficient. The relationship between aerodynamic torque ' $T_a$ ' and the aerodynamic power is given in equation (1.5).

$$P_a = T_a \omega_r \quad (1.5)$$

where

$$T_a = \frac{1}{2} \rho \pi R^3 C_q(\lambda, \beta) v^2 \quad (1.6)$$

$C_q$  is the torque coefficient and is given by

$$C_q(\lambda, \beta) = \frac{C_p(\lambda, \beta)}{\lambda} \quad (1.7)$$

Substituting equation (1.7) in equation (1.6) result in

$$T_a = \frac{1}{2} \rho \pi R^3 \frac{C_p(\lambda, \beta)}{\lambda} v^2 \quad (1.8)$$

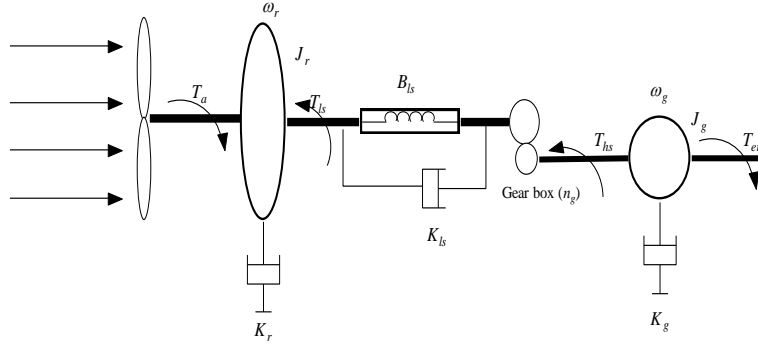


Figure 1.3: Two mass model of the wind turbine.

Figure 1.3 shows the two mass model of the wind turbine. Equation (1.9) represents dynamics of the rotor speed with rotor inertia driven by the aerodynamic torque.

$$J_r \dot{\omega}_r = T_a - T_{ls} - K_r \omega_r \quad (1.9)$$

Breaking torque acting on the rotor is the low speed shaft torque that can be derived by using the relation given in equation (1.10).

$$T_{ls} = B_{ls} (\theta_r - \theta_{ls}) + K_{ls} (\omega_r - \omega_{ls}) \quad (1.10)$$

Equation (1.11) represents dynamics of the generator speed ‘ $\omega_g$ ’ with generator inertia ‘ $J_g$ ’ driven by the high speed shaft torque ( $T_{hs}$ ) and braking electromagnetic torque ( $T_{em}$ )

$$J_g \dot{\omega}_g = T_{hs} - K_g \omega_g - T_{em} \quad (1.11)$$

Gearbox ratio is defined as

$$n_g = \frac{T_{ls}}{T_{hs}} = \frac{\omega_g}{\omega_{ls}} \quad (1.12)$$

From equation (1.11) the high speed shaft torque ‘ $T_{hs}$ ’ can be expressed as

$$T_{hs} = J_g \dot{\omega}_g + K_g \omega_g + T_{em} \quad (1.13)$$

Transforming the generator side dynamics into the low speed shaft side yields

$$n_g^2 J_g \dot{\omega}_g = T_{ls} - n_g K_g \omega_g - n_g T_{em} \quad (1.14)$$

If a perfectly rigid low-speed shaft is assumed, the dynamics of the rotor characteristics of a single mass WT model can be expressed by a first order differential equation given as

$$J_t \dot{\omega}_r = T_a - K_t \omega_r - T_g \quad (1.15)$$

where

$$J_t = J_r + n_g^2 J_g \quad (1.16)$$

$$K_t = K_r + n_g^2 K_g \quad (1.17)$$

$$T_g = n_g T_{em} \quad (1.18)$$

## 1.3 LITERATURE SURVEY ON ESTIMATION OF EFFECTIVE WIND SPEED

### 1.3.1 Polynomial Based Estimation

In (Thiringer, T. and Petersson, A. 2005), (Bhowmik, S. and Spee, R. 1998) and (Bhowmik, S. et al. 1999), a polynomial approximation is used for estimating the wind speed and then the roots of the polynomial are determined by an iterative algorithm. In this section the estimation of wind speed is achieved by first, second and  $n^{th}$  order polynomial.

#### 1.3.1.1 First and Second Order Polynomial based estimation

When the generator is operated in speed control mode (below rated speed), the wind speed is estimated from the turbine output power ' $P_a$ ' by using the second order polynomial given in equation (1.19) (Thiringer, T. and Petersson, A. 2005).

$$\hat{\omega}_{s,low} = a_1 + a_2 P_a + a_3 P_a^2 \quad (1.19)$$

' $\hat{\omega}_{s,low}$ ' is the estimated below rated wind speed. In equation (1.19)  $a_1, a_2$  and  $a_3$  are the coefficients of the second order polynomial. When the wind speed is above the rated speed, pitch angle is used for estimating the wind speed by using first order polynomial given in equation (1.20).

$$\hat{\omega}_{s,high} = b_1 + b_2 \beta \quad (1.20)$$

' $\hat{\omega}_{s,high}$ ' is the estimated wind speed at above rated wind speed,  $b_1$  and  $b_2$  are the coefficients of the first order polynomial. The estimated wind speed is low pass filtered as given in equation (1.21).

$$\begin{aligned} \frac{d\hat{\omega}_s}{dt} &= \alpha_{\omega_s} ((1-k_{tr})\hat{\omega}_{s,low} + k_{tr}\hat{\omega}_{s,high} - \hat{\omega}_s) \\ &= \alpha_{\omega_s} \left( (1-k_{tr}) \left( a_1 + a_2 P_{wt} + a_3 P_{wt}^2 \right) + k_{tr} (b_1 + b_2 \beta) - \hat{\omega}_s \right) \end{aligned} \quad (1.21)$$

where ' $\hat{\omega}_s$ ' estimated wind speed, ' $\alpha_{\omega_s}$ ' is the bandwidth of the estimator and ' $k_{tr}$ ' is a transition parameter.

### 1.3.1.2 $n^{th}$ order polynomial based estimation

In (Bhowmik, S. and Spee, R. 1998) and (Bhowmik, S. et al. 1999), based upon the shaft speed and power output of the turbine, the wind speed is estimated by using the  $n^{th}$  order polynomial. The characteristic of the power coefficients of the WT is normally expressed in terms of tip speed ratio  $\lambda$  and is given by

$$C_p(\lambda) = C_{p0} + C_{p1}\lambda + C_{p2}\lambda^2 + \dots + C_{pn}\lambda^n \quad (1.22)$$

where ' $C_p(\lambda)$ ' is the power coefficient of the WT, which depends on the particulars of the blade design and it is expressed in terms of ' $\lambda$ '. The tip speed ratio ' $\lambda$ ' can be derived from the rotor speed and wind speed, using equation (1.3). Power output of the turbine is related to the cube of the wind velocity as given in equation (1.4). By substituting wind speed from equation (1.3) in equation (1.4) we get:

$$P_{wt} = \frac{1}{2} \rho \pi C_p(\lambda) R^5 \frac{\omega_r^3}{\lambda^3} \quad (1.23)$$

The difference between the right hand side and the left hand side of equation (1.23) can be taken as a function of ' $\lambda$ ' which is represented as  $F(\lambda)$  and is given in equation (1.24).

$$F(\lambda) = P_{wt} - \frac{1}{2} \rho \pi C_p(\lambda) R^5 \frac{\omega_r^3}{\lambda^3} \quad (1.24)$$

By substituting the value  $C_p(\lambda)$  given in equation (1.22) in equation (1.24) we obtain

$$F(\lambda) = P_{wt} - \frac{1}{2} \rho \pi R^5 \omega_r^3 [C_{p0} \lambda^{-3} + C_{p1} \lambda^{-2} + C_{p2} \lambda^{-1} + \dots + C_{pn} \lambda^{n-3}] = 0 \quad (1.25)$$

$$\frac{\partial F(\lambda)}{\partial \lambda} = -\frac{1}{2} \rho \pi R^5 \omega_r^3 \left[ -3C_{p0} \lambda^{-4} - 2C_{p1} \lambda^{-3} - C_{p2} \lambda^{-2} \dots - (n-3)C_{pn} \lambda^{n-4} \right] \quad (1.26)$$

Iterative methods such as Newton Rapshon (NR) or Bisection method is used to determine the roots of the polynomial i.e. ‘ $\lambda$ ’. Substituting ‘ $\lambda$ ’ in equation (1.3) the wind speed is estimated. As the optimal tip speed ratio ‘ $\lambda_{opt}$ ’ is a known quantity, with the estimation of wind speed the optimal rotor speed is determined by using equation (1.27).

$$\omega_{r_{opt}} = \frac{v \lambda_{opt}}{R} \quad (1.27)$$

Substituting ‘ $\lambda_{opt}$ ’ and ‘ $C_{p_{max}}$ ’ (it is a known quantity) and the ‘ $\omega_{r_{opt}}$ ’ in equation (1.23) the optimal turbine output power ‘ $P_{wt}^{max}$ ’, is calculated. The estimated maximum output power of the electrical generator ‘ $P_t^{max}$ ’, can be obtained by using the following relationship.

$$P_t^{max} = \eta_{max}^{DFM} P_{wt}^{max} \quad (1.28)$$

Where  $\eta_{max}^{DFM}$  maximum DFM (Doubly Fed Machines) efficiency.

### 1.3.2 Neural Network Based Estimation

Neural network is a computational model which is inspired by the biological neural system. Most common neural networks are having three layers i.e. input, hidden and output layer. The weights in hidden and output layers are decided by the activation function action of the neural network.

### 1.3.2.1 Multi-Layer Perceptron Neural Network (MLPNN) based estimation

MLPNN based estimation has mainly two applications. 1) NN based wind velocity estimator and 2) NN based pseudo power curves to compensate the potential drift of the wind turbine power coefficient (Li, H. et al. 2004) and (Li, H. et al. 2005).

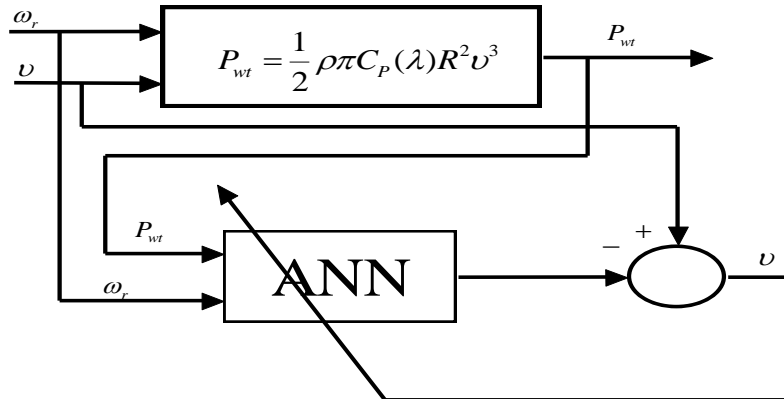


Figure 1.4: NN based training scheme for wind velocity estimator.

Figure 1.4 shows a NN based training scheme for wind speed estimator (Li, H. et al. 2005). In this scheme, sampled data of the turbine power ( $P_{wt}$ ) is obtained from turbine power equation with pre-selected rotor speed and wind velocity samples. As shown in Figure 1.5, both ' $P_{wt}$ ' and ' $\omega_r$ ' samples are used as an input vector to the given NN, and the wind velocity acts as a target vector to train the NN. The NN is configured with two linear neurons in the input layer, five tan-sigmoid neurons in the hidden layer, and one linear neuron in the output layer.

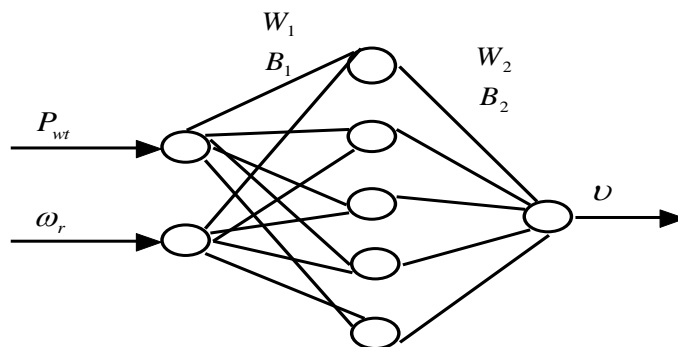


Figure 1.5: NN based Wind velocity estimation with five tan-sigmoid neurons and one linear neuron.

A supervised NN is used to implement the high precision wind speed estimation in (Li, H. et al. 2005). This training scheme of the NN that estimates wind speed ' $v$ ' is shown

in Figure 1.6. The inputs of the NN are generated from the generator power ‘ $P_e$ ’ and synchronous electrical frequency ‘ $\omega$ ’ which is given in equation (1.29) and (1.30) respectively.

$$\omega_r = \frac{2}{P} \omega \quad (1.29)$$

$$P_{wt} = J\omega_r \frac{d\omega_r}{dt} + P_e \quad (1.30)$$

To avoid the noise sensitivity in the equation (1.30) the derivative operation is implemented via the “Approximate Derivative” and the electrical power ‘ $P_e$ ’ is derived from stator currents and voltages. With estimation of wind speed by using NN, maximum power point tracking (MPPT) is obtained with help of the rotor speed reference. This rotor speed reference is generated through the gain  $K = \frac{\lambda_{opt}}{R}$  as shown in Figure 1.6. Figure 1.6 shows the NN based control of wind turbine rotor speed (Li, H. et al. 2005).

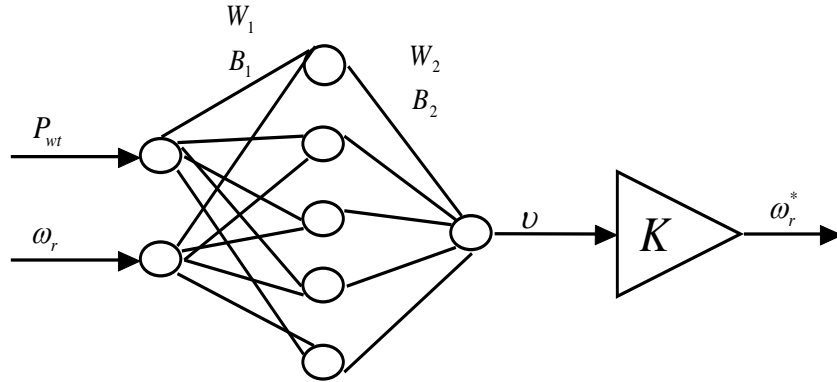


Figure 1.6: NN based control of wind turbine rotor speed.

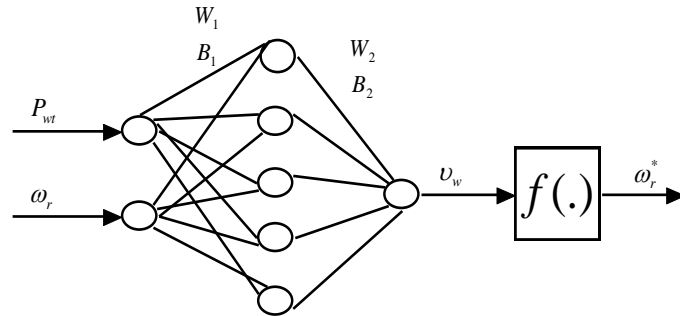


Figure 1.7: NN-based control module of rotor speed with compensation function.

The drift error may occur in the power coefficients because of time and change in environment. When a drift error occurs, the compensation should be done in the control system. In Figure 1.7, for maximum tracking a compensation function is used, instead of ‘ $K$ ’. This function has been derived from the collection of data in pseudo power curves by using NN. The PI controller is used to bring the actual rotor speed to the desired value by varying the duty ratio of the pulse width modulated (PWM) inverter. Figure 1.8 shows the block diagram of small wind turbine driven by permanent magnet synchronous generator (PMSG) and PI controller (Li, H. et al. 2005).

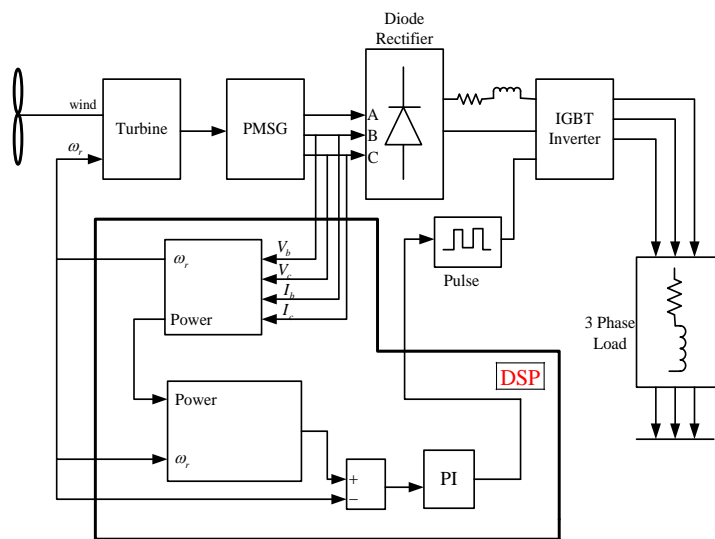


Figure 1.8: Block diagram of small wind turbine driven PMSG and PI controller.

NN based wind speed estimator for variable speed WT is presented in (Barambones, O. et al. 2010), where multilayer feed forward neural network (MLFFNN) with added momentum is adopted as a neural network paradigm. The neural network has three inputs i.e. mechanical power, rotor speed and blade pitch angle and single output as wind speed. The authors (Barambones, O. et al. 2010), discussed about a NN based sensor less control which is having the following drawbacks. 1) Requires more memory space, 2) Requires more complex and time-consuming calculations, and 3) Not accurate for real time control. The authors have proposed a multilayer feed forward network with so-called back propagation with momentum algorithm which is a gradient descent algorithm of the performance function. In order to achieve the maximum wind power extraction, the optimal DFIG rotor speed command is determined from the estimated wind speed.



In (Qiao, W. et al. 2012), simple back propagation artificial neural network (BPANN) is used to estimate the wind speed by using the rotor speed and mechanical power. To determine the optimal rotor speed or power reference to the permanent magnet generator (PMG) the estimated wind speed is used. Three layered BPANN provides a nonlinear mapping between input and output where the input to the NN are mechanical power and rotor speed and output is estimated wind speed.

### 1.3.2.2 SOFT SENSOR BASED SUPPORT VECTOR MACHINE

In (Yang, X. et al. 2006), estimation of effective wind speed is based on modeling of soft sensor by utilizing the support vector machine (SVM). This gives the estimation with high precision compared to other KF (Kalman Filter) techniques. In general, soft sensor technique gives a nonlinear relation between the measured (secondary) and measurable (estimated) variables. The estimated value is obtained from the measured variable through a transformation and computation of the measurable variables. The mathematical model of the soft sensor is built from group of measured variable (secondary variables) associated with estimated variable (master variables), where measured variables acts as input and estimated variable acts as output. The mathematical model of the soft sensor can be derived from the secondary variables and optimal estimation of master variables.

Futher the secondary variables are considered as rotor speed, generator output power and pitch angle, and master variable is the effective wind speed. Based on optimization theory the estimation process is performed. Black box modeling is used for soft sensor modeling, where SVM approximates the mapping between the input and output variables. Wind turbine acts as an anemometer to estimate the wind speed. Effective wind speed is a nonlinear function of rotor speed ( $\omega_r$ ), generator output power ( $P_e$ ) and pitch angle ( $\beta$ ), given in equation (1.31).

$$v = f(\omega_r, P_e, \beta) \tag{1.31}$$

### 1.3.2.3 Gaussian Radial Basis Function Network (GRBFN) Based Wind Speed Estimation

In (Qiao, W. 2008) and (Tian, L. et al. 2011), wind speed estimation is based on GRBFN which is used to provide a nonlinear input-output mapping for the wind turbine aerodynamic characteristics. The wind speed is estimated by taking the measured electrical power with losses, and nonlinear dynamics of the shaft system. Figure 1.9 shows the GRBFN based wind speed estimation (Qiao, W. 2008).

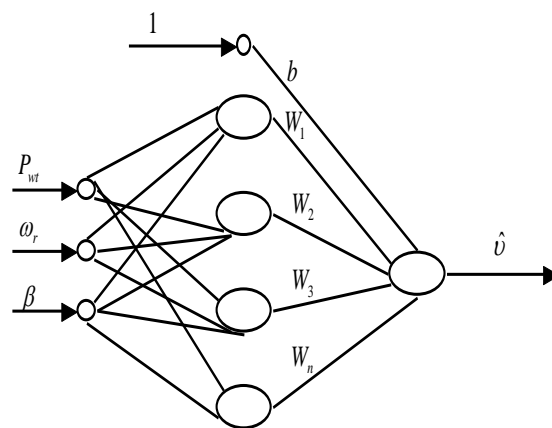


Figure 1.9: GRBFN-based wind speed estimation.

In practice the variation of the wind speed is fast and random, but due to the inertia of the wind turbine its response is relatively slow. So, to achieve a smooth rotor speed command to the turbine a low pass filter is necessary. Figure 1.10 shows the Block diagram of the GRBFN based sensor less maximum wind power tracking (Qiao, W. 2008).

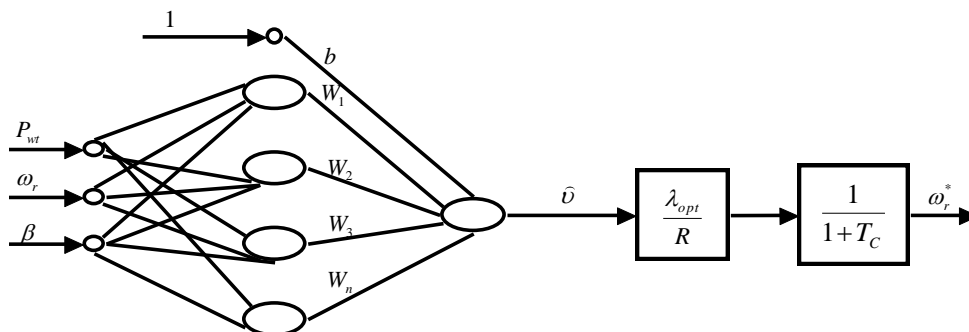


Figure 1.10: Block diagram of the GRBFN-based sensor less maximum wind power tracking.

In order to track the optimal rotor speed of the generator for maximum power extraction PI (Proportional Integral) controller is employed for both rotor side control (RSC) and grid side control (GSC) (Qiao, W. 2008). The stator oriented flux vector control is reported in (Tian, L. et al. 2011).

#### **1.3.2.4 SUPPORT VECTOR REGRESSION BASED WIND SPEED ESTIMATION**

The relationship between the system input and output from the available samples or training data can be obtained by using regression method. It is desirable that the relationship should be determined in such a way, that minimizes the error between the system output and real value i.e. the system output should match the real value as close as possible. The inputs of the SVR (Support Vector Regression) are wind turbine power and rotational speed. Then the wind speed is determined online from the instantaneous input (Abo-Khalil, A.G. and Lee, D.C. 2008), (Ji, G. et al. 2008) and (Abo-Khalil, A.G. and Abo-Zied, H. 2012). The rotor speed and turbine power are input to the SVR and the output is estimated wind speed.

Let ‘ $x_i$ ’ and ‘ $y_i$ ’ denote the input and output spaces respectively and ‘ $n$ ’ is the dimension of training data. The general function of SVR estimation can be expressed as given in equation (1.32)

$$f(x) = (W \cdot \varphi(x)) + b \quad (1.32)$$

Where ‘ $W$ ’ is a weight matrix, ‘ $b$ ’ is a bias term, ‘ $\varphi$ ’ denotes a nonlinear function transformation from ‘ $n$ ’ dimension space to higher dimension feature space. In (Abo-Khalil, A.G. and Abo-Zied, H. 2012) polynomial kernel function and radial basis function are used for approximating  $f(x)$ . In (Abo-Khalil, A.G. and Lee, D.C. 2008) and (Ji, G. et al. 2008) radial basis function are used for approximating  $f(x)$ .

#### **1.3.2.5 ECHO STATE NETWORK (ESN) BASED REAL TIME WIND SPEED ESTIMATION**

In (Qiao, W. 2009), the nonlinear dynamical electrical power wind speed characteristics of the wind turbine systems are approximated by an ESN. By using the dynamical ESN model, the wind speed is directly estimated from measured wind turbine power output.

The wind turbine is controlled by using the estimated wind speed in real time. Figure 1.11 shows the principle of wind speed estimation (Qiao, W. 2009).

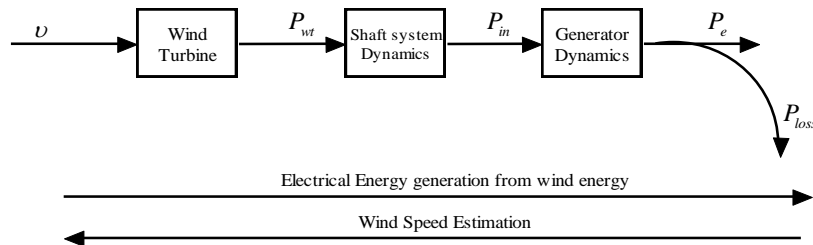


Figure 1.11: The principle of wind speed estimation.

The wind turbine aerodynamic model is represented by the conversion of wind energy to turbine mechanical power. The turbine mechanical power is represented as a nonlinear function of wind speed ' $v$ ', shaft speed ' $\omega_r$ ' and blade pitch angle ' $\beta$ '. The mechanical power is transferred to the generator and the generator converts the mechanical power to the electrical power, losses are also taken into account (referred to the generator side). ESN helps in involving the approximate inverse model for getting the estimated wind speed. In this case, the inputs to the inverse model are ' $P_m$ ', ' $\beta$ ' and ' $\omega_r$ '. The major advantage of this method is that the modelling exercise is free of complex mathematics. Using neural network, the turbine generating system is considered as a black box containing the nonlinear dynamics from  $(v, \beta, \omega_r)$  to  $P_e$ . Following it, ESN is used to estimate the wind speed ' $v$ ' in real time from the measured data  $(P_e, \beta, \omega_r)$ . Figure 1.12 shows the estimation of wind speed by using ESN.

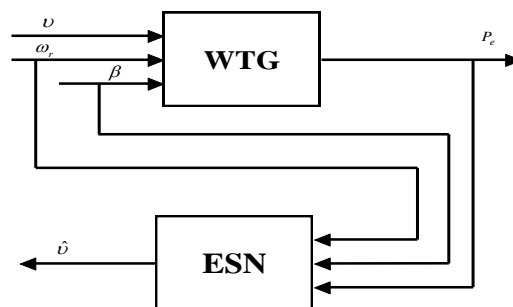


Figure 1.12: Wind speed estimation using an ESN.

### **1.3.2.6 ADAPTIVE NEURO FUZZY INFERENCE SYSTEMS (ANFIS)**

In (Mohandes, M. 2011), the estimation of wind profile is done by the clustering algorithm based on ANFIS. In that the wind speed is estimated up to a height 100 meters based on the knowledge of 10, 20, 30, 40m. ANFIS contains five layers. First layer is called input layer, which is used to map the crisp input to membership function. Second layer performs the connective AND operation. Third layer performs the normalized operation, and fourth layer performs the fuzzy rule which is adaptive with output. Finally fifth layer deals the weighted average of all rule outputs. ANFIS architecture contains four inputs, one output and five fuzzy rules. Finally the estimated wind speed from the model output is compared with the real wind speed at 40m height and the mean absolute error was found to be within 3%.

In (Shamshirband, S. et al. 2014), ANFIS is used to estimate the effective wind speed. The inputs to the ANFIS are wind turbine power coefficients, rotational speed and blade pitch angle and the output is effective wind speed. NN is used to adjust the membership function in fuzzy logic. After training the ANFIS, model is used for online, and performance of the model is evaluated by root mean square error and correlation coefficients.

### **1.3.3 Particle Filter**

In (Ciric, I. et al. 2011), fuzzy control is proposed for aero turbine control which gives the optimal power at below rated wind speed. Effective wind speed is not available for direct measurement, so a wind speed estimator based on sequential Monte Carlo technique is developed. From the knowledge of aerodynamic torque ' $T_a$ ' and measured rotor speed ' $\omega_r$ ', the estimation of effective wind speed is done by particle filter. The main advantage of particle filter is that, it does not depend on any local linearization or functional approximation like EKF (Extended Kalman Filter) at the same time, it can estimate in nonlinear non Gaussian scenarios (Ciric, I. et al. 2011). The dynamic state estimation based on Bayesian approach depends on a posterior probability density function for all state variables which are based on available information that includes the set of received measurements. This density function having the complete statistical

information about the dynamic state, so it may possible to have a complete solution to the estimation problem (Arulampalam, M.S. et al. 2002) and (Pang, W.K. et al. 2001).

### 1.3.4 Statistical model based estimation

In (Tan, K. and Islam, S. 2004), Autoregressive statistical model is used for wind speed prediction, and sensor less control to maximize the power of the wind turbine generator. Generally the prediction model requires previous set of time frame captured by the wind system which is used for the next time frame set. Figure 1.13 shows the sensor less wind energy conversion system (WECS) based control (Tan, K. and Islam, S. 2004).

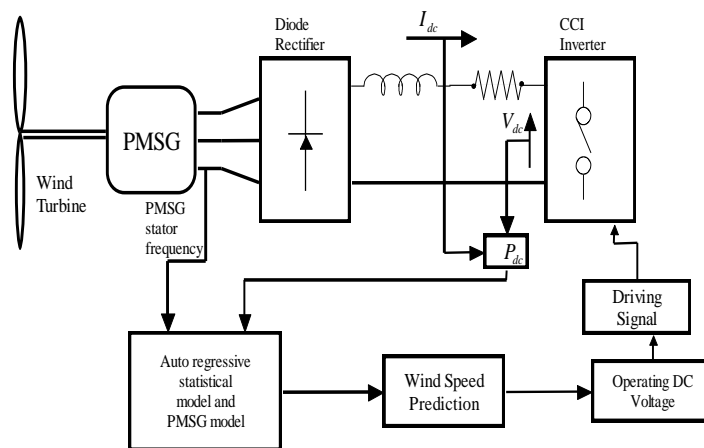


Figure 1.13: Block diagram of the wind prediction sensor less WECS-controlled system.

In (Diaz-Guerra, L. et al. 2012), the wind speed is estimated from the linear time invariant transfer function relating to rotor angular speed and generator torque. This transfer function is obtained from the MATLAB identification tool. The signals used in the identification process are wind speed at hub height, rotor speed and generator torque. After removing the mean from those signals an auto regressive exogenous (ARX) model was obtained from identification tool. The estimated wind speed time series compared with real wind speed and found to 79.75% fit.

### 1.3.5 Data Fusion

Anemometer accuracy is poor because of response speed of an anemometer and some susceptible factors such as the wind turbulence, tower vibration, wind shear, and the roughness of ground. In general, the static accuracy of generator signal is good. But the dynamic response of this generator signal is slow due to large lag and delay of the rotator. The characteristics of these two signals i.e. anemometer data and the generator power are complementary in frequency domain. The estimation error will reduce by fusion of those two signals for estimating the effective wind speed. So, by combining these two sensors the effective wind speed can be calculated with higher accuracy as shown in Figure 1.14.

In (Xu, Z. et al. 2011), the estimation of effective wind speed is based on the data fusion technique. The spectrums of measurement of anemometer and generator power are analysed. From the analysis, it was found that the two signals are complementary in the frequency domain. To design an observer for estimation of effective wind speed, frequency domain data fusion is discussed. Figure 1.14 shows the schematic diagram of the effective wind speed filter.

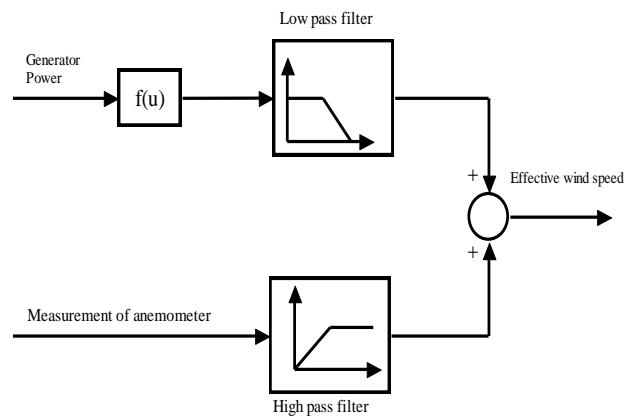


Figure 1.14: Schematic diagram of the effective wind speed filter.

### 1.3.6 Extreme learning machine (ELM) based wind speed estimation

The authors in (Wu, S. et al. 2012) have discussed the estimation of wind speed for variable speed variable pitch generation system. The mapping between the nonlinear input-output is done by using the ELM which gives more accuracy. This proposed method is independent of the environmental air density, so the ELM based wind speed

estimation is robust to air density variation. MPPT control of variable speed variable pitch generation system is achieved by determining the optimal rotor speed from the estimated wind speed. Whenever the wind turbine operates more than rated speed, an ELM pitch control is applied. This control is much faster than the conventional pitch control systems. The input vectors to the NN are the turbine power ' $P_{wt}$ ', the rotational speed ' $\omega_r$ ' and the blade pitch angle ' $\beta$ ' and the output is estimated wind speed. This is the one of the technique for estimation of wind speed where pitch control system is also activated. In above rated wind speed the generated power exceeds its rated value, an ELM based pitch angle controller is used to limit the captured power by activating the pitch control system. Figure 1.15 shows the entire sensor less control scheme for variable pitch PMSG wind turbine power generation system (WTPGS) (Wu, S. et al. 2012).

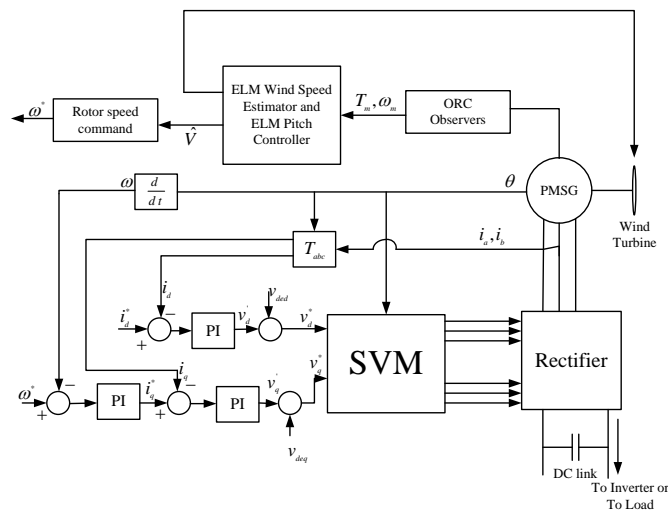


Figure 1.15: Entire sensorless control scheme for variable-pitch PMSG WTPGS.

In (Khamlichi, A. et al. 2011), a direct estimation of wind velocity by means of the nonlinear EKF is used without estimating the aerodynamic torque. The idea consists of using a time dependent Riccati like equation to construct a robust continuous observer for estimating effective wind speed. It is capable of rejecting system perturbations and disturbances acting on the generator torque ' $T_g$ '. In (Mirzaei, M. et al. 2011a) and (Mirzaei, M. et al. 2011b), an EKF is used to estimate the wind speed and this estimated wind speed is used for finding the optimal point of the wind turbine. Uncertainties of the drive train system also considered. These uncertainties are considered as parametric uncertainties in the model and the robust controller is implemented using DK iteration



method. The sources of the uncertainties are drive train stiffness, damping factor and linearized model. The review of estimation of rotor effective wind speed is given in (Soltani, M.N. et al. 2013), which is completely based on linear and nonlinear state /input estimation techniques. Five major estimators are discussed i.e. Power balance estimator, EKF based estimator, KF (Kalman Filter) based estimator, DAC (disturbance accommodating control) based estimator, Unknown input estimator and finally immersion and invariance (I&I) estimator. A comparison has been made among the estimators where KF, I&I and power balance estimator give much better results. From the field test analysis it is found that EKF based estimator at lower turbulence, power balance estimator at high turbulence, and I&I based estimator at all turbulence intensities gives best results.

#### 1.4 LITERATURE SURVEY ON ESTIMATION OF EFFECTIVE WIND SPEED BASED CONTROL

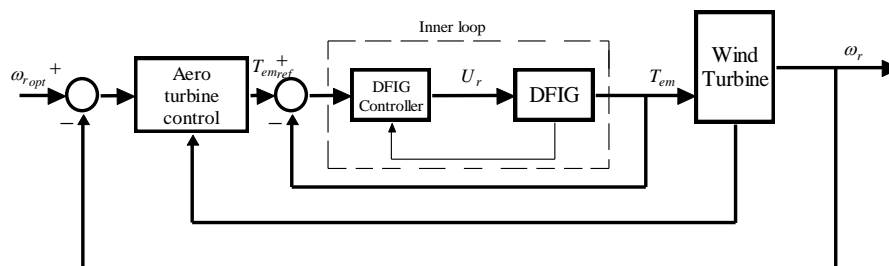


Figure 1.16: WT control.

Generally variable speed WT has two region of control which are below rated speed and above rated speed. In below rated speed, the objectives are to maximize the energy capture from the wind and reduce the drive train oscillations. Figure 1.16 shows the WT control schemes. The schematic diagram comprises of two control loop i.e. inner and outer loop. The inner control loop consists of electrical generator with power converters whereas, the outer loop having the aero turbine control which gives the reference to the inner loop. In this work, we presume that the inner loop is well controlled. Classical vector control is used to control the DFIG (Double Fed Induction Generator) and is connected to the grid.

In (Ma, X. 1997), (Vihriala, H. 2002), (Boukhezzar, B. and Siguerdidjane, H. 2005), (Boukhezzar, B. et al. 2006), (Boukhezzar, B. and Siguerdidjane, H. 2009a), (Boukhezzar, B. and Siguerdidjane, H. 2009b), (Boukhezzar, B. and Siguerdidjane, H. 2011), (Bourlis, D. and Bleijs, J.A.M. 2010) and (Nam, Y. et al. 2011), the authors have addressed various issues about single and two mass model based WT control schemes. In these investigations aerodynamic torque, rotor speed, low speed shaft torque and generator speed are estimated from measured generator speed and control input. For single mass model generator torque acts as control input where as for two mass model electromagnetic torque ( $T_{em}$ ) acts as control input. In (Ma, X. 1997), (Boukhezzar, B. and Siguerdidjane, H. 2005), (Boukhezzar, B. et al. 2006), (Boukhezzar, B. and Siguerdidjane, H. 2009a), (Boukhezzar, B. and Siguerdidjane, H. 2009b), (Boukhezzar, B. and Siguerdidjane, H. 2011) and (Bourlis, D. and Bleijs, J.A.M. 2010), the authors have determined the optimal rotor speed based on EEWS (estimation of effective wind speed). This optimal rotor speed is taken as reference rotor speed for controlling the generator torque. The control technique used is the static and dynamic nonlinear feedback control for getting the maximum power (Boukhezzar, B. and Siguerdidjane, H. 2005), (Boukhezzar, B. et al. 2006), (Boukhezzar, B. and Siguerdidjane, H. 2009a) and (Boukhezzar, B. and Siguerdidjane, H. 2011). The static feedback control technique is not robust for higher order dynamics. To track the higher order dynamics a dynamic state feedback linearization is used. In (Boukhezzar, B. and Siguerdidjane, H. 2009a) and (Boukhezzar, B. and Siguerdidjane, H. 2011), two mass models are considered for EEWS, where the generator torque is controlled with static and dynamic nonlinear state feedback control and the KF is used as estimator. Figure 1.17 shows the nonlinear static and dynamic state feedback control with estimator control scheme (Boukhezzar, B. and Siguerdidjane, H. 2011).

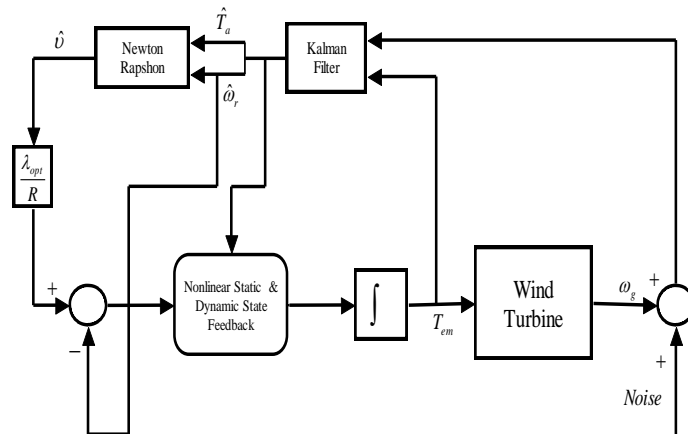


Figure 1.17: Nonlinear Static and Dynamic state feedback control with estimator control scheme.

In (Boukhezzar, B. and Siguerdidjane, H. 2005), (Boukhezzar, B. et al. 2006), (Boukhezzar, B. and Siguerdidjane, H. 2009a) and (Boukhezzar, B. and Siguerdidjane, H. 2011), a nonlinear static and dynamic state feedback with higher order tracking dynamics is introduced. But it requires complex control law and higher order derivatives. In (Boukhezzar, B. and Siguerdidjane, H. 2009b), the controller used is based on the classical PI controller with nonlinear state feedback applied to a linearized wind turbine system. Figure 1.18, shows the nonlinear state space feedback linearization with PI controller and wind speed estimator (Boukhezzar, B. and Siguerdidjane, H. 2009b).

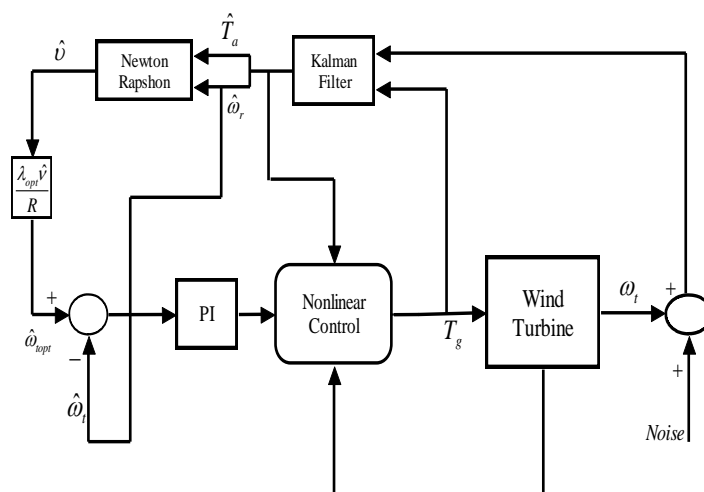


Figure 1.18: Nonlinear state space feedback linearization with PI controller and wind speed estimator.

In multi megawatt (MW) wind turbine the dynamic response of the turbine to sudden change in wind speed is usually slow because of slow pitch control system. Figure 1.19 shows the feed forward pitch control with estimator and 3D lookup table for multi MW wind turbine (Nam, Y. et al. 2011). In this case, the estimated aerodynamic torque, pitch angle and the rotor speed acts as an input to the lookup table and the output is the estimated wind speed (Nam, Y. et al. 2011). The pitch angle is calculated from the knowledge of estimated wind speed and rotor speed. Where  $\left(\frac{\partial\beta}{\partial v}\right)_0$  and  $\left(\frac{\partial\beta}{\partial\Omega_r}\right)_0$  are the feed forward controller gains.

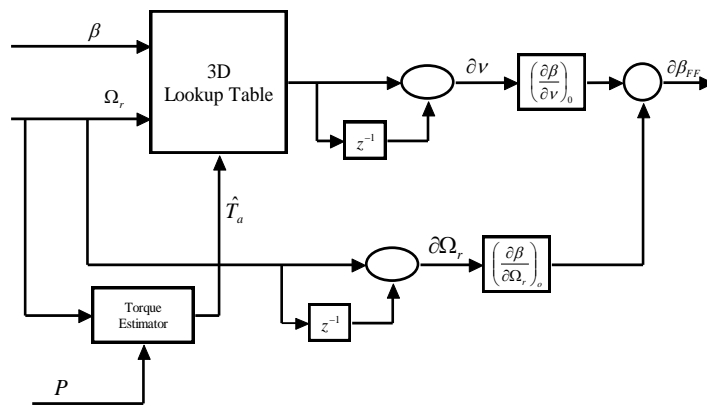


Figure 1.19: Feed forward pitch control with estimator and 3D lookup table.

A classical approach of linear quadratic regulator (LQR) controller is discussed in (Ma, X. 1997), where the KF is used to estimate states and NR is used to estimate the wind speed. LQR and PI controller regulates the pitch for above rated wind speed by maintaining the generator torque constant. Figure 1.20 shows the LQR control of wind turbine (Ma, X. 1997). In (Vihriala, H. 2002) KF is used to estimate the aerodynamic torque and rotor speed. The generator torque control is achieved by ATF control and Fuzzy control.

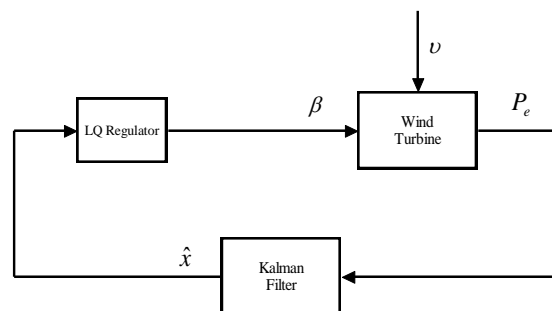


Figure 1.20: LQR control of wind turbine.

In (Bourlis, D. and Bleijs, J.A.M. 2010) KF is used for estimation of states such as rotor speed and aerodynamic torque, and NR is used to estimate the wind speed. NR is used to find the wind speed from the estimated aerodynamic torque. The choice of speed controller for the required torque can be any one of PI, LQG or  $H_\infty$ , which don't affect the estimation algorithm. In (Bourlis, D. and Bleijs, J.A.M. 2010) the noise co-variance matrix ' $Q$ ' and ' $R$ ' are separately estimated in each iteration, unlike (Boukhezzar, B. and Siguerdidjane, H. 2005), (Boukhezzar, B. et al. 2006), (Boukhezzar, B. and Siguerdidjane, H. 2009a), (Boukhezzar, B. et al. and Siguerdidjane, H. 2009b) and (Boukhezzar, B. and Siguerdidjane, H. 2011), where ' $Q$ ' and ' $R$ ' are having fixed co-variance. As the wind changes continuously, for estimation of wind speed the estimation algorithm should be self-adaptive to the changing wind condition and unknown measurement noise. Figure 1.21 shows the control scheme based on aerodynamic torque and effective wind speed estimation (Bourlis, D. and Bleijs, J.A.M. 2010).

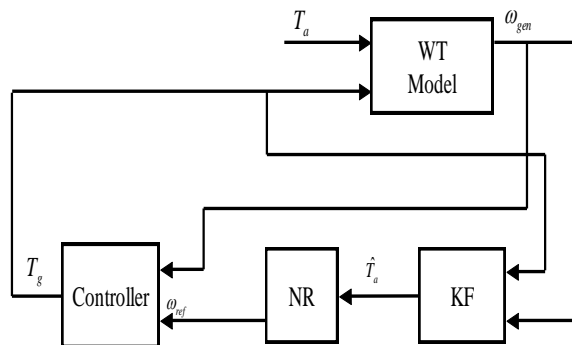


Figure 1.21: Control scheme based on aerodynamic torque and effective wind speed estimation.

## 1.5 CLASSICAL CONTROL TECHNIQUES FOR WIND TURBINE

In this work, the common classical control techniques has been taken into consideration for a WT. Finally the results of these controllers are compared with the other proposed nonlinear control techniques. The classical controllers are ATF, ISC, NSSFE and NDSFE.

### 1.5.1 Aerodynamic Torque Feedforward control for single mass model

In ATF (Aerodynamic torque feed forward), control the variables such as aerodynamic torque and rotor speed are estimated by Kalman Filter (Vihriala, H. et al. 2001).

Equation (1.33) gives the relationship between the estimated variables  $(\hat{T}_a, \hat{\omega}_r)$  and control variable ' $T_g$ '. To track the speed deviation between ' $\omega_{ref}$ ' and ' $\omega_r$ ', a proportional (P) controller is used. The value of ' $\hat{\omega}_{ref}$ ' given in equation (1.34).

$$T_g = K_c(\hat{\omega}_{ref} - \hat{\omega}_r) + \hat{T}_a - K_t \hat{\omega}_r \quad (1.33)$$

$$\hat{\omega}_{ref} = \sqrt{\frac{\hat{T}_a}{K_{opt}}} \quad (1.34)$$

The entire ATF control is considered as P control. For a step change in wind speed this control scheme introduces a steady state error. In order to achieve the exact control action, more precise value of ' $\hat{\omega}_{ref}$ ' is needed, but during the fast wind speed transitions, it introduces the significant power loss. In this work, the aerodynamic torque nonlinearity is approximated by the 5<sup>th</sup> order polynomial and the rotor speed is taken as an output of the WT. The final equation of the proposed method does not contain any estimated quantity given in equation (1.35) and (1.36). By using the same proportional control law given in equation (1.33) the wind turbine generator torque is controlled. The optimal value of proportional gain is found to be  $K_c = 3 \times 10^4$ , where ' $K_c$ ' is the proportional gain.

$$T_g = K_c(\omega_{ref} - \omega_r) + T_a - K_t \omega_r \quad (1.35)$$

$$\omega_{ref} = \sqrt{\frac{T_a}{K_{opt}}} \quad (1.36)$$

## 1.5.2 Indirect Speed Control for single mass model

Operating the WT around its optimal aerodynamic efficiency curve makes it more stable (Leithead, W.E. and Connor, B. 2000). Under constant wind speed and generator torque, an optimal operating point can be derived around which the WT becomes locally stable. The aerodynamic efficiency varies with the variation of wind speed, so under varying wind speed to get the optimal operation, the generator torque should be

chosen properly. By using ISC controller the aerodynamic torque ‘ $T_a$ ’ can be maintained on the aero dynamic efficiency curve by properly choosing the generated torque ‘ $T_g$ ’ that tracks the same value instead of wind speed variation. Fast variation of wind speeds leads to power loss, at the same time the control strategy is not robust with respect to measurement noise and WT disturbance. Equation (1.37) gives the relation between the generator torque and rotor speed for ISC control. Where ‘ $K_t$ ’ is the total external damping in (Nm/rad/sec) for the WT. Equation (1.38) gives the constant value of ‘ $K_{opt}$ ’. Figure 1.22 shows the ISC control for single mass model.

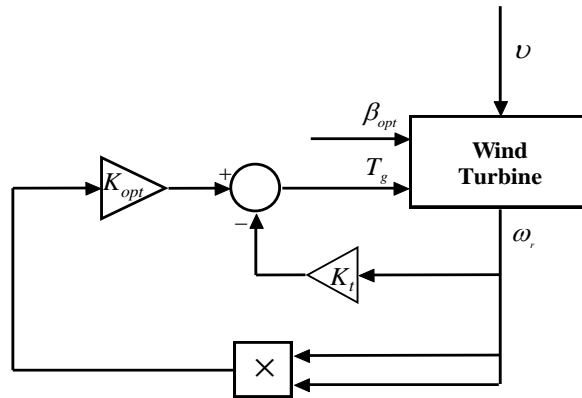


Figure 1.22: ISC Control.

$$T_g = K_{opt} \omega_r^2 - K_t \omega_r \quad (1.37)$$

$$K_{opt} = \frac{1}{2} \rho \pi R^5 C_{popt} \frac{1}{\lambda_{opt}^3} \quad (1.38)$$

### 1.5.3 Nonlinear Static State Feedback with Estimator (NSSFE) for single mass model

The single mass wind turbine given in equation (1.15) can be rearranged in the following form

$$T_g = J_t \left( \frac{T_a}{J_t} - \frac{K_t}{J_t} \omega_r - w_2 \right) \quad (1.39)$$

where  $w_2 = \dot{\omega}_r$

The ‘ $w_2$ ’ is approximated with the first order dynamics in terms of tracking error (Boukhezzer, B. et al. 2006).

$$\dot{e} + a_0 e = 0, a_0 > 0 \quad (1.40)$$

Tracking error is defined as

$$e = \omega_{ropt} - \omega_r \quad (1.41)$$

Finally the control torque ' $T_g$ ' is given in equation (1.42)

$$T_g = T_a - K_t \omega_r - J_t a_0 e - J_t \dot{\omega}_{ropt} \quad (1.42)$$

#### 1.5.4 Nonlinear Dynamic State Feedback with Estimator (NDSFE) for single mass model

By taking the time derivative of the equation (1.15) we get

$$J_t \ddot{\omega}_r = \dot{T}_a - K_t \dot{\omega}_r - \dot{T}_g \quad (1.43)$$

The above equation can be rearranged as

$$\dot{T}_g = \frac{1}{J_t} \left( \frac{\dot{T}_a}{J_t} - \frac{K_t}{J_t} \dot{\omega}_r - w_1 \right) \quad (1.44)$$

where  $w_1 = \ddot{\omega}_r$

The  $w_1$  is approximated with second order differential equation (Boukhezzar, B. et al. 2006) in terms of tracking error ( $e$ ).

$$\ddot{e} + b_1 \dot{e} + b_0 e = 0, b_0, b_1 > 0 \quad (1.45)$$

Finally the control torque ' $T_g$ ' is given in equation (1.46)

$$\dot{T}_g = \dot{T}_a - K_t \dot{\omega}_r - J_t \ddot{\omega}_{ropt} - J_t b_1 \dot{e} - J_t b_0 e \quad (1.46)$$

The time derivatives appeared in the equation (1.46) are obtained using approximated filtered derivatives. Due to the turbulent wind speed, dynamic tracking is required which results in high control inputs. By properly chosen the tracking error dynamics, the smoothness in output power can be achieved.



### 1.5.5 Indirect Speed Control for two mass model

A brief description of the well-known control techniques i.e. ISC and ATF for two mass model are discussed in this section (Vihriala, H. et al. 2001). In ISC, it is assumed that the WT is stable around its optimal aerodynamic efficiency curve. The two mass model control signal is given in equation (1.47). In ISC the WT has to operate at its optimal efficiency curve which introduces more power loss for high varying wind speed.

$$T_{em} = K_{opt_{hs}} \omega_g^2 - K_{t_{hs}} \omega_g \quad (1.47)$$

Where,

$$K_{opt_{hs}} = 0.5 \rho \pi \frac{R^5}{n_g^3 \lambda_{opt}^3} C_{P_{opt}} \quad (1.48)$$

$$K_{t_{hs}} = \left( K_g + \frac{K_r}{n_g^2} \right) \quad (1.49)$$

where ‘ $K_{t_{hs}}$ ’ is the low speed shaft damping coefficient brought up to the high speed shaft.

### 1.5.6 Aerodynamic Torque Feedforward for two mass model

In ATF, proportional control law is used to control the WT. The rotor speed and the aerodynamic torque are estimated using Kalman Filter, which is used to control the WT (Leithead, W.E. and Connor, B. 2000). The control law is given in equation (1.50).

$$T_{em} = \frac{1}{n_g} \hat{T}_a - \left( \frac{K_r}{n_g^2} + K_g \right) \hat{\omega}_g - \frac{K_C}{n_g^2} (\omega_{gref} - \omega_g) \quad (1.50)$$

$$\omega_{gref} = n_g k_w \sqrt{\hat{T}_a} \quad (1.51)$$

$$k_w = \frac{1}{\sqrt{k_{opt}}} = \sqrt{\frac{2 \lambda_{opt}^3}{\rho \pi R^5 C_{P_{opt}}}} \quad (1.52)$$

$$k_{opt} = \frac{1}{2} \rho \pi \frac{R^5}{\lambda_{opt}^3} C_{P_{opt}} \quad (1.53)$$

The optimal value of proportional gain is found to be  $K_c = 3 \times 10^4$ . The above existing control techniques have following three major drawbacks: the ATF control having more steady state error so an accurate value of ' $\omega_{ref}$ ' is needed. Both the controllers are not robust with respect to disturbances.

## **1.6 LITERATURE SURVEY ON CONTROL FOR MAXIMUM POWER EXTRACTION OF VSWT**

In (Sheikhan, M. et al. 2013) the maximum power for VSWT is achieved by PI controller, which is based on the fuzzy system. Error is taken as the input to the controller i.e. difference between the actual and optimal rotor speed, and the output of the controller is generator torque. Further, fuzzy logic systems (FLS) is used for tuning the PI controller gains for various wind speed. PI gains are optimized for different wind speed by particle swarm optimization (PSO). In (Hong, C.M. et al. 2013), radial basis function neural network (RBFNN) and torque observer based control algorithm is used to control the WT for optimal energy capture. RBFNN is trained online by using MPSO (modified particle swarm optimization) training algorithm. In order to achieve the maximum power the difference between the actual and optimal rotor speed to be minimized. In (Kortabarria, I. et al. 2014), a new maximum adaptive algorithm for extraction of optimal power is proposed for small WT. Perturb and observe scheme is adapted for different wind speed to obtain optimum relationship for regulating the maximum power point. In (Merida, J. et al. 2014), two control strategies are developed for optimal power extraction with reduced mechanical stress. The first one is tracking controller with wind speed estimator which ensures the optimal angular speed of the rotor. In second, a robust power tracking is developed by non-homogenous quasi continuous high order sliding mode controller without considering wind velocity. Maximum power extraction from VSWT is achieved by a Takagi–Sugeno–Kang (TSK) fuzzy model which is based on data driven model (Calderaro, V. et al. 2008). In TSK model a combination of fuzzy clustering method with genetic algorithm (GA) is used for the input –output space and least square (LS) algorithm is used for parameter estimation. Feedback torque control is applied for mathematical model FSWT for maximum power extraction. The authors (Liao, M. et al. 2009) have also analyzed the dynamic response and stability of control system by considering both rotor and

generator side rotational speed as the feedback signal in torque control. In order to achieve the maximum power point in the WT, FLC (Fuzzy logic controller) is tuned by GA (genetic algorithm) (Amine, H.M. et al. 2014). The width of the membership function in FLC is adjusted by GA.

A sensorless based maximum power point tracking is developed by FLC (Belmokhtar, K. et al. 2014). This method enhances the reliability of the system by decreasing the losses of the converter. References (Beltran, B. et al. 2008a) and (Beltran, B. et al. 2008b) discussed higher order sliding mode control (HSMC) of WT at below and above rated speed and concluded that HSMC is more robust with respect to parameter uncertainty of the WT. In (Merabet, A. et al. 2011) and (Boukezzar, B. and M'Saad, M. 2008), conventional SMC based control with adaptive sliding gain is used to control the WT, where the sliding gain is varied by an adaptation algorithm.

Authors in (Liu, J. et al. 2015), introduced a novel MPPT algorithm with an adaptation of fuzzy inference system (FIS) for a 2 MW DFIG based WT. TS fuzzy inference system is obtained to have high efficiency with reduced fluctuations in output power. Compared to conventional INC (incremental conductance) and PSO, the FOINC (fractional order incremental conductance algorithm) found to be better in terms of transient tracking of MPPT and also the steady state response. (Yu, K.N. and Liao, C.K. 2015). It consists of an intelligence online learning based on model free Q learning algorithm. The method is validated through simulation on a 1.5 MW DFIG based WT system. (Wei, C. et al. 2015). An (Petkovic, D. et al. 2013), optimum power coefficient value is estimated by using ANFIS. Membership function parameter in fuzzy logic of FIS is adjusted by NN. Backpropagation training algorithm is used for training the NN. In (Daili, Y. et al. 2015), modified perturbation and observation based MPPT algorithm is used for small wind energy system. In that two models are involved, i.e. normal perturbation and observation mode, prediction mode. During slow wind speed condition, normal perturbation and observation is used for tracking maximum power point. But during rapid changes in wind speed the maximum power point is obtained by switching the algorithm to prediction mode. After that normal perturbation and observation is used to track the true peak point.

In (Lin, W. and Hong, C. 2010), Wilcoxon radial basis function network (WRBFN) with hill-climb searching (HCS) method is proposed for maximum power tracking with various turbine inertia. Back propagation learning algorithm with modified PSO is used for online training of WRBFN. Output maximization control of WRBFN can maintain the system stability and reach the desired performance even with parameter uncertainties. In (Evangelista, C. et al. 2013) adaptive second order SMC is designed for maximum power extraction from the wind with reduced mechanical stress on the shaft. The above controller is tested with different random wind speed in the presence of model uncertainties and external perturbations. An additional controller is also developed based on super twisting algorithm to smooth the converter firing angle that ensures maximum power capture and low mechanical stress. In (Assareh, E. and Biglari, M. 2015), maximum power capture of wind turbine at low wind speeds is achieved by regulating the PI controller gains using RBFNN. Gravitational search algorithm (GSA) has provided the optimal data set to train the neural network. Through GSA, optimal gains are obtained so that a cost function i.e. integral square error (ISE) is minimized. The simulations are implemented in 5MW FAST wind turbine system. In (Kumar, D. and Chatterjee, K. 2016), authors have focused on comprehensive review of different MPPT algorithms for VSWT. The algorithms are classified into three categories, i.e. indirect, direct and hybrid power control. From this study it is clear that TSR, OT (optimal torque) and PSF (power signal feedback) algorithms are comparatively very fast algorithms as compared to HCS (Hill climb search), INC (incremental conductance) and ORB (optimal relation based). The authors found that adaptive soft computing based MPPT algorithms are mostly used due to its higher efficiency and more flexibility. In (Abdullah, M.A. et al. 2012) the authors have reviewed MPPT for wind energy conversion systems. In this study three selected methods are compared in terms of efficiency and speed of response. From this analyses, OTC (optimal torque control) found to be optimal in terms of simplicity and accuracy, but it depends on the WT characteristics. P&O (Perturbation and observation) is simple and flexible, but efficiency is less, also the determination of step size is problematic.

## **1.7 WIND TURBINE SIMULATORS**

The numerical simulations are performed on the CART (Controls Advanced Research Turbine) WT model. The CART is located at the NREL (National Renewable Energy Laboratory) National Wind center near Golden, Colorado. The CART3 is a three blade variable speed, variable pitch WT with nominal power rating of 600kW. It has mainly three parts i.e. rotor, tower and nacelle. The rotor includes blade and their attachment points is called hub which is maintained by the low speed shaft. The tower is a cantilever beam which supports a yaw bearing and nacelle. The yaw bearing allows the turbine to rotate in the wind speed direction. The nacelle houses contains the complete drive train assembly. It contains the gearbox, generator and low speed shaft. The gearbox is directly connected to the squirrel cage induction generator through high speed shaft. The generator is connected to the grid through power electronics that can directly control generator torque (Fingersh, L.J. and Johnson, K. 2002). The power electronics consists of three phase PWM (Pulse Width Modulation) converters with a constant dc link voltage. The main objective of the grid side converter is to maintain the dc link voltage constant (Ottersten, R. 2003) and (Pena, R. et al. 2001).

### **1.7.1 Nonlinear FAST Wind Turbine Simulator**

FAST is an aero elastic WT simulator which is developed by NREL. It can able to model both two and three blade horizontal axis wind turbine (HAWT). This FAST code can able to predict both extreme and fatigue loads. The tower and flexible blade are modeled by using the “assumed mode method”. Other components are modeled as rigid bodies. An advanced certified code is used in FAST to model the aerodynamic behavior of the WT. WT loads are calculated by using BEM (Blade Element Momentum) and multiple component of wind speed profile (Hansen, M.O.L. et al. 2006). FAST code is approved by the Germanischer Lloyd (GL) WindEnergie GmbH for calculating onshore WT loads for design and certification (Manjock, A. 2005). Due to the above advantages and exact nonlinear modeling of the WT, the proposed controllers are validated by using FAST. In general three blade turbine have 24 DOF (Degree of Freedom) to represent the wind turbine dynamics. FAST (Fatigue, Aerodynamics, Structures, and Turbulence) is the simulation tool for modelling of nonlinear wind turbine (Jonkman B.J., and Buhl, M.L. 2005) and TurbSim (Jonkman B.J. and Buhl, M.L.

2009) is a stochastic turbulent wind simulator which is developed by the NREL and it generates the turbulent wind inflow used by NREL. In this work five DOF are considered for WT dynamics i.e. variable generator, rotor speed and three flap wise blade mode. FAST codes are interfaced with S-function and implemented with Simulink model. FAST uses an AeroDyn file as an input for aerodynamic part. AeroDyn file contains aerodynamic analysis routine and it requires status of a WT from the dynamic analysis routine (Laino, D.J. and Hansen, A.C. 2002).

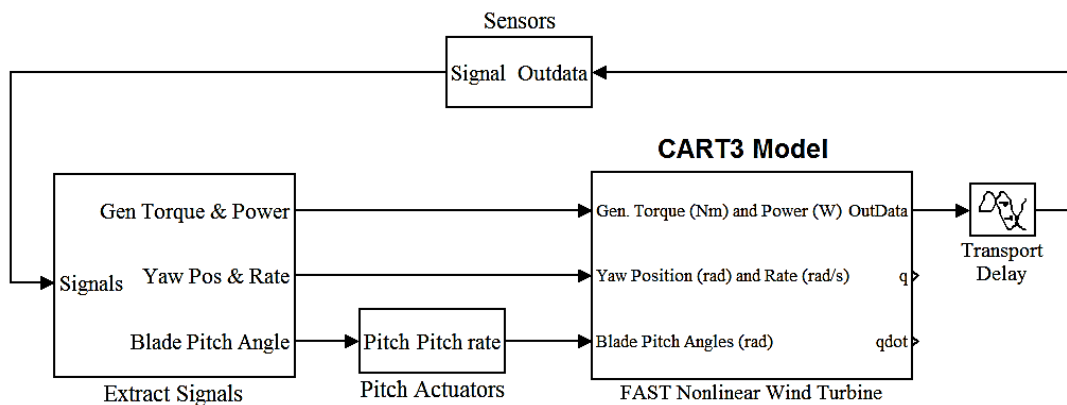


Figure 1.23: Simulink model for simulating the FAST nonlinear turbine with controller and pitch actuator.

Figure 1.23 shows the nonlinear FAST model which is implemented in MATLAB Simulink environment as S-function in ‘.Mex32’ format. Generally two predefined input files are required to run FAST model that are ‘.fst’ and ‘.ipt’. These two files contains information about structural and aerodynamic data of WT model.

### 1.7.2 TurbSim

Wind profile acts as the input file for AeroDyn. The wind input file is generated by using TurbSim is developed by the NREL (Jonkman B.J. and Buhl, M.L. 2009). The test wind profile with full field turbulence is generated. TurbSim is a wind simulator, which consist of stochastic full filled turbulent. It numerically simulates the time series of three dimensional wind velocity vectors at points in a vertical rectangular grid. Output of the TurbSim can be used as input to the AeroDyn code. In TurbSim simulation, it is assumed that the time series are stationary process. To simulate the non-stationary process, TurbSim has superimpose coherent turbulent structure onto the time series.

## 1.8 MOTIVATION OF THE WORK

Wind turbine regions are classified into three. Region 1 (below 5m/s) represents the wind speed below the cut in speed. Region 2 (range between 5 to 9 m/sec) represents the wind speed between cut in and rated speed. In this region 2 the main objective is to maximize the energy capture from the wind with reduced oscillation on the drive train. Region 2.5 (range between 9 to 12 m/sec) represents the wind speed nearer to the rated speed i.e. transient period. Region 3 (above 12 m/sec) describes the wind speed above the rated speed. In this region 3 pitch controller is used to maintain the WT at its rated power. The time response of WT electrical system is much faster than the other parts of the WT. This makes it possible to decouple the generator and the aero turbine control designs and thus define a cascaded control structure around two control loops. In this work, it is assumed that the inner loop is well controlled.

- 1) The inner control loop consists of electrical generator with power converters.
- 2) The outer loop having the aero turbine control which gives the reference to the inner loop.

Figure 1.24 shows the proposed nonlinear control scheme for all the WT regions. Modified Newton Rapshon (MNR) based estimator is used to estimate the wind speed which is used to get the optimal/reference rotor speed. At region 2, torque control can able to extract the maximum power form the wind. Once the generator speed reached 98.5% of the rated speed then the rated torque control signal is sent to the WT. Generator speed based fuzzy PI pitch control for region 3 is also proposed in this work. The objectives of torque control is optimal power extraction with reduced oscillation on the drive train at below rated wind speed.

To achieve the above objective (Region 2 and 2.5) the blade pitch angle ( $\beta_{opt}$ ) and tip speed ratio ( $\lambda_{opt}$ ) are set be its optimal value. In order to achieve the optimal tip speed ratio the rotor speed must be adjusted to the reference/optimal rotor speed ( $\omega_{ropt}$ ) by adjusting the control input i.e. generator torque. The objective of the pitch controller is to vary the pitch angle according to the difference between the nominal speed and output generator speed by fuzzy based gain scheduling PI controller, provided the torque control input set at the rated value.

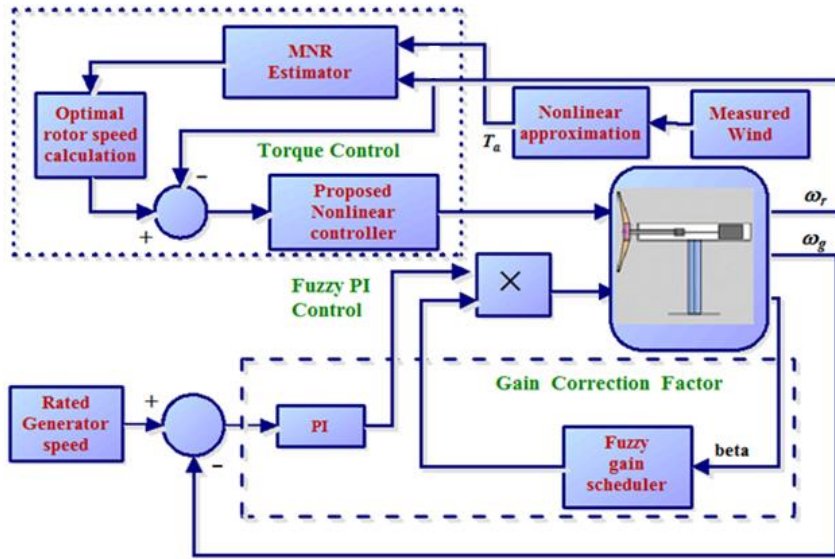


Figure 1.24: Proposed control scheme for WT

## 1.9 CONTRIBUTION OF THE THESIS

In chapter 2 the estimation of effective wind speed at below rated wind speed is done by different estimation techniques such as MNR, Neural Network trained with different algorithms and nonlinear time series based estimation. In this chapter, a single mass model based WT is considered. Initially without estimation of wind speed the conventional control techniques such as ISC and ATF are considered. Due to the lack of performance in the conventional techniques, existing nonlinear controllers are adapted i.e. nonlinear static state feedback linearization with estimator (NSSFE) and nonlinear dynamic state feedback linearization with estimator (NDSFE). For those two nonlinear controllers six different nonlinear wind speed estimators are proposed. Among those wind speed estimators Hammerstein Wiener model (HWM) and Nonlinear auto regressive exogenous model (NARX) with NDSFE control found to be better in terms of standard deviation (STD) and power spectral density (PSD) of the control input.

Generally, wind turbine disturbance are not predictable in nature, so the conventional controller results in poor tracking performance and introduces more power loss. In order to overcome the above drawbacks SMC, ISMC, FSMC and AFISM (Adaptive fuzzy integral sliding mode controller) are proposed. The proposed controllers are tested with different mean wind speed and disturbances. From this analysis it is found



the AFISMC gives better performance and robust to the input disturbances compared to other controller performances.

In chapter 3 the WT dynamics are considered as the two mass model and the simulation are carried out through the FAST NREL 600kW. Initially the conventional control technique such as ATF and ISC are adapted to the WT. However the performance of those techniques does not take into account the dynamical aspect of the wind and aero turbine, leading to significant power loss. In addition it is found that, they are not robust with respect to disturbances. In order to overcome the above drawbacks modified nonlinear static state with feedback estimator (MNSSF), SMC and ISMC with MNR wind speed estimator are proposed at below rated wind speed. The simulations of the conventional and proposed controllers are tested with different mean wind speed and turbulences. Finally it is seen that for a good control performance a trade-off is to be maintained between the maximum power capture and the transient load on the drive train. Higher tracking dynamic will ensure maximum power capture at the cost of high turbulence in the control action. Conversely a slower tracking dynamic ensures smooth torque i.e. less transient load on the drive train at the cost of low power capture. A comparative study between the proposed and conventional techniques are presented.

Chapter 4 mainly focuses on the control of VSVPWT for maximization of extracted power at below rated wind speed (region 2) and regulation of extracted power when operating at above rated wind speed (region 3). Initially, the nonlinear controllers i.e. SMC and ISMC are proposed for region 2 whereas a conventional PI control is adapted for region 3 of a VSVPWT. The proposed controller is combined with MNR wind speed estimator to estimate the wind speed. The control law is derived for region 2 which is also adapted for the transition period between region 2 and region 3 (region 2.5). The dynamic simulations are tested with nonlinear FAST WT. Finally ISMC with fuzzy based pitch controller is compared with baseline + PI controller. Different types of wind speed profile are chosen for all the wind speed region. In this chapter the analysis is completely emphasized on the transition region i.e. region 2.5.

Chapter 5 discusses about the application of an ISMC and terminal sliding mode (TSMC) in region 2 and a fuzzy based PI for region 3 with different actuator fault and

sensor faults. Same ISMC and TSMC is adopted for the switching between operating regions (transition region 2.5), so the control input maintains the continuity at the moment of switching. Finally, the performance of the proposed controllers are tested with nonlinear FAST WT model and the results are compared with the existing baseline controllers.

Finally chapter 6 concludes the whole thesis and gives a salient idea on the future extension of work.

## **1.10 CONCLUSION**

This chapter focuses on the modeling of a variable speed wind turbine. The brief description about the operation of a wind turbine control, principle of extraction of energy from the wind are presented. Generally the WT control techniques are based on wind speed. The main objective at low wind speed is to capture the maximum power with reduced oscillation on the drive train. For high wind speed, the objective of the controller is to regulate the power by pitch controller. A brief literature survey is given for estimation of effective wind speed based control. The nonlinear NREL WT simulator and stochastic TurbSim wind simulator are also presented.

Next chapter will mainly focus on single mass model based different nonlinear controllers such as SMC, FSMC, ISMC and AFISM. Also an accurate estimation of effective wind speed using different artificial intelligence based techniques and the time series based HMM and NARX model will be presented.

## **CHAPTER 2**

### **2 DESIGN AND IMPLEMENTATION OF NONLINEAR ESTIMATOR AND CONTROLLER FOR SINGLE MASS MODEL WIND TURBINE**

#### **2.1 INTRODUCTION**

In a wind turbine system the exact control depends on the accurate estimation of effective wind speed, which can't be measured directly. In this chapter the effective wind speed is accurately estimated using different estimation algorithms. Initially without estimating effective wind speed, the conventional control techniques were applied to the control of WT. However, due to the weak performance of those control techniques different types of nonlinear wind speed estimation based nonlinear controllers are employed for the WT. In this chapter, estimation of effective wind speed at below rated wind speed is done by different estimation techniques such as MNR, NN based algorithms and nonlinear time series based estimation. Six different nonlinear wind speed estimators are proposed. Out of which HWM (Hammerstein Wiener model) and NARX (Nonlinear auto regressive exogenous model) with NDSFE control found to be better in terms of standard deviation (STD) and power spectral density (PSD) of the control input.

This chapter also discusses nonlinear controllers for VSWT. The main objective of the nonlinear controller is to capture the optimal power from the wind with reduced oscillation on the drive train. Initially the conventional control techniques such as ATF, ISC, NSSFE, NDSFE and SMC are adapted to the single mass model of the WT. The performance of the proposed controllers such as FSMC, ISMC and AFISMC are compared with the conventional controller. Generally WT disturbance are not predictable in nature and the conventional controller having poor tracking performance, introduces more power loss in the presence of high disturbance. The proposed

controllers are tested in the presence of the different types disturbances with different mean wind speed variation. Finally from the results it is found that proposed AFISMC gives better performance and is more robust to the input disturbances compared to other controllers.

## 2.2 PROBLEM FORMULATION

Generally WT is classified into two types i.e. fixed and variable speed WT. Variable speed WT has more advanced and flexible operation than fixed speed WT. Operating regions in variable speed WT are divided into three. Figure 2.1 shows the power operating region of WT.

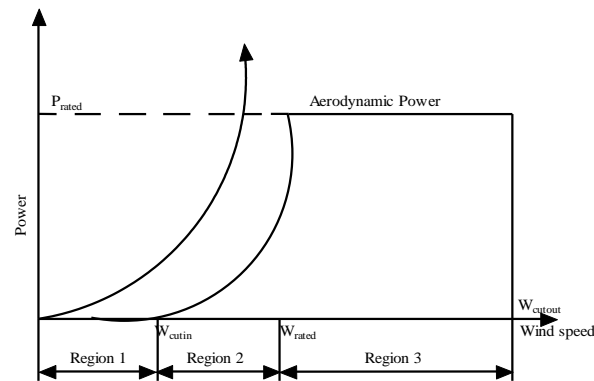


Figure 2.1: Power operating region of wind turbines.

Region 1 represents the wind speed below cut-in wind speed, this is used for starting up the turbine. Region 2 represents the wind speed between cut-in and cut-out. In region 2 the main objective is to maximize the energy capture from the wind with reduced mechanical stress. Region 3 describes the wind speed above the cut-out speed. In this region pitch controller is used to maintain the WT at its rated power.

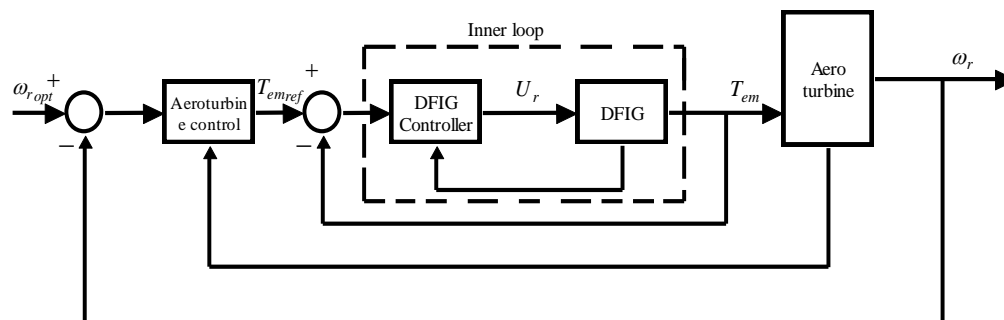


Figure 2.2: WT control scheme.

To achieve the above objective (Region 2) the blade pitch angle ( $\beta_{opt}$ ) and tip speed ratio ( $\lambda_{opt}$ ) are set to its optimal value. In order to achieve the optimal tip speed ratio the rotor speed must be adjusted to the reference/optimal rotor speed ( $\omega_{ropt}$ ) which is done by adjusting the control input i.e. generator torque ( $T_g$ ). Equation (2.1) defines the reference/ optimal rotor speed for a WT.

$$\omega_{ropt} = \omega_{ref} = \frac{\lambda_{opt} \hat{v}}{R} \quad (2.1)$$

Figure 2.2 shows the control scheme of WT having two control loops i.e. inner and outer loop. The inner control loop consists of electrical generator with power converters. The outer loop consists of aero turbine control which provides reference input to the inner loop. In this work we made an assumption that, the inner loop is well controlled.

### 2.3 ESTIMATION OF WIND SPEED AND CONTROL

In a wind turbine system, it is not possible to directly measure the effective wind speed. In order to estimate the exact wind speed, nonlinear estimation techniques are used. Generally, the classical iterative technique used to estimate the wind speed is Modified Newton Rapshon (MNR) method. The disadvantage of MNR is that, it requires more estimation time, so computationally inefficient. To avoid this we have applied a NN based estimation technique with different training algorithms such as Back propagation NN (BPNN), NN trained by Particle Swarm Optimization (PSO), and NN trained by Differential Evolution (DENN). Further, we verified nonlinear identification model based estimation such as HWM and NARX. Based on the estimated wind speed, the reference rotor speed ' $\omega_{ropt}$ ' is derived. Finally, the controller tracks the ' $\omega_{ropt}$ ' by adjusting the generator torque.

## 2.4 ITERATIVE METHODS FOR ESTIMATION OF EFFECTIVE WIND SPEED ESTIMATION

In a WT system the aerodynamic torque and power nonlinearly depends on the wind speed. It is necessary to have a good estimation of wind speed to ensure better control of the closed loop system. The estimation of effective wind speed is initially achieved by the iterative algorithms such as Newton Rapshon (NR) and modified Newton Rapshon (MNR).

### 2.4.1 Newton Rapshon (NR) Method

Solution of the nonlinear equation in the form  $f(x) = 0$  is achieved by NR method. In order to find the solution, one initial guess  $(x_i)$  is needed to start the iterative process and subsequently find the roots of the nonlinear equation.

Algorithm for NR method to find the root of the equation  $f(x) = 0$ , is explained below

1) Evaluate  $f'(x)$

where  $f'(x)$  is the derivative of  $f(x)$  with respect to  $x$

2) By using the initial guess of the root  $(x_i)$  estimate new value of the root i.e.  $(x_{i+1})$

3) Determine the absolute relative approximate error  $|\varepsilon_\alpha|$

$$|\varepsilon_\alpha| = \left| \frac{x_{i+1} - x_i}{x_{i+1}} \right| \times 100$$

4) Compare the absolute relative approximate error with pre specified relative error tolerance  $\varepsilon_s$ . If  $|\varepsilon_\alpha| > \varepsilon_s$  then go the step 2 otherwise stop the iteration.

#### 2.4.1.1 NR method for estimation of effective wind speed

At time instant ' $t$ ', the estimation of effective wind speed ' $\hat{v}(t)$ ' is calculated from aerodynamic torque ' $T_a$ ' and rotor speed ' $\omega_r$ ', using the NR method (Gourdin, A. and Boumahrat, M. 1995).

The NR algorithm is implemented by the following iterative mechanism.

Initialize  $\phi_{\min}$  and  $n_{\max}$ , where  $\phi_{\min}$  is the absolute relative error and  $n_{\max}$  maximum iteration.

Step 1:  $v_0 = \hat{v}(t - T_s)$

Step 2:  $\bar{v}_{n+1} = \bar{v}_n - G_n^{-1}h_n$

Step 3:  $n = n + 1$

Step 4: Stop the iteration if  $n > n_{\max}$  or  $|\bar{v}_n - \bar{v}(n-1)|/\bar{v}_n < \phi_{\min}$  else go to step 2.

Where ' $\bar{v}_n$ ' the result of the first ' $n$ ' iteration and ' $T_s$ ' is the sampling rate fixed as 1 sec. ' $G_n$ ' and ' $h_n$ ' are defined by the following expression.

$$G_n = -\rho\pi R^3 C_q(\bar{\lambda}_n) \bar{v}_n + \frac{1}{2} \rho\pi R^4 \omega_r \frac{\partial C_q(\bar{\lambda}_n)}{\partial \lambda}$$

$$h_n = T_a - \frac{1}{2} \rho\pi R^3 C_q(\bar{\lambda}_n) \bar{v}_n^2$$

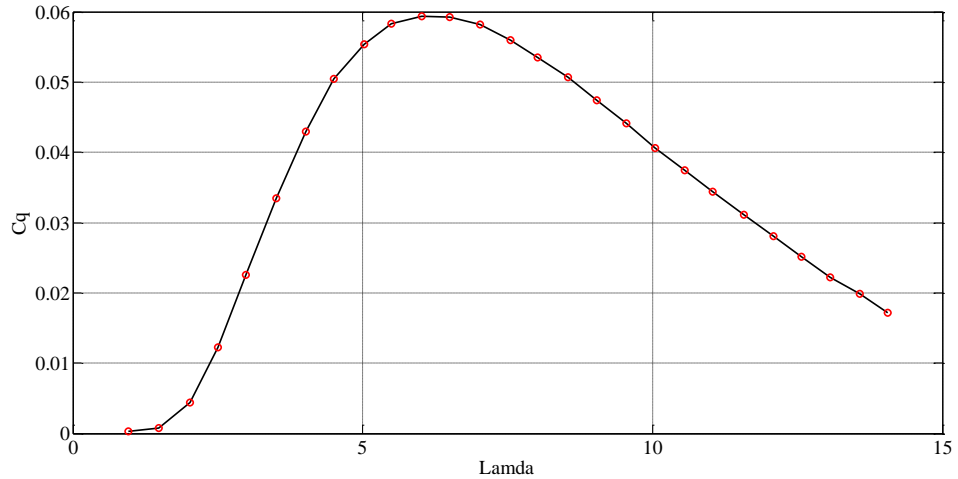


Figure 2.3:  $C_q$  vs Lamda curve.

Figure 2.3 shows the  $C_q$  vs Lamda characteristics. The torque coefficient  $C_q$  is numerically approximated by the 5<sup>th</sup> order polynomial of  $\lambda$  which is given in (2.2).

$$C_q(\lambda) = \sum_{i=0}^{n_c} a_i \lambda^i \quad \text{where } n_c = 5 \quad (2.2)$$

## 2.4.2 Modified Newton Rapshon (MNR) method

Equation (2.3) gives the aerodynamics torque expansion for WT. The estimation of effective wind speed is related to aerodynamic torque and rotor speed provided the pitch angle is at optimal value.

$$T_a = \frac{1}{2} \rho \pi R^3 \frac{C_p(\lambda)}{\lambda} v^2 \quad (2.3)$$

where

$$C_p(\lambda) = C_p(\lambda, \beta_{opt})$$

The aero dynamic power coefficient is approximated by a 5<sup>th</sup> order polynomial as given in equation (2.2). Equation (2.3) can be written as

$$F(v) = T_a - \frac{1}{2} \rho \pi R^3 C_q(\lambda) v^2 \quad (2.4)$$

$F(v)$  is the function of 'v'. The estimated wind speed can be obtained by solving (2.4) using MNR. The MNR algorithm is given by the following steps (Griffiths, D.V. and Smith, I.M. 2006). Initialize  $\varepsilon_{\min}, n_f$

$$\text{Step 1: } v_0 = \hat{v}(t - T_s)$$

$$\text{Step 2: } v_{n+1} = \bar{v}_n - \frac{F(v) \times F'(v)}{(F'(v))^2 - (F(v) \times F''(v))}$$

$$\text{Step 3: } n = n + 1$$

$$\text{Step 4: Stop if } n > n_{\max} \text{ or } \frac{|v_n - v(n-1)|}{v_n} < \varepsilon_{\min} \text{ go to step 2}$$

$$\text{Step 5: } n_f = n$$

Where  $v_n$  is the result of the first  $n$  iterations, and  $T_s$  is the sampled rate fixed here as 1 sec.

$$F'(v) = -\rho \pi R^3 C_q(\lambda) v - 0.5 \rho \pi R^3 v^2 \frac{\partial C_q(\lambda)}{\partial v}$$

$$F''(v) = -\rho \pi R^3 C_q(\lambda) + 0.5 \rho \pi R^4 \omega_r \frac{\partial C_q(\lambda)}{\partial \lambda} - 0.5 \frac{\rho \pi R^5 \omega_r}{v^2} \frac{\partial}{\partial v} \left( \frac{\partial C_q(\lambda)}{\partial \lambda} \right)$$

$$\frac{\partial C_q}{\partial v} = \frac{\partial C_q}{\partial \lambda} \frac{\partial \lambda}{\partial v}$$



$$\frac{\partial}{\partial v} \left( \frac{\partial C_q(\lambda)}{\partial \lambda} \right) = \frac{\partial}{\partial v} \left[ \frac{\partial C_q(\lambda)}{\partial \lambda} \right] \frac{\partial \lambda}{\partial \lambda} = \frac{\partial}{\partial \lambda} \left[ \frac{\partial C_q(\lambda)}{\partial \lambda} \right] \frac{\partial \lambda}{\partial v}$$

## 2.5 NEURAL NETWORK BASED EFFECTIVE WIND SPEED ESTIMATION

This section discusses about NN based estimation algorithm for wind speed. In this approach, NN is trained by different training algorithm such as Back propagation, PSO based training and DE based training. The input to the NN is aerodynamic torque and rotor speed, output is estimated wind speed. The sampled data are taken from the results of MNR which is used for training the NN. Figure 2.4 shows the fundamental block diagram for nonlinear wind speed estimator with controllers. The effective wind speed estimation is based on different nonlinear algorithms with nonlinear controllers. In this chapter, two nonlinear controllers are adapted i.e. NSSFE and NDSFE. The effective wind speed estimation is dependent on two variables i.e. measured rotor speed and aerodynamic torque. The analysis has been made using different combination of nonlinear estimator with NSSFE and NDSFE controllers.

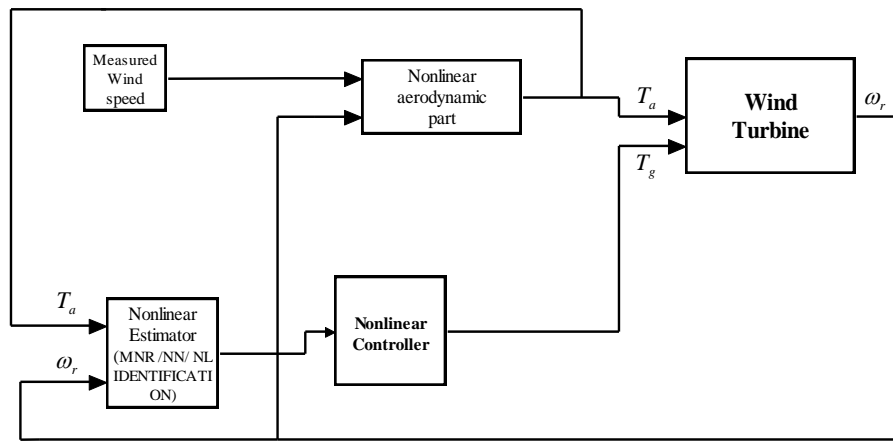


Figure 2.4: Fundamental block diagram for wind speed nonlinear estimator with controller.

### 2.5.1 Neural Networks

Artificial neural networks which are commonly referred to as ‘neural networks’, were first studied to understand and imitate the function of the human brain. They consist of highly interconnected processing elements known as neurons that have the ability to respond to input stimuli, and learn to adapt to environment. They have the advantageous

capabilities of learning from training data, recalling memorized information, and generalizing to the unseen patterns. These capabilities do show great potential in such application areas as control (Hunt, K.J. et al. 1992), signal processing (Widrow, B. and Winter, R. 1998), and pattern recognition (Bishop, C.M. 1995). There are altogether more than hundred neural network structures and algorithms proposed by people from varying standpoints (Hertz, J.A. et al. 1991). However, the most widely used neural networks are limited to just a few.

### 2.5.2 Feed Forward Artificial Neural Networks

Figure 2.5 shows the schematic of a single neuron which takes multiple inputs, sum them and then apply an activation function to the sum before putting it as output (Haykin, S. 2002) and (Jena, D. 2010). The information is stored in the weights. The weights can be positive (excitatory), zero, or negative (inhibitory).

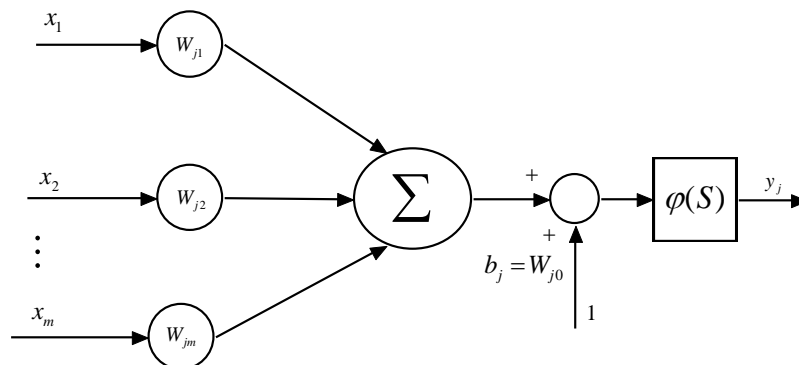


Figure 2.5: Schematic of a single neuron.

The argument ‘ $s$ ’ of the activation (or squashing) function ‘ $\phi(s)$ ’ is related to the inputs through

$$s_j = \sum_{i=0}^m W_{j,i} x_i = \sum_{i=1}^m W_{j,i} x_i + b_j \quad (2.5)$$

where ‘ $b_j$ ’ is the *threshold*; the term bias, which is considered to be an additional input of magnitude 1 and weight ‘ $b_j$ ’. ‘ $x_i$ ’ is the input to the neuron ‘ $j$ ’. The output of the neuron ‘ $j$ ’ is given by

$$y_j = \phi(s_j) \quad (2.6)$$

The commonly used activation functions ‘ $\varphi(s)$ ’ with range  $[0; 1]$  (*binary*) and  $[-1; 1]$  (*bipolar*) are given in Table 2.1. The constant  $c$  represents the slope of the sigmoid functions, and is sometimes taken to be unity. The activation function should not be linear so that the effect of multiple neurons cannot be easily combined. For a single neuron the net effect is then

$$y_j = \varphi\left(\sum_{i=0}^m W_{j,i}x_i\right) \quad (2.7)$$

### 2.5.3 Types of feed forward NN

#### *Single-layer feedforward*

This is also called a perceptron. This is a very simple network. It has one input and one output layer. Each input neurons are connected to the output layer through the connection weights. An example of single layer feed forward neural network is shown in Figure 2.6.

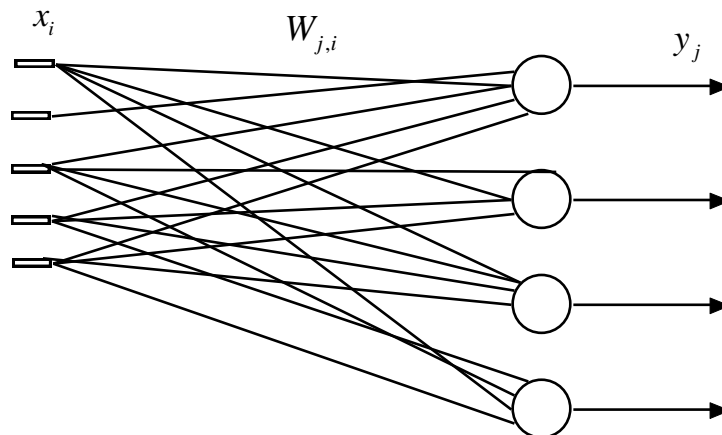


Figure 2.6: Schematic of a single layer network.

#### *Multilayer feedforward*

A two-layer network is shown in Figure 2.7. The limitation of single layer neural network leads to development of one or more hidden layers i.e. multilayer NN. It is used for wide variety of applications. The essential character of this networks is that they map similar input patterns to similar output patterns.

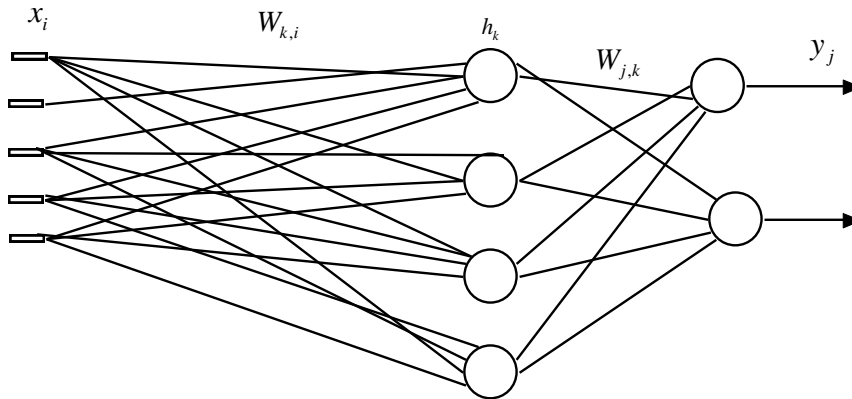


Figure 2.7: Schematic of a multilayer network.

$$\begin{aligned}
 y_j &= \varphi \left( \sum_{k=0}^m W_{j,k} h_k \right) \\
 &= \varphi \left( \sum_{k=0}^n W_{j,k} \sum_{i=0}^m \varphi(W_{k,i} x_i) \right) \\
 \varphi(s) &= 1 / [1 + \exp(-s)]
 \end{aligned} \tag{2.8}$$

Table 2.1: Commonly used activation function

Function	binary $\phi(s) =$	bipolar $\phi(s) =$
Step (Heaviside, threshold)	1 if $s > 0$ 0 if $s \leq 0$	1 if $s > 0$ 0 if $s = 0$ -1 if $s < 0$
Piecewise linear	1 if $s > 1/2$ $s + 1/2$ if $-1/2 \leq s \leq 1/2$ 0 if $s < -1/2$	1 if $s > 1/2$ $2s$ if $-1/2 \leq s \leq 1/2$ -1 if $s < -1/2$
Sigmoid	$\{1 + \exp(-cs)\}^{-1}$ (logistic)	$\tanh(cs/2)$

### 2.5.4 Learning rules

Learning in neural networks is also called “training” because the learning is achieved by adjusting the connection weights iteratively so that trained (or learned) NN’s can perform certain tasks (Jena, D. 2010) and (Haykin, S. 2002). Learning in networks may be of the *unsupervised*, *supervised*, or *reinforcement* type. Unsupervised learning is solely based on the correlations among input data. No information on “correct

output” is available for learning. In supervised learning, on the other hand, there is a set of input-outputs pairs called the training set to which the network tries to adapt itself. It is often formulated as the minimization of an error function such as the total mean square error between the actual output and the desired output summed over all available data. Reinforcement learning is a special case of supervised learning where the exact desired output is unknown. It is based only on the information of whether or not the actual output is correct. The essence of a learning algorithm is the learning rule, i.e., a weight-updating rule which determines how connection weights are changed. Examples of popular learning rules include the delta rule, the Hebbian rule, the anti-Hebbian rule, and the competitive learning rule.

Delta rule is also called the error-correction learning rule. If ‘ $y_j$ ’ is the output of a neuron ‘ $j$ ’ when the desired value should be ‘ $d_j$ ’, then the error is

$$e_j = d_j - y_j \quad (2.9)$$

The weights ‘ $W_{j,k}$ ’ leading to the neuron are modified in the following manner

$$\Delta W_{j,k} = \eta e_j h_k \quad (2.10)$$

The learning rate ‘ $\eta$ ’ is a positive value that should neither be too large to avoid runaway instability, nor too small to take a long time for convergence. One possible measure of the overall error is

$$E = \frac{1}{2} \sum (e_j)^2 \quad (2.11)$$

For simplicity, we will use the logistics activation function

$$y = \varphi(s) = \frac{1}{1 - e^{-s}} \quad (2.12)$$

This has the following derivative

$$\begin{aligned}\frac{dy}{ds} &= \frac{e^{-s}}{(1+e^{-s})^2} \\ &= y(1-y)\end{aligned}\tag{2.13}$$

According to the delta rule

$$\Delta W_{j,k} = \eta \delta_j h_k\tag{2.14}$$

where ‘ $\delta_j$ ’ is the local gradient. We will consider neurons that are in the output layer and then those that are in hidden layers. Figure 2.8 shows the flow chart for BPNN (Haykin, S. 2002) and (Jena, D. 2010).

i) Neurons in output layer: If the target output is ‘ $d_j$ ’ and the actual output is ‘ $y_j$ ’, then the error is given in equation (2.9). The squared output error summed overall output neuron is given in equation (2.11)

We can write

$$\begin{aligned}y_j &= \varphi\left(\sum_{k=0}^m W_{j,k} h_k\right) \\ &= \varphi\left(\sum_{k=0}^n W_{j,k} \sum_{i=0}^m \varphi(W_{k,i} x_i)\right) \\ h_k &= \sum_{i=0}^m \varphi(W_{k,i} x_i)\end{aligned}\tag{2.15}$$

The rate of change of ‘ $E$ ’ with respect to the weight ‘ $W_{i,j}$ ’ is

$$\begin{aligned}\left(\frac{\partial E}{\partial w_{j,k}}\right) &= \left(\frac{\partial E}{\partial e_j}\right) \left(\frac{\partial e_j}{\partial y_j}\right) \left(\frac{\partial y_j}{\partial h_k}\right) \left(\frac{\partial h_k}{\partial w_{j,k}}\right) \\ &= (e_j - 1) (\phi'(y_j)) (h_k)\end{aligned}\tag{2.16}$$

Using a gradient descent

$$\begin{aligned}\Delta W_{j,k} &= -\eta \frac{\partial E}{\partial w_{j,k}} \\ &= \eta e_j \phi'(y_j) h_k \\ &= \eta \delta_j h_k\end{aligned}\tag{2.17}$$

where  $\delta_j = e_j \cdot y_j \cdot (1 - y_j)$  is known as the error term.

ii) Neurons in hidden layer: Consider neurons 'k' in the hidden layer connected to neurons 'j' in the output layer. Then the squared error is given as

$$E = \frac{1}{2} \sum (e_k)^2 \quad (2.18)$$

Calculation of the error term for the respective hidden unit is given by

$$\delta_k^h = h_k (1 - h_k) \sum_{j=1}^l (\delta_j W_{j,k}) \quad (2.19)$$

Where 'l' is number of outputs. Update the network i.e.  $W_{k,i} = W_{k,i} + \Delta W_{k,i}$  where  $\Delta W_{k,i} = \eta \delta_k^h x_i$ . The local gradients in the hidden layer can thus be calculated from those in the output layer.

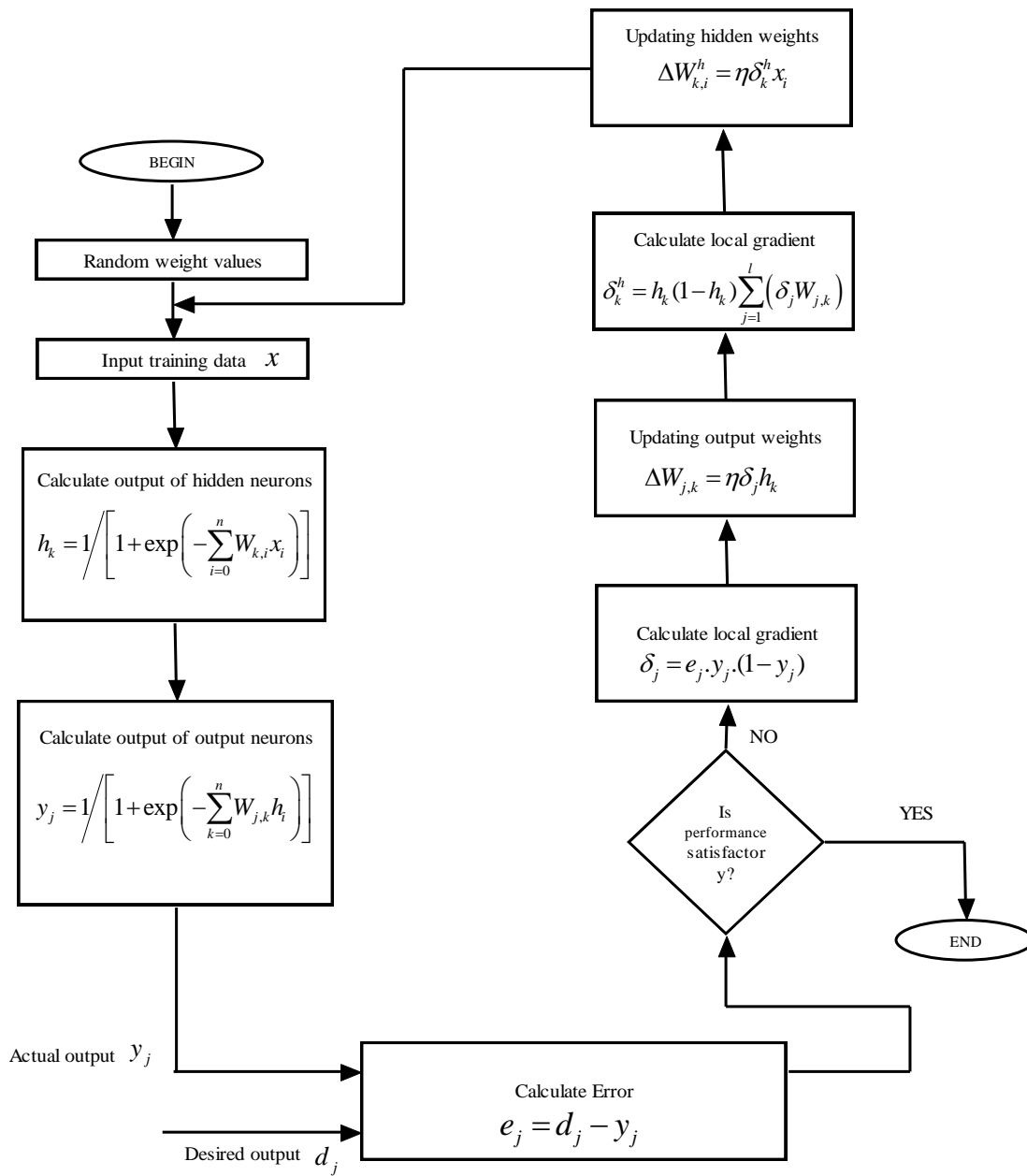


Figure 2.8: Flow chart for BPNN.

### 2.5.5 Differential Evolution NN

Price and Storn developed DE (Differential Evolution) (Storn, R. and Price, K. 1997) to be a reliable and versatile function optimizer that is also easy to use. Like all EAs, DE is a population-based optimizer that attacks the starting point problem by sampling the objective function at multiple, randomly chosen initial points. Each vector is indexed with a number from zero to number of population (i.e.  $P$ ). DE generates new points that are perturbations of existing points, but these deviations are not the samples



from a predefined probability density function, like those in other EAs. Instead, DE perturbs vectors with the scaled difference of two randomly selected population vectors. To produce the trial vector, DE adds the scaled, random vector difference to a third randomly selected population vector. In the selection stage, the trial vector competes against the population vector of the same index, finally the vector with the lower objective function value is marked as a member of the next generation. Once the last trial vector has been tested, the survivors of the competitions become parents for the next generation in the evolutionary cycle.

DE (Zelinka, I. and Lampinen, J. 1999) and (Ilonen, J. and Kamarainen, J.K. 2003) is capable of handling non-differentiable, non-linear and multimodal objective functions. It has been used to train neural networks having real and constrained integer weights. The following steps are describes the algorithm for DE.

### **Step 1: Parameter setup**

Choose the parameters of population size, the boundary constraints of optimization variables, the mutation factor ( $F$ ), the crossover rate ( $C$ ), and the stopping criterion of the maximum number of generations ( $g$ ).

### **Step 2: Initialization of the population**

Set generation  $g=0$ . Initialize a population of  $i=1, \dots, P$  individuals (real-valued  $d$  - dimensional solution vectors) with random values generated according to a uniform probability distribution in the  $d$  dimensional problem space. These initial values are chosen randomly within user's defined bounds.

### **Step 3: Evaluation of the population**

Evaluate the fitness value of each individual of the population. If the fitness satisfies predefined criteria save the result and stop, otherwise go to step 4.

#### **Step 4: Mutation operation (or differential operation)**

Mutation is an operation that adds a vector differential to a population vector of individuals. For each target vector ‘ $x_{i,g}$ ’ a mutant vector is produced using the following relation,

$$v_{i,g} = x_{r_1,g} + F(x_{r_2,g} - x_{r_3,g}) \quad (2.20)$$

In Equation (2.20), ‘ $F$ ’ is the mutation factor, which provides the amplification to the difference between two individuals ( $x_{r_2,g} - x_{r_3,g}$ ). To avoid search stagnation and it is usually taken in the range of  $[0, 1]$ , where  $i, r_1, r_2, r_3 \in \{1, 2, \dots, P\}$  are randomly chosen numbers but they must be different from each other. ‘ $P$ ’ is the number of population.

#### **Step 5: Recombination operation**

Following the mutation operation, recombination is applied to the population. Recombination is employed to generate a trial vector by replacing certain parameters of the target vector with the corresponding parameters of a randomly generated donor (mutant) vector. There are two methods of recombination in DE, namely, binomial recombination and exponential recombination. In binomial recombination, a series of binomial experiments are conducted to determine which parent contributes which parameters to the offspring. Each experiment is mediated by a crossover constant,  $C$ , ( $0 \leq C \leq 1$ ). Starting at a randomly selected parameter, the source of each parameter is determined by comparing ‘ $C$ ’ to a uniformly distributed random number from the interval  $[0, 1]$  which indicates the value of ‘ $C$ ’ can exceed the value 1. If the random number is greater than ‘ $C$ ’, the offspring gets its parameter from the target individual; otherwise, the parameter comes from the mutant individual. In exponential recombination, a single contiguous block of parameters of random size and location is copied from the mutant individual to a copy of the target individual to produce an offspring. A vector of solutions are selected randomly from the mutant individuals when  $rand_j$  ( $rand_j \in [0,1]$ , is a random number) is less than ‘ $C$ ’.

$$t_{j,i,g} = \begin{cases} v_{j,i,g} & \text{if } (rand_j \leq C) \text{ or } j = j_{rand} \\ x_{j,i,g} & \text{otherwise} \end{cases} \quad (2.21)$$

$j = 1, 2, \dots, d$ , where  $d$  is the number of parameters to be optimized.

### **Step 6: Selection operation**

Selection is the procedure of producing better offspring. If the trial vector  $t_{i,g}$  has an equal or lower value than that of its target vector,  $x_{i,g}$  it replaces the target vector in the next generation; otherwise the target retains its place in the population for at least one more generation.

$$x_{i,g+1} = \begin{cases} t_{i,g}, & \text{if } f(t_{i,g}) \leq f(x_{i,g}) \\ x_{i,g} & \text{otherwise} \end{cases} \quad (2.22)$$

Once new population is initialize, the process of mutation, recombination and selection is replaced until the optimum is located, or a specific termination criterion is satisfied, e.g., the number of generations reaches a predefined maximum  $g_{max}$ . At each generation, new vectors are generated by the combination of vectors randomly chosen from the current population (mutation). The upcoming vectors are then mixed with a predetermined target values. This operation is called recombination and produces the trial vector. Finally, the trial vectors is accepted for the next generation if it yields a optimum value of the objective function. This last operation is referred to as a selection. Figure 2.9 shows the block diagram for DE algorithm (Yang, S.H. et al. 2010).

In this work DE is applied for training neural network. DE can be applied to global searches within the weight space of a typical feed forward neural network. Output of a feed forward neural network is a function of synaptic weight ' $W$ ' and input values ' $x$ ', i.e.  $y = f(x, W)$ . In training processes, both the input vector ' $x$ ' and the output vector  $y$  and the synaptic weight are adapted to obtain appropriate functional mapping from the input ' $x$ ' to the output ' $y$ '. Generally, the adaptation can be carried out by minimizing the network function ' $E$ ' which is of the form  $E(y, f(x, W))$ . In this work

we have taken ‘ $E$ ’ as mean square error i.e.  $E = \frac{1}{N} \sum_{k=1}^N [y - f(x, W)]^2$ , where  $N$  is the number of data samples considered. The optimization goal is to minimize the objective function  $E$  by optimizing the values of the network ‘ $W$ ’ where  $W = (W_1, \dots, W_d)$ . An algorithm is developed to obtain the optimal parameters, and is analyzed for convergence aspects.

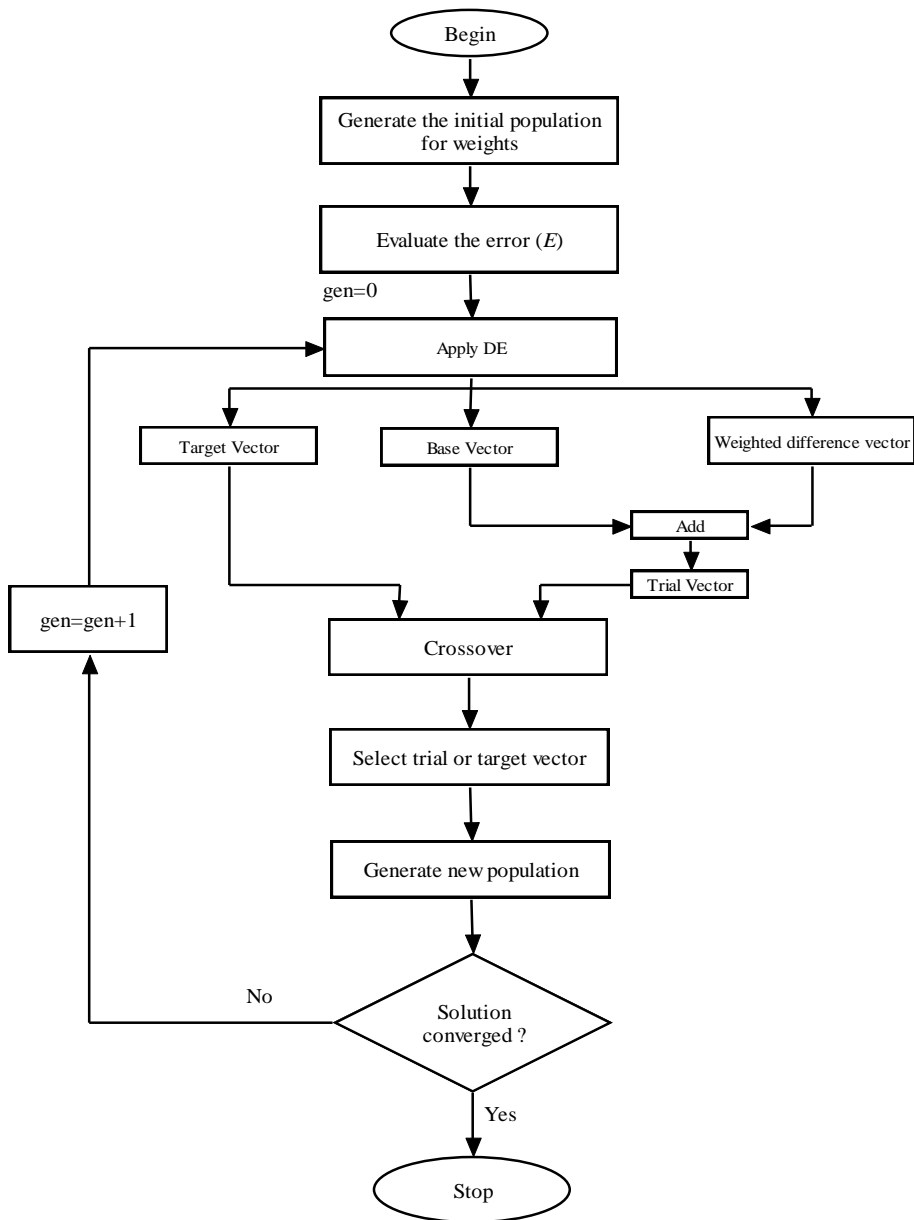


Figure 2.9: Block diagram for DENN algorithm.

### 2.5.6 Particle Swarm Optimization NN

PSO (Chen, S. et al. 2009) and (Agrawal, S. et al. 2008) is a stochastic global optimization method which is based on simulation of social behavior. As in GA and ES, PSO exploits a population of potential solutions to probe the search space. In PSO, no operators inspired by natural evolution are applied to extract a new generation of candidate solutions. Instead of mutation, PSO relies on the exchange of information between individuals, called particles, of the population, called swarm. In effect, each particle adjusts its trajectory towards its own previous best position, and towards the best previous position attained by any member of its neighborhood. In the global variant of PSO, the whole swarm is considered as the neighborhood. Thus, global sharing of information takes place and particles profit from the discoveries and previous experience of all other companions during the search for promising regions of the landscape. Several variants of PSO have been proposed up to date, following Eberhart and Kennedy who were the first to introduce this method (Ge, H.W. et al. 2007).

Initially, assuming that the search space is  $d$  dimensional, so the  $i^{\text{th}}$  particle of the swarm is represented by a  $d$  dimensional vector  $X_i = [X_{i1}, X_{i2}, \dots, X_{id}]$  and the best particle of the swarm, i.e. the particle with the lowest function value, is denoted by index  $g$ . The best previous position (i.e. the position corresponding to the best function value) of the  $i^{\text{th}}$  particle is recorded and represented as  $P_i = [P_{i1}, P_{i2}, \dots, P_{id}]$ , and the position change (velocity) of the  $i^{\text{th}}$  particle is  $V_i = [V_{i1}, V_{i2}, \dots, V_{id}]$ . The particles are manipulated according to the equation (2.23) (the superscripts denote the iteration count):

$$\begin{aligned} V_i^{k+1} &= \chi \left( \omega_a V_i^k + c_1 r_{i_1}^k (P_i^k - X_i^k) + c_2 r_{i_2}^k (P_g^k - X_i^k) \right) \\ X_i^{k+1} &= X_i^k + V_i^{k+1} \end{aligned} \tag{2.23}$$

where  $i = 1, 2, \dots, N$  and ' $N$ ' is the size of the population which is used to control and constrict velocities; ' $\omega_a$ ' is the inertia weight;  $c_1$  and  $c_2$  are two positive constants,

called the cognitive and social parameter respectively;  $r_{i_1}$  and  $r_{i_2}$  are random numbers uniformly distributed within the range [0; 1]. Equation (2.23) is used to determine the  $i^{\text{th}}$  particle's new velocity, at each iteration, as well as new position of the  $i^{\text{th}}$  particle, adding its new velocity, to its current position. The performance of each particle is measured according to a fitness function. In optimization problems, the fitness function is usually identical with the objective function under consideration. The role of the inertia weight ' $\omega_\alpha$ ' is considered important for the PSO's convergence behavior. The inertia weight is employed to control the impact of the previous history of velocities on the current velocity. A large inertia weight facilitates exploration while a small one tends to facilitate exploitation, current search area. A proper value for the inertia weight ' $\omega_\alpha$ ' provides balance between the global and local exploration ability of the swarm, and, thus results in better solutions. Figure 2.10 shows the flow chart for PSOMN (Geethanjali, M. et al. 2008). The following steps are describes the algorithm for PSO.

Step1: Initialize a population of particles with random positions and velocities on  $d$ -dimensions in the problem space.

Step2: For each particle, evaluate the desired optimization fitness function in  $d$  variables.

Step3: Compare particle's fitness evaluation with its ' $pbest$ '. If current value is better than ' $pbest$ ', then set ' $pbest$ ' equal to the current value, and ' $p_i$ ' equals to the current location ' $x_i$ ' in  $d$ -dimensional space

Step4: Identify the particle in the neighbourhood with the best success so far, and assign its index to the variable

Step5: Change the velocity and position of the particle according to equation (2.23)

Step6: Move to step 2) until a criterion is met, usually a sufficiently good fitness or a maximum number of iterations.

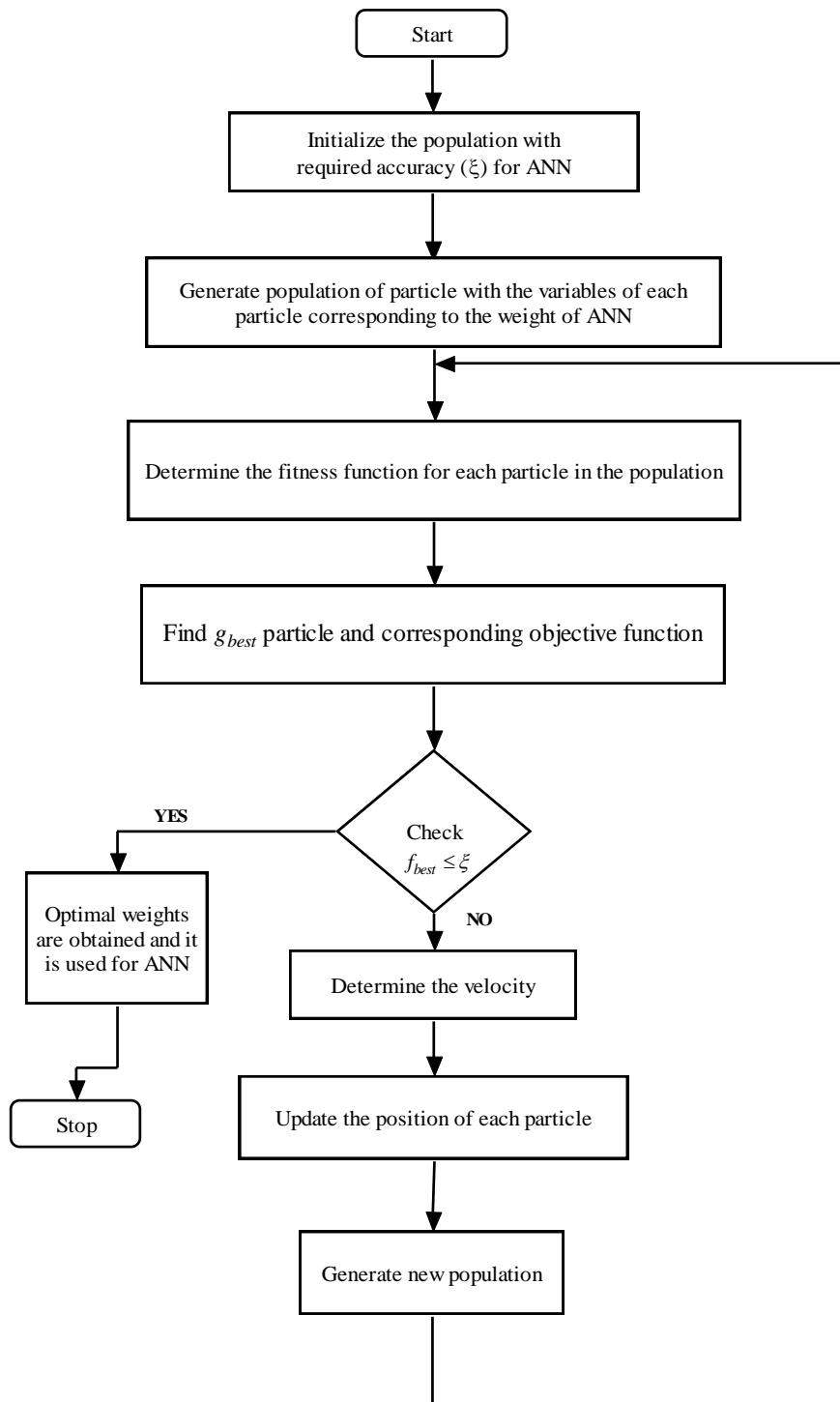


Figure 2.10: Flowchart for PSO NN.

## 2.6 NONLINEAR IDENTIFICATION BASED EFFECTIVE WIND SPEED ESTIMATION

In this method a nonlinear identification model is created for wind speed estimation. Generally we applied two fundamental nonlinear models such as Hammerstein Wiener model (HWM) and Nonlinear Autoregressive Exogenous model (NARX).

### 2.6.1 Hammerstein Wiener Model

The nonlinear dynamical model are called as block oriented model which is configured as linear dynamic block and nonlinear memoryless blocks (Gou, F. 2004). Generally the output of the system depends nonlinearly with its inputs. It is possible to determine the input output relationship by inter connecting the series of blocks linked together. In general Hammerstein model is a cascade connection of static nonlinearity followed by dynamic system. The Wiener model is ordered in way that linear and nonlinear blocks in cascade connection which is a reverse of Hammerstein model. The model where a nonlinear block is present both before and after a linear dynamical system is called as hammerstein wiener model (HWM). Figure 2.11 shows the structure of HWM.

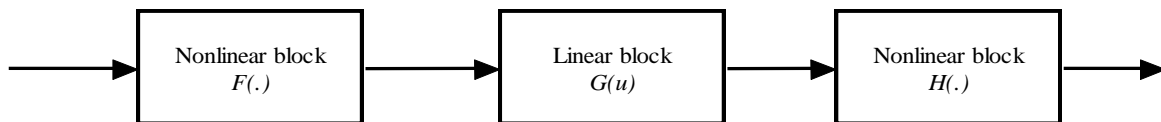


Figure 2.11: HWM structure

In WT the estimated wind speed is a nonlinear function of aerodynamic torque and rotor speed. In order to determine the nonlinear function a Hammerstein Wiener model is used, by configuring the series connection between static nonlinear block and dynamic block.

### 2.6.2 Nonlinear Autoregressive Exogenous Model

Dynamical systems are represented by the nonlinear models. The complete behaviour of the dynamical systems is achieved by nonlinear model with all operating regions. Linear models are only able to approximate the system around the operating point. Block oriented models are one of the nonlinear models, which is the inter connection of linear and nonlinear blocks. The Nonlinear Autoregressive Exogenous Model



(NARX) model structure (Jena, D. 2010) is taken as the nonlinear frame work which is in the form of

$$\begin{aligned} y(k) &= f\left(y(k-1), \dots, y(k-n_y); u(k); u(k-1), \dots, u(k-n_u)\right) \\ z(k) &= \left(y(k-1), \dots, y(k-n_y); u(k); u(k-1), \dots, u(k-n_u)\right) \end{aligned} \quad (2.24)$$

where  $k \in \mathbb{Z}^+$  is the discrete temporal variable

$u(k) \in \mathbb{R}^1$  is the input at time  $k$

$y(k) \in \mathbb{R}^1$  is the output at time  $k$

$f : \mathbb{R}^{n_y+n_u}$  is an unknown nonlinear mapping defined on an open set  $\mathbb{R}^{n_y+n_u}$

$n_y$  is an integer denote maximum lag in the output

$n_u$  is an integer denote maximum lag in the input

$z(k)$  is the regression vector in a NARX model

Since  $f$  is unknown, the objective is to use some type of network approximator  $\Gamma(z, \theta)$  to approximate  $f(z)$ . In the network,  $z \in \mathbb{R}^n$  is the input to the network and  $\theta \in \mathbb{R}^q$  is set of adjustable parameter in vector form of dimension ‘ $q$ ’. The system described in equation (2.24) can be rewritten in the form as

$$y_k = \Gamma(z(k); \theta^*) + e_1(k) \quad (2.25)$$

where  $e_1$  is the modelling error, and defined as

$$e_1(k) = f(z(k)) - \Gamma(z(k); \theta^*) \quad (2.26)$$

In order to obtain successful identification the identified system must be able to reproduce the output of the physical system for any given input. Let  $z(k)$  belongs to some compact set  $Z$  for all  $k > 0$  then we defined the parameter vector  $\theta^*$  as the optimal

value of  $\theta$  in the sense that it minimizes the distance between ' $f$ ' and ' $\Gamma$ ' for all  $z \in Z$ . The optimal parameter vector  $\theta^*$  is defined in equation (2.27)

$$\theta^* = \arg \min \left\{ \sup_{z \in Z} |f(z) - \Gamma(z; \theta)| \right\} \quad (2.27)$$

The optimization problem requires finding a vector ' $\theta \in S_I$ ', that meets chosen optimally criteria where ' $S_I$ ' is the search space. By changing the value of ' $\theta$ ' it is possible to change the input-output response of the network ' $\Gamma$ '. The search space ' $S_I$ ' is defined by a set of maximum and minimum values for each parameter. The vector ' $\theta$ ' is a ' $q$ ' dimensional domain where each element ' $\theta_i$ ' is bounded with ' $\theta_{\min}$ ' and ' $\theta_{\max}$ ', containing the upper bounds of the  $d$  parameter and the lower bounds respectively i.e.  $S_I = \{ \theta \in R^q \mid \theta_{\min,i} \leq \theta_i \leq \theta_{\max,i} \forall i = 1, 2, \dots, q \}$ . The identification process has two stages i.e. model structure selection and parameter estimation. The model structure selection involves the selection of lagged input and output terms while, the parameter estimation involves estimation of coefficient of each regressors. In this work, the effective wind speed estimation model is achieved by the NARX model. The inputs to the NARX model are rotor speed and aero dynamic torque and the output is estimated wind speed. The MATLAB based system identification tool is used for NRAX model identification.

## 2.7 RESULTS AND DISCUSSION FOR WIND SPEED ESTIMATION

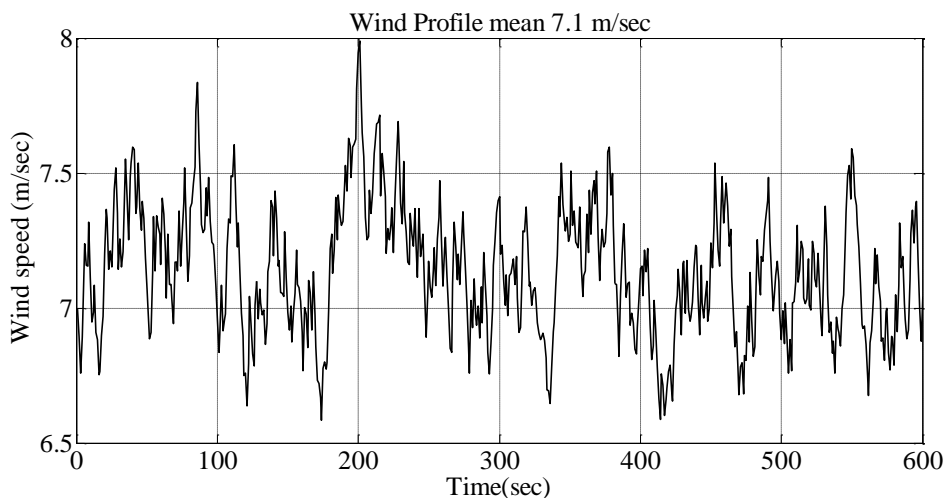


Figure 2.12: Measured hub height wind Profile.

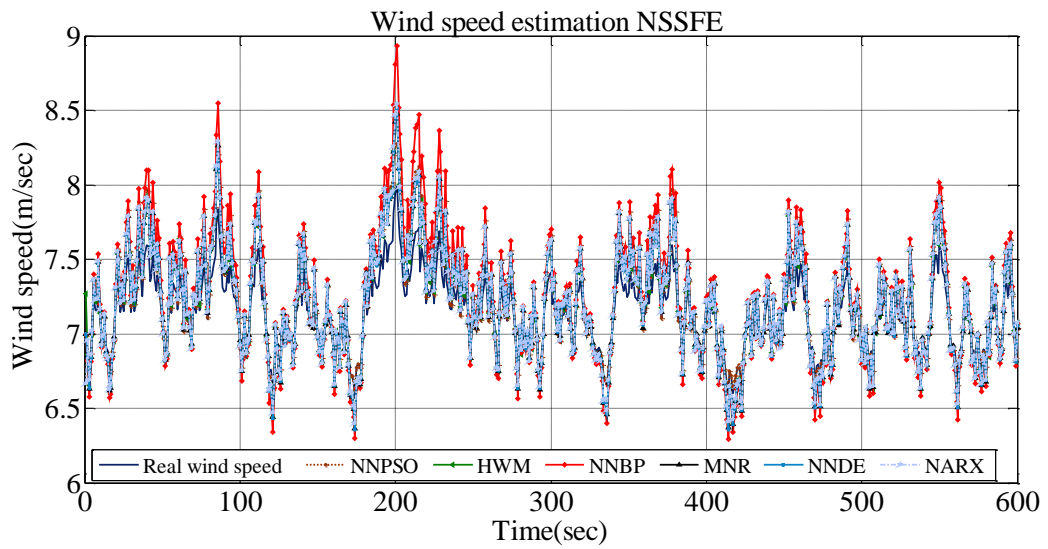


Figure 2.13: Wind speed comparisons for NSSFE.

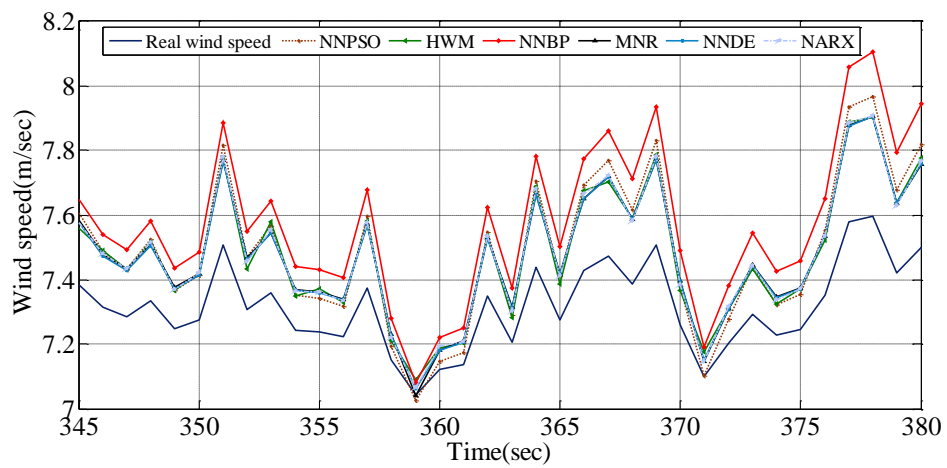


Figure 2.14: Zoomed version of Wind speed comparisons for NSSFE.

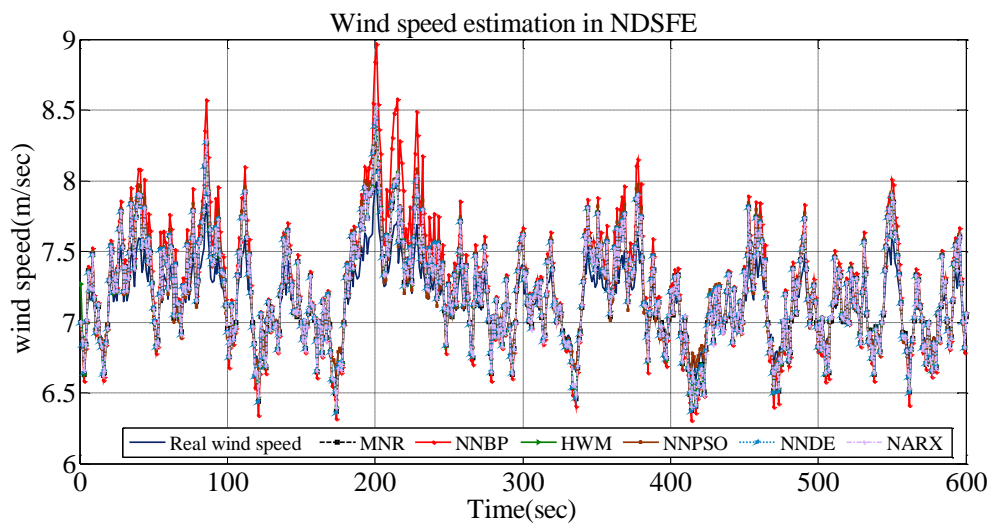


Figure 2.15: Wind speed comparisons for NDSFE.

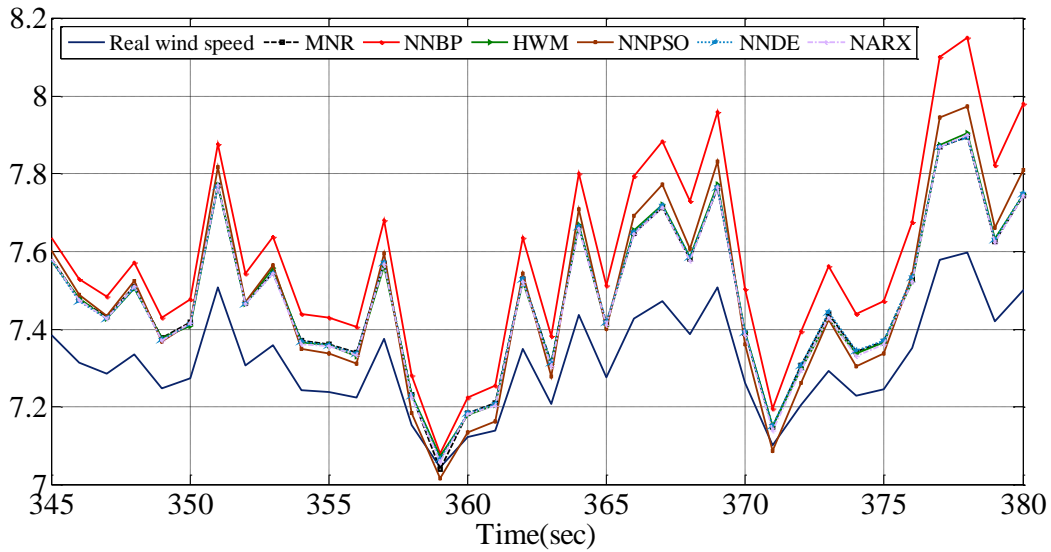


Figure 2.16: Zoomed version of Wind speed comparisons for NDSFE.

Figure 2.12 shows the measured hub height wind profile. The wind speed component is divided into two parts, which are mean wind speed and turbulent component. According to this a 10 min wind speed data set is chosen with mean wind speed of 7.1 m/sec and turbulence intensity of 25% (Kaimal turbulence spectra). This wind profile taken as the excitation of the WT and the analysis is based on energy capture and transient load reduction. Figure 2.13 and Figure 2.15 show the comparison of estimated wind speed using all the six wind speed estimators for NSSFE and NDSFE controller respectively. As all the curves in Figure 2.13 and Figure 2.15 are overlapping over the total time span, it is difficult to differentiate various estimation techniques. So, a zoomed version of the Figure 2.13 and Figure 2.15 within the time span of (340-375 sec) is shown in Figure 2.14 and Figure 2.16 respectively.

## 2.8 RESULTS AND DISCUSSION FOR NSSFE AND NDSFE CONTROLLER

The rotor speed comparison of conventional control techniques and effective wind speed based nonlinear control techniques are shown in Figure 2.17 and 2.19 for NSSFE and NDSFE respectively. Figure 2.17 contains the results of all the approaches with NSSFE control whereas, Figure 2.19 contains the results of NDSFE control. A zoomed version of the Figure 2.17 and Figure 2.19 within the time span of (320 sec - 360 sec)

has been shown in Figure 2.18 and Figure 2.20 respectively. Both the figures contain nine curves out of which one is the optimal rotor speed and rest eight are the rotor speeds obtained from different approaches. Apart from classical control techniques ATF and ISC, which do not require the knowledge of estimated wind speed the rest six are the output of nonlinear controller NSSFE and NDSFE, where the wind speed is estimated by MNR, BPNN,PSO, DENN, HWM and NARX.

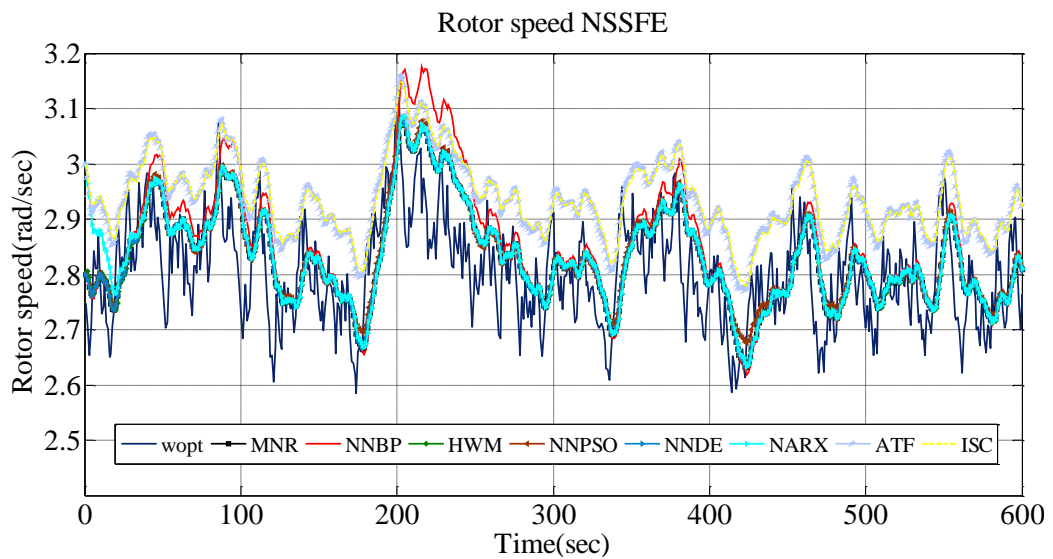


Figure 2.17: Rotor speed comparisons for NSSFE.

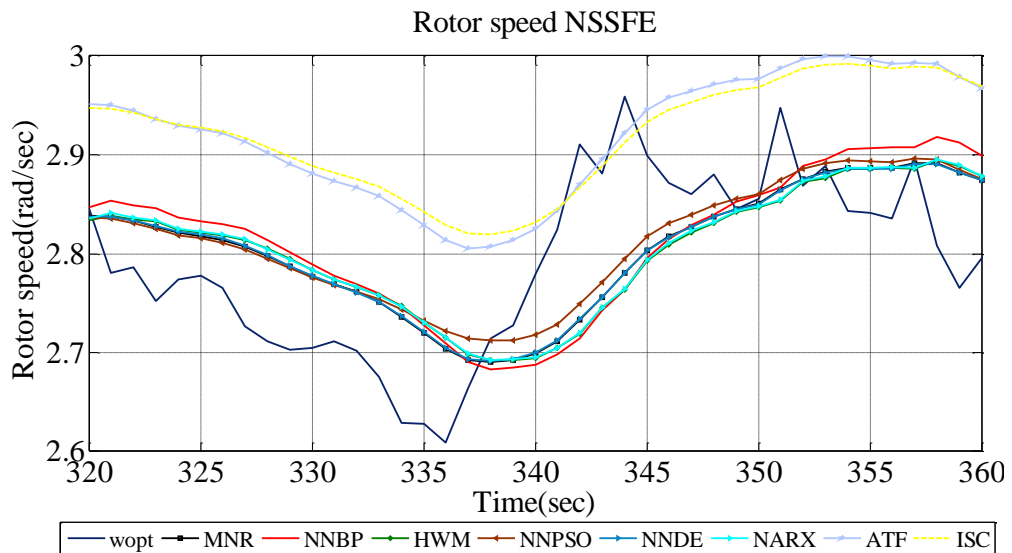


Figure 2.18: Zoomed version rotor speed comparisons for NSSFE.

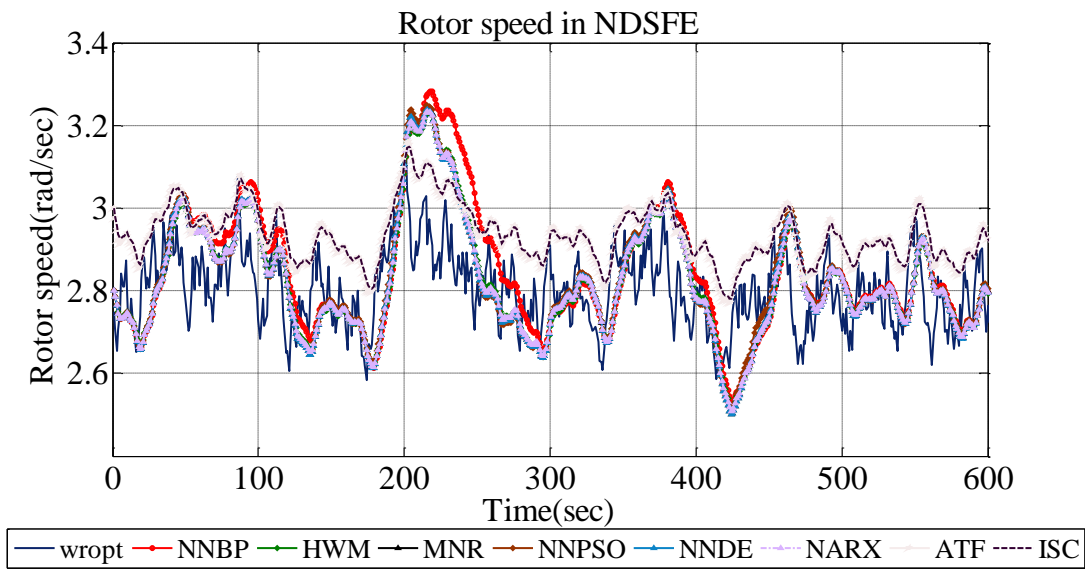


Figure 2.19: Rotor speed comparisons for NDSFE.

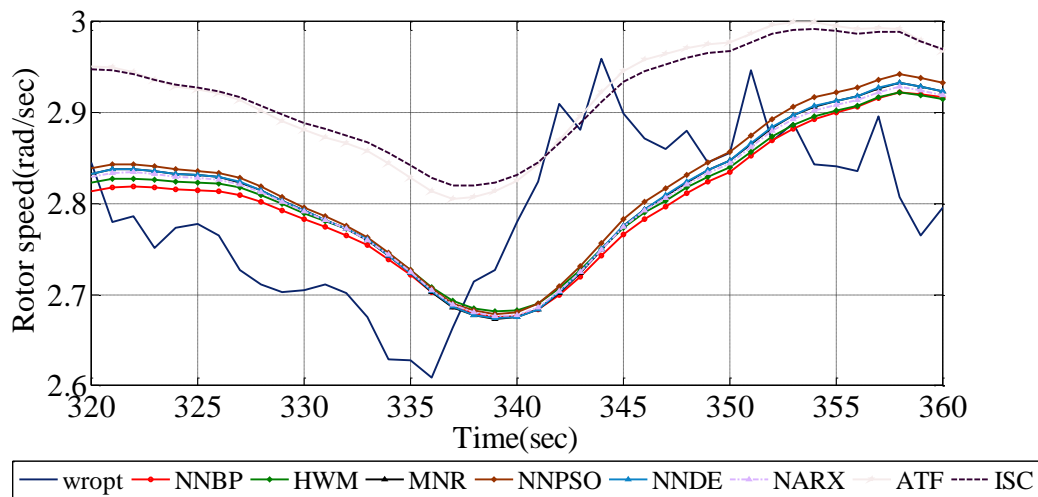


Figure 2.20: Zoomed version of rotor speed comparisons for NDSFE.

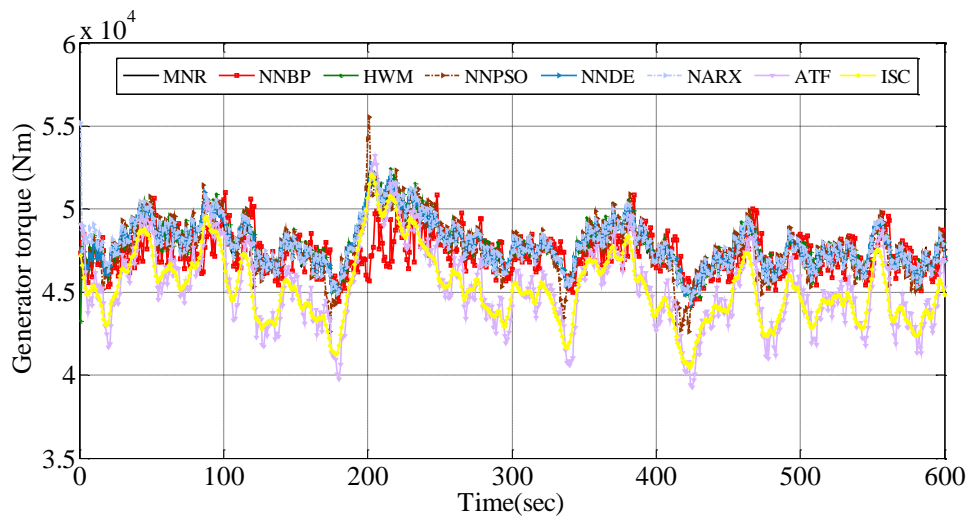


Figure 2.21: Generator torque comparisons for NSSFE.

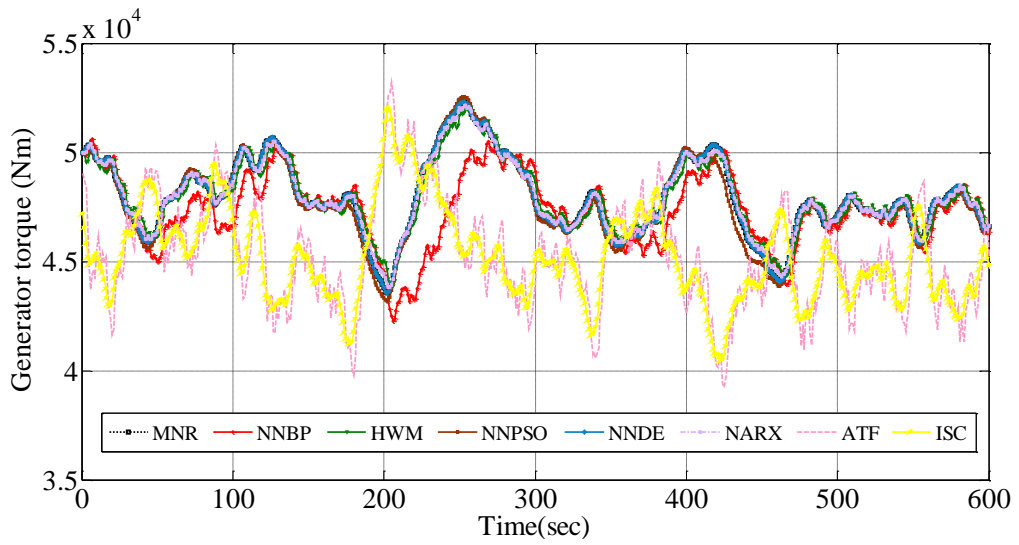


Figure 2.22: Generator torque comparisons for NDSFE.

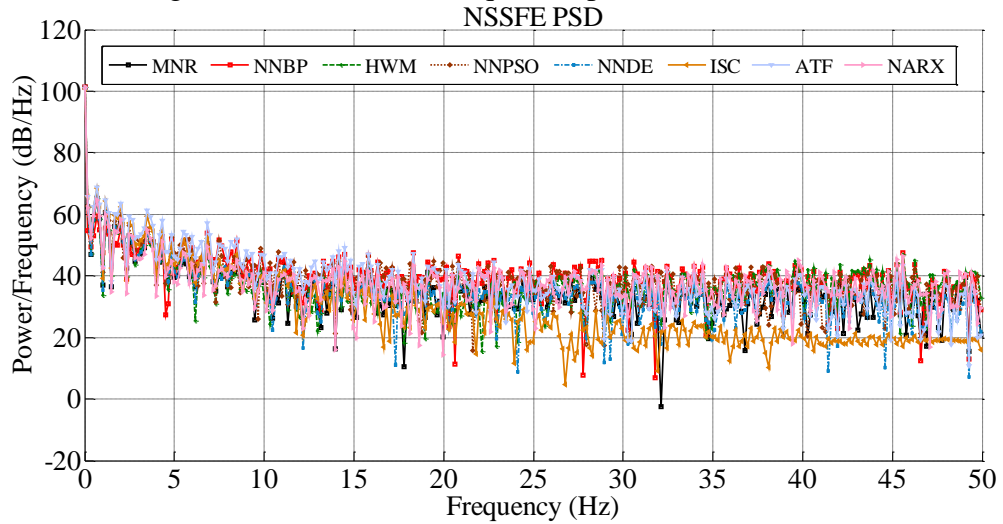


Figure 2.23: Generator torque power spectrum magnitude for NSSFE.

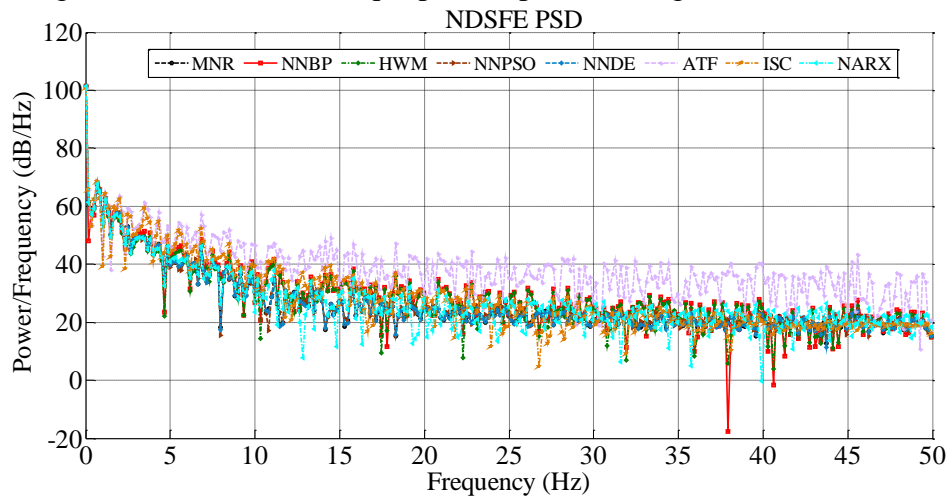


Figure 2.24: Generator torque power spectrum magnitude for NDSFE.

From Figure 2.18 it is clear that, for ATF and ISC the rotor does not track the optimal rotor speed. The rotor speed obtained by using the proposed six nonlinear estimators with NSSFE control almost tracks the optimal rotor speed. It is found that the rotor speed obtained from BPNN based estimation technique is having more tracking error compared with other techniques. From Figure 2.20, it is found that, the classical ATF and ISC control techniques are having demerit of high tracking error. The proposed technique with NDSFE control found to have less tracking error almost over the entire period except the interval between 200 sec to 260 sec. Figure 2.21 and 2.22 gives the comparison of generator torque for all the eight methods with NSSFE and NDSFE respectively. Table 2.2 and 2.3 gives the comparisons of generated torque for different estimation and control strategies. Based on the optimal aerodynamic power, the aerodynamic and electrical efficiency are evaluated, which is given in equation (2.28), where  $P_{aopt} = 0.5\rho\pi R^2 C_{Popt} v^3$  is the optimal aerodynamic power corresponding to the wind profile.

## 2.9 EVALUATION OF PERFORMANCE OF THE CONTROLLERS

The efficiency of the controllers are compared by using the following terms i.e. aerodynamic ( $\eta_{aero}$ ) and electrical ( $\eta_{elec}$ ) efficiency are given in equation (2.28). The following criteria are used to measure the performance of the controllers, under modal uncertainty and added disturbances.

1. Maximization of the power capture is evaluated by the aerodynamic and electrical efficiency which is defined in the equation (2.28).
2. The reduced oscillation on the drive train and smoothness in control torque are measured by the STD (Standard Deviation) and maximum value of control input.

$$\eta_{aero}(\%) = \frac{\int_{t_{ini}}^{t_{fin}} P_a dt}{\int_{t_{ini}}^{t_{fin}} P_{aopt} dt} \quad \text{and} \quad \eta_{elec}(\%) = \frac{\int_{t_{ini}}^{t_{fin}} P_e dt}{\int_{t_{ini}}^{t_{fin}} P_{aopt} dt} \quad (2.28)$$



The result shows that, the aerodynamic efficiency and electrical efficiency are almost same in most of the wind speed estimation based controllers. The efficiency of the controller is evaluated using (2.28) and the minimum transient load on the drive train is measured by the variance and maximum value of the generator torque. From Table 2.2 and 2.3, basing on STD of the controllers with different estimation techniques, it can be concluded that ATF, ISC and NSSFE are having more STD compared with NDSFE control which indicates more oscillation of drive train. It is seen that, for BPNN estimator with NSSFE control having maximum generator torque i.e. around 57.25 kNm that ensures maximum power capture but the STD is highest having 3.8 kNm, which indicates very high excitation to the drive train.

For making a frequency domain analysis, power spectral density (PSD) of the generator torque for all the methods including classical controllers and proposed wind speed estimation based controllers (NSSFE and NDSFE) are shown in Figure 2.23 and Figure 2.24. NSSFE and classical control techniques are having more PSD than NDSFE, which indicates NDSFE controller minimizes the excitation to the drive train. Comparing the data given in Table 2.2 and 2.3 it is found that the nonlinear time series model such as HWM and NARX for NDSFE are having minimum standard deviation which ensures minimum excitation to the drive train. From the results it can be concluded that, the intermediate optimal control (i.e. maximum energy capture with minimum transient load on the drive train) can be achieved by using a nonlinear time series estimator with NDSFE controller.

Table 2.2: Comparisons of different estimation and control strategies for classical, MNR, BPNN and PSONN.

	Classical Control		MNR		BPNN		PSONN	
	ATF	ISC	NSSFE	NDSFE	NSSFE	NDSFE	NSSFE	NDSFE
Max(kNm)	53.23	52.07	55.91	52.33	57.25	50.63	56.95	52.58
STD(kNm)	2.42	2.12	2.75	1.77	3.80	1.64	2.90	1.88
$\eta_{aero}$ (%)	91.6	91.56	93.29	93.09	92.87	92.71	93.23	93.01
$\eta_{elec}$ (%)	89.43	89.37	91.16	90.96	90.74	90.55	91.02	90.87

Table 2.3: Comparisons of different estimation and control strategies for DENN HWM and NARX.

	DENN		HWM		NARX	
	NSSFEE	NDSFE	NSSFEE	NDSFE	NSSFEE	NDSFE
Max(kNm)	55.85	53.32	56.98	52.19	56.92	52.17
STD(kNm)	2.72	1.77	3.06	1.61	3.07	1.67
$\eta_{aero}$ (%)	93.29	93.1	93.26	93.11	93.21	93.11
$\eta_{elec}$ (%)	91.15	91.13	91.16	91.33	91.37	90.98

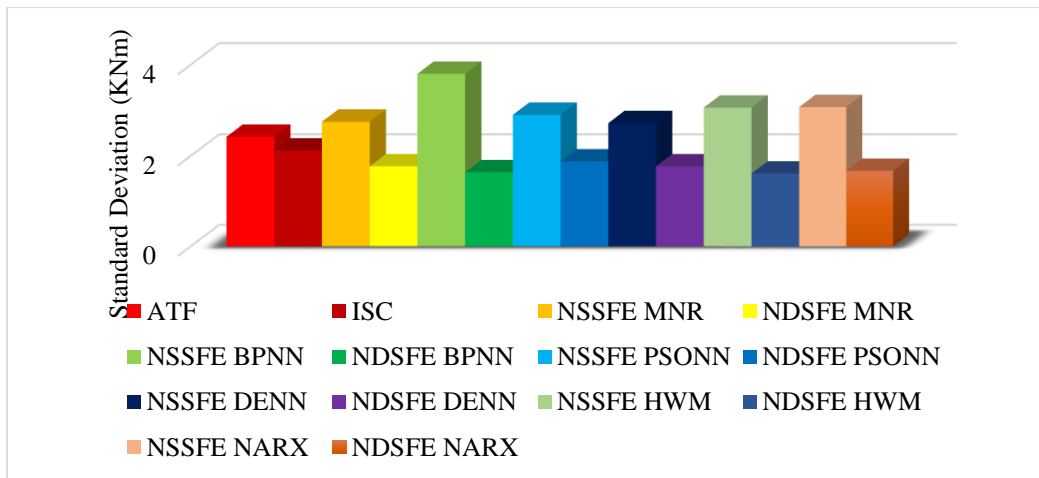


Figure 2.25: Comparison of various Standard deviations for various techniques.

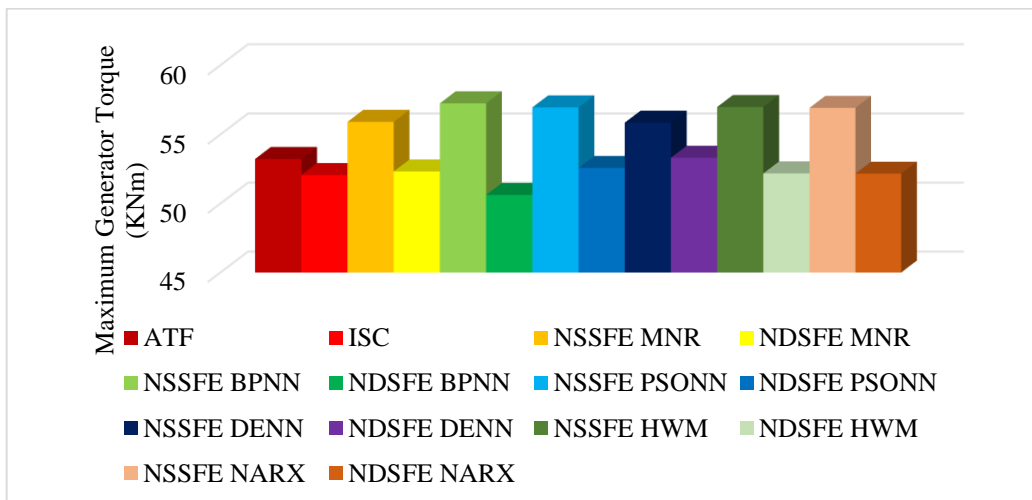


Figure 2.26: Comparison of various maximum generator torques for various techniques.

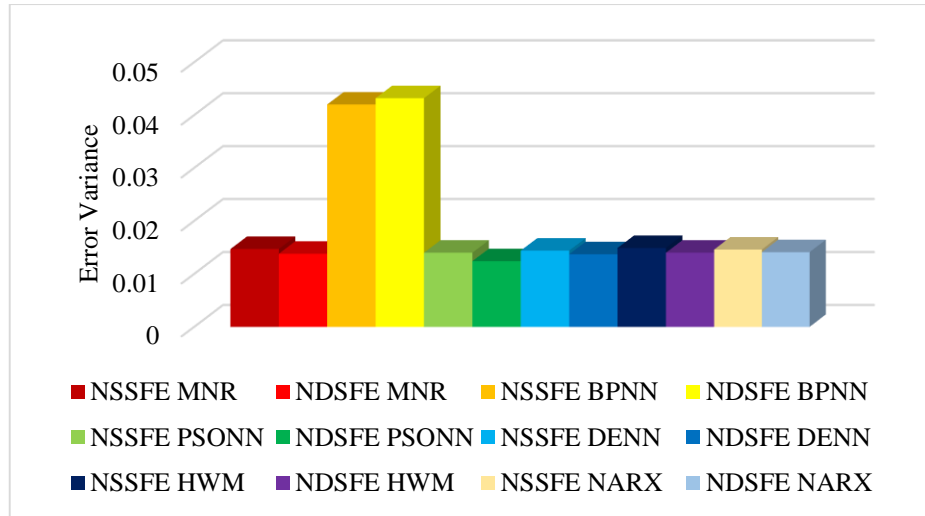


Figure 2.27: Comparison of various error variances for estimation techniques.

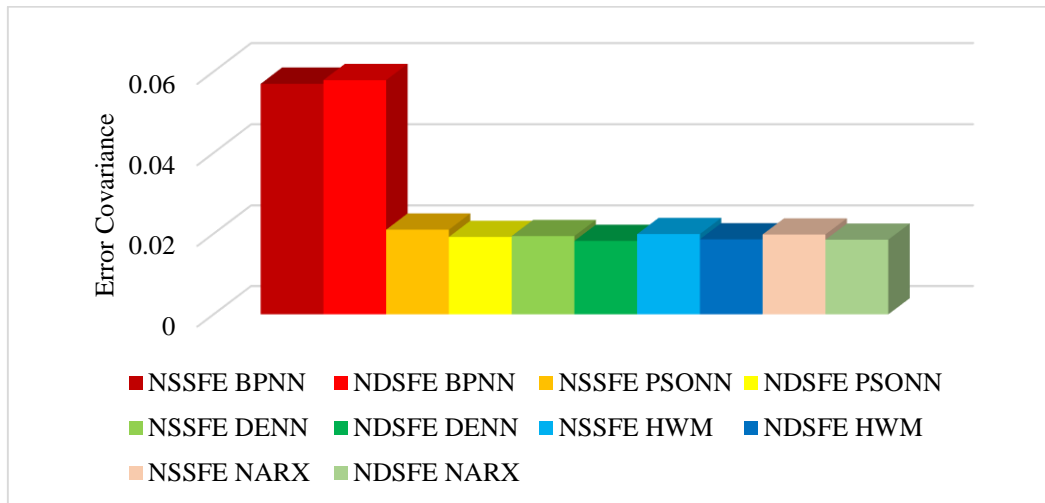


Figure 2.28: Comparison of various error co variances for estimation techniques.

Table 2.4 and 2.5 gives the comparison of estimated error and error co-variance of proposed wind speed estimation techniques. Even though, BPNN with NDSFE control have minimum standard deviation (ref Table 2.2 and 2.3) in control input but variance and error co-variance are high compared to others. For more realistic analysis of the results given in Table 2.2 to 2.4, the bar chart of STD, maximum generator torque, error variance and error co-variance values are shown in Figure 2.25 to Figure 2.28. From these figures it is clear that all NDSFE control having less STD compared to NSSFE. It is seen from Table 2.4 and 2.5 that for NSSFE with PSONN is having less variance of estimation error and DENN having less error co-variance. Similarly for NDSFE control PSONN having less estimation error, but the error co-variance is comparatively

less for DENN, HWM and NARX. Compared to BPNN based estimators, DENN and PSONN are having less variance and error co-variance which gives the advantage of using global search algorithm other than a local search algorithm. BP being a local search algorithm usually trapped by the local minimum whereas DE and PSO having the advantage of searching the global minimum by avoiding the local minimum. Also, it was found that those methods are having less variance and error co-variance compared to other nonlinear time series based estimators such as HWM and NARX. In order to select an intermediate nonlinear controller with estimator a compromise has to be made in between the values of STD, PSD, variance of error and error co-variance. Finally it is seen that the nonlinear time series based estimator with dynamic state feedback linearization controller gives the optimal energy efficiency and reduced load transients.

Table 2.4: MNR, BPNN and PSONN based nonlinear estimation models for wind speed.

Error=real-estimated wind speed	MNR		BPNN		PSONN	
	NSSFE	NDSFE	NSSFE	NDSFE	NSSFE	NDSFE
Variance	0.0147	0.0138	0.042	0.0432	0.014	0.0124
Error co-variance	0.0197	0.0184	0.057	0.0579	0.021	0.0192

Table 2.5: DENN, HWM and NARX based nonlinear estimation models for wind speed.

Error=real-estimated wind speed	DENN		HWM		NARX	
	NSSFE	NDSFE	NSSFE	NDSFE	NSSFE	NDSFE
Variance	0.0144	0.0137	0.0149	0.014	0.0146	0.0141
Error co-variance	0.0194	0.0182	0.0199	0.0186	0.0198	0.0185

Table 2.4 and 2.5 show the performance of different nonlinear wind speed estimators. Performance of different estimators are analyzed by variance and covariance of the error. Among these proposed estimators three are based on neural network based algorithm i.e. BPNN, PSONN, DENN and other two are the time series based algorithm i.e. NARX and HWM. For BPNN the neural network is trained using back propagation which is a local search algorithm. For DENN and PSONN the neural network is trained by the global search algorithm i.e. DE and PSO respectively. For NDSFE and NSSFE

control PSONN gives slight better performance compared to DENN. For all the cases BPNN was having low performance. As, back propagation algorithm is a local search method, there is a fair chance that the optimal solution obtained is not the global optimum point. As the BPNN algorithm gets trapped by local optimum solution its performance is always lower than other global search algorithm such as DENN and PSONN. So BPNN is having more variance and covariance compared to others. Among all the estimators the time series based estimators such as HWM and NARX were found to be better than neural network based estimators. The above discussed algorithms needs more training and testing data, which is obtained from conventional MNR. So, MNR based estimation is taken into consideration for proposed nonlinear control techniques.

## 2.10 PROPOSED CONTROLLERS

In this chapter the following controllers i.e. ISMC, FSMC and AFISM are proposed and tested under varying conditions of mean wind speed, disturbances and uncertainties.

### 2.10.1 Control objectives and structure of sliding mode control for single mass model

To achieve the maximum power at below rated wind speed sliding mode based torque control is proposed in (Merabet, A. et al. 2011). The main objective of this controller is to track the reference rotor speed  $\omega_{ref}$  for maximum power extraction.

For speed control a sliding surface of SMC ( $S_{smc}$ ) is defined in equation (2.29) as

$$S_{smc}(t) = \omega_r(t) - \omega_{ref}(t) \quad (2.29)$$

On differentiating equation (2.29), we obtain as:

$$\dot{S}_{smc}(t) = \dot{\omega}_r(t) - \dot{\omega}_{ref}(t) \quad (2.30)$$

Equation (2.31) obtained by substituting  $\dot{\omega}_r$  (ref equation (1.15)) in equation (2.30) as

$$\dot{S}_{smc} = \frac{1}{J_t} T_a - \frac{K_t}{J_t} \omega_r - \frac{1}{J_t} T_g - \dot{\omega}_{ref} \quad (2.31)$$

Stability of SMC is evaluated by using Lyapunov candidate function as given in equation (2.32)

$$V = \frac{1}{2} S_{smc}^2 \quad (2.32)$$

In order to get  $\dot{V}$  ; we differentitate equation (2.32)

$$\dot{V} = S_{smc} \dot{S}_{smc} = S_{smc} \left[ \frac{1}{J_t} T_a - \frac{K_t}{J_t} \omega_r - \frac{1}{J_t} T_g - \dot{\omega}_{ref} \right] \quad (2.33)$$

if  $\dot{V}$  is negative definite then equation (2.33) can be written as

$$\frac{1}{J_t} T_a - \frac{K_t}{J_t} \omega_r - \frac{1}{J_t} T_g - \dot{\omega}_{ref} \begin{cases} < 0 \text{ for } S_{smc} > 0 \\ > 0 \text{ for } S_{smc} < 0 \end{cases} \quad (2.34)$$

Stability of the controller is achieved provided the torque control satisfies equation (2.35).

$$T_g \begin{cases} < T_a - K_t \omega_r - J_t \dot{\omega}_{ref} \text{ for } S_{smc} > 0 \\ > T_a - K_t \omega_r - J_t \dot{\omega}_{ref} \text{ for } S_{smc} < 0 \end{cases} \quad (2.35)$$

Generally SMC have two parts i.e. equivalent control  $U_{eq}$  and switching control  $U_{sw}$ . Combining these two control result given equation (2.36).

$$U(t) = U_{eq}(t) + U_{sw}(t) \quad (2.36)$$

The switching control is defined in two ways and is given by following pair of equations

$$U_{sw} = k \operatorname{sign} \left( \frac{S_{smc}}{\phi} \right) \quad (2.37)$$

$$U_{sw} = k \tanh \left( \frac{S_{smc}}{\phi} \right) \quad (2.38)$$

Finally the torque control structure with signum function is given in equation (2.39)

$$T_g = T_a - K_t \omega_r - J_t \dot{\omega}_{ref} + J_t k \operatorname{sign} \left( \frac{S_{smc}}{\phi} \right) \quad (2.39)$$

The major drawback of signum function is that, it has discontinued value between +1 and -1, which introduces the chattering in control torque. So the signum function is

replaced by a smoother function i.e. hyperbolic tangent ( $\tanh$ ) with boundary layer ( $\phi$ ). Equation (2.40) gives the final control law for SMC as

$$T_g = T_a - K_t \omega_r - J_t \dot{\omega}_{ref} + J_t k \tanh\left(\frac{S_{smc}}{\phi}\right) \quad (2.40)$$

### 2.10.2 Proposed fuzzy sliding mode control for single mass model

In order to avoid the chattering, the fixed boundary layer ( $\phi$ ) in SMC has been replaced by the varying boundary layer which can be achieved by the FSMC. Where, boundary layer is a function of sliding surface ( $S_{smc}$ ) and derivative of sliding surface ( $\dot{S}_{smc}$ ) (Ben-Tzvi, P. et al. 2011).

Fixed boundary layer thickness may reduce the chattering in regulatory system but it introduces more tracking error particularly with servo systems. In this work we need to avoid the tracking error at the same time the control input to the WT should be as smooth as possible. Fuzzy Logic (FL) is used to improve the performance of the controller. Triangular membership function is used for both input and output variables. FL is used to automatically adjust the thickness of the boundary layer. The input to the fuzzy controller is sliding surface and derivative of the sliding surface and the output is boundary layer thickness. Table 2.6 gives the fuzzy rule base for the input and corresponding output. Equation (2.41) gives the final control law for FSMC.

$$T_g = T_a - K_t \omega_r - J_t \dot{\omega}_{ref} + J_t k \tanh\left(\frac{S_{smc}}{\phi_{Fuzzy}}\right) \quad (2.41)$$

Table 2.6: Fuzzy rules  $S_{smc}$ ,  $\dot{S}_{smc}$  and  $\phi_{Fuzzy}$

	$S_{smc}$				
$\dot{S}_{smc}$	NS	NB	Z	PS	PB
NS	Z	NS	PS	NS	NB
NB	NS	PS	NS	NB	Z
Z	NS	NB	NS	PB	NB
PS	PS	PB	Z	NS	NB
PB	PS	PB	NS	PB	NS

The input fuzzy variables are error and derivative of the error which are varying between the  $\{-0.4, 0.4\}$  and  $\{-0.04, 0.04\}$  respectively. The output variable is boundary layer thickness which is varying between  $\{0.1, 0.6\}$ . The fuzzy variables are defined in the rule base as  $\{NS$  (Negative Small),  $NB$  (Negative Big),  $Z$  (Zero),  $PS$  (Positive Small) and  $PB$  (Positive Big) $\}$ . From the conventional SMC, the knowledge of the boundary layer thickness is obtained. With this knowledge, the fuzzy rules are initially derived by trial and error method. After obtaining the rule base, the simulation is carried out and it is tuned appropriately as per the control objectives. Finally, the derived rule base is given in Table 2.6.

### 2.10.3 Simulation Results for single mass model

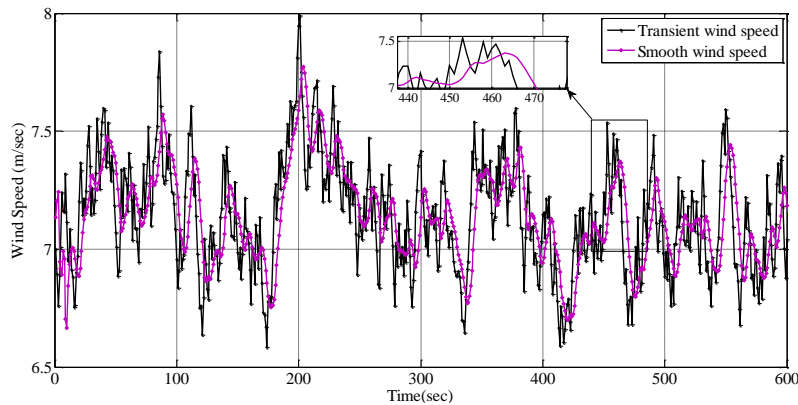


Figure 2.29: Test wind profile of mean 7 m/s.

Initially single mass mathematical model of the WT is considered and the test wind profile is developed with full field turbulent wind. Figure 2.29 shows high wind speed variation with mean wind speed of 7 m/sec. Generally the wind speed is derived from two components i.e. mean wind speed and turbulent component. A 10 min wind data is chosen for this simulation study which is generated by a class A Kaimal spectrum with turbulent intensity of 25%. From this figure it is clear that two different wind speeds are used with different turbulence intensity. Transient and smooth wind speeds are having 10 min wind data with the STD of 0.25 m/sec and 0.19m/sec respectively.

Figure 2.30, shows the rotor speed comparison for proposed FSMC as well as conventional techniques. It is found that both the conventional controllers ATF and ISC are having more tracking error in optimal rotor speed. ATF is generally considered as a proportional controller which always gives the steady state error. Without integral action it not possible to track the sudden wind speed changes. In ISC, during the fast



transient in wind speed, it introduces more power loss and unable to track the optimal rotor speed. The proposed FSMC is almost tracking the optimal rotor speed as compared to other conventional controllers i.e. ATF and ISC. It is clear that, for conventional techniques the obtained rotor speed is unable to track the optimal rotor speed due to inherent disadvantages as explained above.

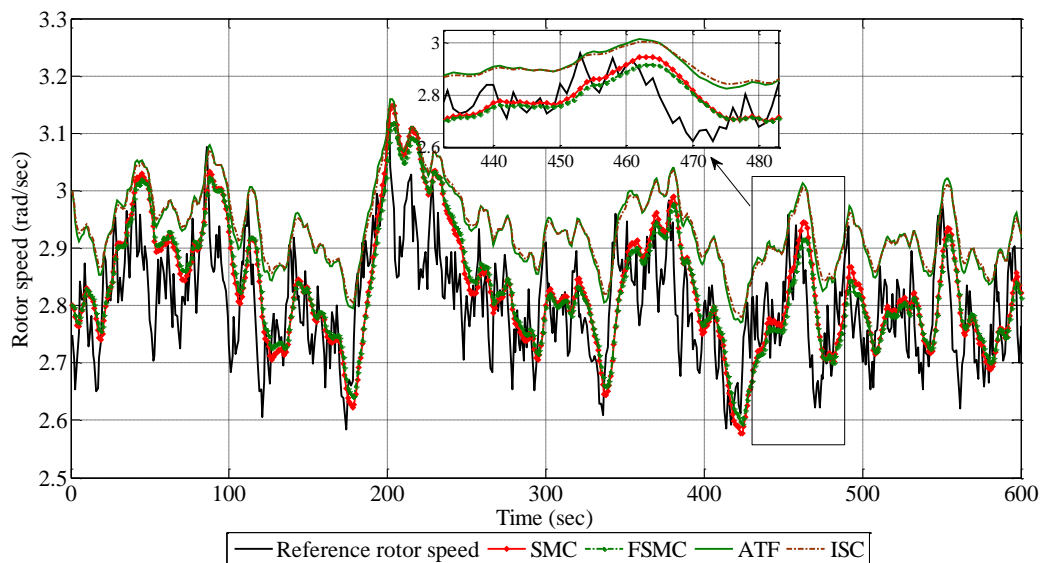


Figure 2.30 : Rotor speed comparisons of ATF, ISC, SMC and FSMC.

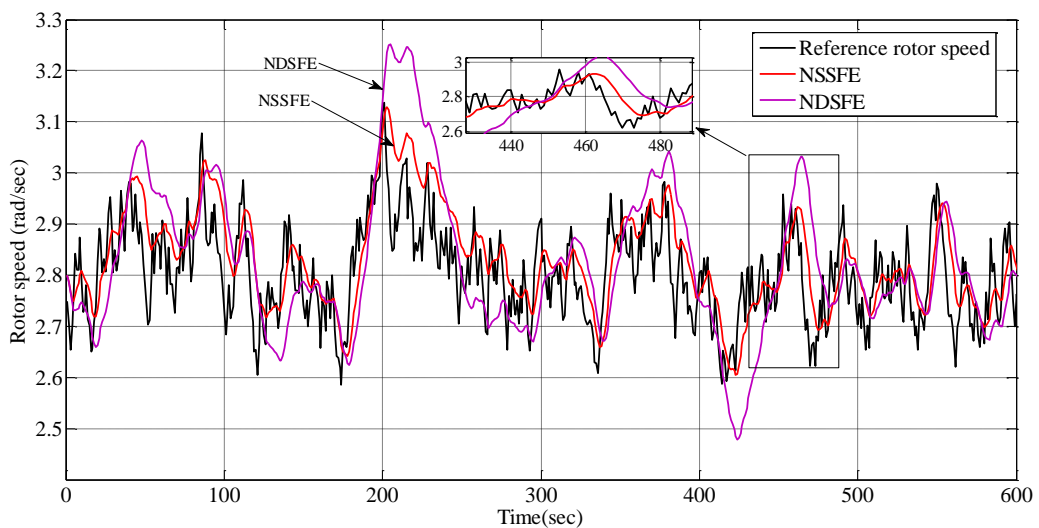


Figure 2.31: Rotor speed comparisons for NSSFE and NDSFE.

Figure 2.31 shows the rotor speed comparison for NSSFE and NDSFE. From this figure it is evident that NSSFE is almost tracking the optimal rotor speed compared with

NDSFE. NDSFE is unable to track the optimal rotor speed in the time interval of 200 sec to 250 sec and 410 sec to 440 sec which is due to the sub-optimal error dynamics coefficient i.e.  $b_o$  and  $b_l$  setting, in NDSFE control.

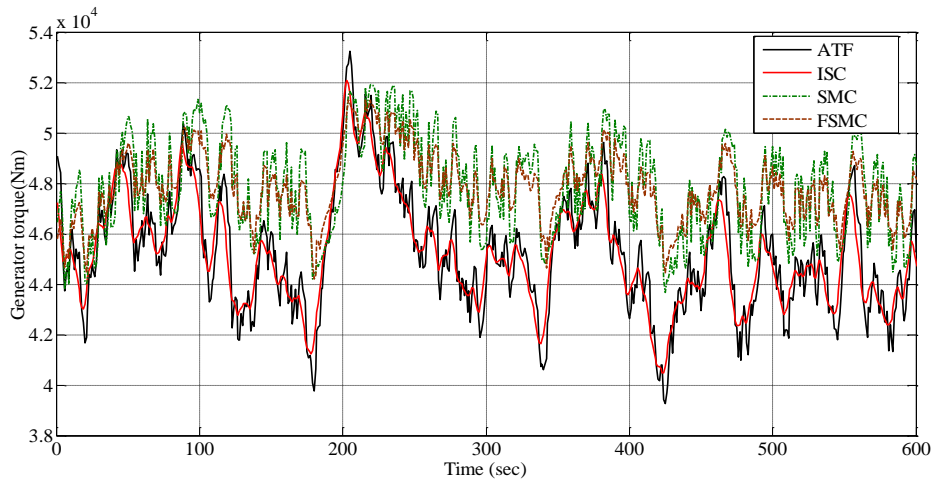


Figure 2.32: Generator torque comparisons of different control strategy.

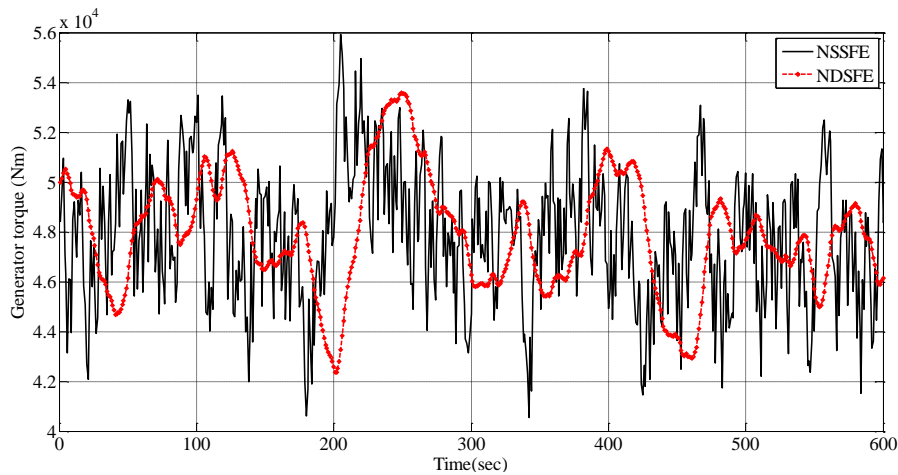


Figure 2.33: Generator torque comparisons NSSFE and NDSFE.

Figure 2.32 and Figure 2.33 show the generator torque comparison for conventional and other nonlinear controllers. From these figures it is clear that NSSFE having more torque variation than NDSFE. However, in Figure 2.31 the tracking error in rotor speed is less for NSSFE. As tracking error is related to maximum power capture, and variation in load torque is dependent on the transient load in drive train, a trade-off has to be made between the tracking error and variation of generator torque.

As shown in Table 2.7 NSSFE is having the highest value of the generator torque (55.91 kNm) which ensures the maximum power capture among all other controllers. At the same time, it is having more transient load on drive train because the STD of ' $T_g$ ' is also having the highest value i.e. 2.753 kNm. For FSMC, the STD of ' $T_g$ ' is lowest compared to the all the controllers i.e. 1.387 kNm, which indicates less transient load on drive train. As both the objectives cannot be achieved simultaneously a compromise has to be made between them. So, for good control a trade-off is to be maintained between the maximum power capture and oscillation in drive train. Analysis of Table 2.7 gives a complete comparison on the results obtained for different controllers which clears that FSMC having almost same electrical and aerodynamic efficiency (i.e. 91.12% and 93.24%) with the NSSFE (i.e. 91.16% and 93.29%), which is highest among all controller. But at the same time, FSMC having lowest standard deviation of control input which ensures reduced transient load on drive train. From Table 2.7 it is clear that FSMC is having better performance in terms of the efficiency and relative variation in generator torque, compared to its counterpart i.e. SMC. In order to analyze the robustness of the controllers a parameter uncertainty is introduced in the WT system parameters i.e. turbine inertia ' $J_t$ ' and turbine damping ' $K_t$ '. The WT parameter is varied between +30% of its nominal values. Table 2.8 gives the controller performance with the presence of +30% parameter uncertainty. From this table it is found that for the proposed FSMC the STD of ' $T_g$ ' is lowest i.e. 2.571 kNm with acceptable tracking error.

Table 2.7 : Different control strategy with high transient wind speed.

Control Strategy	ATF	ISC	NSSFE	NDSFE	SMC	FSMC
Max( $T_g$ )kNm	53.23	52.07	55.91	53.58	51.92	51.31
STD( $T_g$ ) kNm	2.42	2.12	2.753	2.315	1.928	1.387
$\eta_{elec}$ (%)	89.43	89.37	91.16	90.93	91.10	91.12
$\eta_{aero}$ (%)	91.6	91.56	93.29	93.07	93.23	93.24
Relative variation $T_g$ (%)	30.41	25.30	32.08	23.43	17.25	14.83

Table 2.8: Different control strategy with +30% parameter uncertainty.

Control Strategy	NSSF	NDSFE	SMC	FSMC
STD( $T_g$ ) kNm	4.348	3.186	3.471	2.571
$\eta_{elec}$ (%)	90.53	90.28	90.46	90.47
$\eta_{aero}$ (%)	93.29	93.03	93.23	93.24
Relative variation $T_g$ (%)	48.42	32.98	29.36	26.31

For SMC the change in STD of ' $T_g$ ' varies with a higher margin i.e. in the interval [0 to 1.543] (3.471-1.928=1.543 kNm). Whereas, for FSMC this margin comes in the interval [0 to 1.193] (2.571-1.378=1.193 kNm). The electrical and aerodynamic efficiency for both the SMC and FSMC are found to be almost same but the percentage of the relative variation in the generated torque is minimum for FSMC i.e. at 26.31%. This indicates that, for the desired objective of maximum power capture and less oscillation on the drive train, FSMC is more robust than SMC.

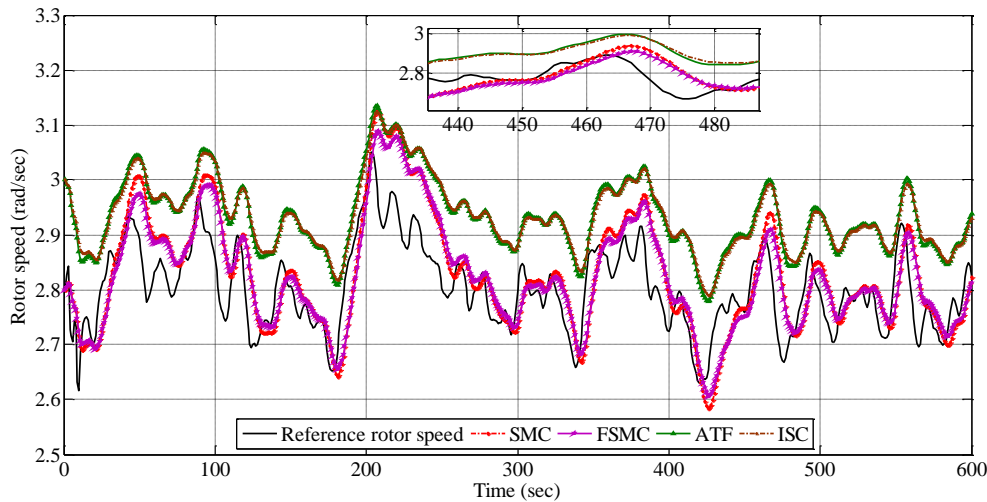


Figure 2.34: Rotor speed comparisons of different control strategy.

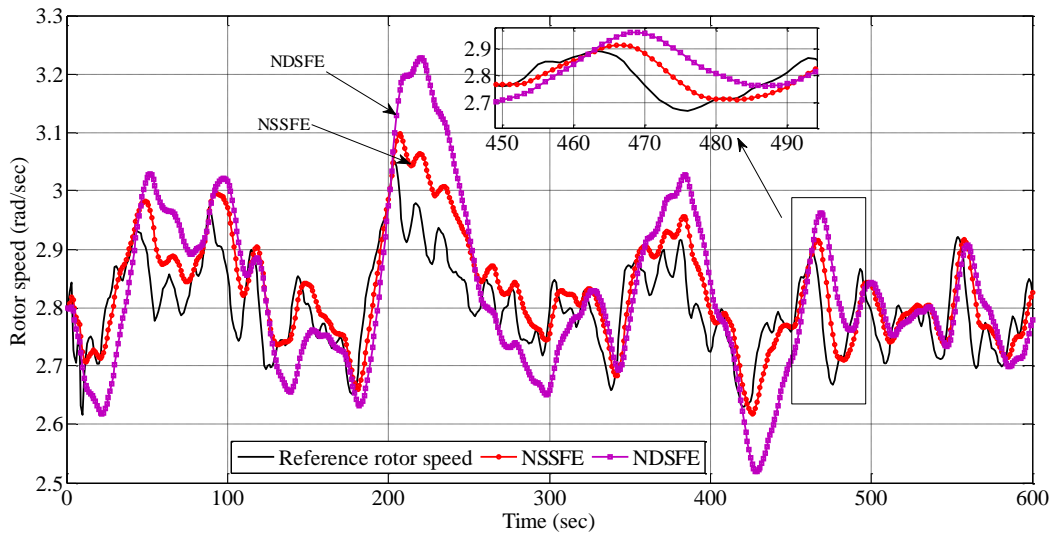


Figure 2.35: Rotor speed comparisons for NSSFE and NDSFE.

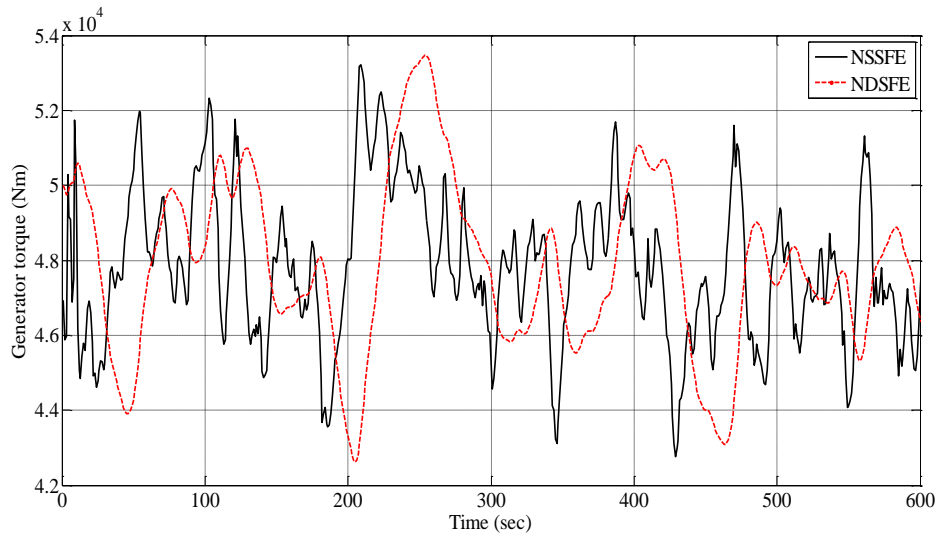


Figure 2.36: Generator torque comparisons NSSFE and NDSFE.

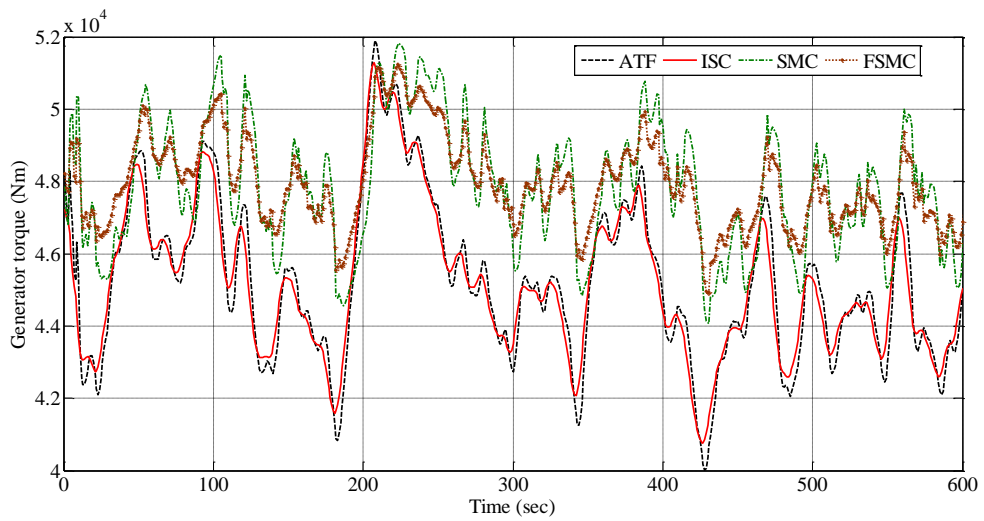


Figure 2.37: Generator torque comparisons of different control strategy.

Figure 2.34 to Figure 2.37 show the comparison of results for the above discussed controllers with a smooth or slow varying wind speed. For a smooth wind speed NDSFE was found to be little better in tracking the optimal rotor speed compared to high varying wind speed, which can be analyzed from the Figure 2.31 and Figure 2.35. In Figure 2.35 it is clear that for smooth wind speed, NDSFE gives more error in optimal rotor speed during the interval of 210 sec to 250 sec and 410 sec to 440 sec. Figure 2.34 shows the rotor speed comparison for FSMC as well as conventional techniques. It clearly reveals that FSMC is able to track the optimal rotor speed without any turbulence.

Figure 2.36 and Figure 2.37 show the generator torque comparisons for different control strategy. All the controller performances are given in Table 2.9. Results in Table 2.9 can be analyzed in the same way as Table 2.7 and it is found that FSMC is having the lowest standard deviation with almost same or better electrical and aerodynamic efficiency compared to all other controllers. This ensures the suitability of FSMC over the other controllers with the objective of maximum power capture and minimum mechanical stress on the drive train.

The robustness of the controllers for smooth varying wind speed is analyzed with the help of parameter uncertainty introduced in the wind turbine system parameter i.e. ' $J_t$ ' and ' $K_t$ '. Table 2.10 indicates the controller performance with +30% parameter uncertainty. From Table 2.9 and Table 2.10 it is evident that the change in STD of generator torque for FSMC with +30% uncertainty varies from 0 to 0.775 (2.037-1.262) whereas for SMC it varies from 0 to 1.088 (2.873-1.785). Nevertheless, the variation range for STD of ' $T_g$ ' for NSSFE is found to be lowest i.e. from 0 to 0.492 (2.495-2.003). Although, its other performances are not comparable with the proposed FSMC.

Table 2.9: Different control strategy with filtered wind speed.

Control strategy	ATF	ISC	NSSF	NDSFE	SMC	FSMC
STD( $T_g$ ) kNm	2.226	2.048	2.003	1.785	1.77	1.262
$\eta_{elec}$ (%)	89.41	89.39	91.16	91.02	91.14	91.22
$\eta_{aero}$ (%)	91.64	91.62	93.36	93.16	93.34	93.4
Relative variation $T_g$ (%)	26.27	23.87	21.88	17.36	16.18	13.19

Table 2.10: Different control strategy with +30% parameter uncertainty.

Control Strategy	NSSFEE	NDSFE	SMC	FSMC
STD( $T_g$ ) kNm	2.911	2.495	2.873	2.037
$\eta_{elec}$ (%)	90.50	90.36	90.48	90.56
$\eta_{aero}$ (%)	93.36	93.12	93.34	93.38
Relative variation $T_g$ (%)	31.18	25.18	24.76	19.01

The adaptability of the controller is analyzed with different mean wind speed profiles at below rated wind speed. Table 2.11 and 2.12 show the performance of all the controllers with a mean wind speed of 8 m/sec and 8.5 m/sec respectively. The results shown in Table 2.11 and 2.12 ensure the suitability of proposed FSMC among other conventional linear and nonlinear controllers that achieves the similar performance even though the mean wind speed changes. From the analysis it is found that, maximum generator torque increases with increase in mean wind speed which indicates the increase in power captured.

Table 2.11: Different control strategy with mean wind speed of 8 m/sec

Control strategy	ATF	ISC	NSSFEE	NDSFE	SMC	FSMC
Max( $T_g$ ) kNm	67.18	67.12	70.19	66.83	67.04	67.94
STD( $T_g$ ) kNm	2.719	2.621	2.493	1.856	1.644	1.461
$\eta_{elec}$ (%)	89.42	89.39	91.42	91.16	91.45	91.54
$\eta_{aero}$ (%)	91.66	91.65	93.38	93.14	93.38	93.49
Relative variation $T_g$ (%)	30.71	28.31	22.61	13.47	15.65	13.82

Table 2.12: Different control strategy with mean wind speed of 8.5 m/sec

Control strategy	ATF	ISC	NSSFEE	NDSFE	SMC	FSMC
Max( $T_g$ ) kNm	73.59	73.65	77.02	73.82	74.69	75.16
STD( $T_g$ ) kNm	2.785	2.742	2.418	1.777	1.424	1.337
$\eta_{elec}$ (%)	89.56	89.53	91.81	91.61	91.79	91.83
$\eta_{aero}$ (%)	91.65	91.65	93.62	93.42	93.58	93.62
Relative variation $T_g$ (%)	26.09	25.70	20.16	12.32	12.56	11.08

Table 2.13: Mean error in rotor speed for different control strategy with different wind profile

Mean Wind speed	NSSFEE	NDSFE	SMC	FSMC
7 m/sec	0.0630	0.0977	0.0714	0.0700
8 m/sec	0.0635	0.0973	0.0693	0.0674
8.5 m/sec	0.0592	0.0947	0.0678	0.0673

Table 2.13 shows the mean error in rotor speed for different control strategy with different wind profile. This table indicates that NSSFE having lowest error in rotor speed but it creates a large variation in generator torque. So that, as seen from Table 2.11 and Table 2.12 an adjustment has to be made between the tracking error dynamics and transient load on drive train. Exact tracking introduces the high turbulence action in control input and vice versa hence, an understanding has been considered between acceptable tracking error and low turbulence action in control input. From the Table 2.12 and 2.13 it is concluded that, compared with other nonlinear controllers FSMC having acceptable tracking error with smooth turbulence on control input for different wind profile.

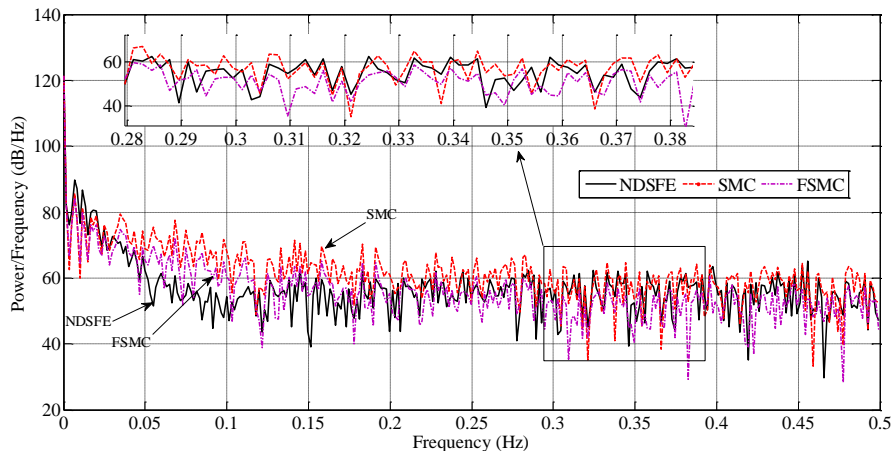


Figure 2.38: Generator torque PSD for SMC and FSMC.

The frequency analysis of the drive train is analyzed by PSD of the generator torque, shown in Figure 2.38. FSMC curve is completely below the SMC curve which ensures less excitation on the drive train. In order to analyze the adaptability of the controller different types of disturbances are given to the WT system.

#### 2.10.4 Integral sliding mode control for single mass model

The steps for designing the equivalent control in ISMC.

- 1) The characteristics of the controller is defined by the user defined sliding surface.
- 2) Required number of sliding surface is taken until the control input is appeared. The equivalent control law is derived by equating the derivative of the sliding surface to zero.



- 3) The switching control law is defined by the user and it is used to keep the system state in equilibrium point.
- 4) The summation of two control strategies is gives the final control input.

To improve the sliding surface and overcome the steady state error, the integral action is included in the sliding surface (Eker, I. and Akinal, S.A 2005). An integral sliding surface ( $S_{ismc}$ ) is defined as

$$S_{ismc}(t) = \left( \lambda + \frac{d}{dt} \right)^{n-1} e(t) + k_i \int_0^{\infty} e(t) dt \quad (2.42)$$

where  $k_i$  is the integral gain.

For first order ( $n=1$ ), the sliding surface is modified as

$$S_{ismc}(t) = e(t) + k_i \int_0^{\infty} e(t) dt \quad (2.43)$$

The major objective of the controller is that, the tracking error  $e(t)$  should converge to zero. Equation (2.44) is obtained by taking the time derivative of the (2.43)

$$\dot{S}_{ismc}(t) = \dot{e}(t) + k_i e(t) \quad (2.44)$$

The stability of the controller is determined by using the Lyapunov candidate function given in (2.45) with  $V(0)=0$  and  $V(t)>0$  for for  $S \neq 0$ .

$$V = \frac{1}{2} S_{ismc}^2 \quad (2.45)$$

Equation (2.46) is derived by taking the time derivative of equation (2.45)

$$\dot{V} = \dot{S}_{ismc} S_{ismc} = S_{ismc} \left[ \frac{1}{J_t} T_a - \frac{K_t}{J_t} \omega_r - \frac{1}{J_t} T_g - \dot{\omega}_{ref} + k_i e(t) \right] \quad (2.46)$$

If  $\dot{V}$  is negative definite then equation (2.46) can be written as given in equation (2.47)

$$\frac{1}{J_t} T_a - \frac{K_t}{J_t} \omega_r - \frac{1}{J_t} T_g - \dot{\omega}_{ref} + k_i e(t) \begin{cases} < 0 \text{ for } S_{ismc} > 0 \\ > 0 \text{ for } S_{ismc} < 0 \end{cases} \quad (2.47)$$

Stability of the controller is achieved provided the torque control satisfies equation (2.48)

$$T_g \left\{ \begin{array}{l} \frac{1}{J_t} T_a - \frac{K_t}{J_t} \omega_r - \frac{1}{J_t} T_g - \dot{\omega}_{ref} + k_i e(t) \text{ for } S_{ismc} > 0 \\ \frac{1}{J_t} T_a - \frac{K_t}{J_t} \omega_r - \frac{1}{J_t} T_g - \dot{\omega}_{ref} + k_i e(t) \text{ for } S_{ismc} < 0 \end{array} \right\} \quad (2.48)$$

In general ISMC having two parts i.e. equivalent control and switching control is given in equation (2.37) and (2.38) respectively. The final control expression for ISMC is given in equation (2.49)

$$T_g = T_a - K_t \omega_r - J_t \dot{\omega}_{ref} + J_t k_i e(t) + J_t k \tanh\left(\frac{S_{ismc}}{\phi}\right) \quad (2.49)$$

*Remark 1*

In order to prove the stability of the proposed ISMC the final control law in equation (2.49) is substituted in equation (2.46)

$$\begin{aligned} \dot{V} &= S_{ismc} \left[ \frac{1}{J_t} T_a - \frac{K_t}{J_t} \omega_r - \frac{1}{J_t} \left( T_a - K_t \omega_r - J_t \dot{\omega}_{ref} + J_t k_i e(t) + J_t k \tanh\left(\frac{S_{ismc}}{\phi}\right) \right) - \dot{\omega}_{ref} \right. \\ &\quad \left. + k_i e(t) \right] \\ &= -S_{ismc} k \tanh\left(\frac{S_{ismc}}{\phi}\right) \end{aligned} \quad (2.50)$$

Equation (2.50) gives the stability of proposed ISMC.  $\dot{V}$  is always negative semi definite with irrespective value of  $S_{ismc}$ .

### 2.10.5 Adaptive fuzzy integral sliding mode control for single mass model

In order to accommodate the input disturbances, the fixed gain ‘ $k$ ’ in ISMC has been replaced by the variable gain which is achieved by AFISMCM. The main aim of the AFISMCM controller is to achieve robustness with respect to disturbances. In Fuzzy SMC, variable boundary layer ( $\phi$ ) is a function of  $S_{ismc}$  and  $\dot{S}_{ismc}$  (Ben-Tzvi, P. et al. 2011). In this problem, we need to avoid more tracking error in the presence of disturbance in the control input like generator torque. Fuzzy Logic (FL) is used to improve the performance of the controller, FL automatically adjust the variable gain

based on sliding surface and derivative of the sliding surface. The input to the fuzzy controller is sliding surface and derivative of the sliding surface, and the output is variable gain. Equation (2.51) defines the control input for AFISMCM.

*Remark 1:*

A variable sliding gain layer is introduced to smooth out the discontinuity which ensures reduced chattering effect. The condition  $S_{ismc}=0$  indicates the tracking error is zero, and the switching control is also zero. But during simulation, it may not be possible to achieve the tracking error to zero because of high tracking dynamics in the reference signal. So the varying fuzzy sliding gain is introduced in the ISMC control. Equation (2.51) gives the control law for AFISMCM.

$$T_g = T_a - K_t \omega_r - J_t \dot{\omega}_{ref} + J_t k_t e(t) + J_t k_{fuzzy} \tanh\left(\frac{S_{ismc}}{\phi}\right) \quad (2.51)$$

Table 2.14: Fuzzy rules  $S_{ismc}$ ,  $\dot{S}_{ismc}$  and  $k_{fuzzy}$

$U(t)$	$\dot{S}_{ismc}(t)$				
$S_{ismc}(t)$	NB	NS	Z	PS	PB
NB	Z	NS	PS	NS	NS
NS	NS	PS	NS	NS	Z
Z	NB	NS	NB	PB	NS
PS	PS	PB	Z	NS	NS
PB	PS	PB	NS	PB	NS

The triangular membership function is used for both inputs and output fuzzy variables. The inputs are error and derivative of the error which is varying between the  $\{-0.4, 0.4\}$  and  $\{-0.04, 0.04\}$  respectively. The output variable is sliding gain which is varying between  $\{0.006, 0.2\}$ . The fuzzy variables are defined in the rule base as  $\{NS$  (Negative Small),  $NB$  (Negative Big),  $Z$  (Zero),  $PS$  (Positive Small) and  $PB$  (Positive Big) $\}$ . From the conventional ISMC, the knowledge of the sliding gain is obtained. With this knowledge, the fuzzy rules are initially derived by trial and error method. After obtaining the rule base, the simulation is carried out and it is tuned appropriately as per the control objectives. Finally, the derived rule base is given in Table 2.14 and is validated for different disturbances and different mean wind speed conditions. From

the results, it is found that the rule base is optimal for achieving the given control objectives. A typical fuzzy control rule of the proposed AFISM is expressed as:

$$R^{(i)} :: \text{IF } S_{smc}(t) \text{ is } H_i^1 \text{ and } \dot{S}_{smc}(t) \text{ is } H_i^2 \text{ THEN } k_{fuzzy} \text{ is } M^i$$

Where  $H_i^1$  and  $H_i^2$  are the labels of the input fuzzy sets and  $M^i$  is the labels of the output fuzzy sets  $i=1, \dots, p$  represents the number of IF-THEN fuzzy rules.

## 2.11 SIMULATION RESULTS AND DISCUSSION FOR SINGLE MASS MODEL

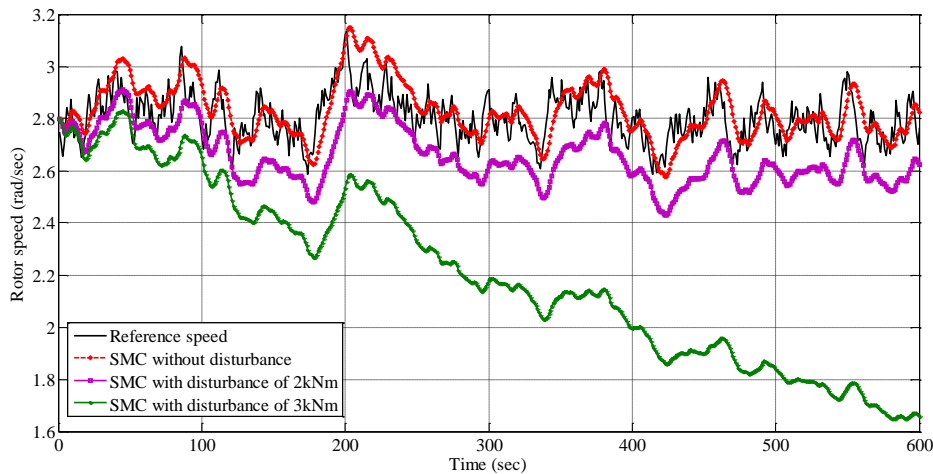


Figure 2.39: Comparison of rotor speed with different level of constant disturbance for SMC (Transient wind speed)

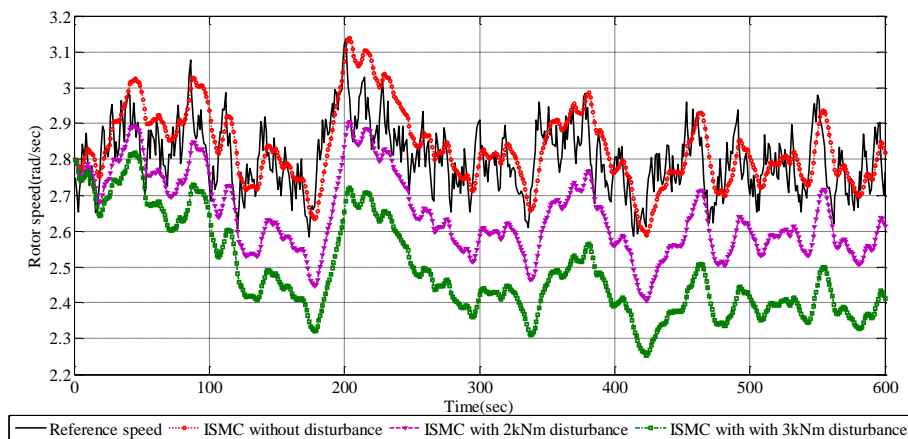


Figure 2.40: Comparison of rotor speed with different level of constant disturbance for ISMC (Transient wind speed)

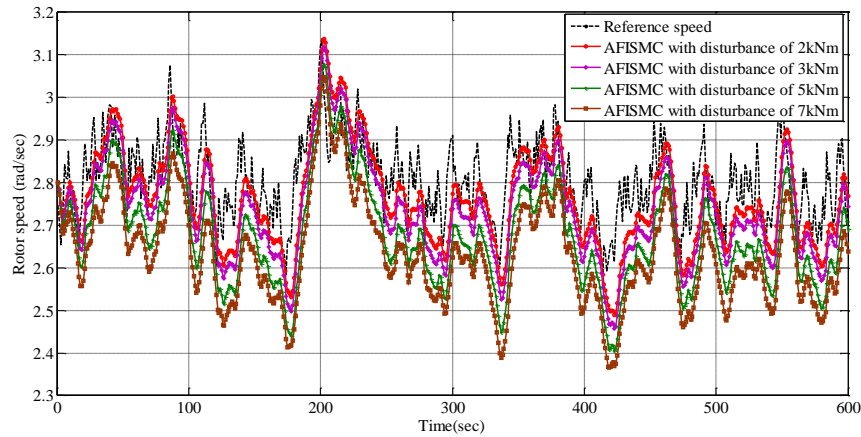


Figure 2.41: Rotor speed comparisons for AFISM with different level of constant disturbance (Transient wind speed).

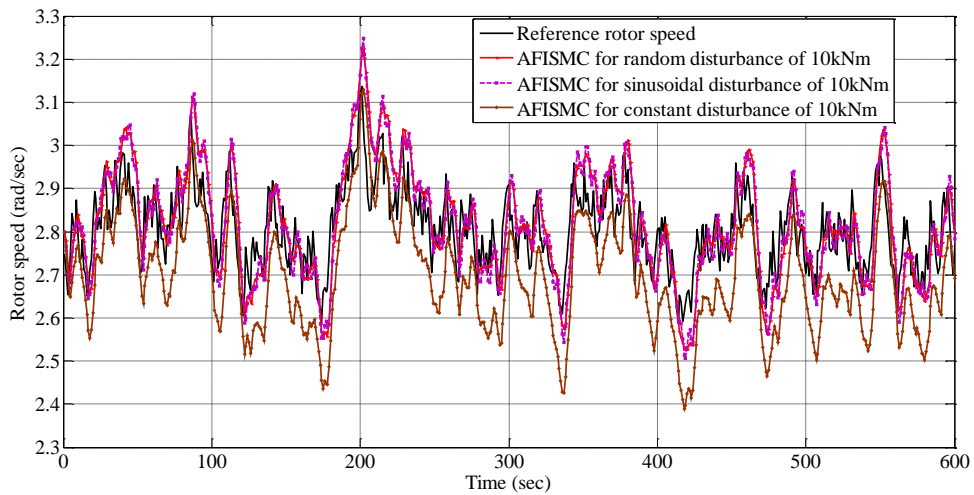


Figure 2.42: Comparison of rotor speed with different types of disturbance for AFISM (Transient wind speed)

Figure 2.39 and Figure 2.40 show the rotor speed comparisons for SMC and ISMC considering both with and without input disturbances. From these figures it is clear that without any input disturbance, the obtained rotor speed for SMC and ISMC are almost following the reference rotor speed. An increase in constant input disturbance level from 2kNm to 3kNm leads to significant increase in tracking error due to which the rotor is unable to track the reference speed, which further results in more power loss and reduced electrical efficiency. Figure 2.41 shows the rotor speed comparison for AFISM with different level of constant input disturbances ranging from 2 kNm to 7 kNm. Figure 2.42 shows the comparison of rotor speed for AFISM with different types of input disturbances such as constant, sinusoidal and random disturbances of magnitude 10kNm.

From Figure 2.41 and Figure 2.42, it is observed that the performance of the WT with the proposed adaptive fuzzy based ISMC is able to track the maximum power delivery point in the presence of different types as well as the different level of input disturbances. Table 2.15 shows the performance of SMC for different input disturbances. From these results, it is clear that with an increase of disturbance level, the STD of the generated torque increases, which ensures more oscillation on the drive train. Also, it is found that the electrical and aerodynamic efficiency decreases with the increase in disturbance level, which introduces more power loss. Analyzing the results given in Table 2.15 and Figure 2.37, it is concluded that conventional SMC is not robust to a disturbance level of more than 3kNm.

Table 2.16 shows the performance of ISMC in terms of efficiency and STD of input torque. This table ensures that an increase in disturbance level introduces more power loss and more drive train oscillation. For a disturbance level of 3kNm, the electrical efficiency decreases to 87.86% for ISMC and 81.17% for SMC respectively, which indicates that SMC and ISMC controllers are not robust with respect to disturbance of more than 3kNm. Generally, WT system disturbance is not predictable and the controller should accommodate the disturbance with maximum power capture and reduced oscillation.

Table 2.15: Performance analysis of SMC with and without constant disturbances (wind speed 7 m/sec)

SMC with and without constant disturbances	SMC without disturbance	SMC with disturbance of 2kNm	SMC with disturbance of 3kNm
Max( $T_g$ ) kNm	51.92	55.20	61.44
Electrical Efficiency (%)	91.10	89.50	81.17
Aerodynamic Efficiency (%)	93.23	94.86	85.82
STD ( $T_g$ ) kNm	1.928	1.705	3.232

Table 2.16: Performance analysis of ISMC with and without constant disturbances (wind speed 7 m/sec)

ISMC with and without constant disturbances	ISMC without disturbance	ISMC with disturbance of 2kNm	ISMC with disturbance of 3kNm
Max( $T_g$ ) kNm	51.58	55.26	57.44
Electrical Efficiency (%)	91.07	89.56	87.86
Aerodynamic Efficiency (%)	93.21	94.71	94.05
STD ( $T_g$ ) kNm	1.606	1.744	2.064

Table 2.17 shows the performance of AFISMC with an objective of maximum energy extraction from the wind and reduced mechanical stress on the drive train. Different types of disturbances are given to the AFISMC controller i.e. random, sinusoidal and constant disturbances with the magnitude of 10kNm. From this table it is clear that in the presence of 10kNm disturbance, the AFISMC is able track the reference rotor speed, whereas for SMC and ISMC, the WT is unable to track the reference for a disturbance level more than 3 kNm. The electrical and aerodynamic efficiency are almost found to be same for sinusoidal and random disturbances, but with constant disturbance the electrical efficiency is 18% less compared to other two disturbances. From the Table 2.15, Table 2.16 and Table 2.17, it is concluded that SMC and ISMC are not robust to disturbances more than 3kNm, but AFISMC is able to track the optimal rotor speed with different types of disturbances of magnitude 10kNm.

Table 2.17: Performance analysis of AFISMC with different types of disturbances (7 m/sec wind profile)

AFISMC with different types of disturbances (7m/sec wind speed)	AFISMC with constant disturbance of 10kNm	AFISMC with sinusoidal disturbance of 10kNm	AFISMC with random disturbance of 10kNm
Max( $T_g$ ) kNm	61.69	72.03	70.97
$\eta_{elec}$ (%)	73.77	91.25	91.38
$\eta_{aero}$ (%)	94.56	93.44	93.45
STD ( $T_g$ ) kNm	10.257	9.484	9.414

Table 2.18: Performance analysis of AFISMC with different types of disturbances (8 m/sec wind profile)

AFISMC with different types of disturbances (8m/sec wind speed)	AFISMC with constant disturbance of 10kNm	AFISMC with sinusoidal disturbance of 10kNm	AFISMC with random disturbance of 10kNm
Max( $T_g$ ) kNm	71.56	67.93	80.00
$\eta_{elec}$ (%)	75.59	89.31	89.39
$\eta_{aero}$ (%)	93.27	91.88	91.88
STD ( $T_g$ ) kNm	9.289	8.301	7.987

In order to analyze the performance of the controllers critically two different wind profiles are tested for simulation. The results for the mean wind speed of 8 m/sec and 8.5m/s are given in Table 2.18 and 2.19 respectively. Results given in the table can be analyzed in the same way as discussed in the previous sections. Finally, it is concluded that with increase in wind speed there is an increase in electrical and aerodynamic efficiency.

Table 2.20 shows that, the increase in disturbance level decreases the efficiency of AFISMC. It can be observed that even though the efficiency decreases from 88.25% to 80.89% for a constant disturbance range of 2 kNm to 7 kNm, the WT with AFISMC control is able to track the reference speed with minimum tracking error (Mean square error) and maximum efficiency. In comparison with SMC and ISMC, the tracking error of AFISMC was found to be minimum with improved electrical efficiency.

Table 2.19: Performance analysis of AFISMC with different types of disturbances. (8.5m/sec wind profile)

AFISMC with different types of disturbances (8.5 m/sec wind speed)	AFISMC with constant disturbance of 10kNm	AFISMC with sinusoidal disturbance of 10kNm	AFISMC with random disturbance of 10kNm
Max( $T_g$ ) kNm	76.69	86.87	86.26
$\eta_{elec}$ (%)	76.93	89.53	89.58
$\eta_{aero}$ (%)	93.25	92.04	92.04
STD ( $T_g$ ) kNm	8.875	7.891	7.487

Table 2.20: Analysis of electrical efficiency with respect to different level of disturbance for a wind speed of 7 m/sec.

AFISMC with disturbances	AFISMC with 2kNm disturbance	AFISMC with 3kNm disturbance	AFISMC with 5kNm disturbance	AFISMC with 7kNm disturbance
$\eta_{elec}$ (%)	88.25	86.82	83.83	80.89
Mean square error	0.008	0.011	0.023	0.037

Figure 2.43 and 2.44 show the rotor speed comparisons for SMC and ISMC with and without input disturbances, where a smooth variation in wind is considered. From these



Figures, it is clear that without any disturbance the obtained rotor speed for SMC and ISMC are almost following the reference rotor speed.

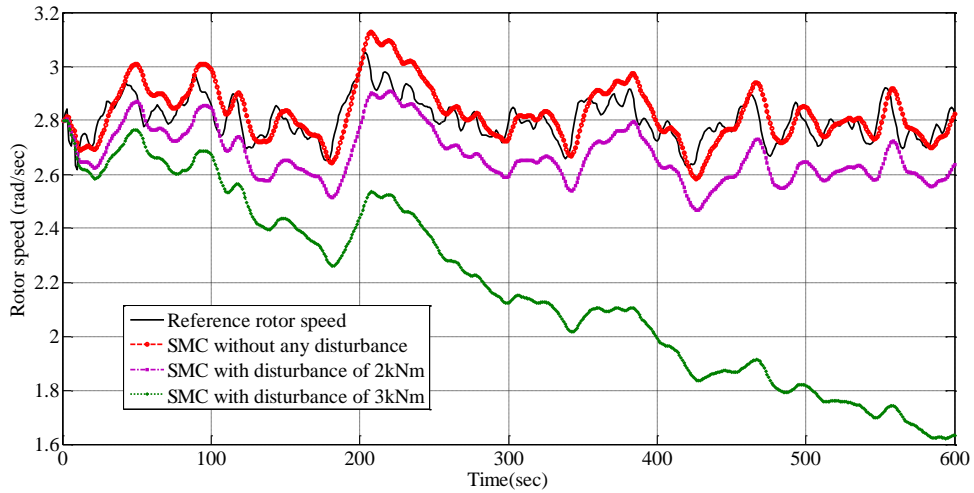


Figure 2.43: Comparison of rotor speed with different disturbance for SMC (smooth wind speed).

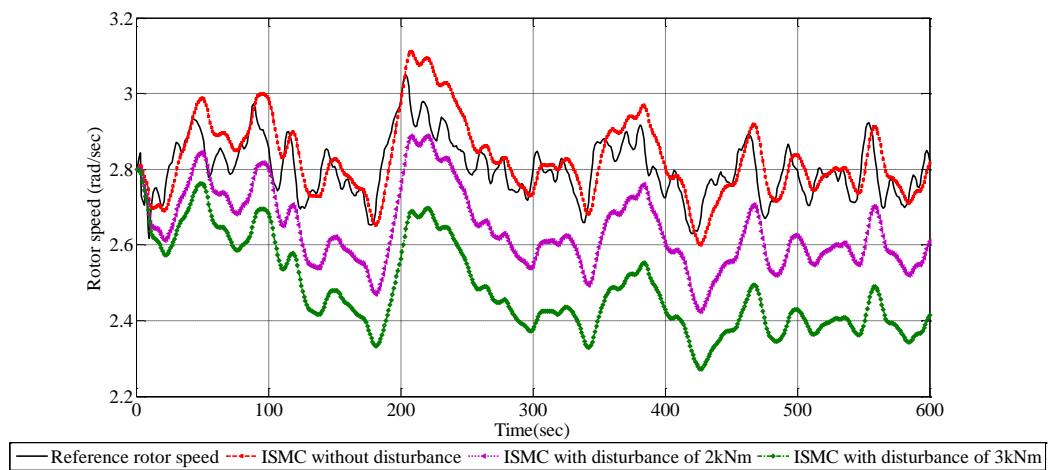


Figure 2.44: Comparison of rotor speed with different disturbance for ISMC (smooth wind speed).

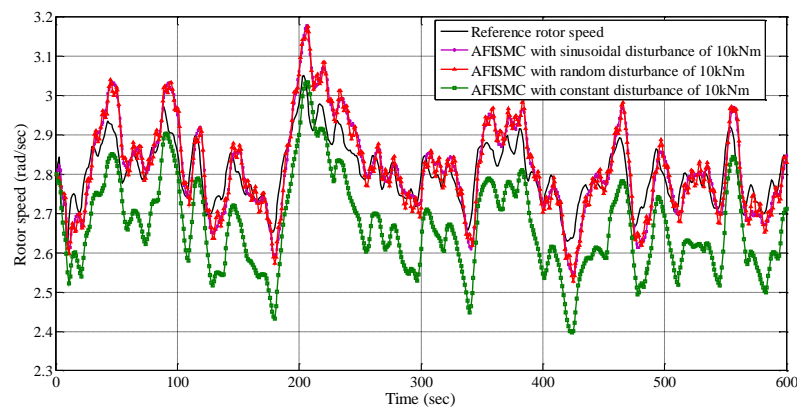


Figure 2.45: Comparison of rotor speed with different disturbance for AFISMC (smooth wind speed).

As shown in the Figure 2.43 and Figure 2.44, with an increase in input disturbance level from 2 kNm to 3 kNm, there is a significant increase in tracking error due to which the rotor is unable to track the reference speed. Figure 2.45 shows different types of disturbance with the magnitude of 10kNm applied for the WT in the presence of AFISMC controller. For smooth wind speed with different level of disturbance level of 10 kNm, AFISMC is able to track the reference that ensures the maximum power capture from the wind.

Table 2.21: Performance analysis of SMC with and without constant disturbances for smooth wind speed of 7 m/sec

SMC with and without constant disturbances	SMC without disturbance	SMC with disturbance of 2kNm	SMC with disturbance of 3kNm
Max( $T_g$ ) kNm	51.82	53.29	60.97
$\eta_{elec}$ (%)	91.14	89.40	80.64
$\eta_{aero}$ (%)	93.34	94.73	85.23
STD ( $T_g$ ) kNm	1.77	1.423	3.114

Table 2.22: Performance analysis of ISMC with and without constant disturbances for smooth wind speed of 7 m/sec

ISMC with and without constant disturbances	ISMC without disturbance	ISMC with disturbance of 2kNm	ISMC with disturbance of 3kNm
Max( $T_g$ ) kNm	51.12	54.11	56.91
$\eta_{elec}$ (%)	91.15	89.61	87.94
$\eta_{aero}$ (%)	93.34	94.82	94.18
STD ( $T_g$ ) kNm	1.388	1.482	1.865

Table 2.21 to 2.23 gives the performance of SMC, ISMC and the proposed AFISMC for smooth wind speed of 7 m/sec respectively. The performance of the controller can be analyzed in the same way of analysis done for transient wind speed profile of 7 m/sec. The only difference between two wind speed profiles is that, for a smooth variation of wind speed the efficiency of the WT increases at the same time, the STD of the input torque reduces. This indicates a smooth variation in control torque for a smooth varying wind speed.

Table 2.23: Performance analysis of AFISMC with different types disturbances for smooth wind speed of 7 m/sec

AFISMC with different types of disturbances	AFISMC with constant disturbance of 10kNm	AFISMC with sinusoidal disturbance of 10kNm	AFISMC with random disturbance of 10kNm
Max( $T_g$ ) kNm	53.37	64.81	65.53
$\eta_{elec}$ (%)	76.20	91.31	91.37
$\eta_{aero}$ (%)	94.79	93.53	93.53
STD ( $T_g$ ) kNm	5.612	4.814	4.962

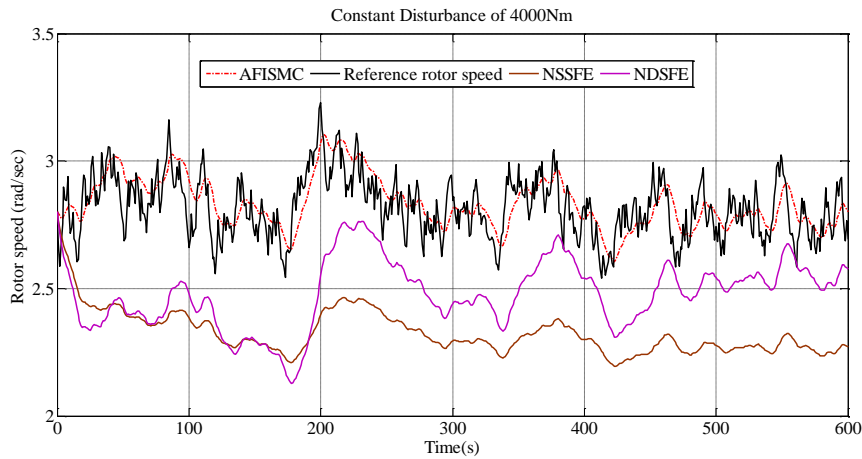


Figure 2.46: Rotor speed comparison for NSSFE, NDSFE and AFISMC with constant 4kNm disturbance.

Figure 2.46 shows the rotor speed comparison for NSSFE, NDSFE and AFISMC with constant 4kNm disturbance. From this figure it is clear that AFISMC can able to track the reference, but other nonlinear controllers are unable to track reference speed. With increase in disturbance level more than 4kNm both NSSFE and NDSFE are unable to track the reference speed. From this analysis it is found that the proposed AFISMC controller is robust with respect to disturbances.

Table 2.24: Performance comparison for NSSFE, NDSFE and AFISMC

	NSSFE	NDSFE	AFISMC
STD( $T_g$ ) kNm	2.761	2.464	1.267
$\eta_{ele}$ (%)	71.99	75.73	91.06

Table 2.24 shows the performance comparison for NSSFE, NDSFE and AFISMC controllers. From this table it is observed that STD is less for AFISMC at the same time,

electrical efficiency is also more compared to other nonlinear controllers, which ensures the robustness of the proposed AFISMC.

## **2.12 COMPARISON BETWEEN SINGLE-MASS AND TWO-MASS MODEL**

Wind turbine is a device which converts the kinetic energy of the wind into electric energy. Simulation complexity of the wind turbine purely depends on the type of control objectives. In case of wind turbine modelling complex simulators are required to verify the dynamic response of multiple components and aerodynamic loading. Generally, dynamic loads and interaction of large components are verified by the aero elastic simulator. For designing a wind turbine controller, instead of going with complex simulator, the design objective can be achieved by using simplified mathematical model. In this work, wind turbine model is described by the set of nonlinear ordinary differential equation with limited degree of freedom. This work describes the control law for a simplified mathematical model and FAST with the objective of optimal power capture at below and above rated wind speed.

The power system transient stability includes the variable speed generator system, which can be modelled by six-mass, three-mass, two-mass and single-mass drive train models. From (S. Muyeen, S. et al. 2007) this study it is found that two mass-model is sufficient to analyze the transient stability of wind energy conversion systems. In (Melicio, R. et al. 2010), three different mass-model and three different power electronics converter topologies are presented to analyze the harmonic assessment with fractional order controller. A three-mass model increases the order of the overall system, which includes both shaft and blade flexibilities. Effective two-mass model is developed with acceptable accuracy (Ramtharan, G. et al. 2007).

Two-mass model is a very generalized model, which can be applied to any size of wind turbine. Especially the control law derived from this model is adapted for high flexibility wind turbine, which cannot be properly modelled with single-mass model. In case of the single mass model, much dynamics are not involved so that the control law developed is not able to adopt the high flexibility wind turbines.

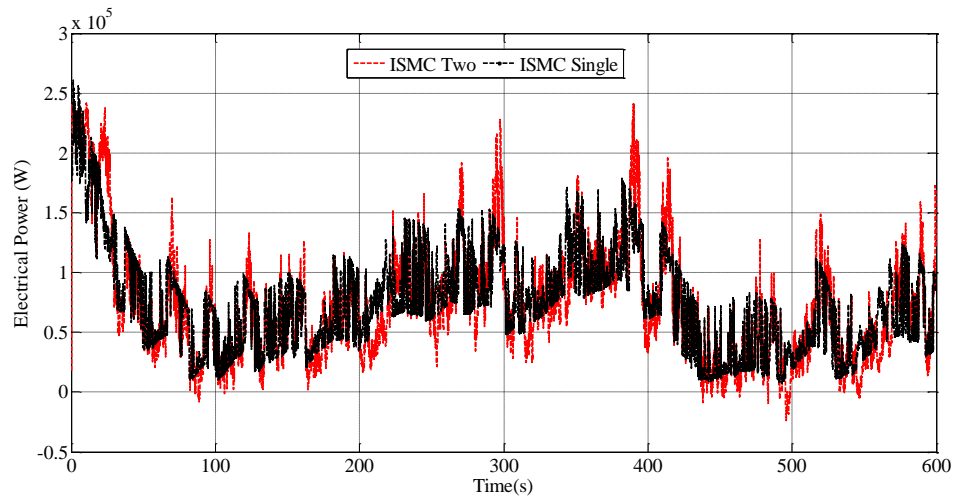


Figure 2.47: Comparison for single and two mass model based control law for FAST model

Figure 2.47 shows the comparison electrical power where the control law is derived from single and two mass model dynamics and applied to ISMC controller. From this figure, it is clear that two mass model based control law extracts more power compared to the single mass model. Two mass model based control law involves more parameter, i.e. DOF is more compared to single mass model. From this analysis it is concluded that for high flexibility turbines, two mass model based control law is more accurate compared to single mass model.

## 2.13 CONCLUSION

The estimation of effective wind speed at below rated wind speed is done by different estimation techniques such as MNR, NN trained by different algorithms, and nonlinear time series based estimation. In this chapter, a single mass model based WT is considered. Without estimation of wind speed the conventional control techniques such as ISC and ATF are considered. Due to the lack of performance in the conventional techniques, existing nonlinear controllers with wind speed estimators are adapted i.e. NSSFE and NDSFE. Six different nonlinear wind speed estimators are proposed. NN based different training algorithm and nonlinear time series are found to be suitable for wind speed estimation. Out of that, HWM and NARX with NDSFE control found to be better in terms of STD and PSD of the control input i.e. generator torque. But such algorithms needs more training and testing data, which is obtained from conventional MNR.

In order to avoid the drawbacks of conventional controllers, the proposed controllers namely FSMC, ISMC and AFISM are developed. Initially FSMC is compared with all the conventional controllers for different mean wind speed in the presence of uncertainty and disturbances. From these analyses it is found that FSMC is better compared to other conventional controllers. As the disturbances in the WT systems are unpredictable, the objective is to design robust controllers that maximize the energy extracted from the wind while reducing mechanical stress on the drive train. Finally the controllers are tested for different input disturbances with different magnitude. SMC and ISMC are found to give weak performance particularly in the presence of input torque disturbance of more than 3 kNm. In order to overcome the above drawbacks fuzzy based AFISM controller is proposed and is found to be more robust in achieving the above objectives in the presence of input torque disturbance varying from 2 kNm to 10 kNm. To prove the efficiency of the proposed AFISM control, the simulation has been conducted for different wind speed profiles with different turbulence component. From this analysis it is clear that AFISM is the robust controller for single mass model of the WT.

In next chapter the nonlinear controllers such as MNSSFE, SMC and ISMC are designed for real time FAST NREL 600kW WT model. The control law is derived for two mass model WT and applied to five DOF FAST model. It is clear that, once the SMC and ISMC is designed the artificial intelligence like FL can be incorporated after gaining a sufficient knowledge on those conventional controllers. So, the next chapter is fully dedicated towards the design of SMC and ISMC for real time wind turbine system at below rated wind speed for optimal power extraction.

## **CHAPTER 3**

### **3 DESIGN AND IMPLEMENTATION OF NONLINEAR CONTROLLERS FOR TWO MASS MODEL OF WIND TURBINE WITH FAST NREL**

#### **3.1 INTRODUCTION**

In this chapter, the exact wind turbine model i.e. two mass model of the WT is chosen with FAST NREL 600kW WT. The FAST has more DOF compared to the mathematical model. It gives the complete model of the WT. In this work, five DOF is considered in FAST WT model. The wind speed is also programmed by the TurbSim package which is developed by the NREL. Initially, the conventional controllers such as ATF and ISC were adapted. It was found that they are not robust to disturbance and parameter uncertainty. However, due to the inherent disadvantages of these control techniques MNSSFE, SMC and ISMC with MNR wind speed estimator are proposed at below rated wind speed. The simulations of conventional and proposed controllers were tested with different mean wind speed and turbulences. Higher tracking dynamic will ensure maximum power capture at the cost of high turbulence in the control action. Conversely, a slower tracking dynamic ensures smooth torque i.e. less transient load on the drive train at the cost of low power capture. A comparative study between the proposed and conventional techniques is presented. All the controllers are simulated by MATLAB/Simulink with NREL FAST model. Different types of mean wind speed and turbulence with parameter uncertainty and disturbances are also analyzed for the proposed and conventional controllers.

### 3.2 MODIFIED NONLINEAR STATIC STATE FEEDBACK LINEARIZATION WITH ESTIMATOR (MNSSFE) FOR TWO MASS MODEL

In (Boukhezzar, B. and Siguerdidjane, H. 2011) the authors have explained Nonlinear static state feedback with Kalman filter based estimator where the second derivative of the rotor speed and first derivative of the low speed shaft are considered to express the control law. In order to avoid higher derivatives and complex control law, a modified nonlinear static state feedback with estimator is proposed in this section. Rearranging the terms in equation (1.19) we will get as

$$\dot{\omega}_r = \frac{1}{J_r} T_a - \frac{K_r}{J_r} \omega_r - \frac{1}{J_r} T_{ls} \quad (3.1)$$

By using the relationship given in equation (1.12) and (1.14) we will get as

$$\dot{\omega}_r = \frac{1}{J_r} T_a - \frac{K_r}{J_r} \omega_r - \frac{1}{J_r} \left( n_g \left( J_g \dot{\omega}_g + K_g \omega_g + T_{em} \right) \right) \quad (3.2)$$

By separating the control input ' $T_{em}$ ' finally the control torque can be expressed as

$$T_{em} = \frac{T_a}{n_g} - \frac{K_r}{J_r} \omega_r - J_g \dot{\omega}_g - K_g \omega_g - \frac{J_r}{n_g} \dot{\omega}_r \quad (3.3)$$

where ' $\dot{\omega}_r$ ' is approximated by the new input ' $w_3$ '

$$\dot{\omega}_r = w_3 \quad (3.4)$$

$$T_{em} = \frac{T_a}{n_g} - \frac{K_r}{J_r} \omega_r - J_g \dot{\omega}_g - K_g \omega_g - \frac{J_r}{n_g} w_3 \quad (3.5)$$

The first order error dynamics can be written as

$$\dot{e} + a_0 e = 0, a_0 > 0 \quad (3.6)$$

$$e = \omega_{ropt} - \omega_r \quad (3.7)$$

From the above equation (3.6) the new input ' $w_3$ ' is defined as

$$w_3 = \dot{\omega}_{ropt} + a_0 e \quad (3.8)$$



By substituting  $w_3$  in equation (3.5) we get the final control law for the WT two mass model.

$$T_{em} = \frac{T_a}{n_g} - \frac{K_r}{n_g} \omega_r - J_g \dot{\omega}_g - K_g \omega_g - \frac{J_r}{n_g} (\dot{\omega}_{ropt} + a_0 e) \quad (3.9)$$

### 3.3 SMC DESIGN FOR TWO MASS MODEL

The proposed control strategy combines MNR based estimator with second order SMC. It is one of the effective nonlinear robust approaches with respect to system dynamics and invariant to uncertainties. Lyapunov stability approach is used in SMC to keep the nonlinear system under control. In general, design of SMC has two steps. First to find the sliding surface and second is to develop the control signal  $U$ .

Time varying sliding surface ( $S_{smc}$ ) is given in equation (3.10)

$$S_{smc} = \left( \lambda_1 + \frac{d}{dt} \right)^{n-1} e(t) \quad (3.10)$$

Where  $e(t)$  is defined as the difference between rotor speed and reference rotor speed, 'n' is the order of the system and ' $\lambda_1$ ' is positive constant.

$$e(t) = \omega_r(t) - \omega_{ref}(t) \quad (3.11)$$

Finally the sliding surface is defined as

$$S_{smc}(t) = \lambda_1 e(t) + \dot{e}(t) \quad (3.12)$$

Generally, three types of reaching law are proposed (Ben-Tzvi, P. et al. 2011). Direct switching function method is applied in this work having the condition:

$$S_{smc} \dot{S}_{smc} \leq 0 \quad (3.13)$$

The control should be chosen in such a way that the following candidate Lyapunov function satisfies Lyapunov stability criteria. Lyapunov candidate function is defined as

$$V = \frac{1}{2} S_{smc}^2 \quad (3.14)$$

A sufficient condition for the system output is that it should stay on the sliding surface i.e.  $S_{smc}(t)$ . When  $S_{smc}(t) = 0$ , ensures the asymptotic stability. Therefore  $e \rightarrow 0$  and  $\dot{e} \rightarrow 0$ , the satisfactory condition is that  $S_{smc} \dot{S}_{smc} < 0$ . This ensures that the control law can track the time varying reference speed i.e. reference rotor speed.

If  $V(0)=0$  then  $\frac{dV}{dt} = 0$ , from this  $\frac{dV}{dt} = S_{smc} \frac{dS_{smc}}{dt}$  so  $\frac{dS_{smc}}{dt} = 0$

$$\frac{dV}{dt} = S_{smc} \frac{dS_{smc}}{dt} = S_{smc} (\lambda_1 \dot{e}(t) + \ddot{e}(t)) \quad (3.15)$$

The convergence condition is given by the Lyapunov equation which makes the sliding surface attractive and invariant. At steady state, the rotor should track the optimal rotor speed asymptotically i.e.  $\omega_r(t) \rightarrow \omega_{ref}(t)$  as  $t \rightarrow \infty$ .

$$\dot{V} = S_{smc} \dot{S}_{smc} = S_{smc} (\lambda_1 \dot{e}(t) + \ddot{e}(t)) = S_{smc} [\lambda_1 (\dot{\omega}_r(t) - \dot{\omega}_{ref}(t) + \ddot{e}(t))] \quad (3.16)$$

$\dot{V} \leq 0$  meets the following condition

$$\lambda_1 (\dot{\omega}_r - \dot{\omega}_{ref}) + \ddot{e}(t) \begin{cases} < 0 \text{ for } S_{smc} > 0 \\ = 0 \text{ for } S_{smc} = 0 \\ > 0 \text{ for } S_{smc} < 0 \end{cases} \quad (3.17)$$

The values of control variable are to be set in such a way that the system will become stable. These control variables are given as follows:

$$U \begin{cases} < T_{em} \text{ for } S_{smc} > 0 \\ = T_{em} \text{ for } S_{smc} = 0 \\ > T_{em} \text{ for } S_{smc} < 0 \end{cases} \quad (3.18)$$

In order to derive the control input i.e. ' $T_{em}$ ', the following conversion has been made.

By substituting the  $\dot{\omega}_r(t)$  in the (3.16) we get as

$$\lambda_1 \left( \frac{1}{J_r} T_a - \frac{K_r}{J_r} \omega_r - \frac{1}{J_r} T_{ls} - \dot{\omega}_{ref} \right) + \ddot{e}(t) = 0 \quad (3.19)$$

By using the relationship given in equation (1.12) and (1.13) finally will get as

$$\lambda_1 \left( \frac{T_a}{J_r} - \frac{K_r}{J_r} \omega_r - \frac{n_g J_g \dot{\omega}_g}{J_r} - \frac{n_g K_g \omega_g}{J_r} - \frac{n_g}{J_r} T_{em} - \dot{\omega}_{ref} \right) + \ddot{e}(t) = 0 \quad (3.20)$$

The control structure is defined in equation (3.21)

$$T_{em} = \frac{T_a}{n_g} - \frac{K_r}{n_g} \omega_r - J_g \dot{\omega}_g - K_g \omega_g - \frac{J_r}{n_g} \dot{\omega}_{ref} + \frac{J_r}{\lambda_1 n_g} \ddot{e}(t) \quad (3.21)$$

The switching control technique is used to avoid the parameter uncertainty and disturbances. The equivalent control is used to control the overall system behavior.

$$U(t) = U_{eq}(t) + U_{sw}(t) \quad (3.22)$$

The Switching control is defined in two ways

$$U_{sw}(t) = k \text{sign}(S_{smc}) \text{ or } k \tanh\left(\frac{S_{smc}}{\phi}\right) \quad (3.23)$$

Generally the SMC with signum function introduces the chattering phenomenon in the system. This chattering introduces high frequency dynamics in the WT system which is undesirable. To neglect this chattering, a smooth control discontinuity is introduced. As the signum function varies between -1 to +1 discontinuously, it is replaced by a tangent hyperbolic function (tanh). Finally the torque control structure is given in equation (3.24).

$$T_{em} = \frac{T_a}{n_g} - \frac{K_r}{n_g} \omega_r - J_g \dot{\omega}_g - K_g \omega_g - \frac{J_r}{n_g} \dot{\omega}_{ref} + \frac{J_r}{\lambda_1 n_g} \ddot{e}(t) + \frac{J_r}{n_g \lambda_1} k \tanh\left(\frac{S_{smc}}{\phi}\right) \quad (3.24)$$

Where 'k' is the sliding gain whose value is based on the empirical results from the simulation. In summary, the controller performance depends on the sliding gain and the boundary layer thickness. By using trial and error method, the sliding gain was found to be 0.2 and boundary layer thickness is 1 for simulation. If the gain value increases more than 0.2, it introduces more oscillation on the low speed shaft. The boundary layer is chosen arbitrarily that depends on the system performance.

### 3.4 INTEGRAL SLIDING MODE CONTROLLER DESIGN FOR TWO MASS MODEL

To improve the sliding surface and overcome the steady state error, the integral action is included in the sliding surface.

A sliding surface defined for ISMC ( $S_{ismc}$ ) is given in (3.25)

$$S_{ismc}(t) = \left( \lambda_1 + \frac{d}{dt} \right)^{n-1} e(t) + K_i \int_0^{\infty} e(t) dt \quad (3.25)$$

where  $K_i$  is the integral gain.

The order of the system is 2 i.e.  $n=2$  then the sliding surface is modified as

$$S_{ismc}(t) = \left( \lambda_1 + \frac{d}{dt} \right)^1 e(t) + K_i \int_0^{\infty} e(t) dt = \lambda_1 e(t) + \dot{e}(t) + K_i \int_0^{\infty} e(t) dt \quad (3.26)$$

By taking the same Lyapunov function as mentioned in SMC with the same condition.

$$\begin{aligned} \dot{V} = S_{ismc} \dot{S}_{ismc} &= S_{ismc} (\lambda_1 \dot{e}(t) + \ddot{e}(t) + K_i e(t)) = \\ &S_{ismc} \left[ \lambda_1 (\dot{\omega}_r(t) - \dot{\omega}_{ref}(t) + \ddot{e}(t)) + K_i e(t) \right] \end{aligned} \quad (3.27)$$

$\dot{V} \leq 0$  meets the following condition

$$\lambda_1 (\dot{\omega}_r - \dot{\omega}_{ref}) + \ddot{e}(t) + K_i e(t) \begin{cases} < 0 \text{ for } S_{ismc} > 0 \\ = 0 \text{ for } S_{ismc} = 0 \\ > 0 \text{ for } S_{ismc} < 0 \end{cases} \quad (3.28)$$

In order to derive the control input i.e. ' $T_{em}$ ', the following conversion has been made.

By substituting the  $\dot{\omega}_r(t)$  in the (3.27) we get as

$$\lambda_1 \left( \frac{1}{J_r} T_a - \frac{K_r}{J_r} \omega_r - \frac{1}{J_r} T_{ls} - \dot{\omega}_{ref} \right) + \ddot{e}(t) + K_i e(t) = 0 \quad (3.29)$$

Finally the torque control structure is given in equation (3.30).

$$\begin{aligned} T_{em} &= \frac{T_a}{n_g} - \frac{K_r}{n_g} \omega_r - J_g \dot{\omega}_g - K_g \omega_g - \frac{J_r}{n_g} \dot{\omega}_{ref} + \frac{J_r}{n_g \lambda_1} \ddot{e}(t) \\ &+ \frac{J_r}{n_g \lambda_1} K_i e(t) + \frac{J_r}{n_g \lambda_1} k \tanh \left( \frac{S_{ismc}}{\phi} \right) \end{aligned} \quad (3.30)$$

The necessary condition of ISMC is to eliminate the steady state error in the conventional SMC. Let us assume the linear sliding surface ( $\sigma_1$ ) is defined in (3.11) as

$$\sigma_1(t) = e(t) + \lambda_1 \dot{e}(t) \quad (3.31)$$

By taking the Laplace transform of above equation,

$$\sigma_1(s) = E(s)[s + \lambda_1] \quad (3.32)$$

The steady state error is calculated by applying the Final Value Theorem (FVT) to conventional sliding surface.

$$\lim_{t \rightarrow \infty} e(t) = \lim_{s \rightarrow 0} s \times E(s) = \lim_{s \rightarrow 0} \frac{s}{s + \lambda_1} \sum(s) = \frac{1}{\lambda_1 k} \phi \quad (3.33)$$

The equation (3.33) represents the conventional SMC having steady state error which is proportional to boundary layer thickness ( $\phi$ ) and inversely proportional to the coefficient ' $\lambda_1$ ' and sliding gain ' $k$ '.

Let us assume the integral sliding surface is ( $\sigma_2$ ), then the steady state error is calculated by applying the final value theorem (FVT) to integral sliding surface ( $\sigma_2$ ).

$$\dot{\sigma}_2(t) = \lambda_1 \dot{e}(t) + k_i e(t) + \ddot{e}(t) \quad (3.34)$$

By taking the Laplace transform of above equation.

$$s \times \sigma_2(s) = E(s)[s^2 + \lambda_1 s + k_i] \quad (3.35)$$

$$\lim_{t \rightarrow \infty} e(t) = \lim_{s \rightarrow 0} s \times E(s) = \lim_{s \rightarrow 0} \frac{s}{s^2 + \lambda_1 s + k_i} \lim_{s \rightarrow 0} s \sum(s) = 0 \quad (3.36)$$

### 3.5 SIMULATION RESULTS AND DISCUSSION FOR TWO MASS MODEL

#### Case 1: Results for mathematical model

Initially, the proposed controllers were tested on the two mass mathematical WT model. Figure 3.1 shows the wind speed profile. The parameters of the two mass model are given in reference (Boukhezzer, B. and Siguerdidjane, H. 2011).

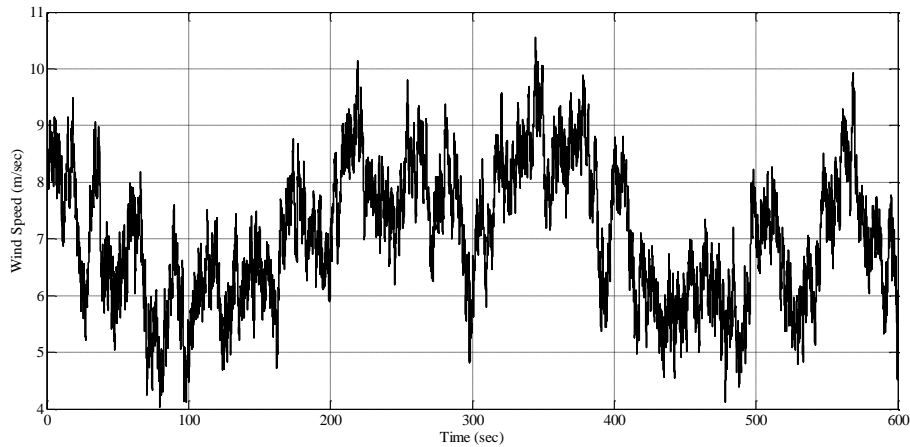


Figure 3.1: Test Wind Speed Profile

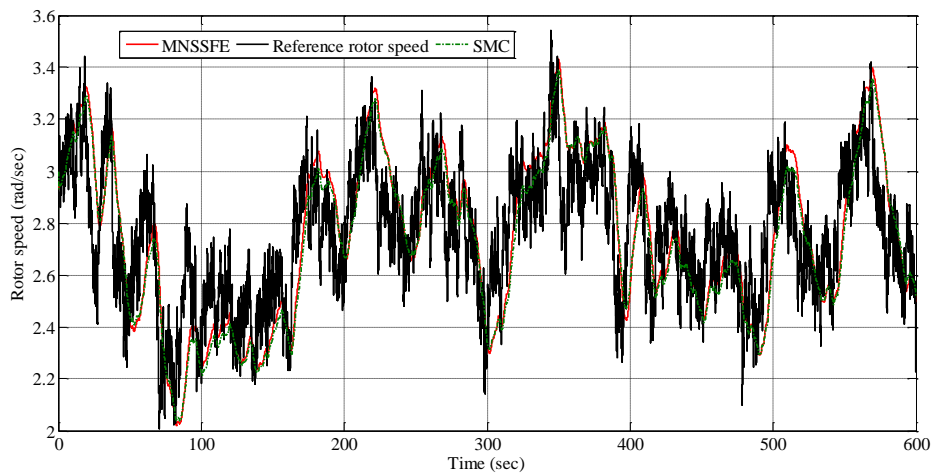


Figure 3.2: Rotor speed comparison using mathematical model.

Using the mathematical model, the rotor speed for two different controllers are shown in Figure 3.2. The objective is to minimize the tracking error in the rotor speed. From this figure it is observed that SMC is able to track the optimal rotor speed without any turbulence. In MNSSFEE, the obtained rotor speed has more turbulence compared to SMC, which indicates that the control torque having more variations and the electrical efficiency is almost same.

Table 3.1: Comparison of different control strategy based on two mass model using mathematical model.

Control Strategy	MNSSFEE	SMC
STD ( $T_{ls}$ ) kNm	8.135	7.509
STD ( $T_{em}$ ) kNm	0.176	0.145
Electrical Efficiency (%)	89.29	89.64

Table 3.1 gives the performance comparison of SMC and MNSSFE for mathematical model. From this table it was found that, compared to SMC, MNSSFE has more standard deviation in control torque and low speed shaft torque i.e. 0.176 kNm and 8.135 kNm respectively. This indicates transient load on the drive train is more for MNSSFE. From the results it is clear that both nonlinear controllers have almost similar electrical efficiency, but in terms of smooth control action, SMC is better than MNSSFE.

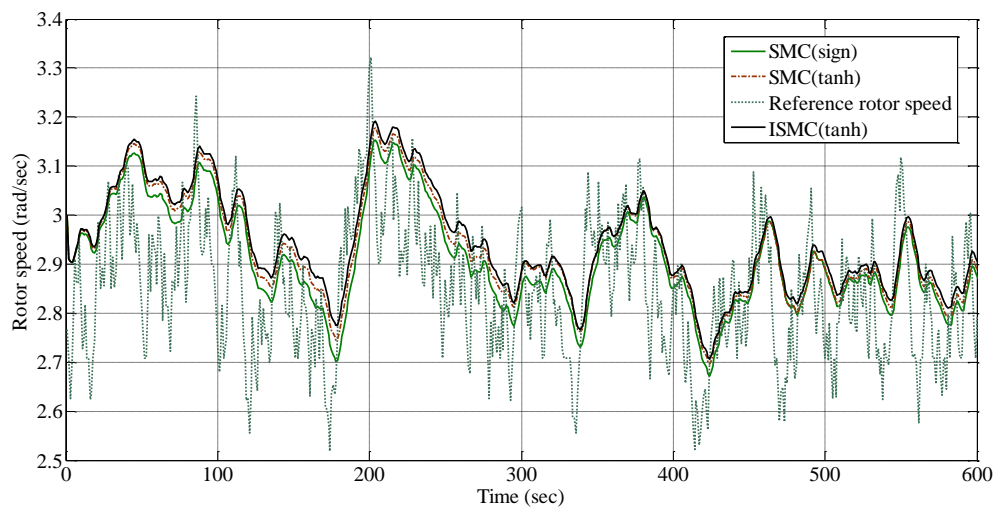


Figure 3.3: Rotor speed comparison for SMC and ISMC for two mass model.

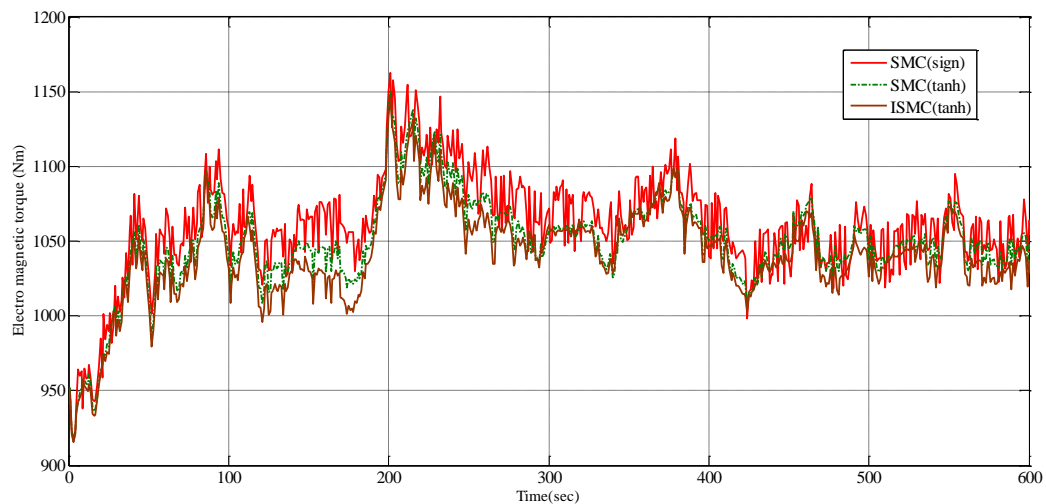


Figure 3.4: Electromagnetic torque comparison for SMC and ISMC.

Figure 3.3 shows the rotor speed comparison for SMC and ISMC for two mass model. Figure 3.4 shows the electromagnetic torque comparison for SMC and ISMC for two mass model. In order to understand the control action performance of the controllers, the electromagnetic torque ( $T_{em}$ ) and low speed shaft torque ( $T_{ls}$ ) are very useful. By

referring Table 3.2, the maximum value of ' $T_{em}$ ' is 1.375 kNm for ATF, and minimum value of 1.146 kNm for ISMC (tanh). Figure 3.5 shows the comparison for low speed shaft torque for SMC and ISMC.

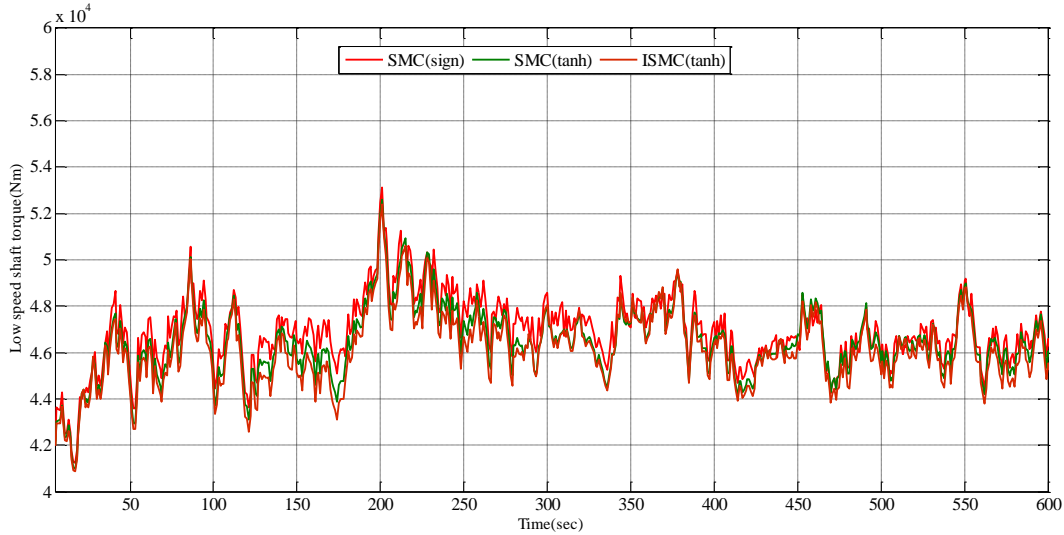


Figure 3.5: Low speed shaft torque comparison for SMC and ISMC.

Table 3.2: Comparisons for various control strategy (Two mass model)

	ATF	ISC	SMC (sign)	SMC (tanh)	ISMC (tanh)
STD( $T_{em}$ )Nm	53.07	53.28	34.76	32.24	32.03
Max( $T_{em}$ )kNm	1.375	1.331	1.162	1.151	1.146
$\eta_{elec}$ (%)	93.0	90.72	89.97	89.61	89.33
$\eta_{aero}$ (%)	94.3	92.53	91.92	91.56	91.32
Std( $T_{ls}$ )	2.62	2.48	1.58	1.57	1.60
Max( $T_{ls}$ )	60.94	59.21	53.12	52.6	52.37
Relative variation ( $T_{em}$ )(%)	27.01	24.87	23.18	22.36	22.17
Relative variation ( $T_{ls}$ )(%)	53.29	50.04	26.67	25.86	25.62

## Case 2: FAST Results

The rotor speed comparisons for FAST simulator are shown in Figure 3.6. From Figure 3.6 it is clear that at initial wind condition 0-30 sec, both controllers SMC and MNSSFE are not able to track the optimal rotor speed due to the initial setting in the AeroDyn input file. At high wind speed variations such as 220, 350 and 550 sec, the SMC is tracking the reference rotor speed in a better way compared to MNSSFE. Except MNSSFE and SMC, all the other controllers have more tracking error in rotor speed.



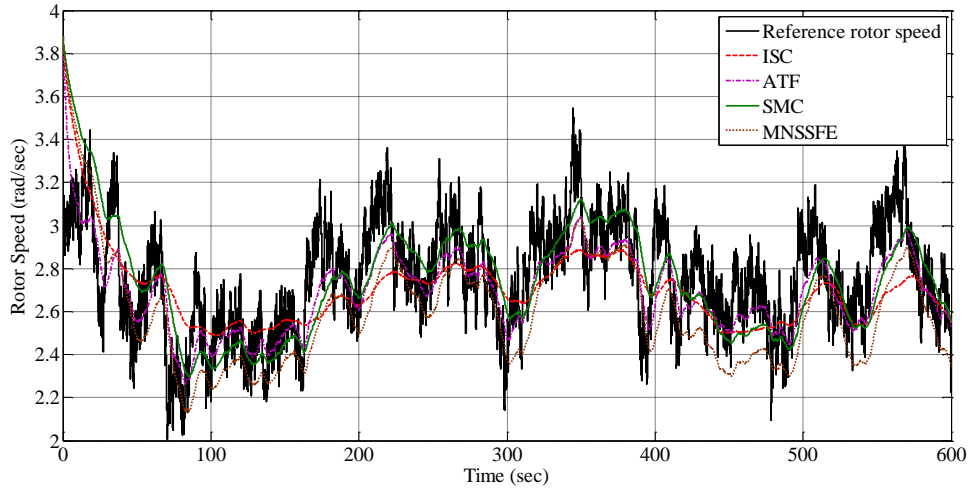


Figure 3.6: Rotor speed comparison for ATF, ISC, MNSSFE and SMC for FAST simulator

Table 3.3 gives the performance analysis of all the conventional and proposed SMC controller. From Table 3.3 it is clear that the STD of ' $T_{em}$ ' and ' $T_{ls}$ ' is lowest for SMC and highest for ATF controller. ISC having very less STD of ' $T_{em}$ ' and ' $T_{ls}$ ', at the same time the efficiency is very low compared to all the controllers. The ISC control only depends on the generator speed which is not suitable and for higher variation in wind speed and introduces significant power loss. So, a compromise is to be made between the efficiency and the fatigue load on drive train. Except SMC, the ATF and MNSSFE have more standard deviation which ensures more drive train transient load. Compared to ISC and ATF, the aerodynamic and electrical efficiency of the proposed SMC and MNSSFE are better.

Table 3.3: Comparison of different control strategy based on two mass model using FAST simulator

Control Strategy	ISC	ATF	MNSSFE	SMC
STD( $T_{ls}$ ) (kNm)	9.629	23.03	23.13	17.23
Max( $T_{ls}$ ) (kNm)	45.62	130.8	136.7	105.7
STD( $T_{em}$ ) (kNm)	0.142	0.369	0.280	0.208
Max( $T_{em}$ ) (kNm)	1.010	2.500	1.807	1.450
$\eta_{elec}$ (%)	69.73	72.87	76.23	75.35
$\eta_{aero}$ (%)	85.59	85.06	94.67	94.32

To analyze the controller performances in a more detailed fashion, Figure 3.7 and Figure 3.8 show the box plot for low speed shaft torque and generator torque with the mean, median,  $\pm 25\%$  quartiles (notch boundaries),  $\pm 75\%$  quartiles (box ends),  $\pm 95\%$

bounds and the outliers. From the size of the boxes shown, it is clear that the ISC experiences minimum variation than others. It ensures that ISC has the minimum transient load on the drive train, at the same time we can find from Table 3.3 that the efficiency of ISC is not comparable with other controllers. Comparing the box plot of SMC and MNSSFE, it was seen that SMC has less variation in low speed shaft torque and generator torque.

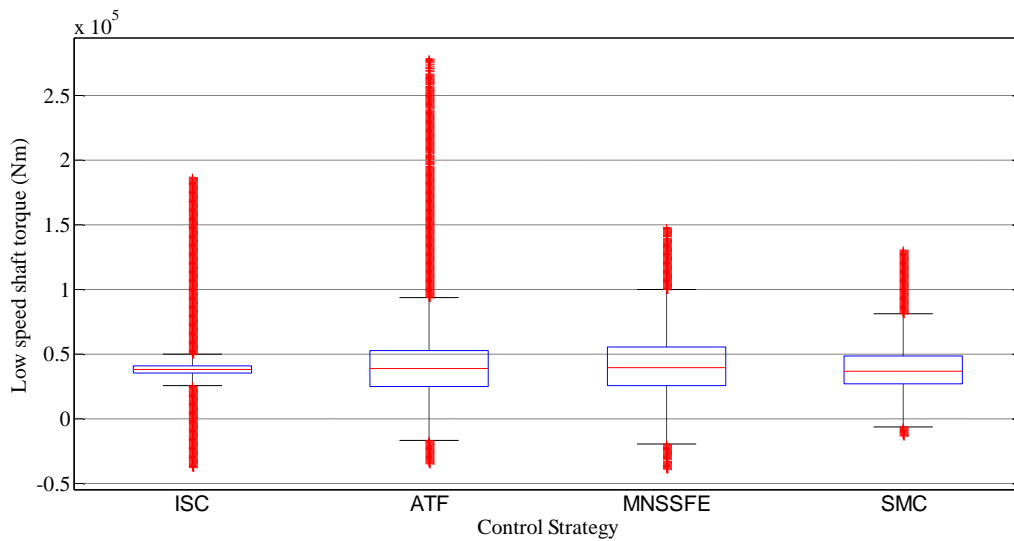


Figure 3.7: Boxplot for Low Speed Shaft Torque using FAST Simulator.

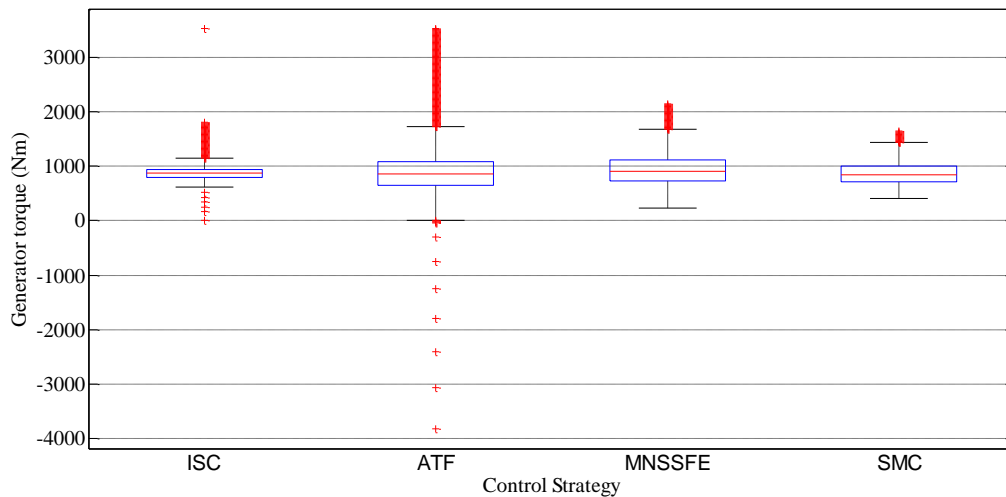


Figure 3.8: Boxplot for generator torque using FAST Simulator.

Figure 3.9 shows the box plot for rotor speed for FAST simulator. It was observed that apart from SMC and MNSSFE, other controllers such as ATF and ISC have more variations with respect to reference speed.

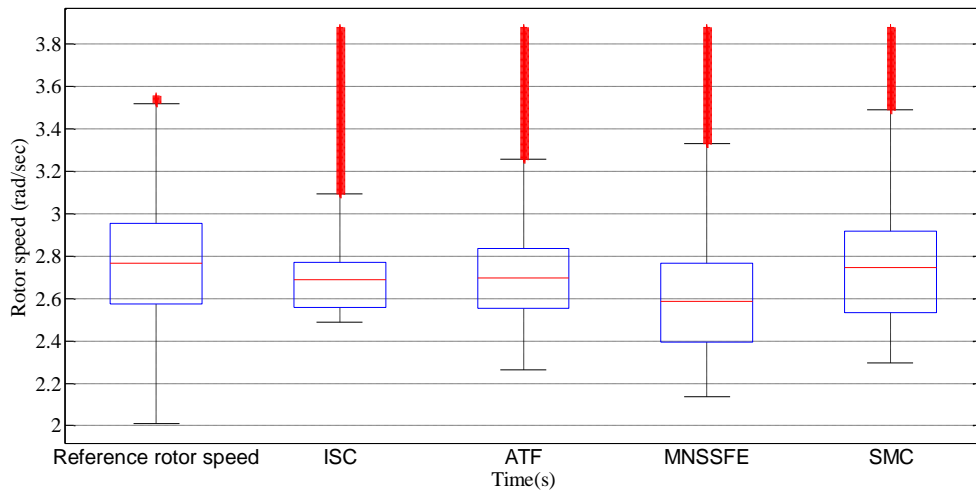


Figure 3.9: Boxplot for rotor speed using FAST Simulator.

The frequency analysis was carried out using the PSD on the low speed shaft torque which is shown in Figure 3.10. The MNSSF plot is completely above the SMC plot, so low speed shaft torque variation is more for MNSSF than SMC.

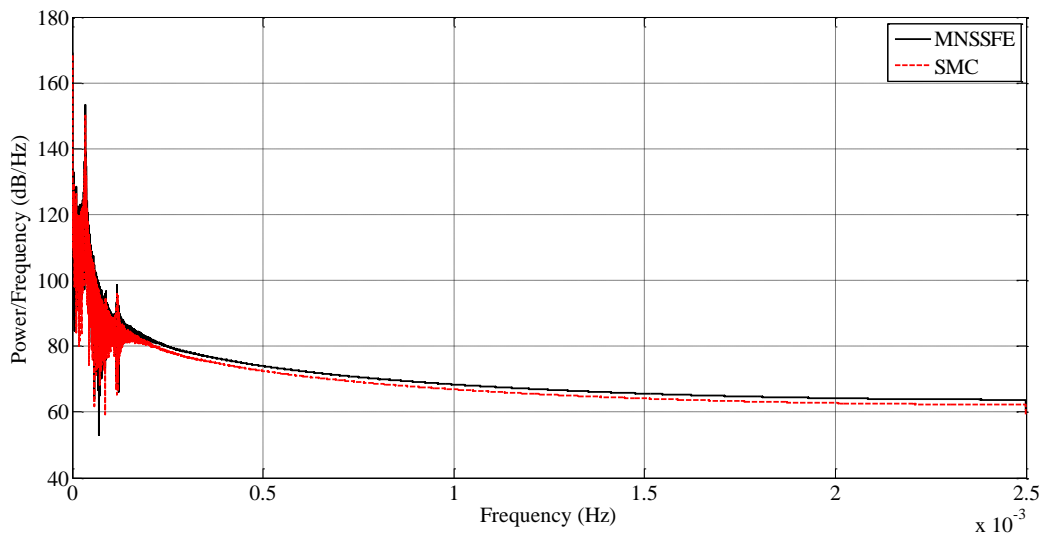


Figure 3.10: PSD for Low Speed Shaft Torque using FAST Simulator.

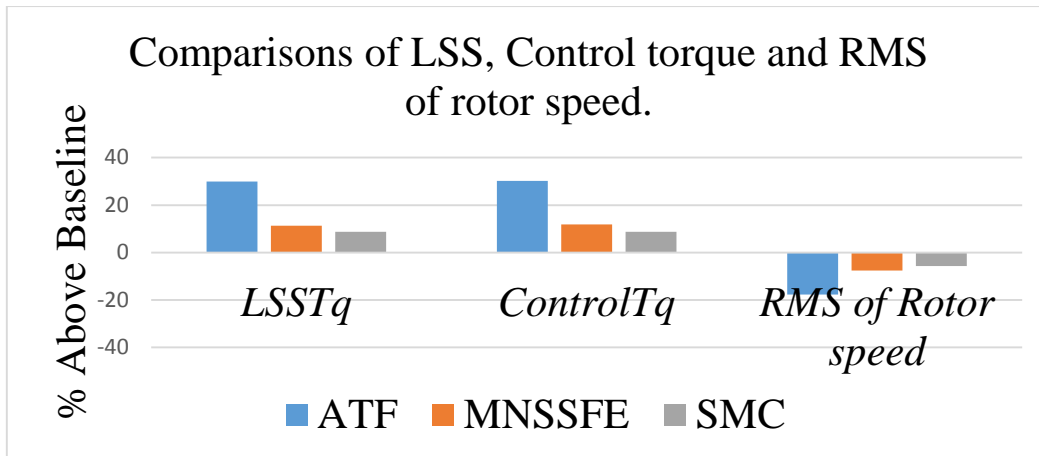


Figure 3.11: Comparison for baseline control with other controllers for LSS, Control torque and RMS of rotor speed.

Figure 3.11 shows comparison of low speed shaft torque, Control torque and RMS of the rotor speed for ATF, MNSSF and SMC by considering ISC as baseline control. All low speed shaft torques (*LSSTq*) and control torques (*ControlTq*) have higher values compared to the baseline controller.

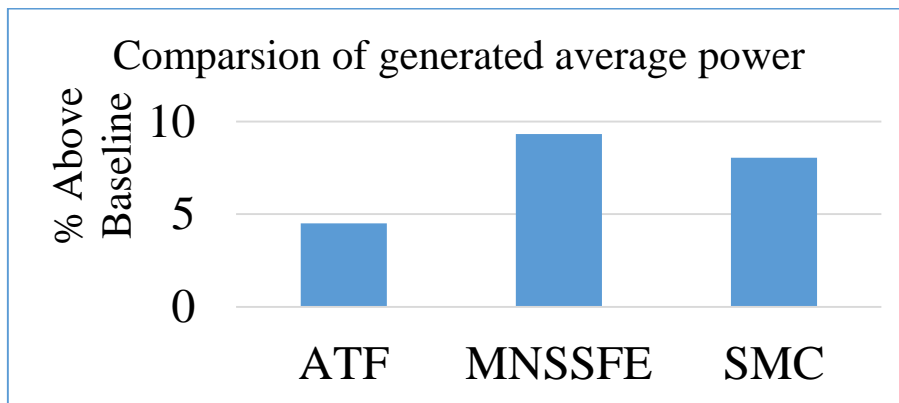


Figure 3.12: Comparison for baseline control with other controllers for generated average power.

As shown in Figure 3.12, the MNSSF controller has improved power capture of 0.9% compared to SMC. So the efficiency of MNSSF is almost 1% more than SMC. Fast tracking introduces more variation in control input. So an intermediate tracking has to be chosen and a compromise has been made between efficiency and load mitigation. From this analysis, even though MNSSF gives a little better efficiency than SMC, by considering transient load on drive train and smooth control input, SMC is found to be optimal.

Table 3.4: SMC performance for different wind speed profiles.

Mean Wind speed (m/sec)	Electrical Efficiency (%)	$T_{ls}$ Standard Deviation kNm	Max ( $T_{em}$ )kNm
7 (m/sec)	75.35	17.23	1.450
8 (m/sec)	73.45	16.87	1.585
8.5 (m/sec)	73.30	15.96	1.728

Table 3.5: MNSSFEE performance for different wind speed profiles.

Mean Wind speed (m/sec)	Electrical Efficiency (%)	$T_{ls}$ Standard Deviation kNm	Max ( $T_{em}$ )kNm
7 (m/sec)	76.23	23.13	1.807
8 (m/sec)	74.85	23.35	1.995
8.5 (m/sec)	74.52	23.58	2.076

In order to avoid the torsional resonance mode by choosing the proper tracking dynamics, a trade-off is made between power capture optimization with smooth control and reduced transient load on low speed shaft torque. A good dynamic tracking i.e. as similar to WT fast dynamics gives better power capture but it requires more turbulence in control torque. Conversely, slow tracking gives smooth control action with less power capture. The simulations were performed with different wind speed profiles with the mean wind speed at below rated value. The results are given in Table 3.4 and Table 3.5. From these tables it was observed that with an increase in mean wind speed, the maximum value of the control input ( $T_{em}$ ) also increases. In all the cases, both SMC and MNSSFEE controllers have almost same efficiency but the transient load reduction is better for SMC. As the mean wind speed increases, the standard deviation also increases for MNSSFEE compared to SMC. It was observed that when wind speed undergoes high variation, the SMC can produce better power capture with reduced mechanical stress on the drive train.

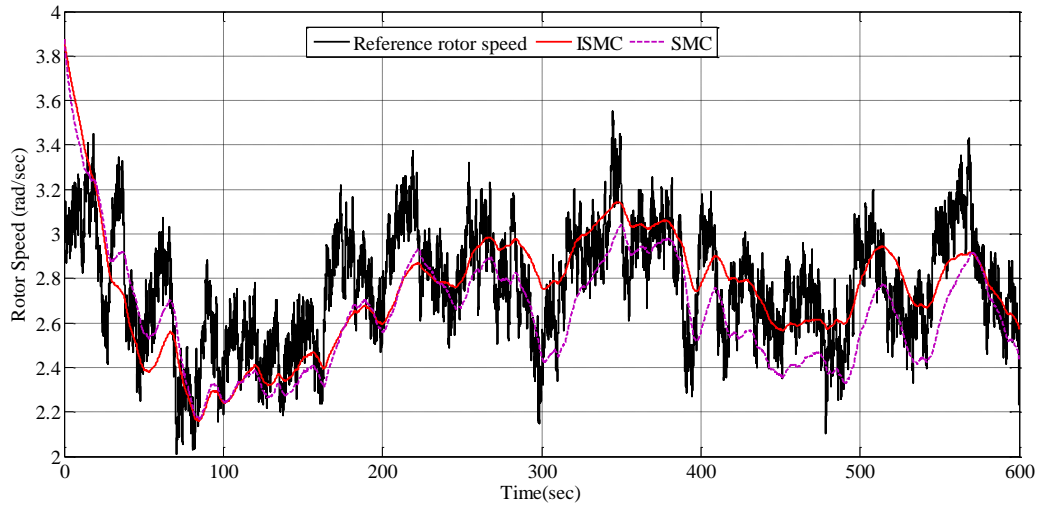


Figure 3.13: Rotor speed comparison for SMC and ISMC for FAST simulator.

Figure 3.13 shows the rotor speed comparisons for ISMC and SMC. Table 3.6 gives the performance analysis of all the conventional and proposed controllers with disturbances of  $5/n_g$  kNm. The STD of  $T_{em}$  and  $T_{ls}$  is less for ISMC compared to SMC and ATF. This ensures the smoothness of the control input and low speed shaft torque in ISMC compared to SMC and ATF. Table 3.6 data shows that ISC has lowest STD of  $T_{em}$  and  $T_{ls}$ , but its efficiency is very low (69.73%) compared to all other controllers.

Table 3.6: Comparison of different control strategy based on two mass model using FAST simulator

Control Strategy	ISC	ATF	SMC	ISMC
STD( $T_{ls}$ ) (kNm)	9.629	23.03	21.84	13.59
Max( $T_{ls}$ ) (kNm)	45.62	130.8	131.4	73.4
STD( $T_{em}$ ) (kNm)	0.142	0.369	0.252	0.198
Max( $T_{em}$ ) (kNm)	1.010	2.500	1.690	1.260
$\eta_{elec}$ (%)	69.73	72.87	76.89	76.26
$\eta_{aero}$ (%)	85.59	85.06	96.78	96.56

Figure 3.14 and Figure 3.15 show the box plot for low speed shaft torque and generator torque with the mean, median,  $\pm 25\%$  quartiles (notch boundaries),  $\pm 75\%$  quartiles (box ends),  $\pm 95\%$  bounds and the outliers. It is clear that the ISC experiences minimum variation at the same time, efficiency of ISC is not comparable with other controllers. Comparing the box plot of ISMC and SMC, ISMC has less variation in low speed shaft torque and generator torque.

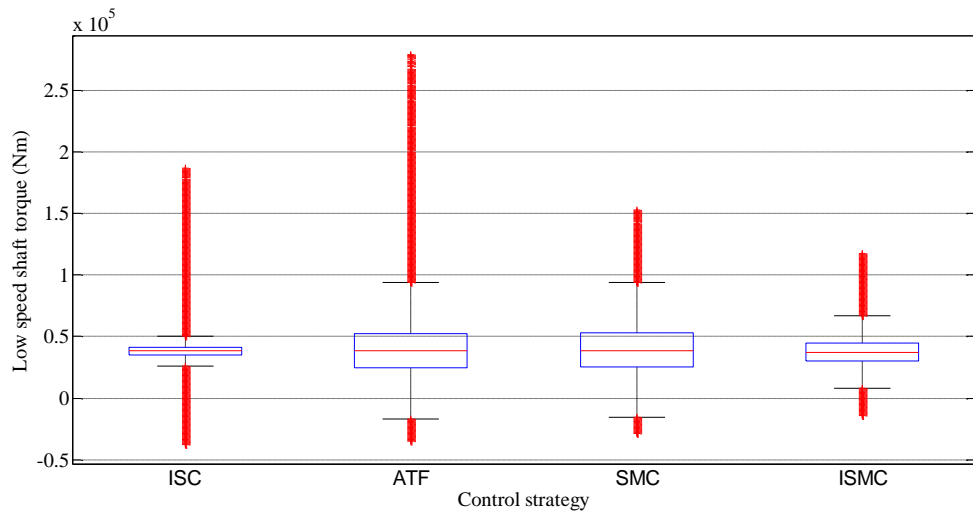


Figure 3.14: Boxplot for Low Speed Shaft Torque using FAST Simulator.

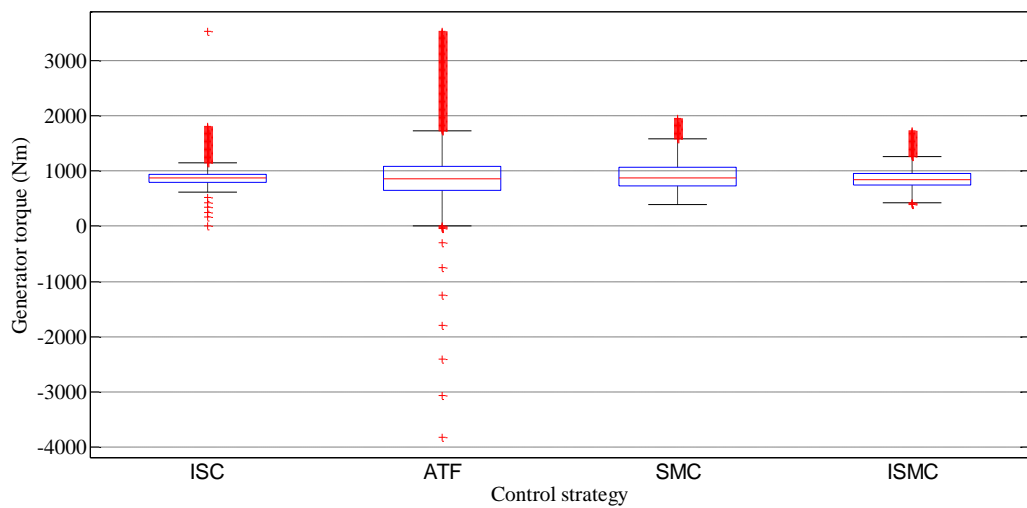


Figure 3.15: Boxplot for generator torque using FAST Simulator.

Figure 3.16 shows the box plot for rotor speed for FAST simulator. From this figure it is observed that ISMC and SMC have almost same variation in the reference rotor speed. Apart from ISMC and SMC, other controllers such as ATF and ISC have more variations in reference speed.

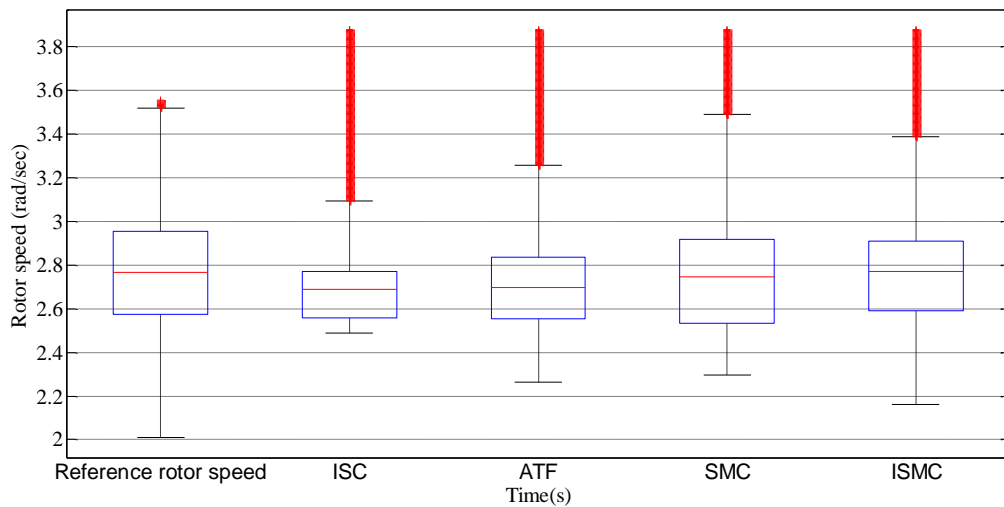


Figure 3.16: Boxplot for rotor speed using FAST Simulator.

The frequency analysis was carried out by using the PSD on the low speed shaft torque which is shown in Figure 3.17. As the SMC plot is completely above the ISMC plot, it can be concluded that low speed shaft torque variation is more for SMC than ISMC.

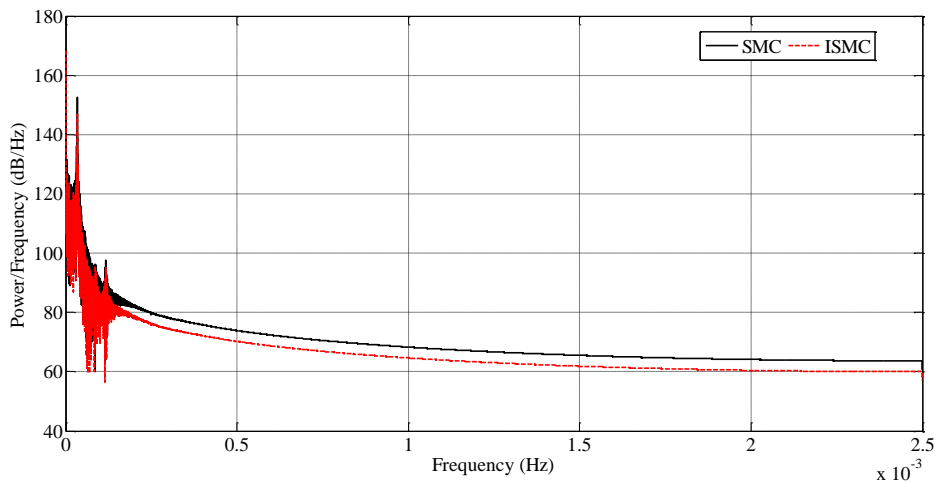


Figure 3.17: PSD for Low Speed Shaft Torque using FAST Simulator.

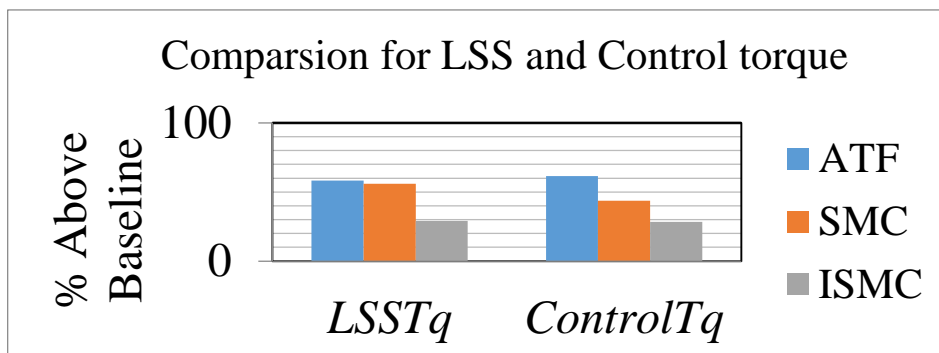


Figure 3.18: Comparison for baseline control with other controllers for LSS, and Control torque.



Figure 3.18 shows comparison of low speed shaft torque and control torque for ATF, SMC and ISMC by considering ISC as baseline control. The entire low speed shaft torques ( $LSST_q$ ) and control torques ( $ControlT_q$ ) have higher values compared to baseline controller.

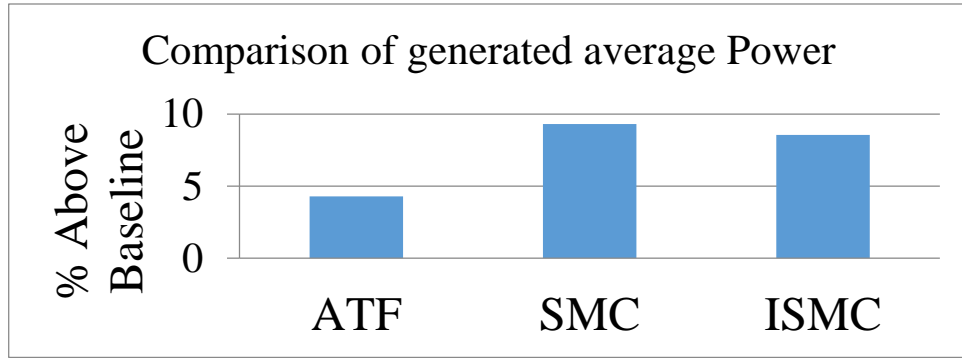


Figure 3.19: Comparison for baseline control with other controllers for generated average power.

Figure 3.19 shows the SMC controller has improved power capture by 0.75% compared to ISMC. From the above analysis and results given in Table 3.6 it was observed that even though SMC is slightly more efficient than ISMC, by considering transient load on drive train and smooth control input, ISMC was found to be optimal.

Table 3.7: SMC performance for different wind speed profiles

Mean Wind speed (m/sec)	Electrical Efficiency (%)	$T_{ls}$ Standard Deviation kNm	Max ( $T_{em}$ )kNm
7 (m/sec)	76.89	21.84	1.690
8 (m/sec)	74.51	20.31	1.783
8.5 (m/sec)	74.22	20.11	1.922

Table 3.8: ISMC performance for different wind speed profiles

Mean Wind speed (m/sec)	Electrical Efficiency (%)	$T_{ls}$ Standard Deviation kNm	Max ( $T_{em}$ )kNm
7 (m/sec)	76.26	13.59	1.260
8 (m/sec)	74.49	11.72	1.526
8.5 (m/sec)	74.68	11.98	1.762

The simulations were performed with different mean wind speed at region 2. The results are given in Table 3.7 and Table 3.8. From these tables it was observed that with an increase in mean wind speed, the maximum value of the control input ( $T_{em}$ ) also increases. In all the cases, both SMC and ISMC controllers have almost same efficiency but the transient load reduction is better for ISMC. As the mean wind speed increases,

the rate of increase of STD is more for SMC than ISMC. It was observed that when wind speed undergoes high variation, the ISMC can produce better power capture with reduced transient load on the drive train.

### **3.6 CONCLUSION**

In this chapter, two mass model based mathematical model for variable speed wind turbine was discussed. Initially, some of the conventional controllers were adapted for the WT systems. The objective was to design a robust controller that maximizes the energy extraction from the wind with load mitigation. To meet above requirements, MNSSFE, SMC and ISMC nonlinear controllers were proposed for two mass model. These controllers have the ability to reject disturbance and accommodate parameter uncertainty. The performances of these controllers were compared with the conventional ATF and ISC using mathematical model and FAST aero elastic simulator. From this analysis it was found that ISMC has less drive train oscillation compared to other controllers. Finally it was concluded that a trade-off is to be maintained between the efficiency and mechanical stress on the drive train. To prove the efficiency of the proposed ISMC control, the simulation was conducted for different wind speed profiles with different turbulence component.

The main focus in this chapter was the control design for below rated wind speed. The next chapter will mainly focus on the separate control design in both below rated and above rated wind speed at the same time it will discuss about the control of WT in region 2.5 i.e. the transient period between below rated wind speed to above rated wind speed.

## **CHAPTER 4**

### **4 CONTROLLER DESIGN FOR ABOVE RATED WIND SPEED AND TRANSITION REGION**

#### **4.1 INTRODUCTION**

This chapter mainly focuses on the control of variable speed variable pitch wind turbine (VSVPWT) for maximization of extracted power, regulation of extracted power and smooth transition between the regions. Initially, the nonlinear controllers i.e. SMC and ISMC were proposed for region 2 whereas a conventional PI control was adapted for region 3 of a VSVPWT. The proposed controller was combined with MNR wind speed estimator to estimate the wind speed. The control law is derived for region 2 which was also adapted for the transition period (region 2.5). The dynamic simulations were tested with nonlinear FAST WT. Finally ISMC with fuzzy based pitch controller was compared with an industrial state of the art baseline + PI controller. Different types of wind speed profiles were chosen for all the wind speed regions.

The baseline + PI controller was considered as the conventional baseline controller with conventional PI as pitch controller. In order to analyze the transition region, the wind speeds were considered between above and below rated wind speeds. In some cases the wind speed profile was taken from below rated wind speed and was raised up to cutout wind speed, again comes down to same speed with a step of 1m/sec. It was seen that in region 3, both the conventional PI and proposed fuzzy PI were almost working in a similar way but, in some cases fuzzy PI was found to generate less actuating control signal to pitch actuator compared to conventional PI. In transition region (region 2.5) the control law was derived based on generator speed, which introduced switching in baseline controller and led to more oscillation on the control input compared to proposed controllers.

## 4.2 CONVENTIONAL BASELINE CONTROLLER OF THE INDUSTRIAL STATE OF ART

The baseline control of industrial state of the art (Darrow, P.J. 2009) is discussed in this section. The control law derivation is based on the operating regions which is given in equation (4.1). The maximum generator speed is 1600rpm, efficiency of the generator is 92% and the rated generator torque is 3524.37 Nm. If the generator speed exceeds the rated speed, then generator torque is considered as the maximum torque and the pitch controller comes into action. Once the generator speed attains 94% to 98.5% of the rated speed, then the region 2.5 torque control comes into action. Figure 4.1 shows the simulation model of the CART 3 WT.

$$T_{em}(\omega_g) = \begin{cases} k_1 \omega_g^2 & \text{Region 2} \\ T_1 + \frac{T_{em_{rated}} - T_1}{\omega_{g_{rated}} - \omega_{g_1}} (\omega_g - \omega_{g_1}) & \text{Region 2.5} \\ T_{em_{rated}} & \text{Region 3} \end{cases} \quad (4.1)$$

Where

$$k_1 = 0.5 \rho \pi \frac{R^5}{n_g^3 \lambda_{opt}^3} C_{p_{opt}}$$

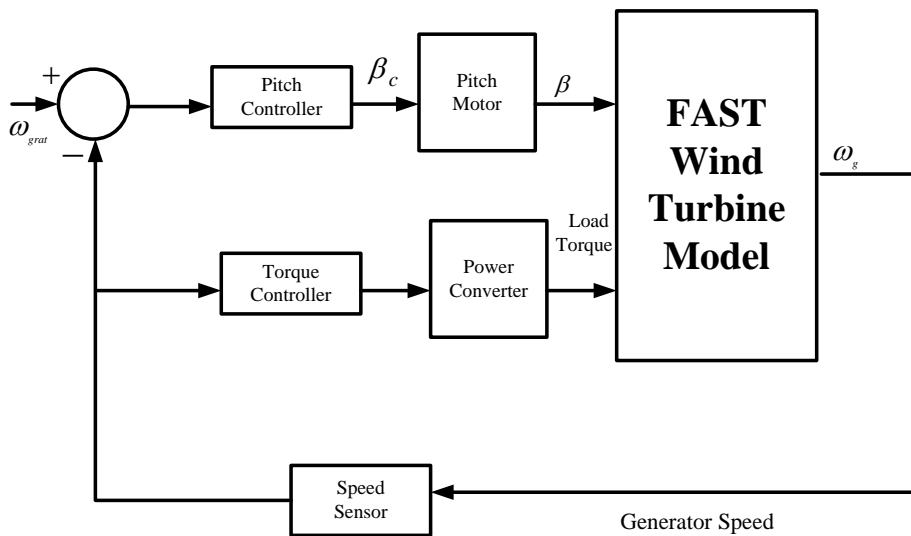


Figure 4.1: Simulation model for the CART3 baseline Controller.

### 4.3 CONVENTIONAL PITCH CONTROLLER FOR ABOVE RATED WIND SPEED

Gain scheduled proportional-integral (PI) controller was used for full span rotor collective blade pitch angle. The speed error was defined as the difference between the measured generator speed and the rated generator speed. The blade pitch angle controller design was based on the WT model. The main aim of the blade pitch angle control system was to regulate the generator speed (Jonkman, J. et al. 2009). In order to compute the control gains, drive train model is considered which is given in equation (4.2)

$$T_a - \eta_g T_g = (I_{Rotor} + \eta_g^2 I_{gen}) \frac{d}{dt} (\Omega_0 + \Delta\Omega) = I_{Drivetrain} \Delta\dot{\Omega} \quad (4.2)$$

where ( $I_{Rotor}$ ) is the rotor inertia, ( $I_{gen}$ ) is the generator inertia, ( $I_{Drivetrain}$ ) is the drive train inertia,  $\Omega$  low speed shaft rotational speed,  $P_0$  is the rated mechanical power and  $\Omega_0$  rated low speed shaft rotational speed. The generator torque control maintains constant power at region 3 provided that generator torque is inversely proportional to the generator speed as given in equation (4.3)

$$T_g (n_g \Omega) = \frac{P_0}{n_g \Omega} \quad (4.3)$$

Assuming that rotor speed is having negligible effect on aerodynamic torque, the region 3 torque can be expressed as:

$$T_a(\theta) = \frac{P(\theta, \Omega_0)}{\Omega_0} \quad (4.4)$$

where  $P$  is the mechanical Power and ' $\theta$ ' is the full span rotor collective blade pitch angle. Using the Taylor series expansion of equations (4.3) and (4.4) we get as,

$$T_g \approx \frac{P_0}{n_g \Omega_0} - \frac{P_0}{n_g \Omega_0^2} \Delta\Omega \quad (4.5)$$

and

$$T_a \approx \frac{P_0}{\Omega_0} + \frac{1}{\Omega_0} \left( \frac{\partial P}{\partial \theta} \right) \Delta \theta \quad (4.6)$$

where ‘ $\Delta\theta$ ’ small perturbation of the blade pitch angle around the operating point. These rotor speed perturbations are related to PID control given in equation (4.7)

$$\Delta \theta = K_p n_g \Delta \Omega + K_I \int_0^t n_g \Delta \Omega dt + K_D n_g \dot{\Delta \Omega} \quad (4.7)$$

The equation of motion for the rotor speed error given in equation (4.8) can be obtained by setting  $\dot{\varphi} = \Delta \Omega$  and combining the above expressions.

$$\left[ \underbrace{I_{Drivetrain} + \frac{1}{\Omega_0} \left( -\frac{\partial P}{\partial \theta} \right) n_g K_D}_{M_\varphi} \right] \ddot{\varphi} + \left[ \underbrace{\frac{1}{\Omega_0} \left( -\frac{\partial P}{\partial \theta} \right) n_g K_P - \frac{P_0}{\Omega_0^2}}_{C_\varphi} \right] \dot{\varphi} + \left[ \underbrace{\frac{1}{\Omega_0} \left( -\frac{\partial P}{\partial \theta} \right) n_g K_I}_{K_\varphi} \right] \varphi = 0 \quad (4.8)$$

Idealized PID controlled rotor speed error given in equation (4.8) represents the second order system with the natural frequency ‘ $\omega_{\varphi n}$ ’ and damping ratio ‘ $\zeta_\varphi$ ’

$$\omega_{\varphi n} = \sqrt{\frac{K_\varphi}{M_\varphi}} \quad (4.9)$$

and

$$\zeta_\varphi = \frac{C_\varphi}{2\sqrt{K_\varphi M_\varphi}} = \frac{C_\varphi}{2M_\varphi \omega_{\varphi n}} \quad (4.10)$$

The sensitivity of the aerodynamic power to the rotor collective pitch blade pitch angle is negative  $\left( \frac{\partial P}{\partial \theta} \text{ is negative} \right)$ . In region 3, drop in generator torque introduces the

increasing speed error which is clearly indicated in equation (4.8) by the term  $\frac{-P_0}{\Omega_0^2}$ . To

neglect the derivative gain, ignoring the negative damping from the generator torque controller (Hansen, M.H. et al. 2005). The response characteristics is given by  $\omega_{\varphi n} = 0.6$

rad/s and  $\zeta_\varphi = 0.6$  to  $0.7$ . The given time response specifications decides the appropriate

PI gains provided  $\frac{\partial P}{\partial \theta}$  is known.

$$K_P = \frac{2I_{Drivetrain}\Omega_0\zeta_\varphi\omega_{\varphi n}}{n_g \left( -\frac{\partial P}{\partial \theta} \right)} \quad (4.11)$$

and

$$K_I = \frac{I_{Drivetrain}\Omega_0\omega_{\varphi n}^2}{n_g \left( -\frac{\partial P}{\partial \theta} \right)} \quad (4.12)$$

$$\frac{\partial P}{\partial \theta} = \left[ \frac{\frac{\partial P}{\partial \theta}(\theta=0)}{\theta_k} \right] \theta + \left[ \frac{\partial P}{\partial \theta}(\theta=0) \right] \quad (4.13)$$

$$\frac{1}{\frac{\partial P}{\partial \theta}} = \frac{1}{\frac{\partial P}{\partial \theta}(\theta=0) \left( 1 + \frac{\theta}{\theta_k} \right)} \quad (4.14)$$

Table 4.1: Sensitivity of the aerodynamic power to blade pitch angle in region 3 (above rated wind speed)

Wind speed (m/s)	HSS Speed (RPM)	Rotor Speed (RPM)	Pitch Angle (degrees)	$\frac{\partial P}{\partial \theta}$ (kilawatt/rad)	$\frac{\partial P}{\partial \theta}$ (watt/rad)
12	1576	36.51190807	3.7	-4.43E+03	-4.43E+06
12.5	1600	37.06792698	4.2	-4.94E+03	-4.94E+06
13	1600	37.06792698	7.095	-5.99E+03	-5.99E+06
14	1600	37.06792698	9.86	-7.30E+03	-7.30E+06
15	1600	37.06792698	11.877	-8.29E+03	-8.29E+06
16	1600	37.06792698	13.589	-9.27E+03	-9.27E+06
17	1600	37.06792698	15.124	-1.02E+04	-1.02E+07
18	1600	37.06792698	16.5495	-1.09E+04	-1.09E+07
19	1600	37.06792698	17.8977	-1.16E+04	-1.16E+07
20	1600	37.06792698	19.812	-1.25E+04	-1.25E+07
21	1600	37.06792698	20.4106	-1.32E+04	-1.32E+07

22	1600	37.06792698	21.5977	-1.40E+04	-1.40E+07
23	1600	37.06792698	22.7387	-1.49E+04	-1.49E+07
24	1600	37.06792698	23.841	-1.59E+04	-1.59E+07
25	1600	37.06792698	24.9073	-1.69E+04	-1.69E+07

The blade pitch sensitivity ( $\partial P/\partial\theta$ ) is nothing but the aerodynamic property of the rotor which depends on the wind speed, rotor speed and blade pitch angle. For NREL 600kW turbine, sensitivity of the aerodynamic power to blade pitch angle over region 3 is given in Table 4.1. This makes fixed PI gain not applicable for effective speed control. The variation in pitch sensitivity is related linearly with blade pitch angle as given in equation (4.13).

where  $\frac{\partial P}{\partial\theta}(\theta = 0)$  is the pitch sensitivity at rated speed, and ' $\theta_K$ ' is the blade pitch angle at which pitch sensitivity has doubled from its value at the rated operating point, is given in equation (4.15)

$$\frac{\partial P}{\partial\theta}(\theta = \theta_K) = 2 \frac{\partial P}{\partial\theta}(\theta = 0) \tag{4.15}$$

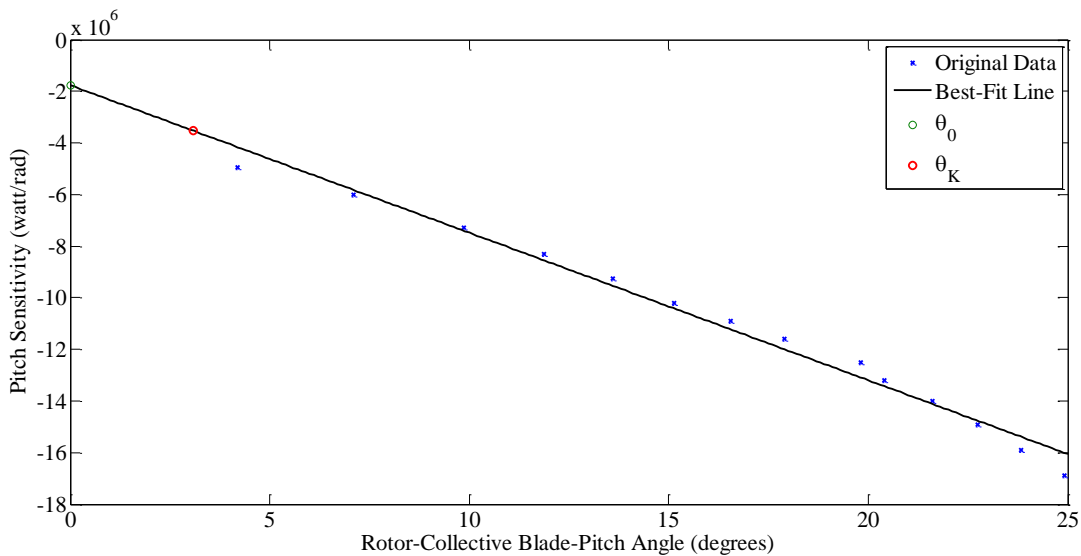


Figure 4.2: Best fit line of the pitch sensitivity in region 3.



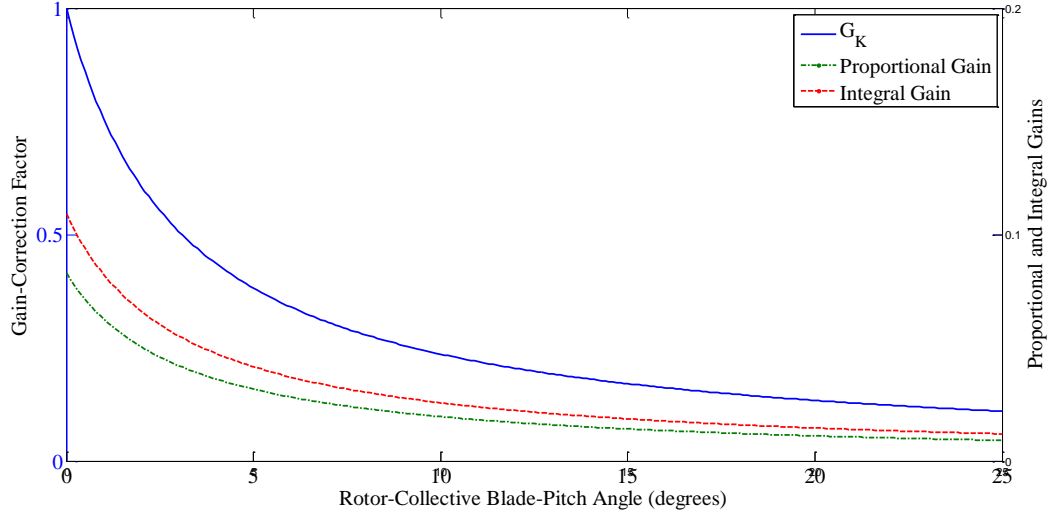


Figure 4.3: Baseline pitch control system gain scheduling law.

Figure 4.2 shows the best line fit of pitch sensitivity in region 3. Figure 4.3 shows the baseline pitch control system gain scheduling law. The linear relation between pitch sensitivity and blade pitch angle presents a simple technique for implementing gain scheduling based on blade pitch angle.

$$K_P(\theta) = \frac{2I_{Drivetrain}\Omega_0\zeta_\varphi\omega_{\varphi n}}{n_g \left( -\frac{\partial P}{\partial \theta}(\theta=0) \right)} G_K(\theta) \quad (4.16)$$

and

$$K_I(\theta) = \frac{I_{Drivetrain}\Omega_0\omega_{\varphi n}^2}{n_g \left( -\frac{\partial P}{\partial \theta}(\theta=0) \right)} G_K(\theta) \quad (4.17)$$

where ‘ $G_K(\theta)$ ’ is the dimensionless gain scheduling factor which depends on blade pitch angle.

$$G_K(\theta) = \frac{1}{1 + \frac{\theta}{\theta_K}} \quad (4.18)$$

Calculation of the gain correction at the next time step, is based on the blade pitch angle from the previous time step (Hansen, M.H. et al. 2005). Figure 4.4 shows the gain scheduling PI controller for blade pitch angle. Gain correction factor is multiplied with PI gains which is used for blade pitch angle.

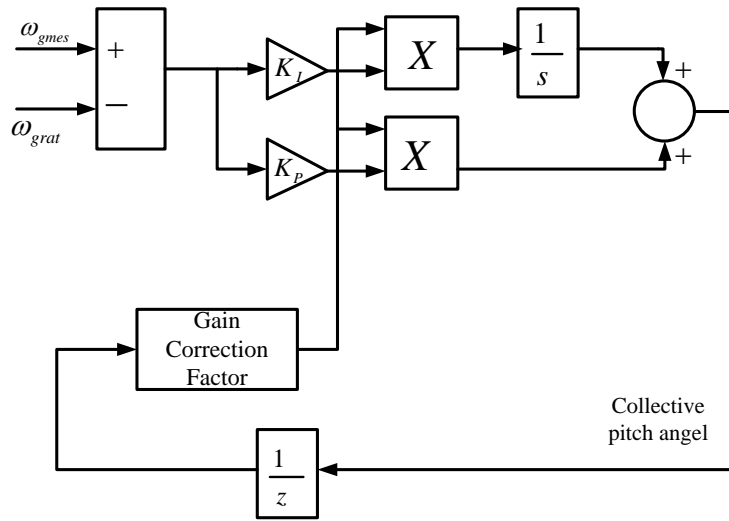
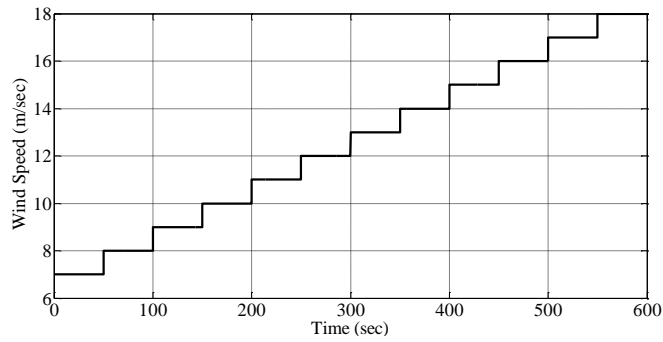
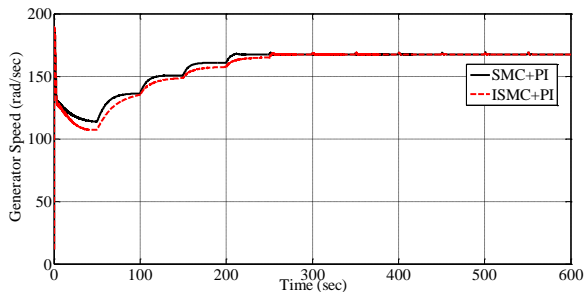


Figure 4.4: Gain scheduling control law.

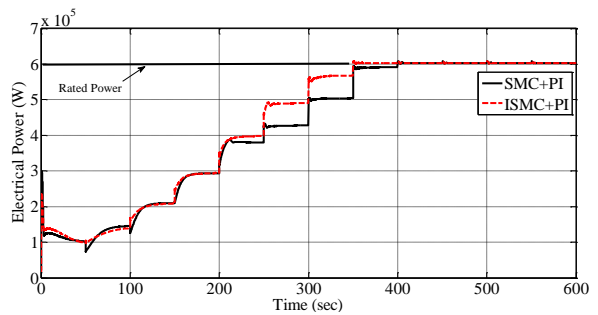
#### 4.4 SIMULATION RESULTS FOR SMC AND ISMC WITH CONVENTIONAL PI PITCH CONTROL



a)



b)



c)

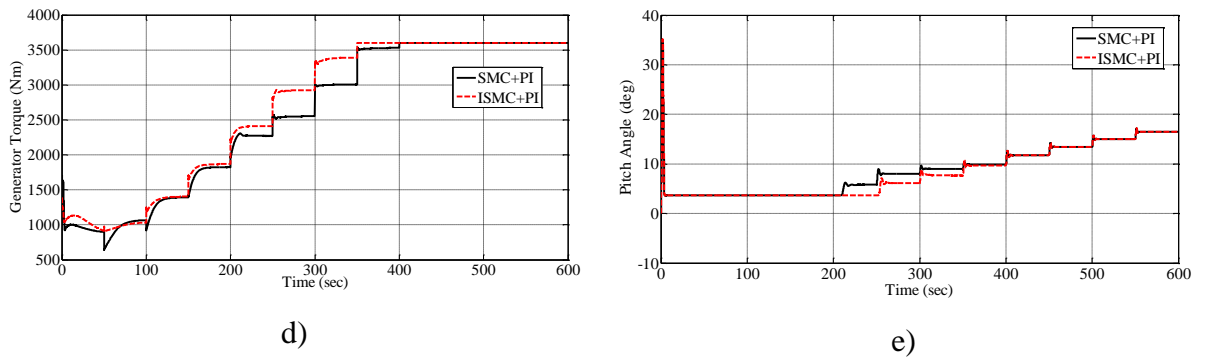


Figure 4.5: Simulation results of 600kW CART 3 WT using SMC and ISMC in full range of operation (Step change wind profile). a) Wind speed profile b) Generator Speed c) Electrical Power d) Generator Torque e) Pitch angle

Figure 4.5 a) Figure 4.6 a) and Figure 4.7 a) show the three different test wind speed consisting of 10min dataset which was generated by the binary file format. The transition regions are 250 sec to 400 sec, 280 sec to 450 sec and 200 sec to 360 sec for Figure 4.5 a), 4.6 a) and 4.7 a) respectively. For below rated wind speed, torque control comes into action with constant pitch angle and for above rated wind speed, pitch control comes into action with rated torque. Figure 4.5 b), 4.6 b) and 4.7 b) show the comparison of generator speed for SMC and ISMC for below and above rated wind speeds corresponding to three different wind profiles. Both controllers achieve the nominal value of the generator speed of 11.5 m/s at 250 sec, 280 sec and 200 sec, which can be seen from Figure 4.5a), 4.6 a) and 4.7 a). As the wind speed approaches towards the rated speed, the WT generator speed reaches the nominal value i.e. 167.55 rad/sec. Figure 4.5 c), 4.6 c) and 4.7 c) show the electrical power comparison for SMC+PI and ISMC+PI in the transition period. At region 2.5, ISMC+PI can extract more power than SMC+PI with almost same mechanical stress on the drive train. Figure 4.5 d), 4.6 d) and 4.7 d) show the generator torque comparison in region 2.5 for SMC+PI and ISMC+PI. It can be observed that ISMC+PI produces more generated torque compared to SMC+PI in region 2.5. The STD of generated torque for SMC and ISMC found to be almost same. Figure 4.5 e), 4.6 e) and 4.7 e) show the pitch angle comparison for SMC+PI and ISMC+PI at region 2.5. Pitch variation is found to be more for SMC+PI compared to ISMC+PI. So the pitch actuator needs more control action for SMC+PI.

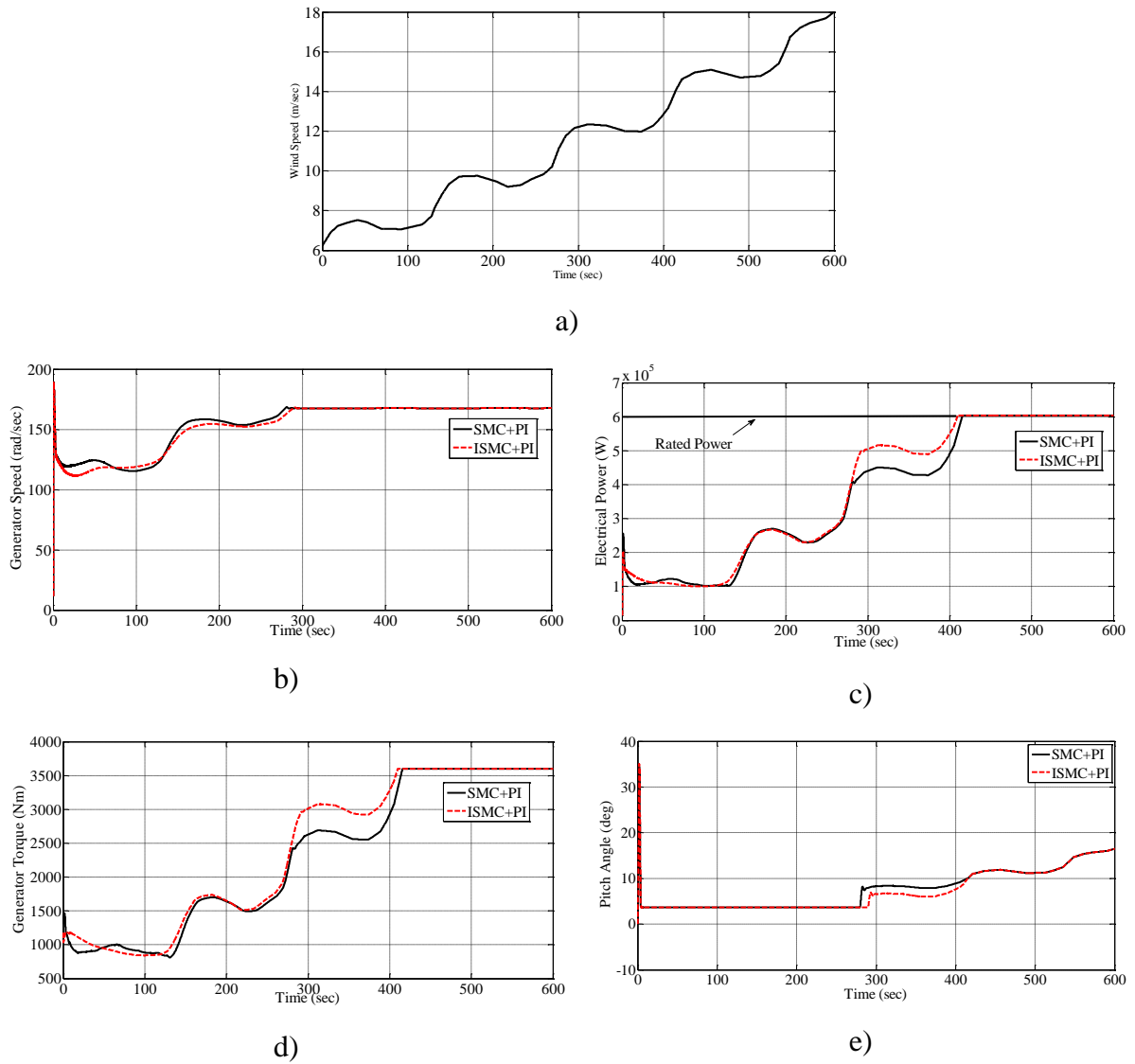
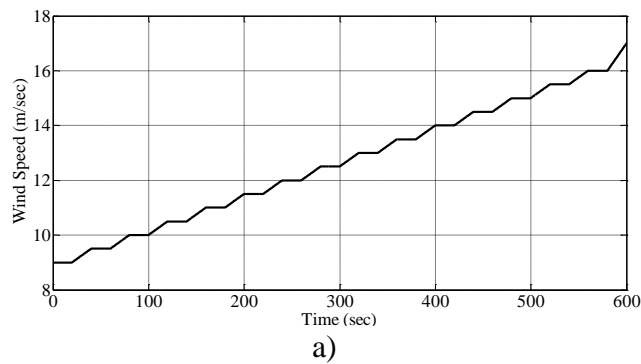


Figure 4.6: Simulation results of 600kW CART 3 WT using SMC and ISMC in full range of operation (Vertical wind profile). a) Wind speed profile b) Generator Speed c) Electrical Power d) Generator Torque e) Pitch angle



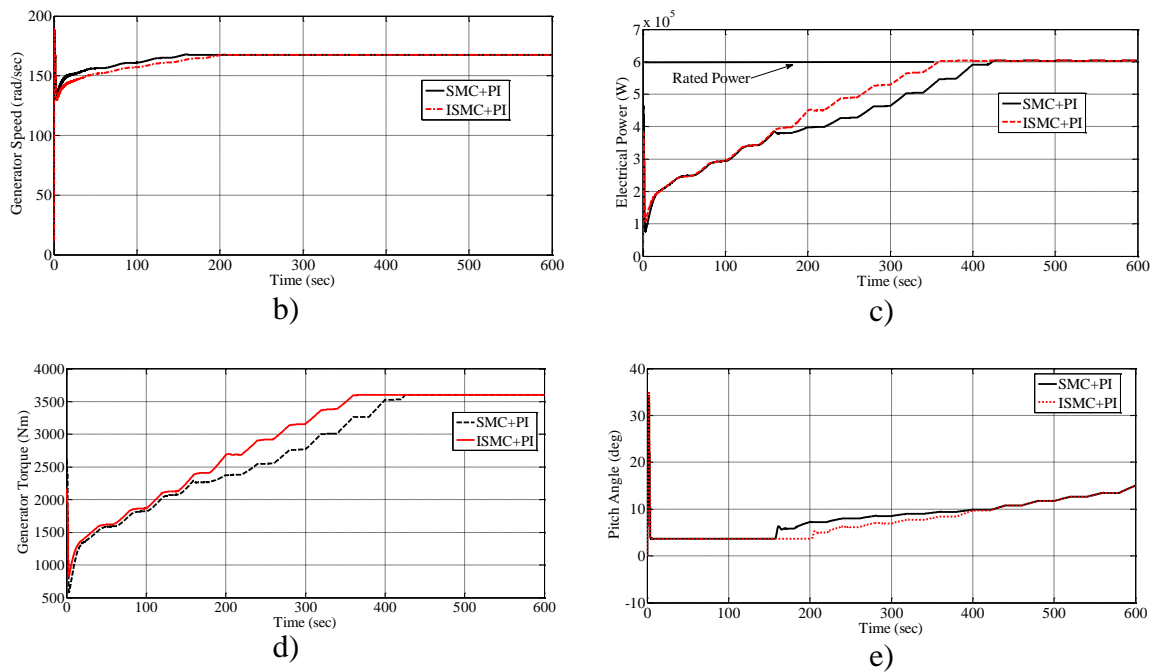


Figure 4.7: Simulation results of 600kW CART 3 WT using SMC and ISMC in full range of operation (Vertical wind profile). a) Wind speed profile b) Generator Speed c) Electrical Power d) Generator Torque e) Pitch angle

Figure 4.8 shows four wind speed profiles out of which one is starting from 5 m/s to 25 m/s with a step increase of 1m/s and again decreasing in the same fashion (represented in 25updown). The other three wind speed profiles show different wind speeds in region 2.5 and are represented as steptest2, steptest3 and steptest4. Table 4.2 shows the controller performance of SMC and ISMC for four wind speed profiles. From Table 4.2 and Figure 4.9, it is found that ISMC can capture higher power than SMC controller.

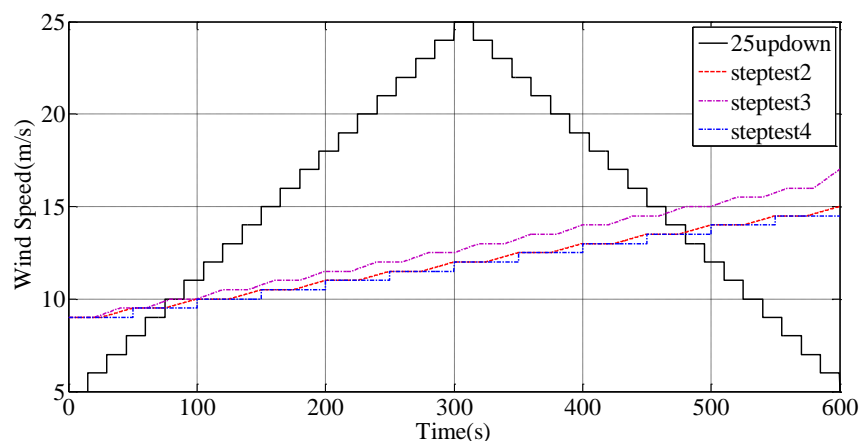


Figure 4.8: Different types of wind speed in region 2.5.

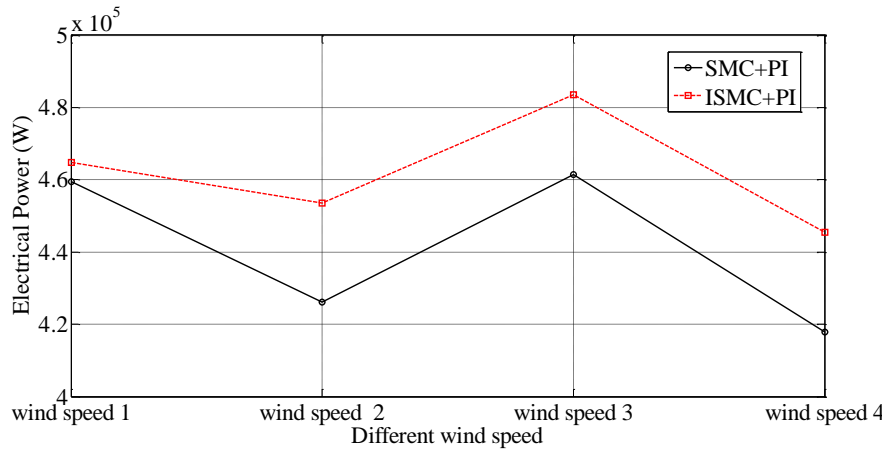


Figure 4.9: Power comparison for SMC and ISMC in region 2.5 for different wind speed profile.

Table 4.2: Performance of SMC and ISMC in region 2.5

Wind speed profile types	Mean power SMC (kW)	Mean power ISMC (kW)	Difference (kW)
25updown	459.37	464.80	5.43
stepstest2	426.12	453.55	27.30
stepstest3	461.43	483.44	22.01
stepstest4	417.84	445.41	27.57

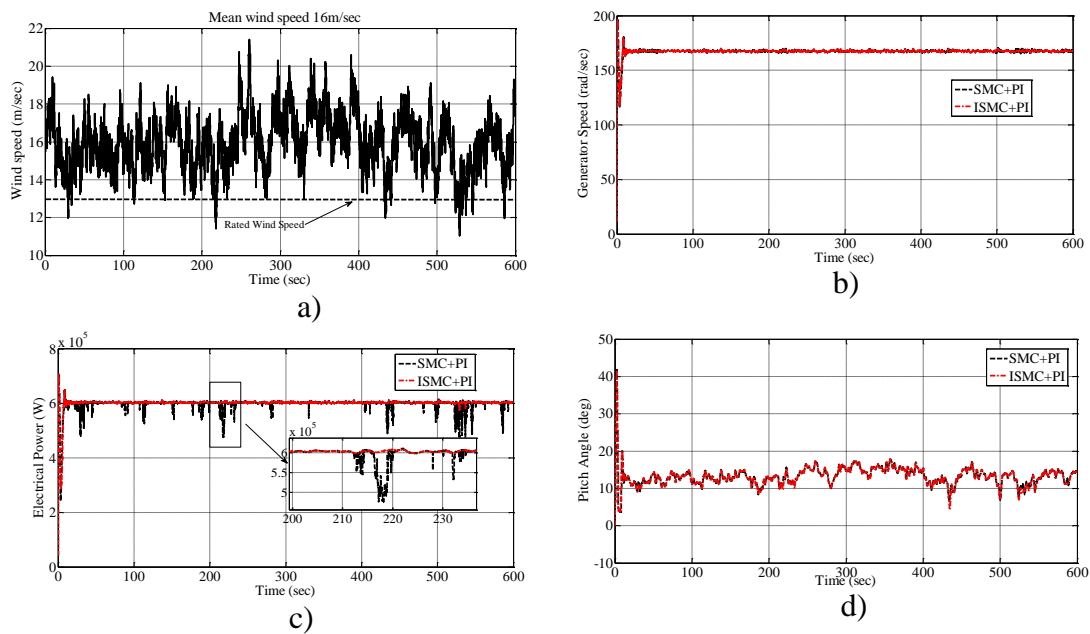


Figure 4.10: Simulation results of 600kW CART 3 WT using SMC and ISMC in full range of operation (above rated wind profile). a) Wind speed profile b) Generator Speed c) Electrical Power d) Pitch angle

Figure 4.10 a) shows the hub height wind speed profile at above rated wind speed. The test wind speed consists of 10 min dataset which was generated using Class A Kaimal turbulence spectra. It has the mean value of 16 m/s at the hub height and turbulence intensity of 25%. Figure 4.10 b) shows the generator speed comparison for SMC and ISMC for above rated wind speed. Both controllers are achieving the nominal generator speed at initial time, because the wind speed is completely above the rated wind speed. Figure 4.10 c) shows the generator power comparison for SMC and ISMC for above rated wind speed. Both controllers are achieving the rated power, but the variation in power is more in SMC compared to ISMC. So, the overall power capture is more in ISMC compared to SMC. Figure 4.10 d) shows the pitch angle comparison for SMC and ISMC with conventional PI for above rated wind speed. From this figure it is clear that pitch angle variation for both the controllers are almost same and finally two curves converge.

#### **4.5 PROPOSED FUZZY PI PITCH CONTROLLER**

In this work, fuzzy system is approximating a nonlinear function between gain correction factor and rotor collective blade pitch angle. In baseline+PI control, the gain correction factor is approximated by a linear function of pitch angle (Hansen, M.H. et al. 2005). The main aim of the proposed fuzzy PI control is to find a nonlinear relation between the pitch angle and the gain correction factor. The input to the fuzzy system is the collective pitch angle and the output is the gain i.e. gain scheduling. Given two nonempty classical sets  $x, y$  a SISO fuzzy IF-THEN rule base can be expressed as,

If  $x$  is  $A_i$  then  $y$  is  $B_i$

Where  $x$  and  $y$  are linguistic variables and  $A_i, B_i$  for  $i = 1, 2, \dots, n$  are the linguistic values taken by the linguistic variable. The main advantage of the fuzzy gain scheduling is that the nonlinear relationship between the gain and pitch angle is approximated by the fuzzy and it can be applicable to any kind of gain scheduling pitch controller. The triangular membership function is used for both input and output fuzzy variables. The input and output vary between  $\{3, 20\}$  and  $\{0, 0.4\}$  respectively. The fuzzy variables are defined in the rule base as  $\{NS$  (Negative Small),  $NB$  (Negative Big),  $Z$  (Zero),  $PS$  (Positive Small) and  $PB$  (Positive Big) $\}$ . From the knowledge of dimensionless gain

correction factor, the fuzzy based gain correction factor is obtained. With this knowledge, the fuzzy rules are initially derived by trial and error method. After obtaining the rule base, the simulation is carried out and it is tuned appropriately as per the control objectives. The SISO fuzzy rule base is given below.

*If input is NS then output is PB*

*If input is NB then output is PS*

*If input is Z then output is Z*

*If input is PS then output is NS*

*If input is PB then output is NB*

#### 4.6 SIMULATION RESULTS FOR BASELINE + PI AND ISMC + FUZZY PI

In this section, comparison is done between (baseline + PI) and proposed (ISMC+Fuzzy PI) where baseline and ISMC for below rated wind speed and PI and fuzzy PI for above rated wind speed.

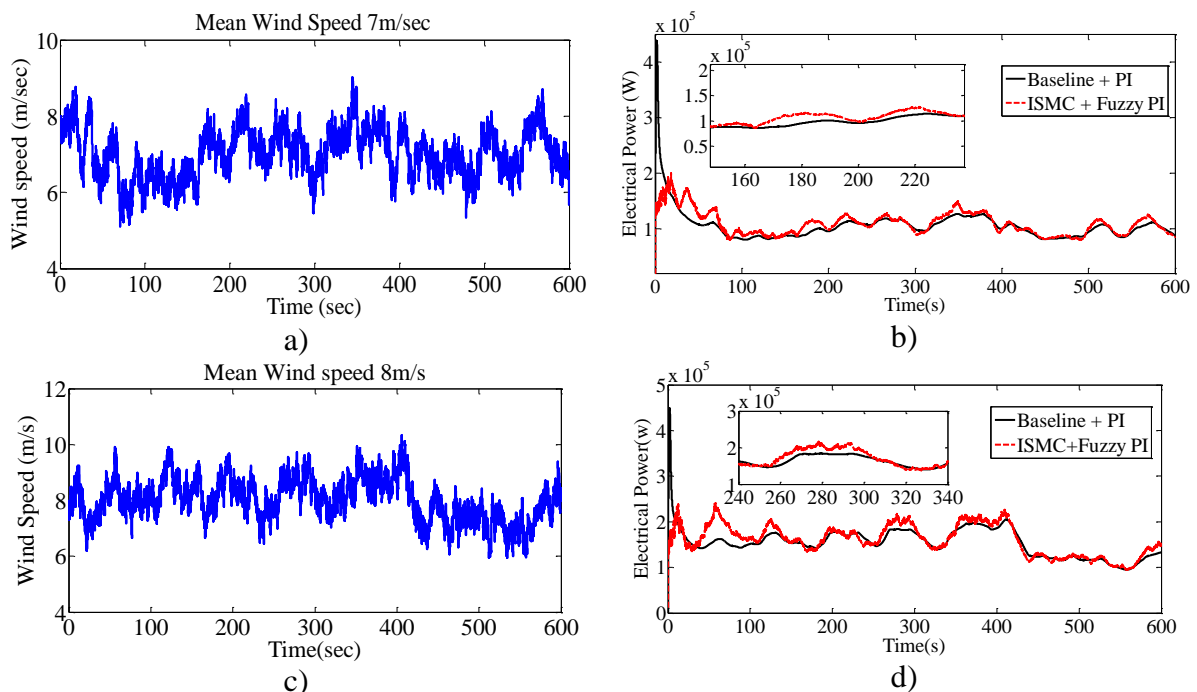


Figure 4.11: Comparison for baseline and ISMC controller a) wind profile with mean 7 m/sec b) Electrical power comparison for 7 m/sec c) wind profile with mean 8 m/sec d) Electrical power comparison for 8 m/sec.



Table 4.3: Power Comparison ISMC and Baseline PI in below rated wind speed

Wind Speed (Below rated wind speed profiles)	7m/s	8m/s
Power comparison for ISMC over Baseline PI	3.5%	4.09%

Figure 4.11 a), b), c) and d) show the wind speed for 25% Kaimal turbulence with 7 m/sec & 8 m/sec mean (completely below rated wind speed) and electrical power comparisons respectively. Table 4.3 shows the power comparison for ISMC and baseline at below rated wind speed. It is clear that at below rated wind speed, ISMC has more power capture compared to baseline control.

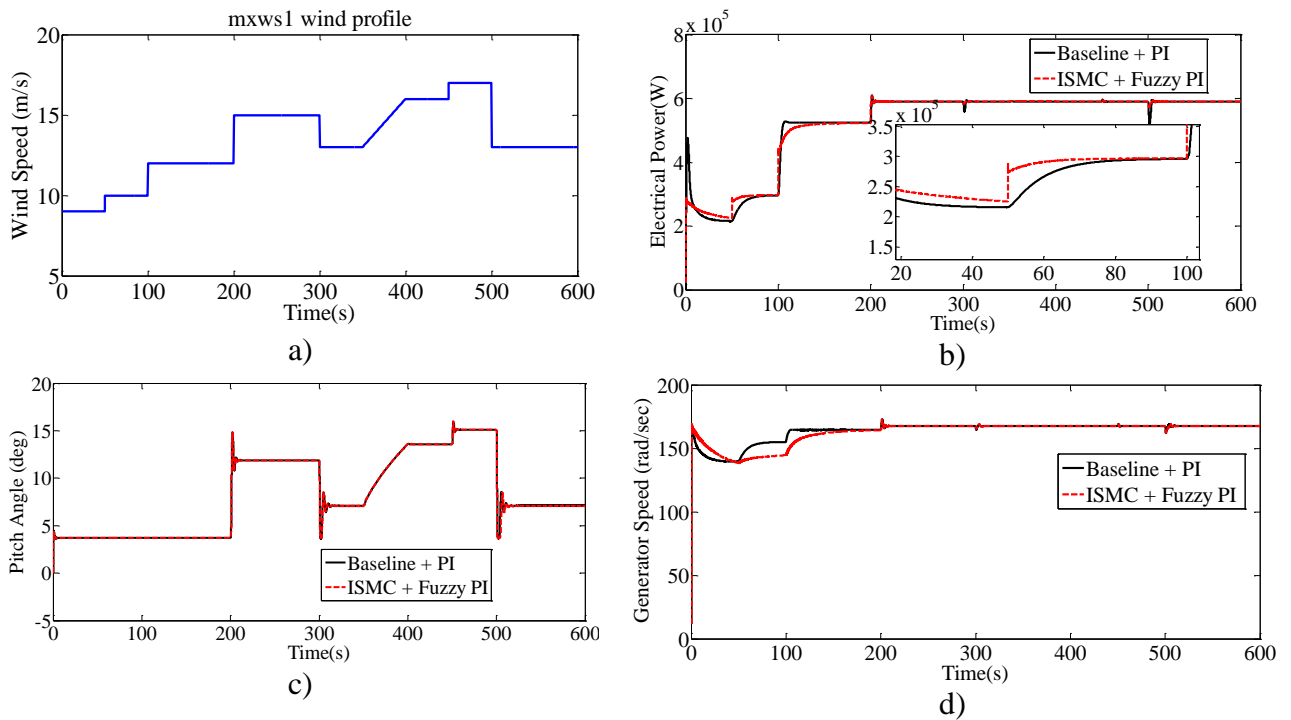


Figure 4.12: Comparison of baseline PI and ISMC + Fuzzy PI a) wind profile mxws1 b) Electrical power comparison c) Pitch angle comparison and d) Generator speed comparison.

Figure 4.12 a), b), c) and d) show the wind speed profile (mxws1), electrical power, pitch angle and generator speed for baseline+PI and ISMC+fuzzy PI controller respectively. The mxws1 wind profile contains all region of wind speed. From the electrical power figure it is clear that ISMC can extract the maximum power in region 2 and baseline can extract the maximum power at region 2.5. But, for any sudden change in wind speed i.e. more than the rated wind speed, the proposed ISMC controller is able to accommodate the changes whereas baseline controller cannot. Both pitch

angle controllers are able to achieve the nominal generator speed in region 3 with almost same variation in the blade pitch angle.

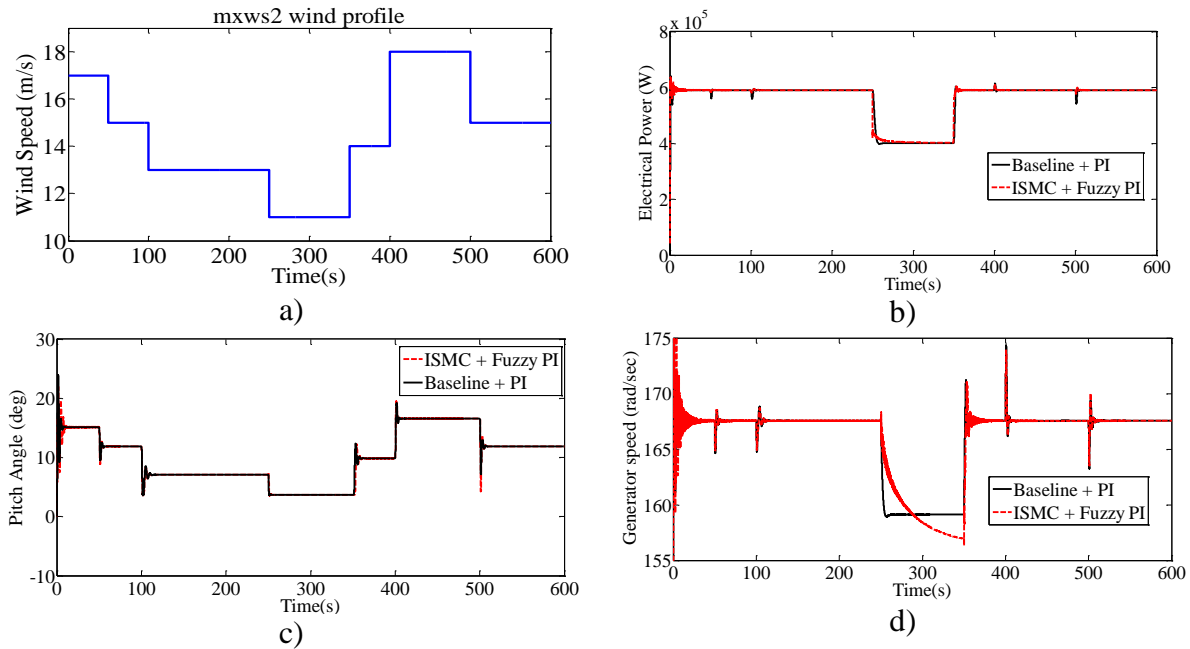
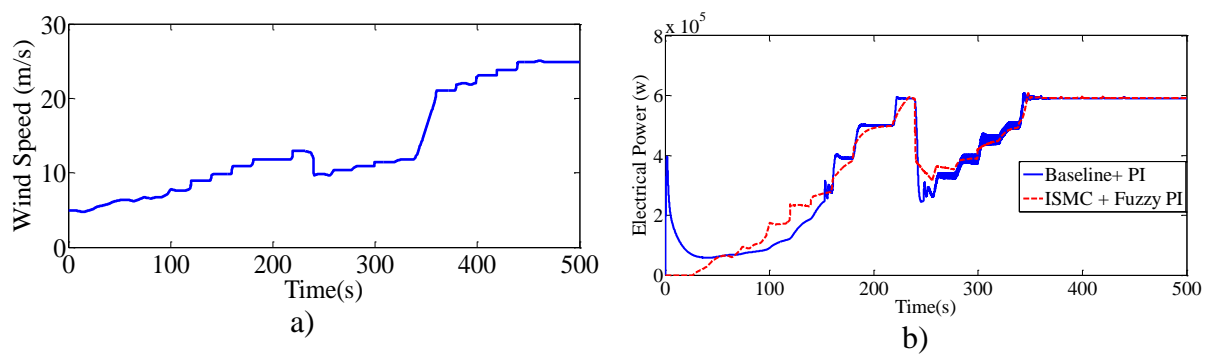


Figure 4.13: Comparison of baseline PI and ISMC + Fuzzy PI a) mxws2 wind profile b) Electrical power comparison c) Pitch angle comparison and d) Generator speed comparison.

Figure 4.13 a), b), c) and d) show the wind speed profile (mxws2), electrical power, pitch angle and generator speed for baseline and proposed controller respectively. The mxws2 wind profile contains region 3 wind profile. When the wind speed is dropping to below the rated speed, baseline torque controller introduces more power loss compared to the proposed controller. The variation in the pitch angle for both controllers give almost the same performance.



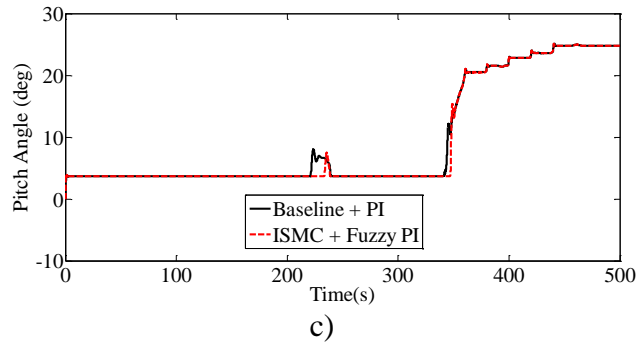


Figure 4.14: Comparison of baseline PI and ISMC + Fuzzy PI a) Darrow wind profile b) Electrical power comparison c) Pitch angle comparison.

Figure 4.14 a), b) and c) show the wind speed profile (Darrow, P.J. 2009), electrical power, and pitch angle for baseline and proposed controller respectively. The given wind profile contains all the regions between below and above rated wind speeds. Up to 150 sec, ISMC can extract the maximum power compared to baseline. In region 2.5, baseline power extraction is almost same with ISMC. When the wind speed drops, baseline has more power oscillation compared to ISMC. Pitch angle variation for both the controller are almost same.

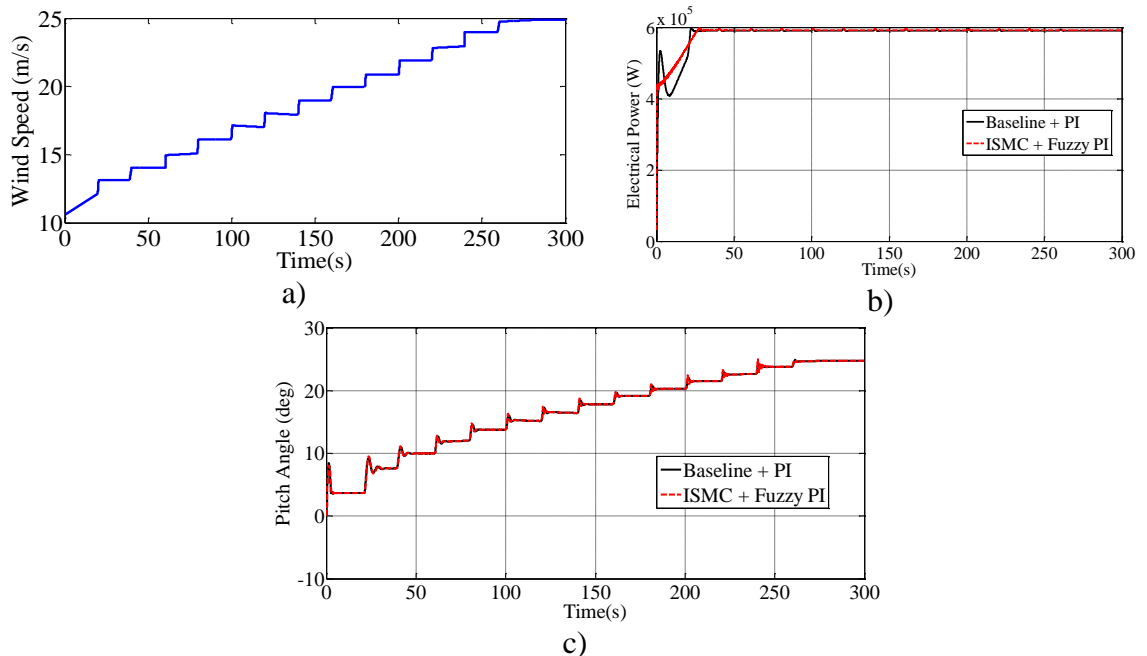


Figure 4.15: Comparison of baseline PI and ISMC + Fuzzy PI a) Hansen wind profile b) Electrical power comparison c) Pitch angle comparison.

Figure 4.15 a), b) and c) show the wind speed profile (Hansen, M.H. et al. 2005), electrical power, and pitch angle for baseline and ISMC controller respectively. The

given wind profile contains wind profile of all the regions i.e. below to above. Up to below rated wind speed, ISMC extracts more power compared to baseline controller.

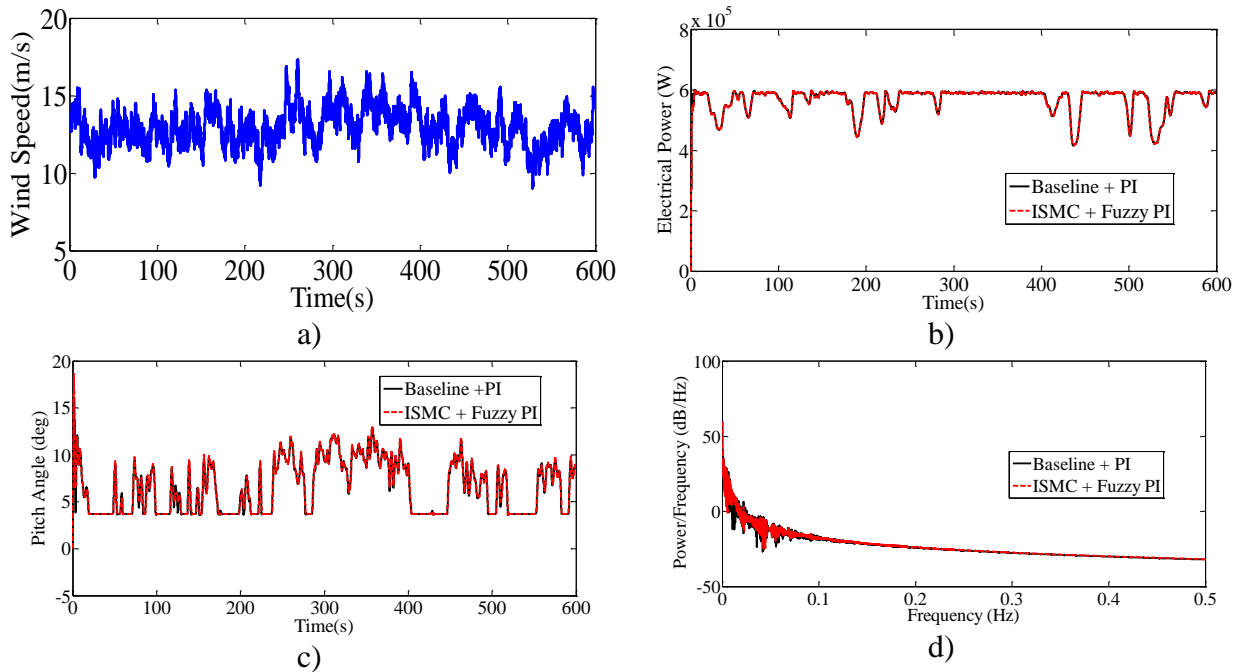


Figure 4.16: Comparison of baseline PI and ISMC + Fuzzy PI a) Mixed wind profile b) Electrical power comparison c) Pitch angle comparison and d) PSD comparison of pitch signal

Figure 4.16 a), b), c) and d) show the wind speed profile (mixed), electrical power, pitch angle and PSD of pitch signal for baseline+PI and proposed controller respectively. The mixed wind profile contains region 2 and region 3 wind profiles. Figure 4.17 a), b), c) and d) show the results for completely above rated wind speed. For both the regions, the performances of baseline+PI and proposed ISMC + fuzzy PI are almost same. The main disadvantage of designing a good baseline control is that, the control law is highly dependent on the accuracy of aerodynamic parameters that may not be well known. At the same time, the baseline controllers do not consider the dynamic aspect of the wind and wind turbine. Unlike baseline, a single nonlinear control law in region 2 and 2.5 is sufficient for ISMC to extract higher power at below rated wind speed.

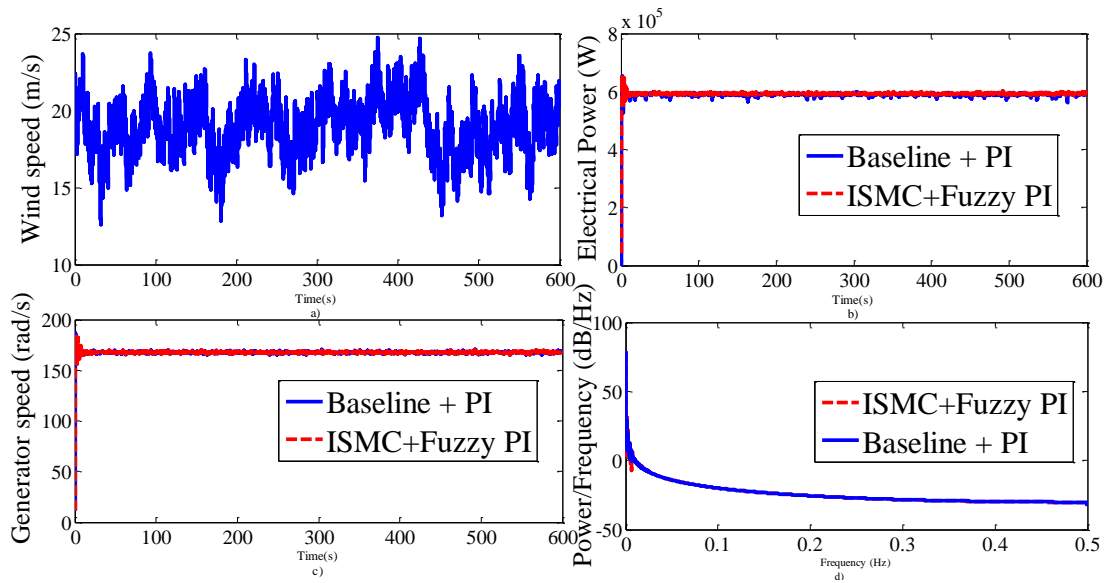


Figure 4.17: Comparison of baseline PI and ISMC + Fuzzy PI a) Above rated wind profile b) Electrical power comparison c) Pitch angle comparison and d) PSD comparison of pitch signal.

Figure 4.18 a), b), c) and d) show the wind speed profile (mixed wind speed from 5 m/s to 25 m/s), electrical power, generator speed, and pitch angle for baseline and proposed controller respectively. The mixed wind profile contains region 2 and region 3 wind profile. For region 2 and the transition region, when the wind speed drops, the proposed ISMC + Fuzzy PI can capture more power than baseline+PI controller. In region 2.5, the baseline+PI controller achieves slight better performance than the proposed; but baseline+PI has more power oscillation in case of drop in wind speed from region 3 to 2.5. In region 3, the performance of baseline+PI and proposed ISMC + fuzzy PI are almost same.

Table 4.4: Turbulence realization by using mean power comparison for different mean wind speed (7 and 11 m/sec)

Controllers	7 m/sec		11 m/sec	
	Baseline + PI	ISMC +Fuzzy PI	Baseline + PI	ISMC+ Fuzzy PI
Turbulence 1	$9.8054 \times 10^4$	$10.311 \times 10^4$	$41.842 \times 10^4$	$41.224 \times 10^4$
Turbulence 2	$9.8054 \times 10^4$	$10.316 \times 10^4$	$42.477 \times 10^4$	$42.882 \times 10^4$
Turbulence 3	$10.341 \times 10^4$	$10.706 \times 10^4$	$42.119 \times 10^4$	$42.554 \times 10^4$
Turbulence 4	$9.817 \times 10^4$	$10.297 \times 10^4$	$41.709 \times 10^4$	$41.851 \times 10^4$
Turbulence 5	$9.974 \times 10^4$	$10.038 \times 10^4$	$42.534 \times 10^4$	$42.734 \times 10^4$

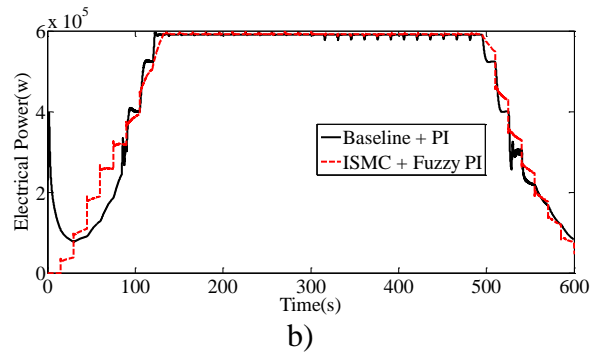
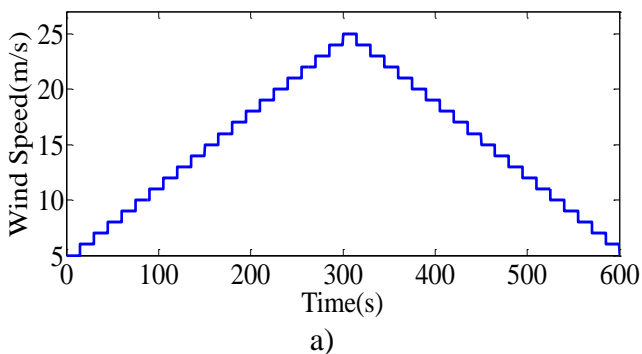
Table 4.5: Turbulence realization by using mean power comparison for different mean wind speed (13 and 15 m/sec)

13 m/sec		15 m/sec	
Baseline + PI	ISMC+ Fuzzy PI	Baseline + PI	ISMC+ Fuzzy PI
$55.988 \times 10^4$	$56.810 \times 10^4$	$59.012 \times 10^4$	$59.229 \times 10^4$
$53.945 \times 10^4$	$54.905 \times 10^4$	$58.536 \times 10^4$	$58.968 \times 10^4$
$52.709 \times 10^4$	$53.568 \times 10^4$	$58.289 \times 10^4$	$58.667 \times 10^4$
$56.176 \times 10^4$	$57.055 \times 10^4$	$59.005 \times 10^4$	$59.232 \times 10^4$
$54.235 \times 10^4$	$55.281 \times 10^4$	$58.599 \times 10^4$	$59.201 \times 10^4$

Table 4.6: Turbulence realization by using mean power comparison for different mean wind speed (17 and 19 m/sec)

Controllers	17 m/sec		19m/sec	
	Baseline + PI	ISMC+ Fuzzy PI	Baseline + PI	ISMC+ Fuzzy PI
Turbulence 1	$59.013 \times 10^4$	$59.234 \times 10^4$	$58.964 \times 10^4$	$59.234 \times 10^4$
Turbulence 2	$58.764 \times 10^4$	$59.115 \times 10^4$	$58.837 \times 10^4$	$59.241 \times 10^4$
Turbulence 3	$58.714 \times 10^4$	$59.051 \times 10^4$	$58.953 \times 10^4$	$59.23 \times 10^4$
Turbulence 4	$58.993 \times 10^4$	$59.235 \times 10^4$	$58.933 \times 10^4$	$59.235 \times 10^4$
Turbulence 5	$58.805 \times 10^4$	$59.207 \times 10^4$	$58.783 \times 10^4$	$59.244 \times 10^4$

Turbulence 1(Kaimal wind model with 10% turbulence), Turbulence 2 (Kaimal wind model with 10% turbulence), Turbulence 3 NWTCUP wind model with 10% turbulence), Turbulence 4 (von Karman wind model with 10% turbulence), Turbulence 5 (von Karman wind model with 15% turbulence)



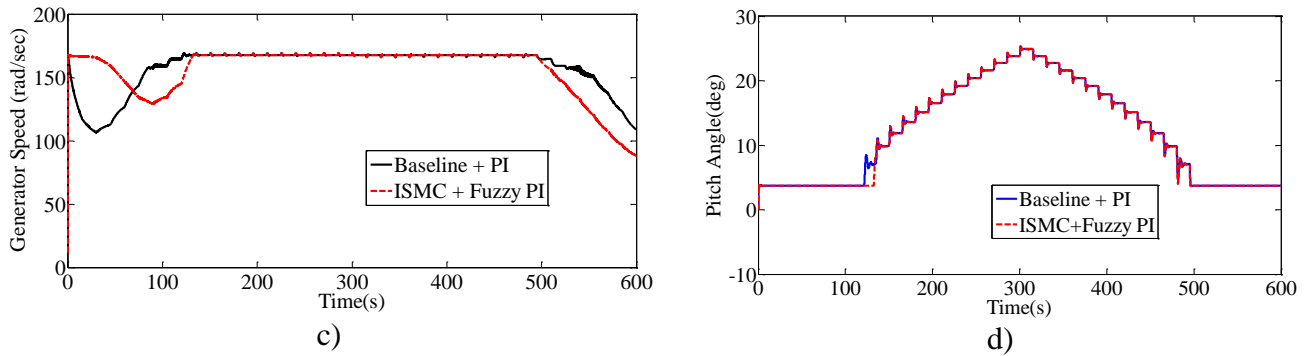


Figure 4.18: Comparison of baseline PI and ISMC + Fuzzy PI a) Mixed wind profile form 5 to 25 m/s b) Electrical power comparison c) Generator speed comparison and d) Pitch angle comparison.

Table 4.4, 4.5 and 4.6 show the different mean wind speed with different turbulence model based mean power for baseline+PI and proposed ISMC + Fuzzy PI controller. By taking different mean wind speed and different turbulence at region 2, ISMC + Fuzzy PI having a mean power extraction of more than 3.5% compared to baseline+PI controller and in region 3, the performance of the controllers are almost same.

Table 4.7: Results of paired t-test

Mean wind speed	'h' value	'p' value
7 m/sec	1	0.0027
11 m/sec	0	0.3799
13 m/sec	1	$1.4076 \times 10^{-6}$
15 m/sec	1	0.0014
17 m/sec	1	$1.0176 \times 10^{-4}$
19 m/sec	1	$1.6584 \times 10^{-4}$

For the performance comparison of the proposed ISMC+Fuzzy PI and baseline+PI controllers, a statistical analysis has been carried out through difference paired t-test using the data given in Table 4.4, 4.5 and 4.6. From Table 4.7 it is clear that for the mean wind speed of 11 m/s with 5 different turbulence realization, the value of 'h=0' and 'p>0.05', which indicates the null hypothesis cannot be rejected. For other mean wind speeds i.e. 7 m/sec, 13 m/sec, 15 m/sec, 17 m/sec and 19 m/sec, the value of 'h=1' and 'p<0.05' concludes the rejection of null hypothesis moving in favour of alternate hypothesis; so the proposed controller has made significant improvement in control performances.

## 4.7 CONCLUSION

In this chapter, a combination of linear and nonlinear control for VSPWT have been analysed. Initially, the proposed nonlinear controller such as SMC and ISMC were designed for wide range of below rated wind speed profiles. The simulation of the controllers were performed by NREL CART 3, 600 kW WT. From the analysis, it was concluded that the proposed ISMC (region 2) with Fuzzy PI controller (region 3) can achieve the maximum power in all the regions of wind speed. Further, the proposed nonlinear controller ISMC + fuzzy PI and baseline + PI controller were tested for wide range of below and above rated wind speed profiles. In region 2, for most of the situation, proposed ISMC was able to extract maximum power with reduced mechanical stress compared to baseline torque control. In region 3, both the performance of conventional PI and fuzzy PI were compared and found to be almost similar. The main advantage of the proposed fuzzy PI control is that it easily handles the nonlinear relation between the pitch angle and the gain correction factor by using fuzzy relations. The main advantage of ISMC is the continuity in control law in transition period, whereas for existing baseline controllers, a separate control law is required in region 2.5 for satisfactory operation.

The main focus of this chapter was the performance of the controller in the transition region for different wind conditions. Generally, the fault in the WT is not predictable. So, in the next chapter, the different types of the fault are considered in WT and the performance of the ISMC is compared to TSMC (terminal sliding mode control) in transient wind speed condition.



## **CHAPTER 5**

# **5 FAULT ANALYSIS OF WIND TURBINE WITH NREL FAST**

## **5.1 INTRODUCTION**

Generally, the fault in the WT is not predictable in nature. In order to make the passive fault tolerant control, the terminal sliding mode control (TSMC) is proposed for single and two mass model of WT. Initially, the generator actuator fault was considered for particular time period. At below rated wind speed, sensor fault was created by using sensor scaling. Here, only generator sensor fault was taken into consideration. This chapter discusses about the application of TSMC in region 2 and a fuzzy based PI for region 3 with different actuator fault and sensor faults. Same TSMC was adopted for the switching between operating regions (transition region 2.5), so that the control input maintains the continuity at the moment of switching. Finally, the performance of the proposed controllers were tested with nonlinear FAST WT model and the results were compared with the existing baseline controllers and ISMC discussed previously in chapter 4. Finally, TSMC + fuzzy PI was simulated with different wind speeds and also compared to baseline + PI controller.

## **5.2 ACTUATOR AND SENSOR FAULTS**

A fault is nothing but an uncontrollable defect in the system which may appear in the system parameter or structure (Shaker, M.S. 2012). It leads to affect the closed loop performance of the system or sometimes it leads to loss of functioning of the system. A fault can affect the normal behavior of the system, so the controller takes remedial measures to overcome the fault. Based on the characteristics, the faults can be classified into three types i.e. abrupt, incipient and intermittent. Figure 5.1 shows the different types of faults (Shaker, M.S. 2012). Based on the fault acting on the location of the

system, the faults are classified into two types i.e. sensor fault and actuator fault. Figure 5.2 shows the actuator fault and sensor fault (Shaker, M.S. 2012).

### *Actuator fault*

According to this fault, the control input is varied either completely or partially. If it is a complete fault, the actuator gives no actuation signal to the system. In partial actuator fault cases, the actuating signal is less from the original signal. In this work, actuator fault is introduced by reducing the control signal by some values at some time period.

### *Sensor faults*

The sensors are used to measure the output signal from the system. Generally, sensor fault is considered as the incorrect reading measured from the system. Sometimes the sensor gives a completely incorrect reading, which is not related to the real signal. The true value of the signal from the sensor are erroneously scaled or stuck. In this work, scaling of the signal is considered as the sensor fault.

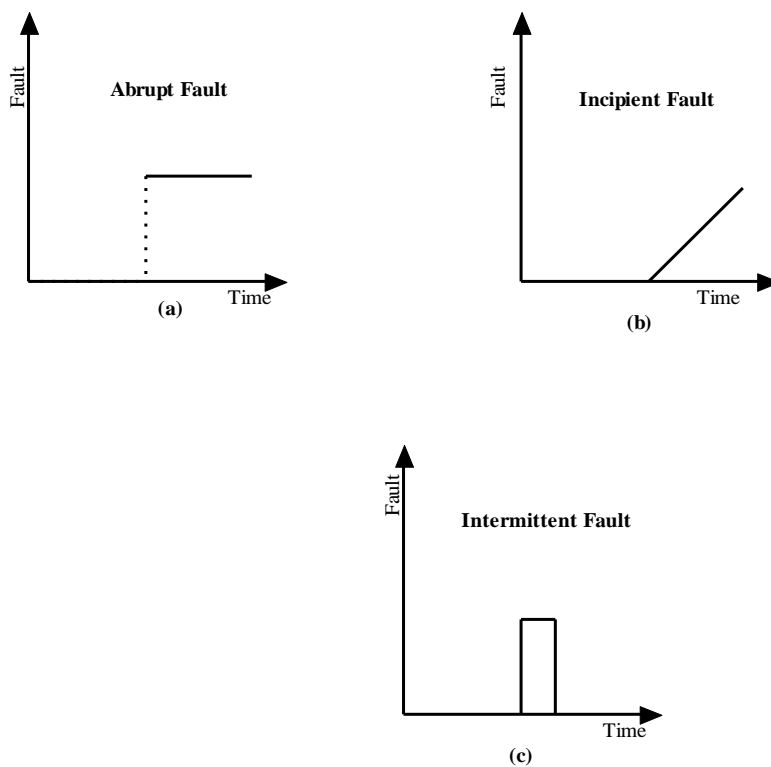


Figure 5.1: Different types of faults

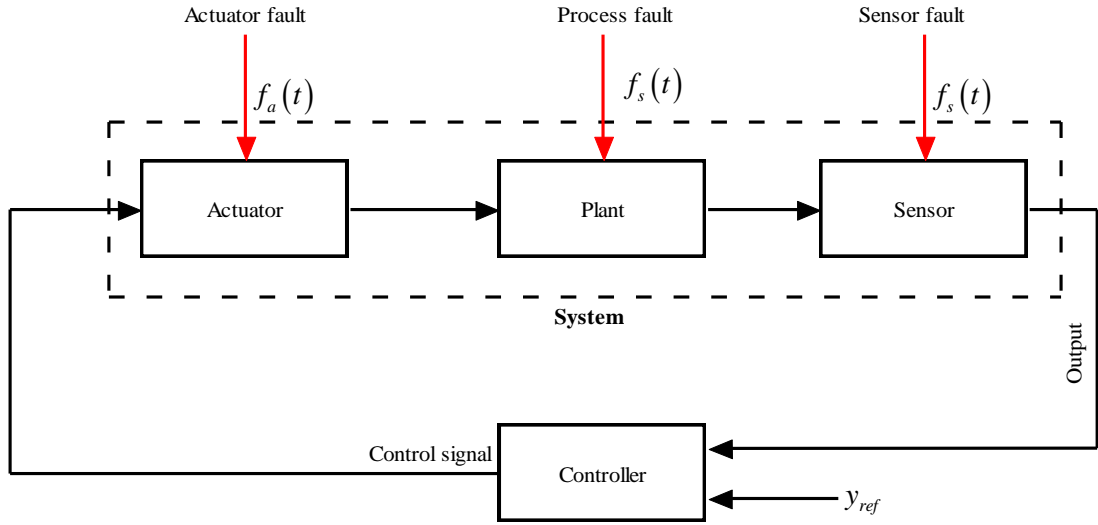


Figure 5.2: Actuator and sensor faults.

### 5.3 TERMINAL SLIDING MODE CONTROLLER FOR SINGLE MASS MODEL

The dynamic WT single mass model can be expressed as

$$J_t \dot{\omega}_r = T_a - K_t \omega_r - T_g + F \quad (5.1)$$

$$F = \Delta(\omega_r, \dot{\omega}_r) + \bar{d} \quad (5.2)$$

$F$  contains both the parameter uncertainty and disturbances ( $\bar{d}$ ). We made the assumptions that the modelling error and the external disturbances in the WT system changes slowly. So that

$$\dot{F} = 0 \quad (5.3)$$

The equation for nonsingular terminal sliding surface (Yu, S. et al. 2005) is defined from the linear sliding surface ( $S_{smc}$ ) given in equation (2.29) as:

$$\sigma = S_{smc} + \beta_1 \left| \dot{S}_{smc} \right|^\gamma \text{sign}(S_{smc}) \quad (5.4)$$

$$\beta_1 > 0, 1 < \gamma < 2$$

The stability of the system was investigated by choosing the following Lyapunov function

$$V = 0.5\sigma^2 \quad (5.5)$$

By taking the derivative of the above equation, we get

$$\begin{aligned}\dot{V} &= \sigma \dot{\sigma} \\ &= \sigma \left( \dot{S}_{smc} + \beta_1 \gamma \left| \dot{S}_{smc} \right|^{\gamma-1} \ddot{S}_{smc} \right)\end{aligned}\quad (5.6)$$

By substituting (2.30) in above equation we get equation (5.7)

$$\dot{V} = \sigma \left( \dot{\omega}_r(t) - \dot{\omega}_{ref}(t) + \beta_1 \gamma \left| \dot{S}_{smc} \right|^{\gamma-1} \ddot{S}_{smc} \right) \quad (5.7)$$

By substituting equation (5.1) in equation (5.7) we get

$$\dot{V} = \sigma \left( \frac{1}{J_t} T_a - \frac{K_t}{J_t} \omega_r - \frac{1}{J_t} T_g + \frac{F}{J_t} - \dot{\omega}_{ref}(t) + \beta_1 \gamma \left| \dot{S}_{smc} \right|^{\gamma-1} \ddot{S}_{smc} \right) \quad (5.8)$$

The terminal sliding mode control law  $T_g$  is defined as

$$T_g = T_a - K_t \omega_r - \bar{F} \text{sign}(\sigma) - J_t \dot{\omega}_{ref} + J_t \gamma \beta_1 \left| \dot{S}_{smc} \right|^{\gamma-1} \ddot{S}_{smc} + J_t K \text{sign}(\sigma) \quad (5.9)$$

By substituting (5.9) into (5.8) the following equation can be obtained

$$\dot{V} = \sigma \left( \begin{array}{l} \frac{1}{J_t} T_a - \frac{K_t}{J_t} \omega_r - \\ \frac{1}{J_t} \left( T_a - K_t \omega_r - \bar{F} \text{sign}(\sigma) - J_t \dot{\omega}_{ref} + J_t \gamma \beta_1 \left| \dot{S}_{smc} \right|^{\gamma-1} \ddot{S}_{smc} \right) + \frac{F}{J_t} - \dot{\omega}_{ref}(t) + \\ \beta_1 \gamma \left| \dot{S}_{smc} \right|^{\gamma-1} S_{smc} \end{array} \right) \quad (5.10)$$

$$\begin{aligned}&\leq \frac{F}{J_t} \sigma - \frac{\bar{F}}{J_t} \sigma \text{sign}(\sigma) - K \sigma \text{sign}(\sigma) \\ &\leq |\sigma| \left( \frac{F}{J_t} - \frac{\bar{F}}{J_t} \right) - K |\sigma| \\ &\leq -K |\sigma|\end{aligned}\quad (5.11)$$

Since the lumped parameter uncertainty and disturbance  $F$  is unknown in practical application and the upper bound  $\bar{F}$  is very difficult to determine, the adaptive control law is adapted for unmodelled dynamic uncertainty  $\hat{F}$ .

The Lyapunov candidate function is chosen as

$$\dot{V}_1 = \dot{V} + \frac{1}{2\varphi} \tilde{F}^2 \quad (5.12)$$

where  $\tilde{F} = F - \hat{F}$  and  $\varphi$  is a positive constants. By taking the derivative of the equation (5.12).

$$\begin{aligned} \dot{V}_1 &= \dot{V} + \frac{1}{2\varphi} \tilde{F} \dot{\tilde{F}} \\ &= \dot{V} - \frac{1}{\varphi} \tilde{F} \dot{\hat{F}} \end{aligned} \quad (5.13)$$

$$= \sigma \left( \begin{array}{l} \frac{1}{J_t} T_a - \frac{K_t}{J_t} \omega_r - \\ \frac{1}{J_t} \left( T_a - K_t \omega_r - \hat{F} - J_t \dot{\omega}_{ref} + J_t \gamma \beta_1 |\dot{S}_{smc}|^{\gamma-1} \ddot{S}_{smc} \right) + J_t K \tanh(\sigma) \\ \frac{\hat{F}}{J_t} - \dot{\omega}_{ref}(t) + \beta_1 \gamma |\dot{S}_{smc}|^{\gamma-1} \ddot{S}_{smc} \end{array} \right) - \frac{1}{\varphi} \tilde{F} \left( \dot{\hat{F}} - \varphi \sigma \right) \quad (5.14)$$

The adaptive control rule can be selected as

$$\dot{\hat{F}} = \varphi \sigma \quad (5.15)$$

According to above equation the terminal sliding mode control law ' $T_g$ ' is defined as

$$T_g = T_a - K_t \omega_r - \hat{F} - J_t \dot{\omega}_{ref} + J_t \gamma \beta_1 |\dot{S}_{smc}|^{\gamma-1} \ddot{S}_{smc} + J_t K \text{sign}(\sigma) \quad (5.16)$$

In order to make the chattering free control law, the signum function can be replaced by 'tanh'

$$T_g = T_a - K_t \omega_r - \bar{F} \text{sign}(\sigma) - J_t \dot{\omega}_{ref} + J_t \gamma \beta_1 |\dot{S}_{smc}|^{\gamma-1} \ddot{S}_{smc} + J_t K \tanh(\sigma) \quad (5.17)$$

Substituting (5.15) into (5.14) the following equation can be obtained

$$\dot{V}_1 \leq -K \sigma \tanh(\sigma) \quad (5.18)$$

The parameters of TSMC controllers are given as follows.  $\gamma=1.5$ ,  $\beta_1=2$ ,  $\varphi=1.5$  and  $K=0.5$ .

## 5.4 RESULT AND DISCUSSION OF TSMC FOR SINGLE MASS MODEL

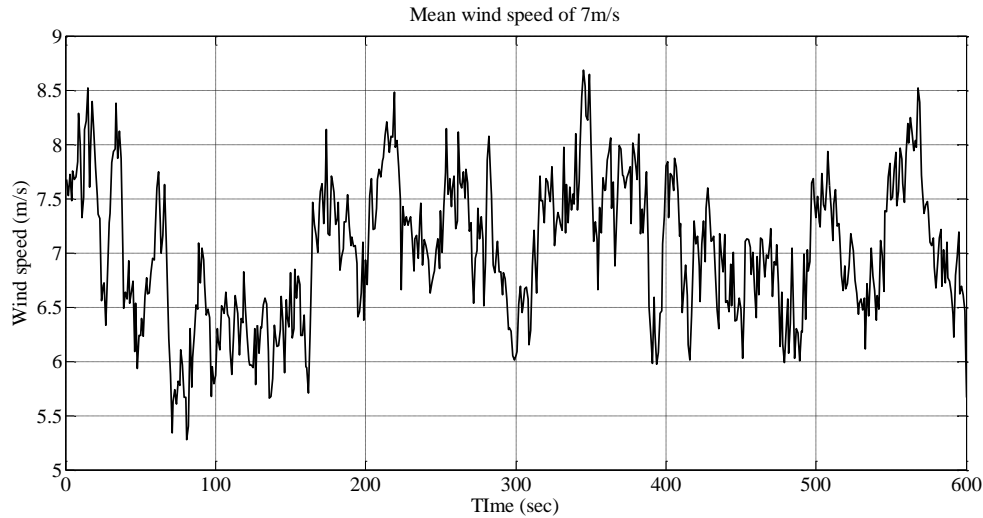


Figure 5.3: Wind speed profile.

Figure 5.3 shows the test wind profile. This wind speed profile is used as the excitation of WT. Figure 5.4 shows the rotor speed comparison for SMC and TSMC controllers without any disturbance and it was found that both controllers have similar performance. In general, the WT disturbance is variable in nature, which is highly unpredictable. Figure 5.5 shows the rotor speed comparison for SMC and TSMC controller with random disturbance between 1000 to 4000Nm throughout the period.

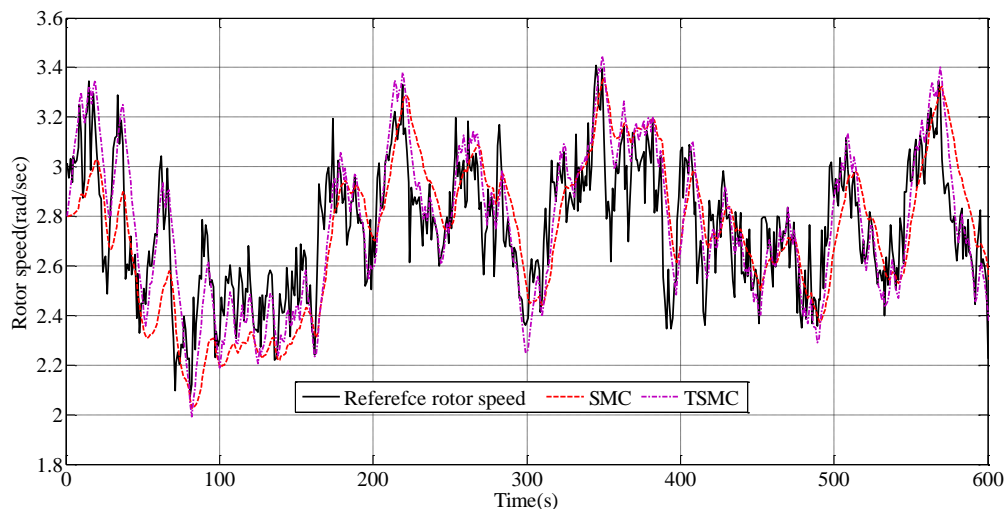


Figure 5.4: Rotor speed comparison for SMC and TSMC controller for mathematical model without disturbance.

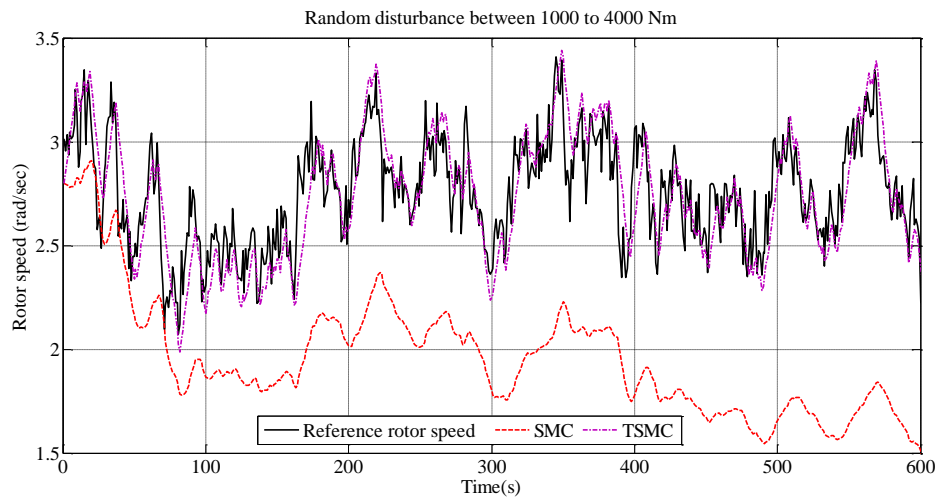


Figure 5.5: Rotor speed comparison for SMC and TSMC controller for mathematical model with random disturbance between 1000 to 4000Nm.

TSMC is able to follow the optimal speed in the presence of random disturbance, but SMC has poor tracking performance. Figure 5.6 shows the rotor speed comparison for SMC and TSMC controllers with presence of actuator offset. The actuator offset is introduced between 300 to 350sec, and 450 to 500sec. In the presence of actuator offset, TSMC was found to track the optimal rotor speed whereas SMC fails to track.

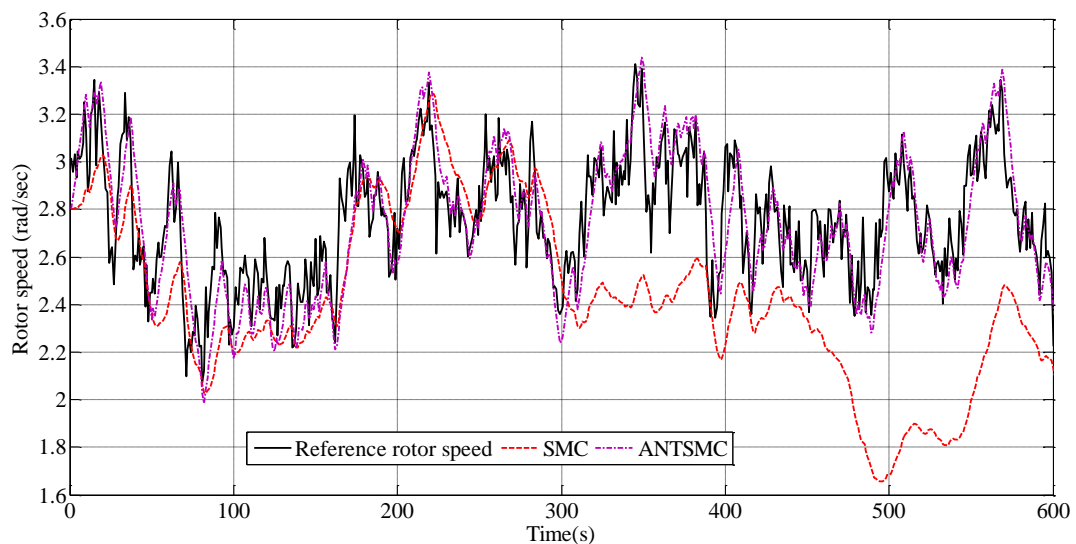


Figure 5.6: Rotor speed comparison for SMC and TSMC controller for mathematical model with presence of actuator offset.

Table 5.1: Comparisons of control strategies without disturbance

Control Schemes	SMC	TSMC
STD( $T_g$ )(kNm)	5.081	18.19
Max( $T_g$ )(kNm)	61.79	81.94
$\eta_{elec}$ (%)	91.06	92.44
$\eta_{aero}$ (%)	92.75	92.83

Table 5.2: Comparisons of control strategies with random disturbance

Control Schemes	SMC	TSMC
STD( $T_g$ )(kNm)	7.465	18.06
Max( $T_g$ )(kNm)	74.48	81.46
$\eta_{elec}$ (%)	78.74	92.91
$\eta_{aero}$ (%)	78.52	93.14

Table 5.1 shows the comparisons of different performance parameter for SMC and TSMC. This table ensures that with no disturbances, the electrical and aerodynamic efficiency of both the controllers are almost same. Finally, the controllers are tested with different disturbances and results are given in Table 5.2 and Table 5.3. Table 5.2 and Table 5.3 shows the comparisons of different performance parameters for SMC and TSMC under random disturbances and actuator offset respectively. The efficiency of TSMC is almost 15% and 8% more than the SMC for random disturbances and actuator offset respectively. This shows more efficiency and robustness of TSMC compared to SMC. Both the tables show that standard deviation in input torque for SMC is lower than TSMC. This reveals that, more power is extracted at the cost of increased input torque variation. In design point of view, it has been the practice to design the gearbox that can withstand a torque around 30% to 40% higher than the rated torque. As the disturbance in the WT varies with time, it can be inferred that TSMC is the preferable controller to achieve the maximum power with acceptable variation in control input.

Table 5.3: Comparisons of control strategies with actuator offset

Control Schemes	SMC	TSMC
STD( $T_g$ )(kNm)	8.073	18.06
Max( $T_g$ )(kNm)	78.76	81.46
$\eta_{elec}$ (%)	84.2	92.91
$\eta_{aero}$ (%)	85.41	93.14



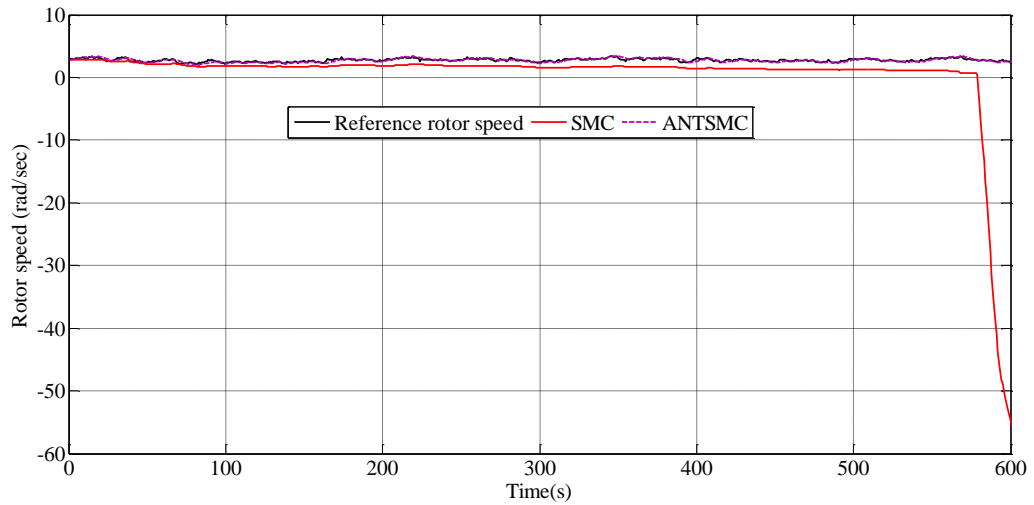


Figure 5.7: Rotor speed comparison for SMC and TSMC controller for mathematical model with presence random disturbance more than 4500kNm.

Figure 5.7 shows the rotor speed comparison for SMC and TSMC controller for mathematical model with presence random disturbance more than 4500 kNm. For the disturbance level more than 4500 kNm, the SMC is completely deviating from the reference rotor speed. This ensures that SMC is not robust with respect to disturbances and it introduces more power loss. Even though the variation in control input is more in TSMC, it can track the optimal reference speed in the presence of various disturbances. Figure 5.8 and Table 5.4 show the mean power comparison for SMC and TSMC at different mean wind speeds. From these results it is clear that at below rated wind speed, TSMC is always extracting more power compared to SMC.

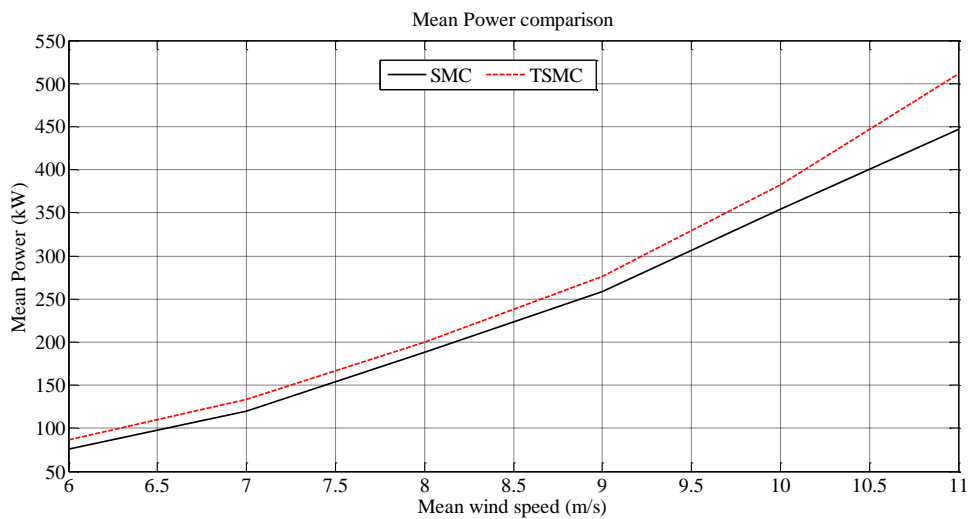


Figure 5.8: Mean power comparison for SMC and TSMC.

Table 5.4: Mean wind power comparison

Mean wind speed (m/s)	Mean power SMC (kW)	Mean power TSMC (kW)	Percentage increase (%)
6	76.23	87.05	14.19
7	119.81	133.49	11.41
8	188.47	199.74	5.97
9	258.53	275.61	6.60
10	354.5	382.5	7.89
11	446.54	511.73	14.59

## 5.5 TSMC FOR OPTIMAL POWER CAPTURE FOR FAST TWO MASS MODEL

Let us consider the linear sliding surface ( $S_r$ ) as

$$S_r = \alpha e + \dot{e} \quad (5.19)$$

The first order derivative of the above equation can be obtained as

$$\dot{S}_r = \alpha \dot{e} + \ddot{e} \quad (5.20)$$

A nonsingular terminal sliding mode manifold (Mondal, S. and Mahanta, C. 2014) is first designed as

$$\sigma = S_r + \beta_2 \dot{S}_r^{p/q} \quad (5.21)$$

where  $\beta_2 > 0$  is a design constant and ' $p$ ' and ' $q$ ' are the positive integer, which satisfy the following condition

$$p > q \text{ or } 1 < p/q < 2$$

The TSMC control is realized by combining the linear sliding surface ' $S_r$ ' with nonsingular terminal sliding mode ' $\sigma$ '. When ' $\sigma$ ' reaches zero at finite time, both ' $S_r$ ' and ' $\dot{S}_r$ ' are bounded to reach zero. This implies that tracking error asymptotically converges to zero.

Suppose ' $t_r$ ' is the time when ' $\sigma$ ' reaches zero from  $\sigma(0) \neq 0$  i.e.  $\sigma = 0$  for all  $t \geq t_r$ , once ' $\sigma$ ' reaches zero it will stay on zero, by using the control law. This ensures the sliding surface ' $S_r$ ' will converge to zero in finite time. The total time from  $\sigma(0) \neq 0$  to ' $S_{tf}$ ' can

be calculated by using the equation  $\dot{S}_r + \beta_2 \dot{S}_r^{p/q} = 0$  from which time taken from  $S_{tr}$  to  $S_{tf}$  is obtained as ‘ $S_{tf}$ ’ to ‘ $S_{tr}$ ’.

$$t_f = t_r + \frac{\left(\frac{p}{q}\right)}{\left(\frac{p}{q}\right)-1} \beta_2^{-(p/q)} \|S_{tr}\|^{(p/q)-1} \quad (5.22)$$

By taking the derivative of the equation (5.21)

$$\dot{\sigma} = \dot{S}_r + \frac{\beta_2 p}{q} \dot{S}_r^{(p/q)-1} \ddot{S}_r \quad (5.23)$$

The stability of the system is investigated by choosing the following Lyapunov function

$$V = 0.5\sigma^2 \quad (5.24)$$

By taking the derivative of the above equation, we will get

$$\begin{aligned} \dot{V} &= \sigma \dot{\sigma} \\ &= \sigma \left( \alpha (\dot{\omega}_r - \dot{\omega}_{ref}) + \ddot{e} + \frac{\beta_2 p}{q} \dot{S}_r^{(p/q)-1} \ddot{S}_r \right) \end{aligned} \quad (5.25)$$

To make the controller more adaptive to uncertainty and disturbances, we introduce the parameter  $F$  which denotes the modelling error and the external disturbances in the WT system change slowly.

$$F = \Delta(\omega_r, \dot{\omega}_r) + \bar{d} \quad (5.26)$$

$$\dot{F} = 0 \quad (5.27)$$

From the two mass model system equation

$$\dot{\omega}_r = \frac{T_a}{J_r} - \frac{K_r}{J_r} \omega_r - \frac{n_g J_g}{J_r} \omega_g - \frac{n_g}{J_r} K_g \omega_g - \frac{n_g}{J_r} T_{em} + \frac{F}{J_r} \quad (5.28)$$

By substituting (5.28) in equation (5.25)

$$\dot{V} = \sigma \left( \alpha \left( \frac{T_a}{J_r} - \frac{K_r}{J_r} \omega_r - \frac{n_g J_g}{J_r} \omega_g - \frac{n_g}{J_r} K_g \omega_g - \frac{n_g}{J_r} T_{em} + \frac{F}{J_r} - \dot{\omega}_{ref} \right) + \ddot{e} + \frac{\beta_2 p}{q} \dot{S}_r^{(p/q)-1} \ddot{S}_r \right) \quad (5.29)$$

According to above equation, the terminal sliding mode control law  $T_{em}$  is defined as

$$\begin{aligned}
T_{em} = & \frac{T_a}{n_g} - \frac{K_r}{n_g} \omega_r - J_g \dot{\omega}_g - K_g \omega_g + \frac{\bar{F}}{n_g} \text{sign}(\sigma) - \frac{J_r}{n_g} \dot{\omega}_{ref} \\
& + \frac{J_r}{n_g \alpha} \ddot{e} + \frac{\beta_2 p}{q} \frac{J_r}{n_g \alpha} \dot{S}_r \left(\frac{p}{q}\right)^{-1} \ddot{S}_r + \frac{J_r}{n_g \alpha} k \text{sign}(\sigma)
\end{aligned} \tag{5.30}$$

By substituting (5.29) into (5.28) the following equation can be obtained

$$\begin{aligned}
\dot{V} = \sigma & \left( \begin{array}{l} \left( \frac{T_a}{J_r} - \frac{K_r}{J_r} \omega_r \right. \\ \left. - \frac{n_g J_g}{J_r} \dot{\omega}_g - \frac{n_g}{J_r} K_g \omega_g \right. \\ \left. \frac{n_g}{J_r} \left( \frac{T_a}{n_g} - \frac{K_r}{n_g} \omega_r - J_g \dot{\omega}_g - K_g \omega_g + \right. \right. \\ \left. \left. \frac{\bar{F}}{n_g} \text{sign}(\sigma) - \frac{J_r}{n_g} \dot{\omega}_{ref} + \frac{J_r}{n_g \alpha} \ddot{e} + \frac{\beta_2 p}{q} \frac{J_r}{n_g \alpha} \dot{S}_r \left(\frac{p}{q}\right)^{-1} \ddot{S}_r + \frac{J_r}{n_g \alpha} k \text{sign}(\sigma) \right) \right) + \\ \left. + \frac{F}{J_r} - \dot{\omega}_{ref} \right) \\ & \left( \ddot{e} + \frac{\beta_2 p}{q} \dot{S}_r \left(\frac{p}{q}\right)^{-1} \ddot{S}_r \right) \\ & \leq \frac{\bar{F}}{n_g} \sigma \text{sign}(\sigma) - k \sigma \text{sign}(\sigma) - \frac{F}{J_r} \sigma \\ & \leq -k |\sigma|
\end{array} \right) \tag{5.31}
\end{aligned}$$

Since the lumped parameter uncertainty and disturbance ‘ $F$ ’ is unknown in practical application and the upper bound ‘ $\bar{F}$ ’ is very difficult to determine, the adaptive control law is adapted for lumped uncertainty ‘ $\hat{F}$ ’.

The Lyapunov candidate function is chosen as

$$V_1 = V + \frac{1}{2\varphi} \tilde{F}^2 \tag{5.32}$$

where  $\tilde{F} = F - \hat{F}$  and  $\varphi$  is a positive constants. By taking the derivative of the equation (5.32)

$$\begin{aligned}
\dot{V}_1 &= \dot{V} + \frac{1}{2\varphi} \tilde{F} \dot{\tilde{F}} \\
&= \dot{V} - \frac{1}{\varphi} \tilde{F} \dot{\hat{F}} \\
&= \sigma \left( \alpha \begin{pmatrix} \left( \frac{T_a}{J_r} - \frac{K_r}{J_r} \right) \omega_r \\ -\frac{n_g J_g}{J_r} \dot{\omega}_g - \frac{n_g}{J_r} K_g \omega_g \\ \left( \frac{T_a}{n_g} - \frac{K_r}{n_g} \right) \omega_r - J_g \dot{\omega}_g - K_g \omega_g + \frac{\hat{F}}{n_g} - \frac{J_r}{n_g} \dot{\omega}_{ref} \\ + \frac{J_r}{n_g \alpha} \ddot{e} + \frac{\beta_2 p}{q} \frac{J_r}{n_g \alpha} \dot{S}_r \left( \frac{p}{q} \right)^{-1} \ddot{S}_r + \frac{J_r}{n_g \alpha} k \text{sign}(\sigma) \\ + \frac{F}{J_r} - \dot{\omega}_{ref} \\ \ddot{e} + \frac{\beta_2 p}{q} \dot{S}_r \left( \frac{p}{q} \right)^{-1} \ddot{S}_r \end{pmatrix} \right) - \frac{1}{\varphi} \tilde{F} \left( \dot{\hat{F}} - \varphi \sigma \right) \quad (5.33)
\end{aligned}$$

The adaptive control rule can be selected as

$$\dot{\hat{F}} = \varphi \sigma \quad (5.34)$$

According to the above equation, the terminal sliding mode control law ' $T_{em}$ ' is defined as

$$\begin{aligned}
T_{em} &= \frac{T_a}{n_g} - \frac{K_r}{n_g} \omega_r - J_g \dot{\omega}_g - K_g \omega_g + \frac{\hat{F}}{n_g} - \frac{J_r}{n_g} \dot{\omega}_{ref} + \frac{J_r}{n_g \alpha} \ddot{e} \\
&\quad + \frac{\beta_2 p}{q} \frac{J_r}{n_g \alpha} \dot{S}_r \left( \frac{p}{q} \right)^{-1} \ddot{S}_r + \frac{J_r}{n_g \alpha} k \text{sign}(\sigma) \quad (5.35)
\end{aligned}$$

In order to make the chattering free control law, the signum function can be replaced by 'tanh'.

$$\begin{aligned}
T_{em} &= \frac{T_a}{n_g} - \frac{K_r}{n_g} \omega_r - J_g \dot{\omega}_g - K_g \omega_g + \frac{\hat{F}}{n_g} - \frac{J_r}{n_g} \dot{\omega}_{ref} \\
&\quad + \frac{J_r}{n_g \alpha} \ddot{e} + \frac{\beta_2 p}{q} \frac{J_r}{n_g \alpha} \dot{S}_r \left( \frac{p}{q} \right)^{-1} \ddot{S}_r + \frac{J_r}{n_g \alpha} k \tanh(\sigma) \quad (5.36)
\end{aligned}$$

Substituting (5.34) into (5.33) the following equation can be obtained as

$$\dot{V}_1 \leq -k\sigma \tanh(\sigma) \quad (5.37)$$

## 5.6 COMPARISON OF RESULTS OF ISMC, TSMC AND BASELINE CONTROLLER FOR TWO MASS MODEL WITH FAST

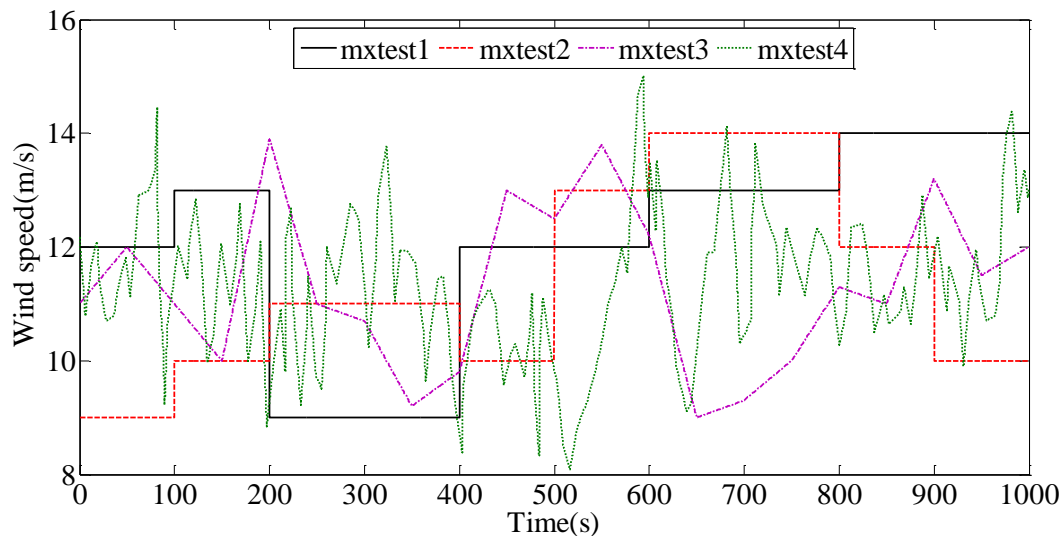


Figure 5.9: Different wind speed profiles

Figure 5.9 shows the different wind speeds which include step changes in wind speed and random wind speed profiles represented as mxtest1, mxtest2, mxtest3 and mxtest4. These wind speed profiles are used to analyze the proposed and existing controllers. This set of turbulence wind speed profile generated by TurbSim software is developed by the NREL. The average wind speed for all wind speed profiles is around 11.5 m/s and the turbulence intensity varies for all wind speed profiles. The wind speed profiles shown in Figure 5.9 ensures that the turbine operates all the wind speed regions.

Figure 5.10 shows the power comparison for mxtest1 and mxtest2 wind speed profile. Figure 5.11 shows the power comparison for mxtest3 and mxtest4 wind speed profile. For any sudden change in wind speed i.e. more than the rated wind speed, the ISMC & TSMC controllers are able to accommodate the changes and can extract more power compared to baseline controller. The power oscillation is more in baseline controller compared to other proposed controllers.

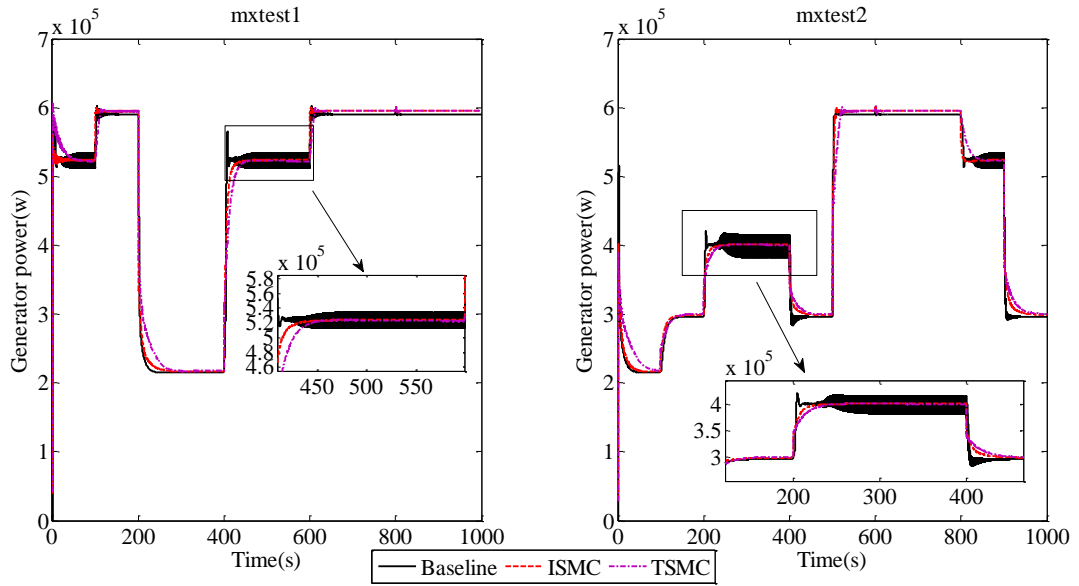


Figure 5.10: Power comparison for mxtest1 and mxtest2 wind speed profiles.

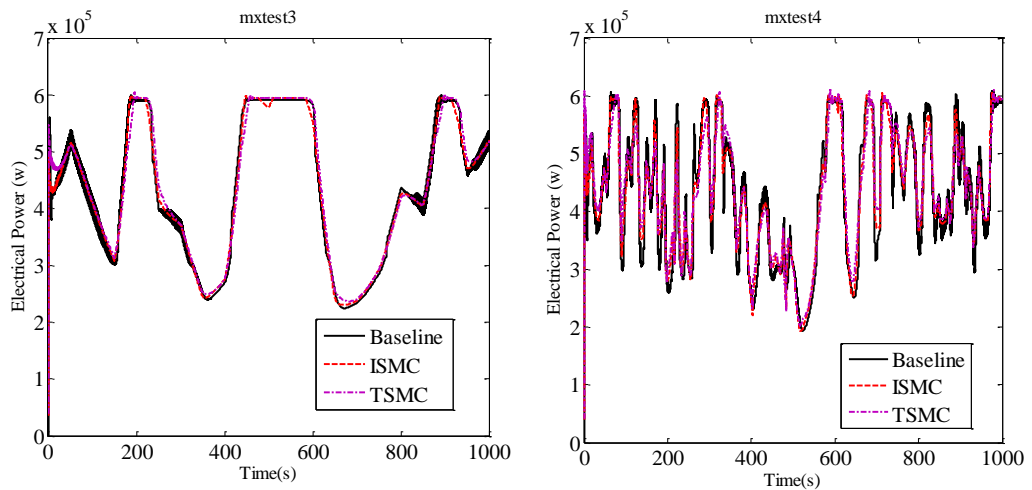


Figure 5.11: Power comparison for mxtest3 and mxtest4 wind speed profiles.

Table 5.5: Standard deviation of the different controllers with different wind speed profiles

	mxtest1	mxtest2	mxtest3	mxtest4
Baseline	757.39	740.63	678.52	635.81
ISMC	737.34	697.11	630.08	553.75
TSMC	594.42	540.79	503.21	467.60

Table 5.5 shows the standard deviation of the different controllers with different wind speed profiles. TSMC gives low standard deviation irrespective of wind speed profiles, which ensures less mechanical stress on drive trains. But other two controllers have more standard deviation compared to TSMC, particularly baseline controllers having

very large standard deviation compared to TSMC and ISMC. Figure 5.12 shows the anova1 plot for different control strategy. In this figure, the red line indicate the mean value of the controllers. From this figure it is clear that TSMC controller having low bounds and mean value ensures less oscillation in control torque compared to other controllers.

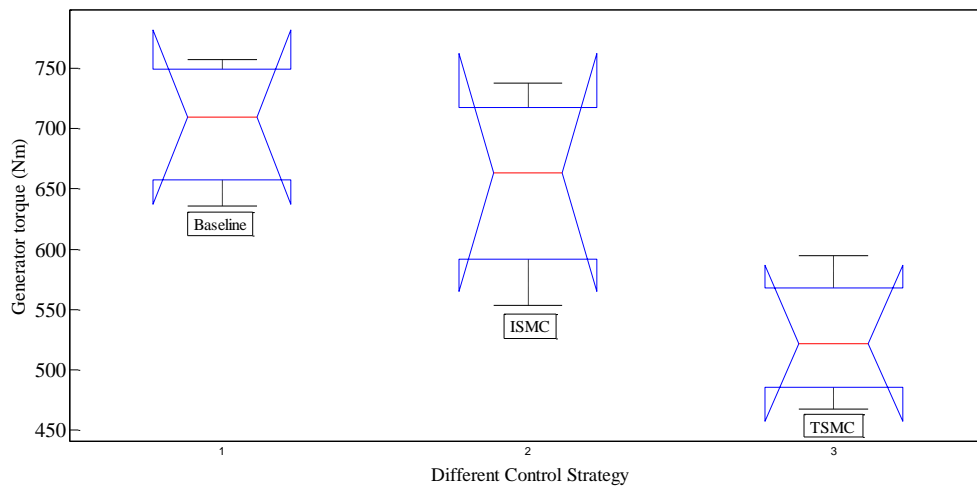


Figure 5.12: Anova1 plot for different control strategy.

Figure 5.13 and Figure 5.14 show the power comparison for different controllers with different types of actuator offset. From these figures it is seen that baseline and TSMC controllers are almost extracting similar power compared to ISMC. But ISMC cannot accommodate the actuator fault and it introduces more power loss. Table 5.6 and 5.7 show the performance comparison for different actuator faults. It is found that TSMC gives maximum electrical efficiency compared to other controllers with actuator offset. The standard deviation of the generator torque is more in case of baseline controller. ISMC cannot accommodate the actuator faults and it introduces more power loss compared to other controllers due to non-adaptiveness in the control law.

Table 5.6: one actuator offset

	Baseline	ISMC	TSMC
$STD(T_{em})$ Nm	656.88	615.26	625.97
$\eta_{elec}$ (%)	71.05	67.18	75.54
$\eta_{aero}$ (%)	88.11	94.90	92.60
Std ( $T_{ls}$ ) Nm	72.20	27.92	28.93



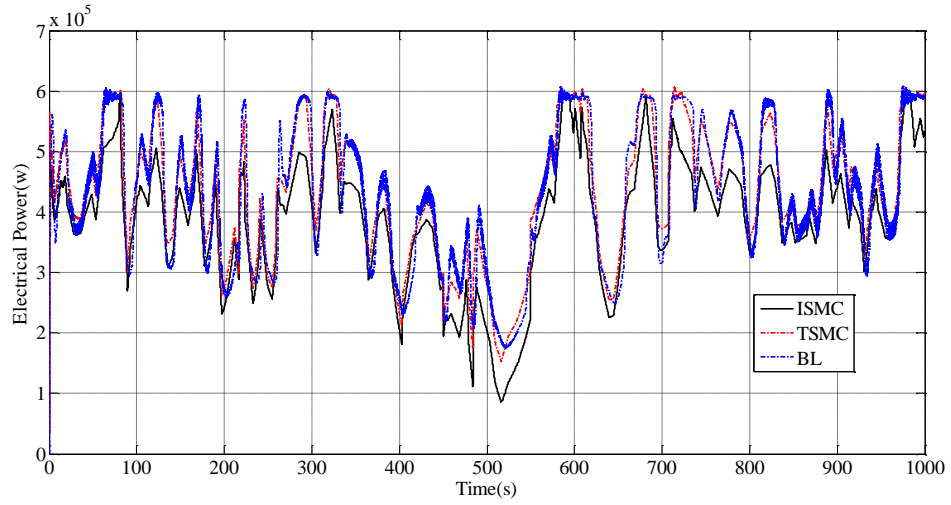


Figure 5.13: Power comparison one actuator fault.

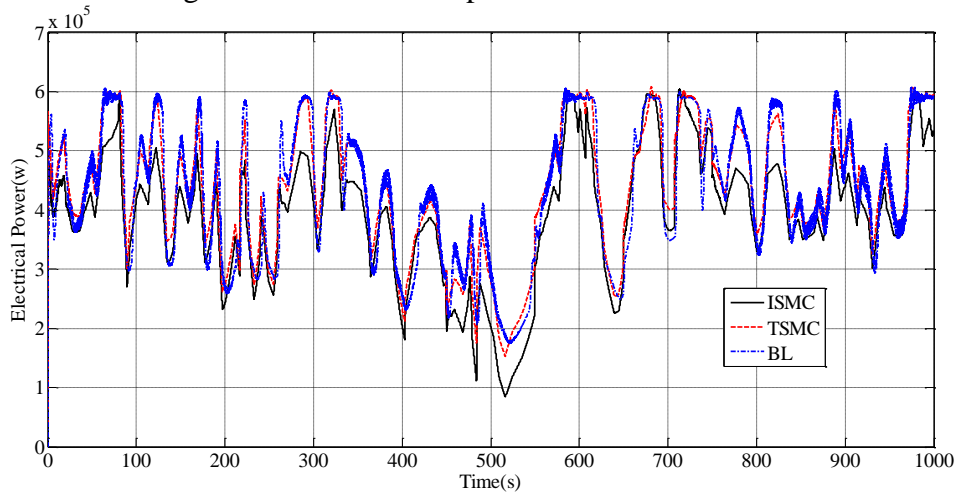


Figure 5.14: Power comparison two actuator fault.

Table 5.7: Two actuator offset

	Baseline	ISMC	TSMC
$\text{Std}(T_{em})$ Nm	653.97	646.02	634.66
$\eta_{elec}$ (%)	71.08	68.11	75.70
$\eta_{aero}$ (%)	88.06	94.85	92.17
$\text{Std}(T_{ls})$ Nm	72.66	29.29	29.41

## 5.7 FAULT DESCRIPTION

Fault scenarios are implemented in the FAST WT model.

Table 5.8 shows the fault scenario.

Table 5.8: Fault Scenarios

S. No	Fault	Type	Active (s)
1	Generator actuator fault	Offset	650-750
2	Generator speed sensor	Scaling	350-400

## 5.8 SIMULATION RESULT FOR BOTH THE FAULTS

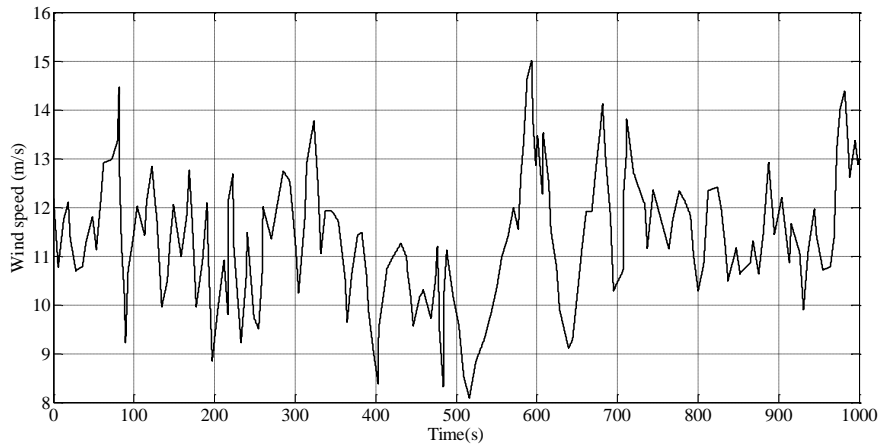


Figure 5.15: Mixed wind profile.

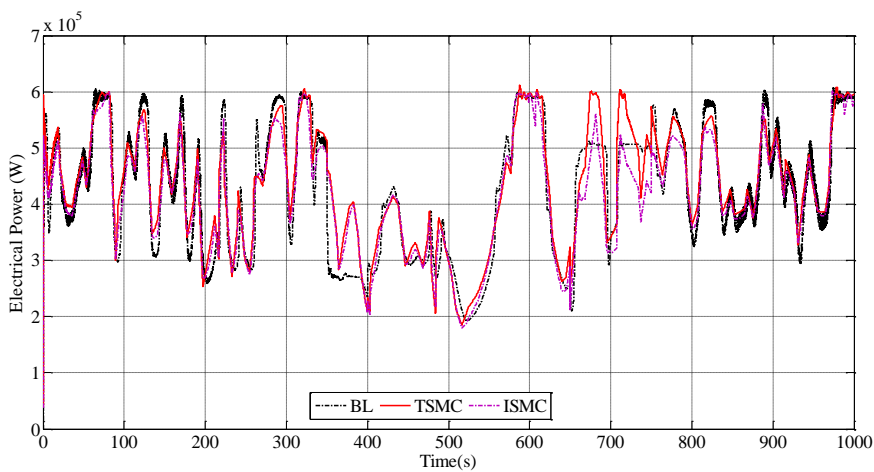


Figure 5.16: Electrical power comparison for conventional, ISMC and TSMC with generator and sensor fault.

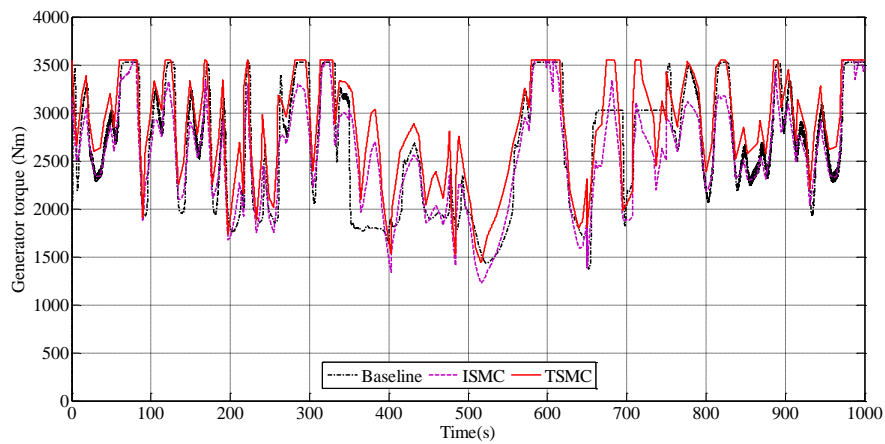


Figure 5.17: Generator torque comparison for conventional, ISMC and TSMC with generator and sensor fault.

Figure 5.15 shows the mixed wind speed profile around the rated wind speed. Figure 5.16 shows the electrical power comparison for baseline ISMC and TSMC controller. In the presence of both the generator sensor and actuator fault, TSMC can achieve optimal power compared to other controllers.

Table 5.9: Performance analysis of different controller in the presence of generator sensor and actuator fault.

Controllers	BL	ISMC	TSMC
STD( $T_{em}$ ) Nm	662.37	586.05	522.25
STD( $T_{ls}$ ) kNm	68.68	26.54	24.03

Figure 5.17 shows the generator torque comparison for baseline ISMC and TSMC controller. In order to analyze the performance of the controller, STD for generator torque and low speed shaft torque are considered. Table 5.9 shows the STD in TSMC is low compared to all the controllers. From the analysis, TSMC is found to be the optimal controller in the presence of both the generator sensor and actuator faults.

## 5.9 CONCLUSION

This chapter discusses the application of an ISMC and TSMC in region 2 with different actuator faults and sensor faults. Initially, TSMC is proposed for maximum power capture of VSWT at below rated wind speed for single mass model. The conventional SMC and TSMC for single mass model were tested with various types of disturbances. Proposed TSMC can extract more power under different input disturbances and actuator offset. This study reveals that the potential gain in power capture can be achieved by improving the tracking that always comes at the cost of increased variations in input torque, which ultimately increases the stress in the system. TSMC is also adapted for two mass model for VSWT. The proposed TSMC is compared with ISMC and conventional baseline controller for generator actuator offset and sensor fault. Same ISMC and TSMC are also adopted for the switching between operating regions (transition region 2.5), so the control input maintains the continuity at the moment of switching. Finally, the performance of the proposed controllers are tested with nonlinear FAST WT model and the results are compared with the existing baseline controllers.



## CHAPTER 6

### 6 CONCLUSIONS AND FUTURE WORK

The simulations were carried out to control a variable speed variable pitch wind turbine operating under different disturbances and turbulent winds. The philosophy behind the control strategy at below and above rated wind speeds is clearly defined. The WT used in this work is the 600 kW FAST NREL. In order to make the controller more robust, different types of disturbances with different mean wind speeds were tested for the proposed controllers. Considering the simulation results, the following conclusions are drawn.

Chapter 2 discussed the exact estimation of effective wind speed. Generally the effective wind speed is not measured directly. The estimation of effective wind speed is achieved by using different estimation algorithm. Initially, without estimation of effective wind speed, the conventional control techniques were adapted to control the WT. Due to the weak performance of those control techniques, different types of nonlinear wind speed estimation based nonlinear controllers were employed for the WT and found to be more effective. Initially the WT dynamics were considered as the single mass model. At below rated wind speed, the power extraction was optimum by adapting  $C_p$  for different wind speeds. The pitch angle was kept at its optimum value. The proposed AFISMIC was applied for single mass model of the WT. Generally, WT disturbances are highly unpredictable in nature. In order to make the controller more robust, different types of disturbances i.e. constant, sinusoidal and random disturbances with different mean wind speed were tested for the conventional and proposed AFISMIC controllers. From this analysis it was seen that the proposed AFISMIC can achieve the above objectives with reduced oscillation in the control torque.

In chapter 3, the exact WT model i.e. two mass model of the WT was chosen with FAST NREL 600kW WT. The FAST has more DOF compared to the mathematical model. It gives the complete model of the WT. In this work, five DOF was considered

in FAST WT model. The wind speed was also programmed by the TurbSim package which was developed by the NREL. Initially, the conventional controllers such as ATF and ISC were adapted. Finally, the nonlinear controllers such as SMC and ISMC were considered and the results were compared to the conventional controllers. All the controllers were simulated by MATLAB/Simulink with NREL FAST model. Different types of mean wind speed and turbulence with parameter uncertainty and disturbances were also analyzed for the proposed and conventional controllers.

In chapter 4, at above rated speed, fuzzy PI based pitch controller was proposed. In region 2.5 i.e. transition region, both the controller actions were involved. A baseline + PI controller suitable for industrial state-of-the-art was considered as the conventional controller. In order to analyze the transition region, the wind speeds were considered for above and below rated wind speed. In some cases, the wind speed was considered from below rated wind speed and was raised up to cutout wind speed, again comes down to same speed with a step of 1m/sec. From the results it was found that at below rated wind speed, the trade-off is to be maintained between the maximum power capture and transient load on the drive train. It was seen that at above rated wind speed, both the conventional PI and proposed fuzzy PI are almost working in a similar way, but in some cases fuzzy PI was found to generate less actuating control signal to pitch actuator compared to conventional PI. In transition region, (region 2.5) due to the switching in the baseline controller, the control law is derived basing on generator speed, which introduces more oscillation on the control input compared to the all proposed controllers.

Fault in the WT is not predictable in nature. In order to make the passive fault tolerant control, the TSMC was proposed in chapter 5. Initially, the generator actuator fault was considered for particular time duration, which is generated by adding external disturbance to the control signal for a small duration. Sensor scaling was also taken into consideration as the sensor fault at below rated wind speed (only generator sensor fault). The proposed ISMC and TSMC with fuzzy PI were simulated with different wind speeds and also compared to baseline + PI controller.

The wind turbine regions are classified into three different categories i.e. region 2, region 2.5 and region 3. The main objective of the controller (torque control) in region

2 and 2.5 is to extract the maximum power from the wind with reduced oscillation on the drive train. At above rated wind speed (region 3), the major objective of the controller (i.e. pitch control) is to maintain the rated power of the wind turbine. Initially, single mass mathematical model based different control law is derived. The controllers are tested with different wind speed. In order to get the exact control on the wind turbine a two mass model is derived. The proposed controllers such as ISMC and TSMC are derived from two mass model and is applied to a FAST wind turbine model. This study reveals that proposed ISMC and TSMC were found to be optimal compared with baseline controller in the presence of disturbances, sensor and actuator fault. At above wind speed i.e. region 3 both the conventional PI and proposed fuzzy based PI controller are working almost similar but some cases fuzzy PI found to generate less actuating control signal to pitch actuator compared to conventional PI.

Future work might also include the observer based fault tolerant control for WT at various operating regions. Design of an integrated fault diagnosis system for the wide range of operating conditions. The drive train/damping controller can be combined with master controller for analysing the performance of WT for different wind speed regions. All proposed controllers with fault tolerant control schemes can be implemented with 5MW off shore WT systems and the stability aspects of controllers with integration of WT in grid can be analysed.

Most of the MPPT algorithm for WT is based on wind speed. Without considering the wind speed, an adaptive intelligent controller can be designed based on the power signal feedback by considering all the dynamics of WT and to be implemented in NREL FAST.





## Appendix I

### CART WT Parameters

Wind CART (Controls Advanced Research Turbine) is installed on the site NWTC (National Wind Technology Center). It is a horizontal axis with a mast 35 m and has two blade.



Figure AI.1: WT CART at NWTC, Golden Co.

Table AI.1: WT Parameters

Parameter	Signification
Rotor Radius	$R=21.65\text{m}$
Air Density	$\rho=1.29\text{kg/m}^3$
Rotor Inertia	$J_r=3.25.105\text{kg.m}^2$
Generator Inertia	$J_g=34.4\text{kg.m}^2$
Shaft damping coefficient	$K_{ls}=9500\text{Nm/rad}$
Shaft stiffness coefficient	$B_{ls}=2.691.105\text{Nm/rad}$
Rotor friction coefficient	$K_r=27.36 \text{ Nm/rad/sec}$
Generator friction coefficient	$K_g=0.2 \text{ Nm/rad/sec}$
Gear ratio	$n_g=43.165$
Cut in wind speed	6 m/sec
Rated Wind speed	13 m/sec
Cut out wind speed	25 m/sec



## Appendix II

### NREL Tools Input Files

#### *TurbSim*

TurbSim Input File. Valid for TurbSim v1.50, 22-Jul-2009; for CART3 simulations.

```
-----Runtime Options-----
511347          RandSeed1          - First random seed (-2147483648 to
2147483647)
RanLux          RandSeed2          - Second random seed (-2147483648 to
2147483647) for intrinsic pRNG, or an alternative pRNG: "RanLux" or
"RNSNLW"
False          WrBHHTTP           - Output hub-height turbulence parameters
in GenPro-binary form? (Generates RootName.bin)
False          WrFHHTTP           - Output hub-height turbulence parameters
in formatted form? (Generates RootName.dat)
False          WrADHH             - Output hub-height time-series data in
AeroDyn form? (Generates RootName.hh)
False          WrADFF             - Output full-field time-series data in
TurbSim/AeroDyn form? (Generates RootName.bts)
True           WrBLFF             - Output full-field time-series data in
BLADED/AeroDyn form? (Generates RootName.wnd)
False          WrADTWR            - Output tower time-series data?
(Generates RootName.twr)
False          WrFMFFF            - Output full-field time-series data in
formatted (readable) form? (Generates RootName.u, RootName.v,
RootName.w)
False          WrACT              - Output coherent turbulence time steps
in AeroDyn form? (Generates RootName.cts)
True           Clockwise          - Clockwise rotation looking downwind?
(used only for full-field binary files - not necessary for AeroDyn)
0              ScaleIEC           - Scale IEC turbulence models to
specified standard deviation [0=none,1=hub,2=all points]?

-----Turbine/Model Specifications-----
17             NumGrid_Z          - Vertical grid-point matrix dimension
17             NumGrid_Y          - Horizontal grid-point matrix dimension
0.05           TimeStep           - Time step [seconds]
650.0          AnalysisTime        - Length of analysis time series
[seconds]
650.0          UsableTime          - Usable length of output time series
[seconds] (program will add GridWidth/MeanHHWS seconds)
37.0           HubHt              - Hub height [m] (should be >0.5*GridHeight)
55.0 45        GridHeight         - Grid height [m]
55.0 45        GridWidth          - Grid width [m] (should be >=
2*(RotorRadius+ShaftLength))
0              VFlowAng           - Vertical mean flow (uptilt) angle
[degrees]
0              HFlowAng           - Horizontal mean flow (skew) angle
[degrees]

-----Meteorological Boundary Conditions-----
```

NWTCUP            TurbModel            - Turbulence model ("IECKAI"=Kaimal, "IECVKM"=von Karman, "GP\_LLJ", "NWTCUP", "SMOOTH", "WF\_UPW", "WF\_07D", "WF\_14D", or "NONE")  
1-ed3            IECstandard        - Number of IEC 61400-x standard (x=1,2, or 3 with optional 61400-1 edition number (i.e. "1-Ed2") )  
"a"              IECturbc            - IEC turbulence characteristic ("A", "B", "C" or the turbulence intensity in percent) ("KHTTEST" option with NWTCUP, not used for other models)  
NTM              IEC\_WindType        - IEC turbulence type ("NTM"=normal, "xETM"=extreme turbulence, "xEWM1"=extreme 1-year wind, "xEWM50"=extreme 50-year wind, where x=wind turbine class 1, 2, or 3)  
default           ETMc                - IEC Extreme turbulence model "c" parameter [m/s]  
PL                WindProfileType    - Wind profile type ("JET"=Low-level jet, "LOG"=Logarithmic, "PL"=Power law, or "default", or "USR"=User-defined)  
37.0             RefHt                - Height of the reference wind speed [m]  
7.0               URef                - Mean (total) wind speed at the reference height [m/s]  
default           ZJetMax             - Jet height [m] (used only for JET wind profile, valid 70-490 m)  
0.2               PLExp               - Power law exponent (or "default")  
default           Z0                   - Surface roughness length [m] (or "default")

-----Non-IEC Meteorological Boundary Conditions-----

default           Latitude            - Site latitude [degrees] (or "default")  
0.05             RICH\_NO            - Gradient Richardson number  
default           UStar               - Friction or shear velocity [m/s] (or "default")  
default           ZI                   - Mixing layer depth [m] (or "default")  
default           PC\_UW               - Hub mean u'w' Reynolds stress (or "default")  
default           PC\_UV               - Hub mean u'v' Reynolds stress (or "default")  
default           PC\_VW               - Hub mean v'w' Reynolds stress (or "default")  
default           IncDec1             - u-component coherence parameters (or "default")  
default           IncDec2             - v-component coherence parameters (or "default")  
default           IncDec3             - w-component coherence parameters (or "default")  
default           CohExp               - Coherence exponent (or "default")

-----Coherent Turbulence Scaling Parameters-----

"Y:\Wind\Archive\Public\Projects\KH\_Billow\EventData"        CTEventPath  
- Name of the path where event data files are located  
"Random"           CTEventFile        - Type of event files ("random", "les" or "dns")  
true               Randomize            - Randomize disturbance scale and location? (true/false)  
1.0                DistScl             - Disturbance scale (ratio of dataset height to rotor disk).  
0.5                CTLy                - Fractional location of tower centerline from right (looking downwind) to left side of the dataset.

```

0.5          CTLz          - Fractional location of hub height
from the bottom of the dataset.
10.0         CTStartTime   - Minimum start time for coherent
structures in RootName.cts [seconds]

```

```

----- User-Defined Profiles (Used only with USR wind profile or
USRVKM spectral model) -----

```

```

5           NumUSRz       - Number of Heights
1.092      StdScale1     - u-component scaling factor for the
input standard deviation
1.0        StdScale2     - v-component scaling factor for the
input standard deviation
0.534      StdScale3     - w-component scaling factor for the
input standard deviation

```

```

.....
.....
Height      Wind Speed      Wind --Direction--      Standard Deviation
Length Scale
(m)          (m/s)          (deg, cntr-clockwise )      (m/s)
-----

```

```

15.0        3              00              .100
3
25.0        4              00              .200
4
35.0        5              00              .300
6
45.0        6              00              .100
9
55.0        7              00              .500
13

```

```

=====
NOTE: Do not add or remove any lines in this file!
=====

```

## ***FAST***

```

-----
-----
----- FAST INPUT FILE -----
-----
FAST Model: CART 3-blades, Operating Point #1, with Region 2.5
Compatible with FAST v6.01.
----- SIMULATION CONTROL -----
-----
False       Echo          - Echo input data to "echo.out" (flag)
1          ADAMSPrep     - ADAMS preprocessor mode {1: Run FAST, 2: use
FAST as a preprocessor to create an ADAMS model, 3: do both} (switch)
1          AnalMode     - Analysis mode {1: Run a time-marching
simulation, 2: create a periodic linearized model} (switch)
3          NumBl        - Number of blades (-)
600        TMax         - Total run time (s)
0.0025     DT           - Integration time step (s)
----- TURBINE CONTROL -----
-----

```

0            YCMode            - Yaw control mode {0: none, 1: user-defined from routine UserYawCont, 2: user-defined from Simulink} (switch)  
 9999.9       TYCON            - Time to enable active yaw control (s) [unused when YCMode=0]  
 2            PCMode            - Pitch control mode {0: none, 1: user-defined from routine PitchCntrl, 2: user-defined from Simulink} (switch)  
 0.            TPCOn            - Time to enable active pitch control (s) [unused when PCMode=0]  
 3            VSContrl        - Variable-speed control mode {0: none, 1: simple VS, 2: user-defined from routine UserVSCont, 3: user-defined from Simulink} (switch)  
 1600 1781.9791 VS\_RtGnSp    - Rated generator speed for simple variable-speed generator control (HSS side) (rpm) [used only when VSContrl=1]  
 3524.36      VS\_RtTq            - Rated generator torque/constant generator torque in Region 3 for simple variable-speed generator control (HSS side) (N-m) [used only when VSContrl=1]  
 0.000924 VS\_Rgn2K        - Generator torque constant in Region 2 for simple variable-speed generator control (HSS side) (N-m/rpm<sup>2</sup>) [used only when VSContrl=1]  
 5.000000000 VS\_SlPc        - Rated generator slip percentage in Region 2 1/2 for simple variable-speed generator control (%) [used only when VSContrl=1]  
 1            GenModel            - Generator model {1: simple, 2: Thevenin, 3: user-defined from routine UserGen} (switch) [used only when VSContrl=0]  
 True         GenTiStr            - Method to start the generator {T: timed using TimGenOn, F: generator speed using SpdGenOn} (flag)  
 True         GenTiStp          - Method to stop the generator {T: timed using TimGenOf, F: when generator power = 0} (flag)  
 9999.9       SpdGenOn            - Generator speed to turn on the generator for a startup (HSS speed) (rpm) [used only when GenTiStr=False]  
 0.0          TimGenOn            - Time to turn on the generator for a startup (s) [used only when GenTiStr=True]  
 9999.9       TimGenOf            - Time to turn off the generator (s) [used only when GenTiStp=True]  
 1            HSSBrMode          - HSS brake model {1: simple, 2: user-defined from routine UserHSSBr} (switch)  
 9999.9       THSSBrDp          - Time to initiate deployment of the HSS brake (s)  
 9999.9       TiDynBrk          - Time to initiate deployment of the dynamic generator brake [CURRENTLY IGNORED] (s)  
 9999.9       TTpBrDp(1)        - Time to initiate deployment of tip brake 1 (s)  
 9999.9       TTpBrDp(2)        - Time to initiate deployment of tip brake 2 (s)  
 9999.9       TTpBrDp(3)        - Time to initiate deployment of tip brake 3 (s) [unused for 2 blades]  
 9999.9       TBDepISp(1)      - Deployment-initiation speed for the tip brake on blade 1 (rpm)  
 9999.9       TBDepISp(2)      - Deployment-initiation speed for the tip brake on blade 2 (rpm)  
 9999.9       TBDepISp(3)      - Deployment-initiation speed for the tip brake on blade 3 (rpm) [unused for 2 blades]  
 9999.9       TYawManS          - Time to start override yaw maneuver and end standard yaw control (s)  
 9999.9       TYawManE          - Time at which override yaw maneuver reaches final yaw angle (s)  
 0.0          NacYawF            - Final yaw angle for yaw maneuvers (degrees)

```

9999.9      TPitManS(1) - Time to start override pitch maneuver for
blade 1 and end standard pitch control (s)
9999.9      TPitManS(2) - Time to start override pitch maneuver for
blade 2 and end standard pitch control (s)
9999.9      TPitManS(3) - Time to start override pitch maneuver for
blade 3 and end standard pitch control (s) [unused for 2 blades]
9999.9      TPitManE(1) - Time at which override pitch maneuver for
blade 1 reaches final pitch (s)
9999.9      TPitManE(2) - Time at which override pitch maneuver for
blade 2 reaches final pitch (s)
9999.9      TPitManE(3) - Time at which override pitch maneuver for
blade 3 reaches final pitch (s) [unused for 2 blades]
3.7         BlPitch(1) - Blade 1 initial pitch (degrees)
3.7         BlPitch(2) - Blade 2 initial pitch (degrees)
3.7         BlPitch(3) - Blade 3 initial pitch (degrees) [unused for
2 blades]
90.0        BlPitchF(1) - Blade 1 final pitch for pitch maneuvers
(degrees)
90.0        BlPitchF(2) - Blade 2 final pitch for pitch maneuvers
(degrees)
90.0        BlPitchF(3) - Blade 3 final pitch for pitch maneuvers
(degrees) [unused for 2 blades]
----- ENVIRONMENTAL CONDITIONS -----
-----
9.80665 Gravity - Gravitational acceleration (m/s^2)
----- FEATURE FLAGS -----
-----
True        FlapDOF1   - First flapwise blade mode DOF (flag)
True        FlapDOF2   - Second flapwise blade mode DOF (flag)
True        EdgeDOF    - First edgewise blade mode DOF (flag)
False      TeetDOF     - Rotor-teeter DOF (flag) [unused for 3 blades]
True        DrTrDOF    - Drivetrain rotational-flexibility DOF (flag)
True        GenDOF     - Generator DOF (flag)
False      YawDOF      - Yaw DOF (flag)
False True  TwFADOF1   - First fore-aft tower bending-mode DOF
(flag)
False      TwFADOF2   - Second fore-aft tower bending-mode DOF
(flag)
True        TwSSDOF1   - First side-to-side tower bending-mode DOF
(flag)
False      TwSSDOF2   - Second side-to-side tower bending-mode DOF
(flag)
True        CompAero   - Compute aerodynamic forces (flag)
False      CompNoise  - Compute aerodynamic noise (flag)
----- INITIAL CONDITIONS -----
-----
0.0         OoPDefl    - Initial out-of-plane blade-tip displacement,
(meters)
0.0         IPDefl     - Initial in-plane blade-tip deflection,
(meters)
0.0         TeetDefl   - Initial or fixed teeter angle (degrees)
[unused for 3 blades]
0.0         Azimuth    - Initial azimuth angle for blade 1 (degrees)
37.0        RotSpeed   - Initial or fixed rotor speed (rpm)
-0.0        NacYaw     - Initial or fixed nacelle-yaw angle (degrees)
0.0         TTDspFA    - Initial fore-aft tower-top displacement
(meters)

```

```

    0.0      TTDspSS      - Initial side-to-side tower-top displacement
(meters)
----- TURBINE CONFIGURATION -----
-----
20.0000000 TipRad      - The distance from the rotor apex to the blade
tip (meters)
    0.816   HubRad      - The distance from the rotor apex to the blade
root (meters)
    1.0000000 PSpnElN   - Number of the innermost blade element which
is still part of the pitchable portion of the blade for partial-span
pitch control [1 to BldNodes] [CURRENTLY IGNORED] (-)
    0.0000000 UndSling  - Undersling length [distance from teeter pin
to the rotor apex] (meters) [unused for 3 blades]
    0.0000000 HubCM     - Distance from rotor apex to hub mass [positive
downwind] (meters)
-4.2570400 OverHang   - Distance from yaw axis to rotor apex [3
blades] or teeter pin [2 blades] (meters)
-0.4020000 NacCMxn    - Downwind distance from the tower-top to the
nacelle CM (meters)
    0.0000000 NacCMyn   - Lateral distance from the tower-top to the
nacelle CM (meters)
    1.7340000 NacCMzn   - Vertical distance from the tower-top to the
nacelle CM (meters)
34.8615000 TowerHt    - Height of tower above ground level [onshore]
or MSL [offshore] (meters)
    1.7340000 Twr2Shft  - Vertical distance from the tower-top to the
rotor shaft (meters)
    0.0000000 TwrRBHt   - Tower rigid base height (meters)
-3.32   ShftTilt     - Rotor shaft tilt angle (degrees)
    0.0000000 Delta3    - Delta-3 angle for teetering rotors (degrees)
[unused for 3 blades]
    0.0000000 PreCone(1) - Blade 1 cone angle (degrees)
    0.0000000 PreCone(2) - Blade 2 cone angle (degrees)
    0.0000000 PreCone(3) - Blade 3 cone angle (degrees) [unused for 2
blades]
    0.0000000 AzimBlUp  - Azimuth value to use for I/O when blade 1
points up (degrees)
----- MASS AND INERTIA -----
-----
    0.0      YawBrMass  - Yaw bearing mass (kg)
23884.1     NacMass    - Nacelle mass (kg)
    6552.    HubMass    - Hub mass (kg)
    0.       TipMass(1) - Tip-brake mass, blade 1 (kg)
    0.       TipMass(2) - Tip-brake mass, blade 2 (kg)
    0.       TipMass(3) - Tip-brake mass, blade 3 (kg) [unused for 2
blades]
36590.     NacYIner   - Nacelle inertia about yaw axis (kg m^2)
46.01   34.4   GenIner   - Generator inertia about HSS (kg m^2)
    3899.7   HubIner   - Hub inertia about rotor axis [3 blades] or
teeter axis [2 blades] (kg m^2)
----- DRIVETRAIN -----
-----
    98.0     GBoxEff    - Gearbox efficiency (%)
    93.0     GenEff     - Generator efficiency [ignored by the Thevenin
and user-defined generator models] (%)
    43.165   GBRatio   - Gearbox ratio (-)
False      GBRevers   - Gearbox reversal {T: if rotor and generator
rotate in opposite directions} (flag)

```



```

8686.4      HSSBrTqF      - Fully deployed HSS-brake torque (N-m)
9999.9      HSSBrDT      - Time for HSS-brake to reach full deployment
once initiated (sec) [used only when HSSBrMode=1]
          DynBrkFi      - File containing a mech-gen-torque vs HSS-
speed curve for a dynamic brake [CURRENTLY IGNORED] (quoted string)
2.47e7 18588500 1.6043e7  DTTorSpr      - Drivetrain torsional spring
(N-m/rad)
1.4e4 2.4e4  DTTorDmp      - Drivetrain torsional damper (N-m/s)
----- SIMPLE INDUCTION GENERATOR -----
-----
0.1          SIG_SlPc      - Rated generator slip percentage (%) [used
only when VSContrl=0 and GenModel=1]
1800.0       SIG_SySp      - Synchronous (zero-torque) generator speed
(rpm) [used only when VSContrl=0 and GenModel=1]
3580.0       SIG_RtTq      - Rated torque (N-m) [used only when VSContrl=0
and GenModel=1]
2.0          SIG_PORT      - Pull-out ratio (Tpullout/Trated) (-) [used
only when VSContrl=0 and GenModel=1]
----- THEVENIN-EQUIVALENT INDUCTION GENERATOR -----
-----
0.0          TEC_Freq      - Line frequency [50 or 60] (Hz) [used only
when VSContrl=0 and GenModel=2]
0            TEC_NPol      - Number of poles [even integer > 0] (-) [used
only when VSContrl=0 and GenModel=2]
0.00         TEC_SRes      - Stator resistance (ohms) [used only when
VSContrl=0 and GenModel=2]
0.00         TEC_RRes      - Rotor resistance (ohms) [used only when
VSContrl=0 and GenModel=2]
0.0          TEC_VLL      - Line-to-line RMS voltage (volts) [used only
when VSContrl=0 and GenModel=2]
0.0          TEC_SLR      - Stator leakage reactance (ohms) [used only
when VSContrl=0 and GenModel=2]
0.0          TEC_RLR      - Rotor leakage reactance (ohms) [used only
when VSContrl=0 and GenModel=2]
0.0          TEC_MR      - Magnetizing reactance (ohms) [used only when
VSContrl=0 and GenModel=2]
----- PLATFORM MODEL -----
-----
0            PtfmModel      - Platform model {0: none, 1: onshore, 2: fixed
bottom offshore, 3: floating offshore} (switch)
          PtfmFile      - Name of file containing platform properties
(quoted string) [unused when PtfmModel=0]
----- TOWER -----
-----
20 17          TwrNodes      - Number of tower nodes used for analysis
(-)
"CART3_Tower_V7.dat" TwrFile - Name of file containing tower properties
(quoted string)
----- NACELLE-YAW -----
-----
0.0          YawSpr      - Nacelle-yaw spring constant (N-m/rad)
0.0          YawDamp      - Nacelle-yaw damping constant (N-m/rad/s)
0.0          YawNeut      - Neutral yaw position--yaw spring force is
zero at this yaw (degrees)
----- FURLING -----
-----
False          Furling      - Read in additional model properties for
furling turbine (flag)

```

```

        FurlFile      - Name of file containing furling properties
        (quoted string) [unused when Furling=False]
----- ROTOR-TEETER -----
-----
        0          TeetMod      - Rotor-teeter spring/damper model {0: none,
1: standard, 2: user-defined from routine UserTeet} (switch) [unused
for 3 blades]
        0.0       TeetDmpP     - Rotor-teeter damper position (degrees) [used
only for 2 blades and when TeetMod=1]
        0.0       TeetDmp      - Rotor-teeter damping constant (N-m/rad/s)
[used only for 2 blades and when TeetMod=1]
        0.0       TeetCDmp     - Rotor-teeter rate-independent Coulomb-damping
moment (N-m) [used only for 2 blades and when TeetMod=1]
        0.0       TeetSSStP    - Rotor-teeter soft-stop position (degrees)
[used only for 2 blades and when TeetMod=1]
        0.0       TeetHStP     - Rotor-teeter hard-stop position (degrees)
[used only for 2 blades and when TeetMod=1]
        0.0       TeetSSSp     - Rotor-teeter soft-stop linear-spring constant
(N-m/rad) [used only for 2 blades and when TeetMod=1]
        0.0       TeetHSSp     - Rotor-teeter hard-stop linear-spring constant
(N-m/rad) [used only for 2 blades and when TeetMod=1]
----- TIP-BRAKE -----
-----
        0.0       TBDrConN     - Tip-brake drag constant during normal
operation, Cd*Area (m^2)
        0.0       TBDrConD     - Tip-brake drag constant during fully-deployed
operation, Cd*Area (m^2)
        0.0       TpBrDT       - Time for tip-brake to reach full deployment
once released (sec)
----- BLADE -----
-----
"CART3_Blades_V7.dat"      BldFile(1) - Name of file containing
properties for blade 1 (quoted string)
"CART3_Blades_V7.dat"      BldFile(2) - Name of file containing
properties for blade 2 (quoted string)
"CART3_Blades_V7.dat"      BldFile(3) - Name of file containing
properties for blade 3 (quoted string) [unused for 2 blades]
----- AERODYN -----
-----
"CART3_AD_V7.ipt"         ADFile      - Name of file containing AeroDyn
input parameters (quoted string)
----- NOISE -----
-----
        NoiseFile      - Name of file containing
aerodynamic noise input parameters (quoted string) [used only when
CompNoise=True]
----- ADAMS -----
-----
        ADAMSFile     - Name of file containing ADAMS-
specific input parameters (quoted string) [unused when ADAMSPrep=1]
----- LINEARIZATION CONTROL -----
-----
"lin_file"                LinFile      - Name of file containing FAST
linearazation parameters (quoted string) [unused when AnalMode=1]
----- OUTPUT -----
-----
True          SumPrint     - Print summary data to "<RootName>.fsm" (flag)

```

```

True          TabDelim    - Generate a tab-delimited tabular output file.
(flag)
"ES10.3E2"   OutFmt       - Format used for tabular output except time.
Resulting field should be 10 characters. (quoted string) [not checked
for validity!]
0.000000000 TStart      - Time to begin tabular output (s)
1.000000000 DecFact     - Decimation factor for tabular output {1:
output every time step} (-)
1.000000000 SttsTime    - Amount of time between screen status
messages (sec)
3.052000000 NcIMUxn     - Downwind distance from the tower-top to
the nacelle IMU (meters)
0.000000000 NcIMUyn     - Lateral distance from the tower-top to
the nacelle IMU (meters)
0.489000000 NcIMUzn     - Vertical distance from the tower-top to
the nacelle IMU (meters)
1.113000000 ShftGagL    - Distance from rotor apex [3 blades] or
teeter pin [2 blades] to shaft strain gages [positive for upwind
rotors] (meters)
1.000000000 NTwGages    - Number of tower nodes that have strain
gages for output [0 to 5] (-)
5.000000000 TwrGagNd    - List of tower nodes that have strain gages
[1 to TwrNodes] (-) [unused if NTwGages=0]
0.000000000 NBlGages    - Number of blade nodes that have strain
gages for output [0 to 5] (-)
3,5,7       BldGagNd    - List of blade nodes that have strain gages
[1 to BldNodes] (-) [unused if NBlGages=0]
OutList      - The next line(s) contains a list of output
parameters. See OutList.txt for a listing of available output
channels, (-)
"RotTorq"
"HSShftTq"
"NcIMURVxs"
"LSSTIPPxa"
"NcIMURVys"
"NcIMURVzs"
"NcIMUTAxS"
"NcIMUTAyS"
"NcIMUTAzS"
"TwrBsMxt"
"TwrBsMyt"
"LSSTipVxa"
"RotCp"
"TSR"
"HSShftPwr"
"RotPwr"
"LSSTipAxa"
"HSShftA"
"GenSpeed"
"WindVxi"
"RootMxb1"
"RootMyb1"
"RootMxb2"
"RootMyb2"
"RootMxb3"
"RootMyb3"
"RotSpeed"
"Azimuth"

```

"PtchPMzc1"  
"PtchPMzc2"  
"PtchPMzc3"  
"LShftTq"  
"TipDxb1"  
"TipDyb1"  
"TwHt1ALxt"  
"YawBrTDyp"  
"TwHt1MLxt"  
"TwHt1MLyt"

END of FAST input file (the word "END" must appear in the first 3  
columns of this last line).

-----  
-----

## References

- Abdullah, M.A., Yatim, A.H.M., Tan, C.W. and Saidur, R. (2012). "A review of maximum power point tracking algorithms for wind energy systems." *Renewable and Sustainable Energy Reviews.*, 16(5), 3220-3227.
- Abo-Khalil, A.G. and Abo-Zied, H. (2012). "Sensorless control for DFIG wind turbines based on support vector regression." *Proc., Annual Conf. on IEEE Industrial Electronics Society*, Montreal, QC, 3475-3480.
- Abo-Khalil, A.G. and Lee, D.C. (2008). "MPPT control of wind generation systems based on estimated wind speed using SVR." *IEEE Trans. Ind. Electron.*, 55(3), 1489-1490.
- Agrawal, S., Panigrahi, B.K. and Tiwari, M.K. (2008). "Multiobjective particle swarm optimization with fuzzy clustering for electrical power dispatch." *IEEE Trans. Evol. Comput.*, 12(5), 529-541.
- Amine, H.M., Abdelaziz, H. and Najib, E. (2014). "Wind turbine maximum power point tracking using FLC tuned with GA." *Energy Procedia.*, 62, 364-373.
- Amirat, Y., Benbouzid, M., Bensaker, B. and Wamkeue, R. (2007). "The state of the art of generators for wind energy conversion systems." *Electromotion.*, 14(4), 163-172.
- Anaya-Lara, O., Jenkins, N., Ekanayake, J., Cartwright, P. and Hughes, M. (2009). *Wind energy generation: Modelling and control*. Wiley Publication.
- Arulampalam, M.S., Maskell, S., Gordon, N. and Clapp, T. (2002). "A tutorial on particle filters for online nonlinear/non-Gaussian Bayesian tracking." *IEEE Trans. Signal Process.*, 50(2), 174-188.
- Assareh, E. and Biglari, M. (2015). "A novel approach to capture the maximum power from variable speed wind turbines using PI controller, RBF neural network and GSA evolutionary algorithm." *Renewable and Sustainable Energy Reviews.*, 51, 1023-1037.
- Bansal, R.C., Zobaa, A.F., and Saket, R.K. (2005). "Some issues related to power generation using wind energy conversion systems: An Overview" *International Journal of Emerging Electric Power Systems.*, 3(2), 1-17.
- Barambones, O., Durana, J.M.G. and Kremers, E. (2010). "A neural network based wind speed estimator for a wind turbine control." *Proc., IEEE Mediterranean Electrotechnical Conf.*, Valletta, 1383-1388.

- Belmokhtar, K., Doumbia, M.L. and Agbossou, K. (2014). "Novel fuzzy logic based sensorless maximum power point tracking strategy for wind turbine systems driven DFIG." *Energy.*, 76, 679-693.
- Beltran, B., Ahmed-Ali, T. and Benbouzid, M.E.H. (2008a). "Sliding mode power control of variable-speed wind energy conversion systems." *IEEE Trans. Energy Convers.*, 23(2), 551-558.
- Beltran, B., Ahmed-Ali, T. and Benbouzid, M.E.H. (2008b). "High-order sliding-mode control of variable-speed wind turbines." *IEEE Trans. Ind. Electron.*, 56(9), 3314-3321.
- Ben-Tzvi, P., Bai, S., Zhou, Q. and Huang, X. (2011). "Fuzzy sliding mode control of rigid –flexible multibody systems with bounded inputs." *J. of Dynamic Systems Measurement and Control.*, 133(6).
- Bhowmik, S. and Spee, R. (1998). "Wind speed estimation based variable speed wind power generation." *Proc., Annual Conf. of Industrial Electronics Society, Aachen*, 596-601.
- Bhowmik, S., Spee, R. and Enslin, J.H.R. (1999). "Performance optimization for doubly fed wind power generation systems." *IEEE Trans. Ind. Appl.*, 35(4), 949-958.
- Bishop, C.M. (1995). "Neural network for pattern recognizataion." Oxford University Press, Oxford., UK.
- Boukezzar, B. and M'Saad, M. (2008). "Robust sliding mode control of a DFIG variable speed wind turbine for power production optimization." *Proc., Mediterranean Conference on Control and Automation, Ajaccio, France*, 795-800.
- Boukhezzar, B. (2011). "On control strategies for power optimization and regulation of variable speed wind turbines." Ph.D thesis, Paris-Sud University, France.
- Boukhezzar, B. and Siguerdidjane, H. (2005). "Nonlinear control of variable speed wind turbines without wind speed measurement." *Proc., IEEE Conf. on Decision and Control, Seville*, 3456-3461.
- Boukhezzar, B. and Siguerdidjane, H. (2009a). "Comparison between linear and nonlinear control strategies for variable speed wind turbine power capture optimization." *Renewable Energy Ecol Vehicles*.
- Boukhezzar, B. and Siguerdidjane, H. (2009b). "Nonlinear control with wind estimation of a DFIG variable speed wind turbine for power capture optimization." *Energy Conversion and Management.*, 50(4), 885-892.

- Boukhezzar, B. and Siguerdidjane, H. (2011). "Nonlinear control of a variable speed wind turbine using a two mass model." *IEEE Trans. Energy Convers.*, 26(1), 149-162.
- Boukhezzar, B., Siguerdidjane, H. and Hand, M.M. (2006). "Nonlinear control of variable speed wind turbines for generator torque limiting and power optimization." *J. of Solar Energy Engineering.*, 128(4).
- Bourlis, D. and Bleijs, J.A.M. (2010). "A wind speed estimation method using adaptive Kalman filtering for a variable speed stall regulated wind turbine." *Proc., Int. Conf. on Probabilistic Methods Applied to Power Systems*, Singapore, 89-94.
- Calderaro, V., Galdi, V., Piccolo, A. and Saino, P. (2008). "A fuzzy controller for maximum energy extraction from variable speed wind power generation systems." *Electrical Power System Research.*, 78(6), 1109-1118.
- Chen, S., Hong, X., Luk, B.L. and Harris, C.J. (2009). "Nonlinear system identification using particle swarm optimisation tuned radial bias function models." *International J. Bio-Inspired Computation.*, 1(4), 246-258.
- Ciric, I., Cojbasic, Z., Nikolic, V. and Petrovic E. (2011). "Hybrid fuzzy control strategies for variable speed wind turbines." *FACTA Universitatis Series Automatic Control and Robotics.*, 10(2), 205-217.
- Daili, Y., Gaubert, J. and Rahmani, L. (2015). "Implementation of anew maximum power point tracking control strategy for small wind energy conversion system without mechanical sensor." *Energy Management and Conversion.*, 97, 298-306.
- Darrow, P.J. (2009). "Wind turbine control design to reduced capital costs." NREL Report., Golden, Colorado.
- Diaz-Guerra, L., Adegas, F.D., Stoustrup, J. and Monros, M. (2012). "Adaptive control algorithm for improving power capture of wind turbines in turbulent winds." *Proc., American Control Conf.*, Montreal, QC, 5807-5812.
- Eker, I. and Akinal, S.A. (2005). "Sliding mode control with integral action and experimental application to an electromechanical system." *Proc., Congress on Computational Intelligence Methods and Applications*, Istanbul, 1-6.
- Evangelista, C., Puleston, P., Valenciaga, F. and Fridma, L.M. (2013). "Lyapunov-Designed Super-Twisting Sliding Mode Control for Wind Energy Conversion Optimization." *IEEE Transactions on Industrial Electronics.*, 60(2), 538-545.

Fingersh, L.J. and Johnson, K. (2002). "Controls advanced research turbine (CART) commissioning and baseline data collection." NREL Report, Golden, Colo, USA.

Fung, K.T., Scheffler, R.L. and Stolpe, J. (1981). "Wind energy – A utility perspective." *IEEE Trans. Power App. Syst.*, 100(3), 1176-1182.

Ge, H.W., Liang, Y.C. and Marchese, M. (2007). "A modified particle swarm optimization based dynamic recurrent neural network for identifying and controlling nonlinear system." *Computer and Structures.*, 85(21), 1611-1622.

Geethanjali, M., Slochanal, S.M.R. and Bhavani, R. (2008). "PSO trained ANN-based differential protection scheme for power transformers." *Neurocomputing.*, 71, 904-918.

Global Wind Energy Council website at <http://www.gwec.net/global-figures/graphs/>

Gou, F. (2004). "A new identification method for Wiener and Hammerstein systems." Ph.D thesis, Karlsruhe Institute of Technology., Germany.

Gourdin, A. and Boumahrat, M. (1995). "Methods Numerical Appliquees." Tec&Doc, 1995.

Griffiths, D.V. and Smith, I.M. (2006). "Numerical Methods for Engineers." CRC Press, Boca Raton.

Hansen, M.H., Hansen, A., Larsen, T.J., Oye, S., Sorensen, P. and Fuglsang, P. (2005). "Control design for pitch regulated variable speed wind turbine." Riso-R Report., Riso National Laboratory, Roskilde, Denmark.

Hansen, M.O.L., Sorensen, J.N., Voutsinas, S., Sorensen, N. and Madsen, H.A. (2006). "State of the art in wind turbine aerodynamics and aeroelasticity." *Progress in Aerospace Sciences.*, 42(4), 285-330.

Haykin, S. (2002). "Neural Network: A Comprehensive Foundation." Pearson Education.

Herbert, G.M.J., Iniyar, S., Sreevalsan, E. and Rajapandian, S. (2007). "A review of wind energy technologies." *Renewable and Sustainable Energy Reviews.*, 11(6), 1117-1145.

Hertz, J.A., Krogh, A.S. and Palmer, R.G. (1991). "Introduction to the theory of neural computing." Addison-Wesley, New York, NY.

Hong, C.M., Chen, C.H. and Tu, C.S. (2013). "Maximum power point tracking-based control algorithm for PMSG wind generation system without mechanical sensors." *Energy Conversion and Management.*, 69, 58-67.



- Hunt, K.J., Sbarbaro, D., Zbikowski, R. and Gawthrop, P.J. (1992). "Neural network for control systems-A survey." *Automatica.*, 28(6), 1083-1112.
- Ilonen, J., Kamarainen, J.K. and Lampinen, J. (2003). "Differential evolution training algorithm for feedforward neural networks." *Neural. Processing Letter.*, 17(1), 93-105.
- Jena, D. (2010). "Evolutionary neuro-computing approaches to system identification." Ph.D thesis, National Institute of Technology Rourkela, India.
- Ji, G., Dong, Z., Qiao, H. and Xu, D. (2008). "SVR-Based soft sensor for effective wind speed of large-scale variable speed wind turbine." *Proc., Int. Conf. on Natural Computation*, Jinan, 193-196.
- Jonkman B.J., and Buhl, M.L. (2005). "FAST user's guide." NREL Report., Golden, Colorado.
- Jonkman B.J., and Buhl, M.L. (2009). "TurbSim user guide: Version 1.50." NREL Report., Golden, Colorado.
- Jonkman, J., Butterfield, S., Musial, W. and Scott, G. (2009). "Definition of a 5-MW reference wind turbine for offshore system development." NREL Report., Golden, Colorado.
- Khamlichi, A., Ayyat, B., Zarouala, R.O.B. and Venegas, C.V. (2011). "Advanced control based on extended Kalman filter for variable speed wind turbine." *Australian J. of Basic & Applied Sciences.*, 5(9), 636-644.
- Kortabarria, I., Andreu, J., Alegria, I.M., Jimenez, J., Garate, J.I. and Robles, E. (2014). "A novel adaptative maximum power point tracking algorithm for small wind turbines." *Renewable Energy.*, 63, 785-796.
- Kumar, D. and Chatterjee, K. (2016). "A review of conventional and advanced MPPT algorithms for wind energy systems." *Renewable and Sustainable Energy Reviews.*, 55, 957-970.
- Laino, D.J. and Hansen, A.C. (2002). "User's guide to the wind turbine aerodynamics computer software AeroDyn." NREL Report, Golden, Colorado, USA.
- Leithead, W.E. and Connor, B. (2000). "Control of variable speed wind turbines: Design task." *International J. of Control.*, 73(13), 1189-1212.
- Li, H., Shi, K.L. and McLaren, P.G. (2004). "Neural network based sensorless maximum wind energy capture with compensated power coefficient." *Proc., Industry Applications Conf.*, Tallahassee, FL, USA, 2600-2608.

- Li, H., Shi, K.L. and McLaren, P.G. (2005). "Neural network based sensorless maximum wind energy capture with compensated power coefficient." *IEEE Trans. Ind. Appl.*, 41(6), 1548-1556.
- Liao, M., Dong, L., Jin, L. and Wang, S. (2009). "Study on rotational speed feedback torque control for wind turbine generator system." *Proc., Int. Conf. on Energy and Environment Technology*, Guilin, Guangxi, 853-856.
- Lin, W. and Hong, C. (2010). "Intelligent approach to maximum power point tracking control strategy for variable-speed wind turbine generation system." *Energy.*, 35(6), 2440-2447.
- Liu, J., Meng, H., Hu, Y., Lin, Z. and Wang, W. (2015). "A novel MPPT method for enhancing energy conversion efficiency taking power smoothing into account." *Energy Management and Conversion.*, 101, 738-748.
- Ma, X. (1997). "Adaptive extremum control and wind turbine control." Ph.D thesis, Technical University of Denmark, Denmark.
- Manjock, A. (2005). "Design codes FAST and ADAMS for load calculations of onshore wind turbines." NREL Report, Golden, Colorado, USA.
- Melicio, R., Mendes, V.M.F. and Catalao, J. P. S. (2010). "Harmonic assessment of variable-speed wind turbines considering a converter control malfunction," *IET Renewable and Power Generation.*, 4(2), 139–152.
- Merabet, A., Beguenane, R., Thongam, J.S. and Hussein, I. (2011). "Adaptive sliding mode control for wind turbine systems." *Proc., 37th Annual Conf. on IEEE Industrial Electronics Society*, Melbourne, VIC., 2461-2466.
- Merida, J., Aguilar, L.T. and Davila, J. (2014). "Analysis and synthesis of sliding mode control for large scale variable speed wind turbine for power optimization." *Renewable Energy.*, 71, 715-728.
- Mirzaei, M., Niemann, H.H. and Poulsen, N.K. (2011a). "DK-iteration robust control design of a wind turbine." *Proc., IEEE Int. Conf. on Control Applications*, Denver, CO, 1493-1498.
- Mirzaei, M., Niemann, H.H. and Poulsen, N.K. (2011b). "A  $\mu$ -synthesis approach to robust control of a wind turbine." *Proc., IEEE Int. Conf. Decision and Control and European Control Conference*, Orlando, FL, 645-650.

- Mohandes, M., Rehman, S. and Rahman, S.M. (2011). "Estimation of wind speed profile using adaptive neuro-fuzzy inference system (ANFIS)." *Applied Energy.*, 88(11), 4024-4032.
- Mondal, S. and Mahanta, C. (2014). "Adaptive second order terminal sliding mode controller for robotic manipulators." *J. of the Franklin Institute*, 351(4), 2356-2377.
- Muyeen, S., et.al. (2007). "Comparative study on transient stability analysis of wind turbine generator system using different drive train models," *IET Renewable and Power Generation.*, 1(2), 131–141.
- Nam, Y., Kim, J., Paek, I., Moon, Y.H., Kim, S.J. and Kim, D.J. (2011). "Feedforward pitch control using wind speed estimation." *J. of Power Electronics.*, 11(2), 211-217.
- Ottersten, R. (2003). "On control of back-to-back converters and sensorless induction machine drives." Ph.D thesis, Chalmers University of Technology, Goteborg, Sweden.
- Pang, W.K., Forster, J.J. and Troutt M.D. (2001). "Estimation of wind speed distribution using Markov chain Monte Carlo techniques." *J. of Applied Meteorology and Climatology.*, 40(8), 1476-1484.
- Pena, R., Cardenas, R., Blasco, R., Asher, G. and Clare, J. (2001). "A cage induction generator using back to back PWM converters for variable speed grid connected wind energy system." *Proc., Annual Conf. of the Industrial Electronics Society*, Denver, CO, 1376-1381.
- Petkovic, D., Cojbasic, Z. and Nikolic, V. (2013). "Adaptive neuro fuzzy approach for WT power coefficient estimation." *Renewable and Sustainable Energy Reviews.*, 28, 191-195.
- Qiao, W. (2009). "Echo-state-network-based real-time wind speed estimation for wind power generation." *Proc., Int. Conf. on Neural Networks.*, Atlanta, GA, 2572-2579.
- Qiao, W., Yang, X. and Gong, X. (2012). "Wind speed and rotor position sensorless control for direct-drive PMG wind turbines." *IEEE Trans. Ind. Appl.*, 48(1), 3-11.
- Qiao, W., Zhou, W., Aller, J.M. and Harley, R.G. (2008). "Wind speed estimation based sensorless output maximization control for a wind turbine driving a DFIG." *IEEE Trans. Power Electron.*, 23(3), 1156-1169.
- Ramtharan, G., Jenkins, N., Anaya-Lara, O. and Bossanyi, E. (2007) "Influence of rotor structural dynamics representations on the electrical transient performance of FSIG and DFIG wind turbines," *Wind Energy*, 10(4), 293–301.

- Sesto, E. and Casale, C. (1998). "Exploitation of wind as an energy source to meet the world's electricity demand." *J. of Wind Engineering and Industrial Aerodynamics.*, 74-76, 375-387.
- Shaker, M.S. (2012). "Active fault tolerant control of nonlinear systems with wind turbine applications." Ph.D thesis., University of Hull., UK.
- Shamshirband, S., Petkovic, D., Anuar, N.B., Kian, M.L.L., Akib, S., Gani, A., Cojbasic, Z. and Nikolic, V. (2014). "Sensorless estimation of wind speed by adaptive neuro-fuzzy methodology." *International J. Electrical Power & Energy Systems.*, 62, 490-495.
- Sheikhan, M., Shahnazi, R. and Yousefi, A.N. (2013). "An optimal fuzzy PI controller to capture the maximum power for variable-speed wind turbines." *Neural Computing and Applications.*, 23(5), 1359-1368.
- Soltani, M.N., Knudsen, T., Svenstrup, M., Wisniewski, R., Brath, P., Ortega, R. and Johnson, J. (2013). "Estimation of rotor effective wind speed: A comparison." *IEEE Trans. Control Syst. Technol.*, 21(4), 1155-1167.
- Storn, R. and Price, K. (1997). "Differential evolution- a simple and efficient heuristic for global optimization over continuous space." *J. of Global Optimization.*, 11(4), 341-359.
- Tan, K. and Islam, S. (2004). "Optimum control strategies in energy conversion of PMSG wind turbine system without mechanical sensors." *IEEE Trans. Energy Convers.*, 19(2), 392-399.
- Thiringer, T. and Petersson, A. (2005). "Control of a variable speed pitch regulated wind turbine." Report, Chalmers University of Technology, Goteborg, Sweden.
- Tian, L., Lu, Q. and Wang, W. (2011). "A gaussian RBF network based wind speed estimation algorithm for maximum power point tracking." *Energy Procedia.*, 12, 828-836.
- Vihriala, H. (2002). "Control of variable speed wind turbines." Ph.D thesis, Tampere University of Technology, Tampere.
- Vihriala, H., Perala, R., Makila, P. and Soderlund, L. (2001). "A gearless wind power drive: Part 2: Performance of control system." *Proc., European Wind Energy Conf.*, Copenhagen, Denmark.

- Wei, C., Zhang, Z., Qiao, W. and Qu, L. (2015). "Reinforcement learning based intelligent MPPT control for wind energy conversion systems." *IEEE Transactions on Industrial Electronics.*, 62(10), 6360-6370.
- Widrow, B and Winter, R (1998). "Neural network for adaptive filtering and adaptive pattern reorganization." *Computer.*, 21(3), 25-39.
- Wu, S., Wang, Y. and Cheng, S. (2013). "Extreme learning machine based wind speed estimation and sensorless control for wind turbine power generation system." *Neurocomputing.*, 102, 163-175.
- Xu, Z., Hu, Q. and Ehsani, M. (2011). "Estimation of effective wind speed for fixed-speed wind turbines based on frequency domain data fusion." *IEEE Trans. Sustainable Energy.*, 3(1), 57-64.
- Yang, S.H., Natarajan, U., Sekar, M. and Palani, S. (2010). "Prediction of surface roughness in turning operations by computer vision using neural network trained by differential evolution algorithm." *International J. Advanced Manufacturing Technology.*, 51(9), 965-971.
- Yang, X., Han, X., Xu, L. and Liu, Y. (2006). "Soft sensor based on support vector machine for effective wind speed in large variable wind." *Proc., Int. Conf. on Control, Automation, Robotics and Vision*, Singapore, 1-4.
- Yu, K.N. and Liao, C.K. (2015). "Applying novel fractional order incremental conductance algorithm to design and study the maximum power tracking of small wind power systems." *Journal of Applied Research and Technology.*, 13(2), 238-244.
- Yu, S., Yu, X., Shirinzadeh, B. and Man, Z. (2005). "Continuous finite time control for robotic manipulators with terminal sliding mode." *Automatica.*, 41(11), 1957-1964.
- Zelinka, I. and Lampinen, J. (1999). "An evolutionary learning algorithm for neural networks." *Proc., Int. Conf. on Soft Computing*, Brno, Czech Republic, 410-414.



## Publications

### International Journals

- 1) Jena, D. and Rajendran, S. (2014). "A review of estimation of effective wind speed based control of wind turbine." *Renewable and Sustainable Energy Reviews.*, 43, 1046-1062. (Elsevier)
- 2) Saravanakumar, R. and Jena, D. (2014). "Nonlinear control of wind turbine based on nonlinear estimation techniques for maximum power extraction." *International J. Green Energy.*, DOI: 10.1080/15435075.2014.952424. (Taylor & Francis)
- 3) Rajendran, S. and Jena, D. (2014). "Variable speed wind turbine for maximum power capture using adaptive fuzzy integral sliding mode control." *J. of Modern Power Systems and Clean Energy.*,2(2), 114-125. (Springer)
- 4) Saravanakumar, R. and Jena, D. (2014). "Adaptive fuzzy sliding mode control of variable speed wind turbine for maximum power extraction." *WSEAS Transaction on Power Systems.*, 9, 281-290.
- 5) Rajendran, S. and Jena, D. (2015). "Load mitigation and optimal power capture for variable speed wind turbine in region 2." *J. of Renewable Energy.*, Article ID 978216, DOI: <http://dx.doi.org/10.1155/2015/978216>. (Hindawi)
- 6) Saravanakumar, R. and Jena, D. (2015). "Validation of an integral sliding mode control for optimal control of a three blade variable speed variable pitch wind turbine." *International J. of Electrical Power & Energy Systems.*, 69, 421-429. (Elsevier)
- 7) Rajendran, S. and Jena, D. (2015). "Backstepping sliding mode control of a variable speed wind turbine for power optimization." *J. of Modern Power Systems and Clean Energy.*,3(3), 402-410. (Springer)
- 8) R. Saravanakumar and Debashisha Jena, "Nonlinear Control of wind turbine with optimal power capture and load mitigation," *Energy Systems* (Springer) DOI: [10.1007/s12667-015-0170-8](https://doi.org/10.1007/s12667-015-0170-8)

## International Conferences

- 1) Saravanakumar, R. and Jena, D. (2012). "Nonlinear estimation and control of wind turbine." *Proc., IEEE Int. Conf. on Electronics, Computing and Commination Technologies*, Bangalore, India, 1-6.
- 2) Saravanakumar, R. and Jena, D. (2013). "Second order ISMC for variable speed wind turbine." *Proc., IEEE Int. Conf. on Industrial and Information Systems (ICIS 2013)*, Peradeniya, Srilanka, 594-598.
- 3) Rajendran, S. and Jena, D. (2014). "Backstepping sliding mode control for variable speed wind turbine." *Proc., IEEE India Conf. (INDICON 2014)*, Pune, India, 1-6.
- 4) Saravanakumar, R. and Jena, D. (2014). "ISMC based variable speed wind turbine for maximum power capture." *Proc., Int. Conf. on Control, Instrumentation, Energy and Communication*, Calcutta, India, 326-330.
- 5) Rajendran, S. Jena, D. (2015). "Adaptive nonsingular terminal sliding mode control for variable speed wind turbine." *Proc., IEEE 28<sup>th</sup> Canadian Conf. on Electrical and Computer Engineering (CCECE 2015)*, Halifax, NS, 937-942.



## **Brief Bio-Data**

### **Saravanakumar Rajendran**

Research Scholar,  
Department of Electrical Engineering,  
National Institute of Technology Karnataka, Surathkal,  
Mangalore, India.  
Ph: 09486076363  
e-mail: sarrajoom@gmail.com

### **Qualification**

- Ph.D (Continuing)  
NITK, Surathkal.
- M.E (Control & Instrumentation Engineering)  
Anna University, Regional Center Coimbatore.
- B.E (Electrical & Electronics Engineering)  
Anna University Chennai.
- +2 (Maths, Physics)  
State Board, Tamilnadu.
- 10<sup>th</sup> (Maths, Science)  
State Board, Tamilnadu.

### **Publications**

- 8 Journal Articles.
- 5 Conference Papers.

### **Date of Birth**

Aug 04, 1987.